

Characterising Combustion in Diesel Engines

using parameterised finite stage
cylinder process models

Yu DING

丁宇

Characterising Combustion in Diesel Engines

using parameterised finite stage
cylinder process models

Proefschrift

ter verkrijging van de graad van doctor
aan de Technische Universiteit Delft,
op gezag van de Rector Magnificus prof.ir. K.C.A.M. Luyben,
voorzitter van het College voor Promoties,
in het openbaar te verdedigen

op woensdag 21 december 2011 om 12.30 uur

door

Yu DING

Marine Engineer
Harbin Engineering University, CHINA
geboren te Qiqihar, CHINA

Dit proefschrift is goedgekeurd door de promotoren:

Prof. ir. D. Stapersma

en copromotor:

Dr. ir. H. T. Grimmelius

Samenstelling promotiecommissie:

Rector Magnificus	voorzitter
Prof. ir. D. Stapersma	Technische Universiteit Delft, promotor
Dr. ir. H. T. Grimmelius	Technische Universiteit Delft, copromotor
Prof.dr.ir. R.S.G. Baert	Technische Universiteit Eindhoven
Prof. MA Xiuzhen	Harbin Engineering University, CHINA
Prof.dr.ir. B.J. Boersma	Technische Universiteit Delft
Prof.dr.ir. T.J.H. Vlugt	Technische Universiteit Delft
Dr. G.P. Theotokatos	National Technical University of Athens, GREECE

Published by:

VSSD
Leeghwaterstraat 42
2628 CA Delft
The Netherlands

E-mail: hlf@vssd.nl
Internet: <http://vssd.nl/hlf>

Keywords: diesel engine, combustion, heat release, Vibe model, Seiliger process, smooth pressure signals, in-cylinder process, characterising, mean value first principle, measurement

ISBN: 978-90-6562-289-1

©Ding Yu, 2011

All rights reserved. No part of this publication may be reproduced, stored in a retrieval system, or transmitted, in any form or by any means, electronic, mechanical, photocopying, recording or otherwise, without the prior written permission of the publisher.

Content

1 Introduction	1
1.1 Research background and relevance.....	2
1.2 Research objectives	5
1.3 Thesis outlines	7
2. Heat Release Calculation Using Simulation Techniques	9
2.1 Introduction	10
2.2 In-cylinder process simulation model.....	11
2.2.1 Introduction	11
2.2.2 Structure of the simulation model.....	11
2.2.3 Heat release model.....	17
2.2.4 Result and analysis	21
2.2.5 Discussions	35
2.3 Heat release calculation model	36
2.3.1 Introduction	36
2.3.2 Structure of the simulation model.....	36
2.3.3 Result and analysis	38
2.3.4 Discussions	49
2.4 Smoothing of the in-cylinder pressure signals.....	50
2.4.1 Introduction	50
2.4.2 Averaging and direct mathematical smoothing of pressure trace	51
2.4.3 Indirect fitting of pressure signal based on multiple Vibe function....	51
2.4.4 Smoothed result and analysis.....	59
2.4.5 Discussions	63
3. Parameters for Finite Stage Cylinder Process Model.....	65
3.1 Introduction	66

3.2 Theory of Advanced Seiliger Process.....	68
3.2.1 Definition of basic and advanced Seiliger process of closed cycle	69
3.2.2 Modeling the in-cylinder process with Seiliger model	72
3.2.3 Systematic investigation of the influence of Seiliger parameters on the in-cylinder process	79
3.3 Fitting measured engine cycle with Seiliger process	88
3.3.1 Determine equivalence criteria and suitable Seiliger parameters	88
3.3.2 Numerical method implementation and calculation procedure	91
3.3.3 Fit versions with three Seiliger parameters.....	95
3.3.4 Fit versions with four Seiliger parameters.....	106
3.3.5 Fit versions with five Seiliger parameters	125
3.3.6 Summary and comparison of Seiliger fit versions	129
3.4 Comparison of Seiliger process with Vibe heat release model.....	136
3.4.1 Seiliger process model based on <i>V3-1</i> fit version.....	137
3.4.2 Seiliger process model based on <i>V4-6</i> fit version.....	142
3.4.3 Summary.....	147
4. Using Measurements to Characterize Combustion.....	149
4.1 Introduction	150
4.2 Flow chart of the simulation procedure	151
4.3 The map of measured series	153
4.4 Result of Seiliger parameter <i>a</i>	156
4.5 Result of Seiliger parameter <i>b</i>	159
4.6 Result of Seiliger parameter <i>c</i>	163
4.7 Result of Seiliger parameter n_{exp}	167
4.8 Result of Seiliger parameter $\Delta E O$	177
4.9 Non-used equivalence criteria	179
4.10 Summary.....	187
5. Conclusions and Recommendations	191
5.1 Summary of thesis work.....	192

5.2 Conclusions	194
5.3 Recommendations	197
Appendix	199
I. Single-zone combustion model	200
II. Properties library.....	205
III. Curve fitting techniques using least square theory	210
IV. Fitting residual analysis.....	213
V. Polytropic process	215
VI. Investigation of diverging in Newton-Raphson numerical method	220
VII. Smoothed heat release measurement of the other three cylinders and cylinder 1 with original hole position.....	229
VIII. Description of the measurement system (based on manufacturer's data)	240
Nomenclature.....	249
Reference.....	255
Summary	267
Acknowledgement	273
Curriculum Vitae	275

Chapter 1

Introduction

1.1 Research background and relevance

Already in 1988, Delft University of Technology (TU Delft) started developing a diesel engine model using a ‘Mean Value First Principle (MVFP)’ approach [Boot, 1991]. Since it uses cycle time scale rather than crank angle, this model can simulate the complete turbocharged diesel engine system rapidly and efficiently, acquiring the diesel engine performance under various operational conditions at a certain level of detail but at the same moment being suitable to be a sub-model in a total propulsion or power generation system simulation [Grimmelius, 2000a]. As such this MVFP diesel engine model is not primarily intended for engine development but is used for system studies of engine users of complex propulsion systems such as in naval ships, and in installations where, next to propulsion, also power is required for other purposes such as in a dredging vessel.

The diesel engine model consists of a number of sub-models: the ‘in-cylinder process’, ‘gas exchange’, ‘thermodynamic-volume’, ‘exhaust process’, ‘turbo-machinery’, etc. In 1998, the model was further developed by Baan and Boëtius in a MATRIXx environment [Boëtius, 1998], to be used for advanced control research [Grimmelius, 1999a], [Grimmelius, 2000b] and for application in an engine room training simulator [Grimmelius 1999b]. The ‘in-cylinder process’ model from the beginning of its development used a Seiliger process model to describe the in-cylinder process between the moment of Inlet valve Closed (IC) and Exhaust valve Open (EO). An empirical fit was used to model the Seiliger parameters as function of some engine operation parameters (e.g. engine speed, ignition delay, in-cylinder temperature) first based on measurements on a test engine at the NLDA (then Royal Netherlands Naval College) [Schulten, 1998] and data from (then) Wärtsilä Netherlands [Baan, 1998]. The ‘gas exchange’ model for the first version was valid only to 4-stroke engines and was developed by Boëtius. Later Boëtius extended it to a 2-stroke engine [Boëtius, 1999], [Grimmelius, 2000a]. In 2002, Paul Schulten transferred the overall model from the MATRIXx to the MATLAB/Simulink environment [Schulten, 2005]. He did not change the ‘in-cylinder process’ model of 1998 based on his own measurements of the MAN4L20/27 and measurements of the Wärtsilä 16V26ST engine, but the major contribution of Schulten was the complete revision of the ‘gas exchange’ model for a 4-stroke engine [Schulten, 2003] with provisions for 2-stroke gas exchange. After that

this 2-stroke engine ‘gas exchange’ model was implemented by Chris Dijkstra and presented in [Dijkstra, 2003a]. Meanwhile the ‘turbo-machinery’ model was replaced by a model using non-dimensional approach [Stapersma, 1997] and Chris Dijkstra also implemented this into the DE B model [Dijkstra, 2003b]. Martijn Kom developed the cylinder process model with a multizone fit [Kom, 2004a] and a Woschni fit [Kom, 2004b] but did not achieve the necessary improvement of the combustion model within the Seiliger cylinder description.

The original Seiliger model, published in [Seiliger, 1922], had three combustion stages, although the cycle that goes by the name now normally has two combustion stages and also is referred to as the dual combustion cycle. The model was refined by [Stapersma, 2002a], who also returned to the original three stages of combustion. This development is completed in this thesis, where a general cycle with four stages of combustion is introduced to describe the net combustion heat of the ‘in-cylinder process’ model. The heat loss (i.e. heat loss during compression and in some cases for expansion) is also part of the cycle description. The result is a generalized finite stage cylinder process model that is completely specified by a finite number of parameters.

The reason to use a finite stage model in the DE II ‘MVFP’ simulation model is that it is capable to characterize the combustion and thus heat input with a finite number of stages and its associated parameters, and further is capable to calculate in a simple way the net work output from all the stages and their parameters. Then the in-cylinder process can be transformed to engine cycle time scale easily and efficiently. Therefore the key point to apply a finite, Seiliger type, model in DE B4 model is to obtain models for the Seiliger parameters (especially the parameters describing net combustion heat). This has been done in this thesis on the basis of both an experimental and theoretical approach.

From the experimental approach, it will be shown that the in-cylinder pressure measurement can be transformed to a Seiliger process definition on the basis of different sets of equivalence criteria to uniquely determine the Seiliger parameters. Then the dependence of Seiliger parameters with engine operating conditions can be obtained, after which the models of the Seiliger parameters in relation to the engine running parameters can be researched. As to the theoretical approach, the commonly used heat release model based on Vibe functions can be implemented in a single zone closed cylinder process simulation. The results also could be transformed to Seiliger

parameters using the same equivalence criteria and then the Vibe driven cylinder simulation could be compared with the Seiliger approximation.

1.2 Research objectives

Characterizing combustion of diesel engines is not only necessary when researching the instantaneous combustion phenomena but also when investigating the change of the combustion process under variable engine operating conditions. An effective way to achieve this goal is to parameterize the combustion process using a finite combustion stage cylinder process model and then the parameters can be modeled to give a global description of diesel engine combustion.

The main objective of this thesis is getting information *how to calculate (simulate) the parameters* defining the finite stage cylinder process model using both theoretical and experimental methods. The latter is essential but also complicated.

In order to achieve the main objective, the *first step* is to reconstruct the heat release during combustion using physical principles, i.e. the gas law and the first law of thermodynamics after carrying out the in-cylinder pressure measurement. Then a smoothing technique should be used to get smoothed and reliable in-cylinder features (e.g. in-cylinder pressure, in-cylinder temperature, heat input, work output).

In implementing this step, some simulation models must be built:

- *In-cylinder process simulation* model: using Vibe heat release model to calculate the in-cylinder features based on a single zone model. It will be used for an exploratory investigation of the engine in-cylinder process.
- *Heat release calculation* model: the reversed model of *In-cylinder process simulation* model, using in-cylinder pressure measurement, fuel consumption measurement, etc. as input to calculate the heat release during combustion. Here some improvements dealing with the dependence of the heat of combustion with cylinder temperature and the effect of heat required for fuel heating and evaporation are introduced.
- *A new smoothing method*: smoothing the combustion reaction coordinate on the basis of multiple Vibe functions to obtain a smoothed pressure and temperature trace, which potentially has a better quality than mathematically (up-front) smoothed signals. This smoothing method needs both the *heat release calculation* model and the *in-cylinder process simulation* model.

The *second step* is to transfer the in-cylinder features to the Seiliger parameters. In this step some goals should be reached:

- The *Seiliger process definition* must be correct and comprehensive.
- The possible *sets of equivalence criteria* are selected which relate the real engine cycle to the theoretical Seiliger process in an unambiguous way. They are used to set up the system of equations to find the solutions for Seiliger parameters.
- A proper *numerical iteration method* should be selected to find the solutions for Seiliger parameters.
- Any problems with *converging* of the iteration must be investigated in order to decide whether problems are caused by the numerical solution or by the non-existence of the roots.
- The different *sets of equivalence criteria* should be *compared* and *evaluated*.

The *third step* is a research into the theoretical method. The transformation of the parameters of the commonly used Vibe heat release model to Seiliger parameters was implemented and investigated. Then, after comparison, the behaviour of Seiliger parameters in the in-cylinder process can be expressed in existing knowledge in terms of Vibe parameters and it can be judged whether the Seiliger process can be used to characterize the combustion and performance of the in-cylinder process.

1.3 Thesis outline

The thesis is structured into five chapters and eight appendixes. Chapter 2 deals with the concept of heat release simulation of the diesel engine cylinder process. The ‘in-cylinder process model’, the ‘heat release calculation model’ including the effect of temperature dependent heat of combustion and heat required for fuel evaporation and a new method to smooth the in-cylinder pressure signals, are presented.

In Chapter 3, the definition of an advanced Seiliger process is given first, after which the most important part of the thesis – fit the real engine cycle to a Seiliger process is presented. Finally a comparison of the Seiliger process model with Vibe heat release model is carried out.

Chapter 4 shows the final result of the trend of Seiliger parameters as function of engine operating conditions based on extensive measurements, from which the combustion process of a real diesel engine is characterized and parameterized.

The thesis ends with Chapter 5, in which the conclusions are drawn and recommendations are given.

Chapter 2

Heat Release Calculation Using Simulation Techniques

2.1 Introduction

Heat release analysis is an important tool in the research of the combustion process in diesel engines. Recently, with the development of new fuel injection technologies, combustion in the diesel engine has changed considerably: with high fuel injection pressures, common rail, variable injection timing and rate shaping, the heat release pattern is different from the traditional engines and is to a certain extent controllable. Following a heat release measurement, there are several methods to investigate the combustion process in the diesel engine. An important application is the case where heat release measurement is required to determine combustion model parameters. Therefore the method to acquire an accurate heat release profile is rather important for the following combustion model parameters analysis.

However, heat release during combustion is not measured directly on the engine. Instead an in-cylinder pressure measurement is used to reconstruct the heat release using physical principles, i.e. the gas law and the first law of thermodynamics. This chapter will present the approach used in this thesis to acquire and process the heat release of a diesel engine after measurement. When the engine parameters (i.e. pressure signals, fuel consumption, engine trapped condition, etc.) are available, the heat release can be calculated based on physical principles. But this calculated heat release shows severe fluctuations, mainly due to the pressure signal measurement. Hence a procedure should be applied in order to smooth the heat release, after which the in-cylinder pressure, temperature, etc. can be reconstructed subsequently and be used for combustion model parameter analysis.

An 'in-cylinder process model' is described first as it is the basis of the 'heat release calculation' model. Moreover it can be used independently to simulate the in-cylinder process to investigate the main features of the cylinder process of the engine. Then the reversed and anti-causal 'heat release calculation model' is presented together with the results for three engine operating points. Last but not least, a new smoothing method based on multiple Vibe functions is presented in order to acquire a smoother and more reliable pressure signal [Ding, 2011a].

2.2 In-cylinder process simulation model

2.2.1 Introduction

The past few decades have witnessed the development and improvement of various methods in modelling of the combustion process in diesel engine. Nevertheless, the thermo-dynamical details of these models that basically are zero-dimensional or quasi-dimensional remain critical and receive high attention nowadays.

Depending on the application, typically three different types of combustion models are distinguished. In order of increasing complexity, according to [Stiesch, 2003], these are the thermodynamic (or zero- dimensional) models (e.g. [Watson, 1980], [Arregle, 2003], [Brown, 1996], [Vibe, 1970]), the phenomenological (or quasi-dimensional) models (e.g. [Hiroyasu, 1983], [Taufia, 2006], [Sahin, 2008]) and CFD (or multidimensional) models (e.g. [Rietz, 1995], [Benkenida, 2004], [Struckmeier, 2010]). The main task for these models is not only to investigate the conditions of the combustion but also to obtain knowledge about the influence of the combustion process on significant parameters in a diesel engine. In this section, a double Vibe model [Vibe, 1970] is used to simulate the cylinder process for a diesel engine and the MATLAB simulation results with respect to the pressure, temperature, heat flow, etc. in the cylinder following from a systematic research of all factors of the Vibe model will be discussed. In addition, the sub-models of the properties library and heat loss to the cylinder wall in the simulation model are critically reviewed in principle and application.

2.2.2 Structure of the simulation model

Figure 2.1 illustrates the overall in-cylinder process simulation model [Ding, 2009]. The final output of the model is the in-cylinder temperature, which is the result of integration of the first law of thermodynamics (equation [2.1]). The heat release model is based on the combustion reaction rate (ζ , fuel burn rate, i.e. mass of fuel burnt per unit time). When multiplied with – a temperature dependent – heat of combustion (u_{comb}) this acts as heat source (\dot{Q}_{comb}) in the first law. The reaction rate after integration also causes a (slight) mass addition in the mass balance. The in-cylinder

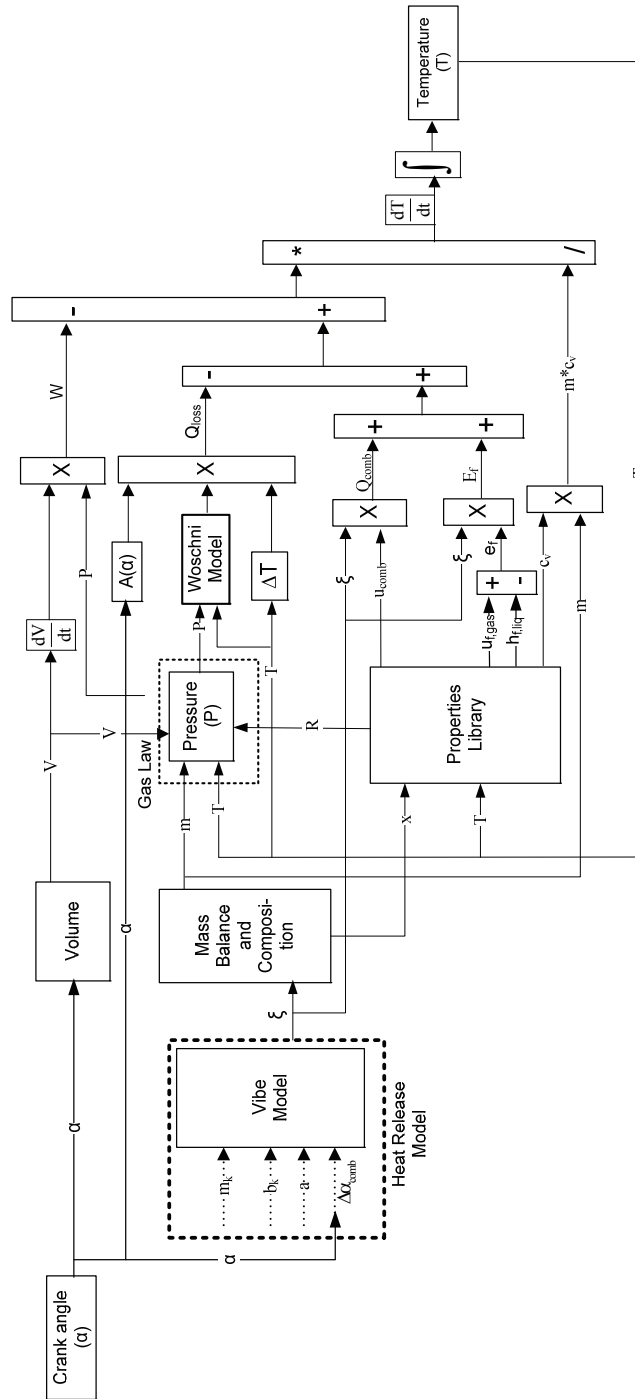


Figure 2.1 General block diagram of in-cylinder process model

volume is calculated using the crank angle (α), cylinder geometry and dimensions, assuming a constant engine speed to calculate the crank angle in equation [2.2], [Stapersma, 2009c]. Both the mass and volume, together with a feedback of the in-cylinder temperature and gas constant, are used in the gas law to calculate in-cylinder pressure. When calculating work and internal energy terms, volume is differentiated: this can be done straightforward in a simulation environment. Woschni's model is used to evaluate the heat transfer coefficient [Woschni, 1967] to calculate heat loss to the walls. All the properties of air, stoichiometric gas and fuel (e.g. gas constant, internal energy, specific heat) are calculated in the 'Properties library'. The energy of fuel (E_f) indicates the fuel carrying energy into cylinder upon entry. The derivation and detailed explanation of the implementation of the first law of thermodynamics in the control volume of this model is presented in Appendix I.

It is noted that the way the initial condition (i.e. p_1 , T_1 , m_1 and x_1) is determined will be presented in section 3.2.2.

$$\frac{dT}{dt} = \frac{\dot{Q}_{comb} - \dot{Q}_{loss} - p \cdot \frac{dV}{dt} + \dot{E}_f}{m \cdot c_v} \quad [2.1]$$

$$V(\alpha) = A_b \cdot L_s \cdot \left[\frac{1}{\varepsilon - 1} + \frac{1}{2} \cdot \left\{ (1 + \cos \alpha) + \frac{1}{\lambda_{CR}} \left(1 - \sqrt{1 - \lambda_{CR}^2 \cdot \sin^2 \alpha} \right) \right\} \right] \quad [2.2]$$

1) Mass balance and composition

The purpose in this sub-model is to acquire the mass in the cylinder and more importantly the composition parameter 'x' which is used in the 'Properties library' to calculate specific heat, internal energy, and enthalpy etc.

In the 'Heat release model', the Combustion Reaction Rate (*CRR* or ξ) is modelled with a double Vibe model that will be discussed later:

$$\xi = \frac{dm_f}{dt} \quad [2.3]$$

Adding the mass of fuel to the trapped mass in *IC* (Inlet valve Closed) condition, the total mass in the cylinder is known according to the mass balance:

$$m = m_1 + \int_{IC}^{EO} \xi \cdot dt \quad [2.4]$$

Last but not least, the composition of gas in terms of the air fraction, which is an important variable in the ‘Properties library’ (presented in the next section), can be calculated using σ (air/fuel ratio). The ‘ x_1 ’ in equation [2.5] is the air fraction of the trapped condition, which is strictly speaking not equal to unity, due to the residual exhaust gas remaining in the cylinder after scavenging.

$$x = \frac{m_1 \cdot x_1 - \sigma \cdot \int_{IC}^{EO} \xi \cdot dt}{m_1 + \int_{IC}^{EO} \xi \cdot dt} \quad [2.5]$$

2) *Properties library*

In order to obtain the in-cylinder gas properties (e.g. c_v , c_p , u and h), the in-cylinder gas is modelled as a mixture of two well defined basic mixtures – air and stoichiometric gas, which are in turn also considered to be mixtures of several species. If these two basic mixtures are supposed to be ideal but non-perfect, the properties of the composing species are only functions of temperature. Then the properties of air and stoichiometric gas can be calculated using species fractions obeying ideal mixture. Finally the in-cylinder properties can be calculated as a function of temperature using a single parameter, in this case the air mass fraction, which is calculated in equation [2.5]. The determination of the entropy is more complicated since it is not only function of temperature and air fraction but also of pressure. The detailed explanation of the ‘Properties library’ is presented in Appendix II.

3) *Heat of combustion*

The quantity Q_{comb} is defined as ‘combustion heat’, for a closed system based on internal energy, and is calculated using the properties of fuel, air and stoichiometric gas, which have been presented in Appendix II. The combustion heat rate is:

$$\begin{aligned} \dot{Q}_{comb} &= \xi \cdot u_{comb} \\ &= \xi \cdot (u_f + \sigma \cdot u_a - (1 + \sigma) \cdot u_{sg}) \end{aligned} \quad [2.6]$$

In most research studies, u_{comb} is set to be constant (e.g. $4.27 \cdot 10^4$ kJ/kg for normal diesel fuel), often also neglecting the small difference between heat of combustion based on enthalpy and based on internal energy. In this thesis all terms in principle are temperature dependent and heat of combustion therefore is not a constant.

The composition of diesel fuel is rather complex. For calculating the stoichiometric composition up to reasonable accuracy only the fractions of carbon, hydrogen and sulphur are required. Then according to [BSI, 1982] also a good estimate of the heat value at reference temperature can be obtained. The detailed composition of fuel becomes important for the fuel thermodynamic properties at higher temperatures.

An approximation of fuel composition has been presented by [van Oosten, 2004] for 15 components and by [Kraaij, 2002] for 26 components. In those two approximations, alkanes occupy a considerable portion. Later, [de Vos, 2008] proposed to simplify the diesel fuel to consist of an alkane ($C_{13}H_{28}$) and a benzene ($C_{13}H_{10}$), the idea being that the chosen species are typical for all alkanes and aromatics and that the specific heat of alkanes and aromatics differ both at reference temperature and in their temperature dependence. The fraction of $C_{13}H_{28}$ and $C_{13}H_{10}$ is calculated from the carbon percentage of the fuel, which is known when the fuel type is determined. Then the $c_{p,f}$, $c_{v,f}$, u_f and h_f are calculated using the same method as described in equation [II.5] – [II.7] and equation [II.9] – [II.11]. The reference value h_f^{ref} in equation [II.6] for fuel is used to match the heat of combustion to the heat value at reference temperature according to [BSI, 1982], adding the fuel evaporation heat at the reference temperature according to [Borman, 1998].

Ultimately the effect of u_f in the heat of combustion (equation [2.6]) is that the heat of combustion *increases* with temperature, i.e. it compensates the effect of u_a and u_{sg} that which tend to *decrease* the heat of combustion with increasing temperature.

4) Energy of fuel

The quantity E_f is defined as ‘energy of fuel’ and for a closed system there are two constituents: one is the difference caused by fuel phase changing from liquid to gas; the other is the difference between fuel injection pressure and in-cylinder pressure. (see Figure I.1 in Appendix I). Therefore it is equal to the difference of total enthalpy of entering (liquid) fuel (i.e. including the kinetic energy caused by the fuel injection pressure) and the internal energy of (gaseous) fuel present in the cylinder. The energy fuel rate is:

$$\dot{E}_f = \dot{m}_{f,in} \cdot e_f = \dot{m}_{f,in} \cdot (h_{f,liquid}^{in+} - u_{f,gas}) \quad [2.7]$$

The fuel enters the cylinder as a fluid at some (low) temperature and after evaporation is assumed to enter the gas phase at cylinder temperature. Both the injection rate and evaporation rate are assumed equal to the combustion rate. One can view this energy flow also as the heat flowing from the gas phase to the (liquid) fuel and required to heat up and evaporate the fuel before combustion. As a result, the ‘effective heat of combustion’ is lower than the nominal value at reference temperature since fuel in a diesel engine enters at a low energy value (as a liquid and at a relatively low temperature). This is illustrated in section 2.2.3, Figure 2.16.

The $h_{f,liquid}^{in}$ in equation [2.7] is the inflow fuel enthalpy in *liquid* phase. The $c_{v,f,liquid}$ and $u_{f,liquid}$ are calculated using the method as described in Appendix II.

5) Heat loss to the walls

During combustion, there is a large temperature difference between the combustion gas and the cylinder wall. The heat loss to the surrounding metal should be taken into account.

$$\dot{Q}_{loss} = \sum_{i=1}^3 \{ \alpha_{g \rightarrow w} \cdot (T - T_{wall,i}) \cdot A_{wall,i} \} \quad [2.8]$$

With: $i=1$, cylinder wall;
 $i=2$, cylinder cover;
 $i=3$, piston crown.

Since it is difficult to measure the surface temperature in these three places and these temperatures do not play a significant role in the heat loss value, these three temperatures are estimated and kept constant. The heat transfer coefficient can be estimated using semi-empirical formulae. In this model, the Woschni method is used ([Woschni, 1965], [Stapersma, 2009d]).

$$\alpha = C_1 \cdot \frac{1}{D_B^{0.214}} \cdot \frac{p^{0.786}}{T^{0.525}} \cdot (C_3 \cdot c_m + C_4 \cdot \frac{p - p_0}{p_1} \cdot \frac{V_s}{V_1} \cdot T_1)^{0.786} \quad [2.9]$$

Note that the p_0 and T_0 here are the pressure and temperature in the ‘no fuel injection’ condition instead of ambient condition. The constants are valid for a heat transfer coefficient in [W/m²K], while pressure must be in [bar], bore in [meter] and temperature in [Kelvin].

The constant C_1 in equation [2.9] will directly affect the heat loss to the walls and further to the heat release during combustion. The influence of this parameter will be discussed in section 2.3.3.

The parameter C_3 is related to the effect of in-cylinder gas swirl velocity w_t and Woschni advised:

During gas exchange:
$$C_3 = 6.18 + 0.417 \cdot \frac{w_t}{c_m} \quad [2.10]$$

During compression and expansion:
$$C_3 = 2.28 + 0.308 \cdot \frac{w_t}{c_m} \quad [2.11]$$

Since it was impossible to measure w_t , the ratio w_t/c_m is unknown. As C_1 will be considered a variable, C_3 cannot very well be determined from measurements as well. According to literature w_t/c_m can vary within the range of 5 to 50, for this engine, it is set to 10 because limited swirl is expected for this engine.

The parameter C_4 is related to the shape of the combustion chamber. Woschni advised:

Direct injection:
$$C_4 = 0.00324 \left[\frac{m}{s \cdot K} \right] \quad [2.12]$$

Pre-chamber:
$$C_4 = 0.00622 \left[\frac{m}{s \cdot K} \right] \quad [2.13]$$

Since the engine used in this thesis has direct injection, equation [2.12] is applied in the heat loss model.

2.2.3 Heat release model

1) Introduction Vibe heat release model

The Vibe combustion profile was originally presented in [Vibe, 1970] but can be found in many textbooks, e.g. [Merker, 2006], [Watson, 1980], [Zhan, 2004]. The Vibe function is based on the first principle of chain reactions [Stapersma, 2009c], where the formation of radicals is proportional to the amount of fuel and the increase of radicals is proportional to the decrease of fuel:

$$\frac{dm_f^+}{dt} = k \cdot m_f \quad \text{and} \quad dm_f^+ = -\mu \cdot dm_f \quad [2.14]$$

And thus the reaction rate:

$$\xi = \frac{dm_f}{dt} = -\frac{k}{\mu} \cdot m_f \quad [2.15]$$

The normalized rate of combustion Z , which is linked to the normalized reaction rate X , can be defined as:

$$Z = \frac{dX}{d\tau} = \xi \cdot \frac{t_{comb}}{m_{f,0}} \quad \text{and} \quad X = \frac{m_f}{m_{f,0}} \quad [2.16]$$

where τ is normalized time:

$$\tau = t/t_{comb} \quad [2.17]$$

Vibe proposed a model assuming a nonlinear time dependency of the reaction constant in equation [2.15]

$$k \propto t^m \quad [2.18]$$

The normalized reaction rate and reaction coordinate then can be shown to be¹:

$$Z = a \cdot (m+1) \cdot \tau^m \cdot e^{-a \cdot \tau^{m+1}} \quad \text{and} \quad X = 1 - e^{-a \cdot \tau^{m+1}} \quad [2.19]$$

If the duration of combustion time and the total injected fuel are given, the *CRR* can be acquired after selecting parameters m and a .

To make the model more suitable for real combustion processes and make a division between the premix and diffusive combustion stages, a double Vibe model is often used (Figure 2.2):

$$Z = b_1 \cdot a \cdot (m_1 + 1) \cdot \tau^{m_1} \cdot e^{-a \cdot \tau^{m_1+1}} + b_2 \cdot a \cdot (m_2 + 1) \cdot \tau^{m_2} \cdot e^{-a \cdot \tau^{m_2+1}} \quad [2.20]$$

$$X = b_1 \cdot \left(1 - e^{-a \cdot \tau^{m_1+1}}\right) + b_2 \cdot \left(1 - e^{-a \cdot \tau^{m_2+1}}\right) \quad [2.21]$$

Here b_1 and b_2 are the ‘weighting factor’ for premix and diffusive combustion, which must obey:

¹ Note that the Vibe function is mathematically equivalent to the Weibull function in statistics and that the time dependent reaction rate equation [2.15] resembles the time dependent failure rate.

$$b_1 + b_2 = 1 \quad [2.22]$$

The parameter a is taken equal for both Vibe functions and then can easily be linked to the combustion efficiency:

$$1 - e^{-a} = \eta_{comb} \quad [2.23]$$

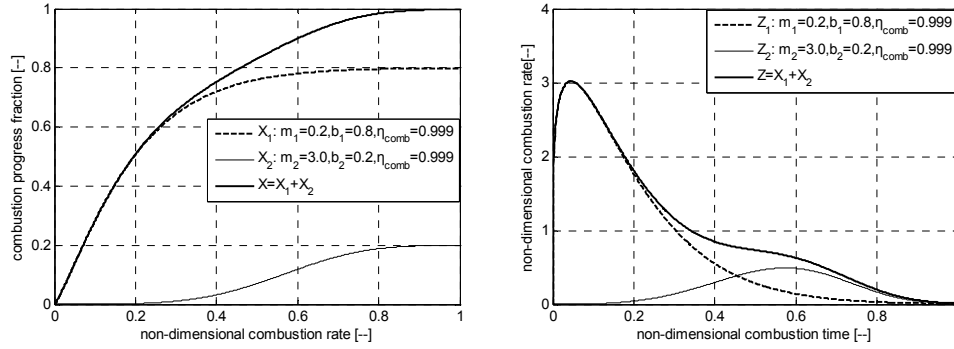


Figure 2.2 Double Vibe heat release profile

A series progression of Vibe functions was proposed in [Knobbe, 2001]:

$$X = \sum_{k=1}^n b_k \cdot X_k = \sum_{k=1}^n b_k \cdot \left(1 - e^{-a \cdot t^{m_k+1}}\right) \quad [2.24]$$

The Vibe function is considered a wavelet from which a series expansion is formed. Each single Vibe function has its own form factor m_k and weight factor b_k but they share the same a and the same duration of combustion.

2) The influence of Vibe parameters on the combustion profile

Table 2.1 Summary of the double Vibe parameters range

Double Vibe Parameter	Base Value	Range
m_1	0.2	0.05 - 0.5
m_2	3	1.5 - 4.0
b_1	0.8	0.3 - 0.9
a	6.9078	3.9120 - 9.2103
(η_{comb})	(0.999)	(0.980 - 0.9999)

Figure 2.3 illustrates the influence of double Vibe parameters (m_1 , m_2 , b_1 and a) on the non-dimensional combustion rate. Since parameter a is linked to η_{comb} in a straightforward manner, the η_{comb} is used instead of parameter a . Table 2.1 gives a realistic range of values for the parameters m_1 , m_2 , b_1 and η_{comb} , in which only one Vibe parameter is changed at a time while the others remain at their base value.

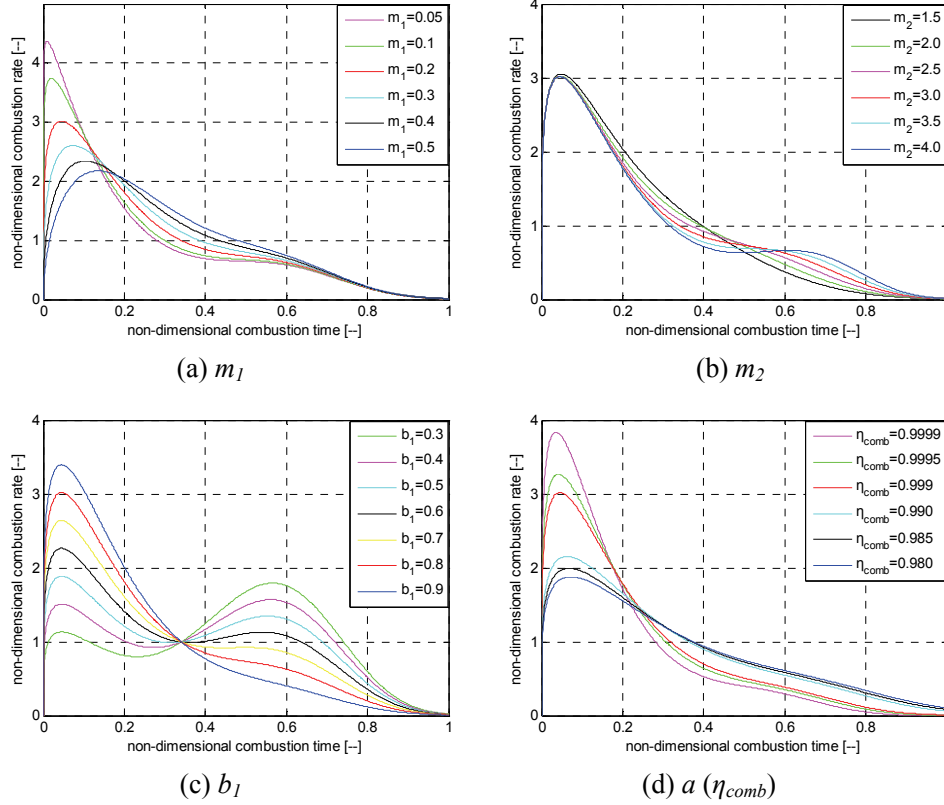


Figure 2.3 The influence of double Vibe parameters to heat release profile

Parameters m_1 and m_2 indicate the shape of ‘premix’ and ‘diffusive’ combustion respectively (Figure 2.3(a) and (b)). There is more heat release during the premix combustion stage and less during the diffusive combustion stage with m_1 descending. In contrast when m_2 decreases, the amount of heat release is decreasing during diffusive combustion and increasing in the premix combustion. Parameter b_1 is the weight factor of premix combustion and $1-b_1$ is the weight factor of diffusive combustion. Therefore it is easy to understand that in Figure 2.3(c) there is more heat release during the premix combustion stage and less during the diffusive combustion stage with b_1 increasing. As

to a (or η_{comb}), its influence is more complicated. First, the amount of heat release during premix combustion stage becomes larger with increasing η_{comb} .

Second, it is noticed that the total combustion terminates earlier for larger η_{comb} , which is the reason why a is sometimes taken larger for the Vibe functions representing premix combustion stage. The effect of changing the a value for the premix combustion phase is shown in Figure 2.4, where the a value is changed from 6.908 ($\eta_{comb} = 0.9990$) to 9.210 ($\eta_{comb} = 0.9999$): the premix combustion phase now terminates earlier (Z_3 and X_3 of the black line in Figure 2.4) resulting in a more pronounced ‘peaky’ combustion. However, to simplify the calculations, a common parameter a is preferred, used in both premix and diffusive combustion stages, also because to a certain extent the same effect can be accomplished by choosing a smaller m_1 value [Stapersma, 2009c].

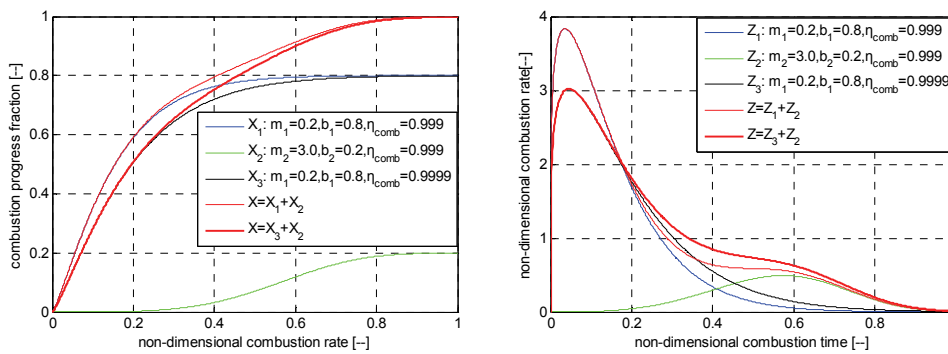


Figure 2.4 Double Vibe heat release profile with the effect of different a value in premix phase

2.2.4 Result and analysis

The model is verified with measurements taken from a MAN 4L 20/27 at NLDA. The general data of the engine are listed in Table 2.2. The full load and maximum speed define the nominal point used in the following simulation and analysis.

Table 2.2 The dimensions of engine used in the model

Parameter	
Model	MAN4L 20/27
Cylinder Number	4
Bore	0.20 m
Stroke	0.27 m
Connection Rod Length	0.52 m
Nominal Engine Speed	1000 rpm
Maximum Effective Power	340 kW
Compression Ratio	13.4[-]
Fuel injection	Plunger pump Direct injection
SOI	4° before TDC
IC	20° after BDC
EO	300° after BDC

1) Input parameters

According to Figure 2.1, the prime input of the simulation model is the ‘heat release’ along with the crank angle. The base values in Table 2.1 are selected as the shape parameters for the double Vibe heat release model. The other two parameters *SOC* (Start Of Combustion) and *EOC* (End Of Combustion) are estimated at 177 degree (the ignition delay is estimated to be 1 degree) and 280 degree after BDC respectively.

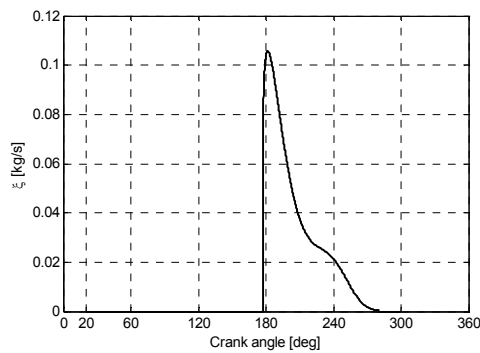


Figure 2.5 Combustion reaction rate

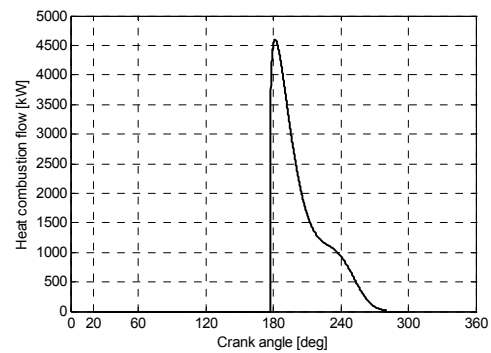


Figure 2.6 Heat combustion flow

Figure 2.5 – Figure 2.7 show the combustion reaction rate, combustion heat flow, and heat input flow separately. The shapes are almost congruent because they are all derived from the Vibe combustion profile, but the non-constant effective heat of combustion causes some distortion. The consequences of these heat releases will be presented in section 2.3.2. Figure 2.8 shows the fuel burnt percentage – also referred to as the reaction coordinate (*RCO*) – which is the integral of *CRR*.

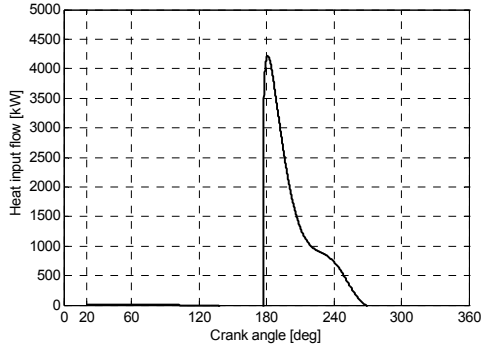


Figure 2.7 Heat input flow

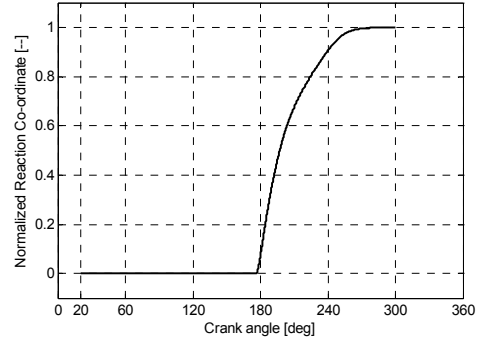


Figure 2.8 Fuel burnt percentage

2) State parameters

Four gas state parameters are shown in Figure 2.9 – Figure 2.12. In Figure 2.9 and Figure 2.10, the dash lines imply the in-cylinder pressure and temperature for ‘no fuel injection’, the p_0 and T_0 as used in equation [2.9] to calculate the heat transfer coefficient. The in-cylinder volume versus crank angle is given in Figure 2.11. The mass in the cylinder (Figure 2.12) increases from the start of combustion – just before TDC – with the mass of fuel injected into the cylinder.

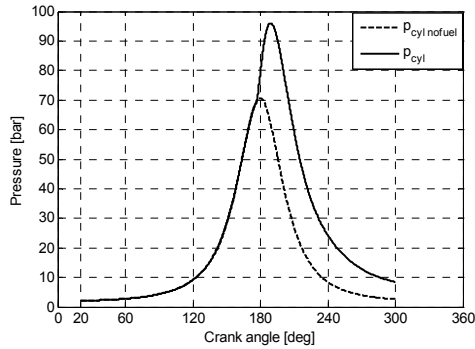


Figure 2.9 In-cylinder pressure

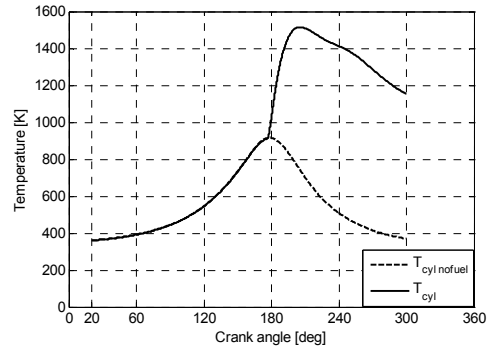


Figure 2.10 In-cylinder temperature

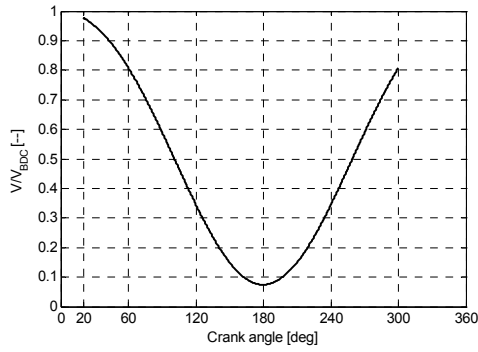


Figure 2.11 In-cylinder volume

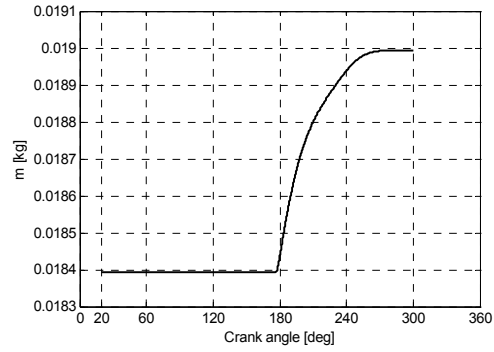


Figure 2.12 In-cylinder mass

3) Gas property parameters

Figure 2.13 illustrates the fresh air fraction in the cylinder. It remains constant ($x_l = 0.95$) during the compression phase and from the point of *SOC* it decreases. Figure 2.14 shows the e_f in equation [2.7]. Since $h_{f,liquid}^{in}$ is a function of fuel injection temperature ($T_{f,inj} = 40$ °C) and $u_{f,gas}$ is a function of in-cylinder temperature, the difference is also function of temperature and is negative, which can be considered to be the net heat loss to the fuel before combustion.

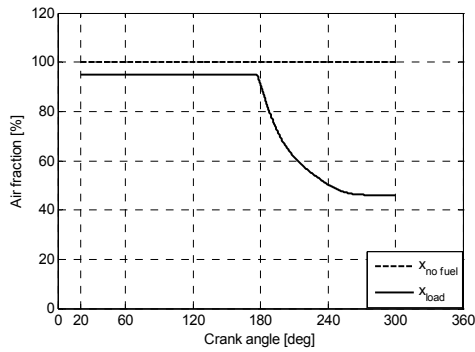


Figure 2.13 In-cylinder air fraction

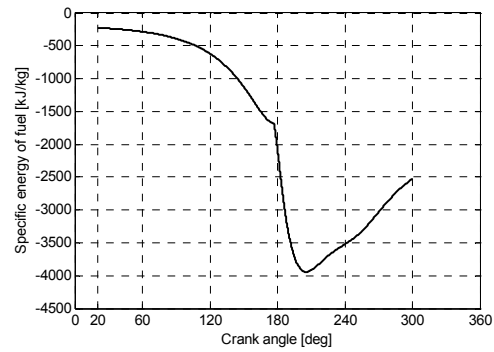


Figure 2.14 Specific energy of fuel

The c_v is illustrated in Figure 2.15 where the c_v of air, stoichiometric gas and in-cylinder gas are displayed separately. In Figure 2.15(b), due to the different air fraction at the same gas temperature before and after T_{max} , there are two different c_v values of the in-cylinder gas between 1200 K and 1500 K.

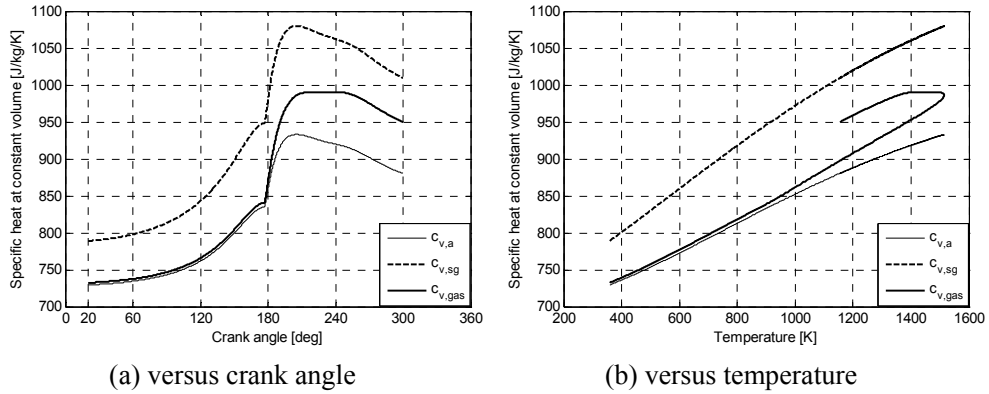


Figure 2.15 Specific heat at constant volume (c_v)

Figure 2.16 shows the ‘heat of combustion’ derived from equation [2.6]. As stated, due to the fact that the in-cylinder process takes place in a closed system, the internal energy should be used to calculate the ‘heat of combustion’ (u_{comb}). However the ‘heat of combustion’ derived from enthalpy (h_{comb}) is also displayed in the figures, which is smaller than u_{comb} . The dark solid curves in Figure 2.16 indicate the ‘the effective heat of combustion’ being ($u_{comb} - e_f$), i.e. after subtracting the heat required to evaporate and heat up the fuel (energy of fuel ‘ E_f ’ derived from equation [2.7]). It is clear that the ‘effective heat of combustion’ is considerably lower than the ‘heat of combustion’, in particular at higher temperature.

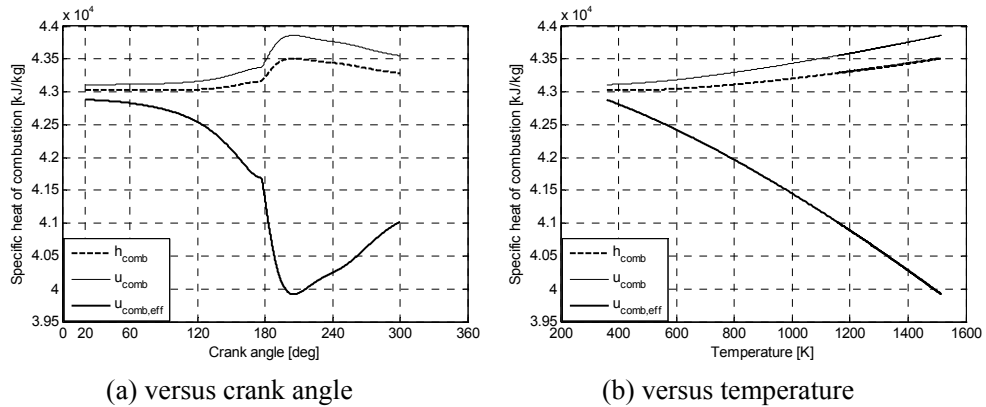


Figure 2.16 Specific ‘heat of combustion’ and ‘effective heat of combustion’

4) *Heat loss to the walls*

Figure 2.17 shows the heat transfer coefficient versus crank angle, estimated with Woschni's model (equation [2.9]). The instantaneous heat loss flow is illustrated in Figure 2.18, for a wall temperature of 400 K for the cylinder wall, 600 K for the piston crown and 580 K for the cylinder head. Since wall temperatures were never measured in this engine, they are estimates. Also for simplicity they are kept constant for all operating points, which will not be true in reality. Due to the uncertainty in the Woschni expression (in particular the value of the constants, see 2.3.3 5)) it was thought not worthwhile to put in a more clever scheme. There is some heat input (negative heat loss flow) at the beginning of the compression stroke, after that the heat flow follows the trend of the in-cylinder pressure.

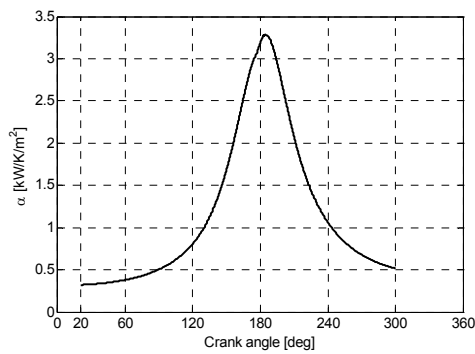


Figure 2.17 Heat transfer coefficient

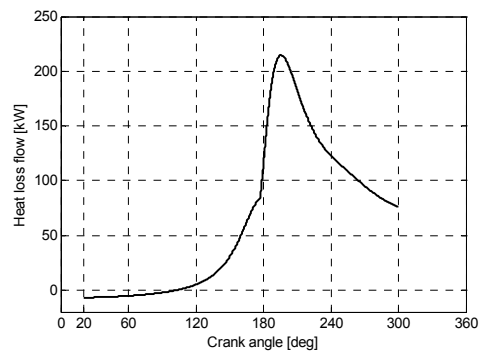


Figure 2.18 Instantaneous heat loss flow

5) *Engine performance*

The principle of energy conversion of a diesel engine is to transform the fuel heat energy into (mechanical) work. The following chain of efficiencies are defined for the energy conversion [Stapersma, 2010a]:

$$Q_f \xrightarrow{\eta_{comb}} Q_{comb} \xrightarrow{\eta_{hl}} Q_i \xrightarrow{\eta_{td}} W_i \xrightarrow{\eta_m} W_e$$

The representative overall efficiencies are ‘indicated efficiency’ (η_i) and ‘effective efficiency’ (η_e):

$$\eta_e = \frac{W_e}{Q_f} \quad \text{and} \quad \eta_i = \frac{W_i}{Q_f} \quad [2.25]$$

The following partial efficiencies are defined to analyse the energy transfer chain:

a). *Combustion efficiency*: specifies the losses due to incomplete combustion. Combustion efficiency can be modelled, see for instance [Betz, 1986]. With the recent development of high pressure injection technology and combustion chamber optimization, η_{comb} is close to 1.

$$\eta_{comb} = \frac{Q_{comb}}{Q_f} \quad [2.26]$$

b). *Heat loss efficiency*: specifies the heat loss to the cylinder walls during combustion. Q_{comb} is difficult to measure or to calculate but the difference between Q_{comb} and Q_i (i.e. Q_{loss}) can be evaluated according to section 2.2.2 5).

$$\eta_{hl} = \frac{Q_i}{Q_{comb}} \quad [2.27]$$

c). *Thermodynamic efficiency*: specifies the conversion efficiency from heat input to indicated work. This efficiency is the ratio of W_i (indicated work in the p - V diagram) and Q_i (heat input in the T - S diagram). The energy loss due to this conversion takes more than the others in the total energy loss.

$$\eta_{td} = \frac{W_i}{Q_i} \quad [2.28]$$

d). *Mechanical efficiency*: specifies the mechanical loss of the engine between piston and output flange. W_i can be calculated based on p - V diagram while W_e can be measured directly from the output power. Otherwise, η_m can be modelled according to methods such as [Chen, 1965] or [Millington, 1968].

$$\eta_m = \frac{W_e}{W_i} \quad [2.29]$$

Figure 2.19 shows the instantaneous indicated power and the instantaneous heat combustion flow, heat input flow and heat loss flow have been shown in Figure 2.6, Figure 2.7 and Figure 2.18 respectively. However, of major concern to engine performance evaluation is not the value of the instantaneous parameters but the mean values per cycle.

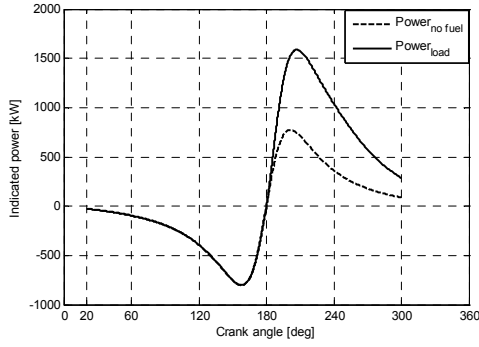


Figure 2.19 Instantaneous indicated power

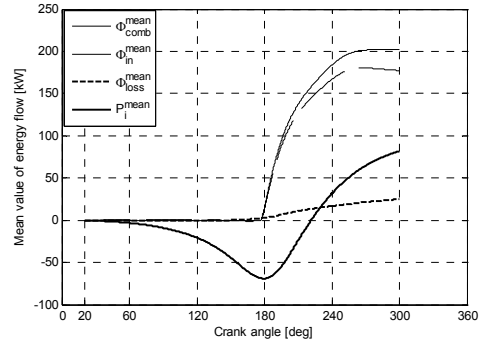


Figure 2.20 Summary of mean value of energy flow

Figure 2.20 shows the mean value of the indicated power, heat combustion flow, heat input flow and heat loss flow, which are calculated based on equation [2.30] – [2.33]. Here ‘ k_{cyc} ’ has value two, as for four-stroke engines there is one combustion every two cycles.

$$\bar{P}_i = \int_{IC}^{EO} p \cdot \frac{dv}{dt} \cdot dt \cdot \frac{n_{eng}}{k_{cyc}} \quad [W] \quad [2.30]$$

$$\bar{Q}_{comb} = \int_{IC}^{EO} \frac{dQ_{comb}}{dt} \cdot dt \cdot \frac{n_{eng}}{k_{cyc}} \quad [W] \quad [2.31]$$

$$\bar{Q}_i = \int_{IC}^{EO} \frac{dQ_i}{dt} \cdot dt \cdot \frac{n_{eng}}{k_{cyc}} \quad [W] \quad [2.32]$$

$$\bar{Q}_{loss} = \int_{IC}^{EO} q_{loss} \cdot dt \cdot \frac{n_{eng}}{k_{cyc}} \quad [W] \quad [2.33]$$

Table 2.3 Summary of energy flow and engine efficiency per cycle and per cylinder

Energy flow and efficiency per cycle	Φ_{comb} [kW]	Φ_i [kW]	Φ_{loss} [kW]	P_i [kW]	η_i [--]	η_{hl} [--]	η_{td} [--]
	202.10	177.18	24.93	81.76	0.41	0.88	0.46

Actually, the end values in Figure 2.20 are the mean values of the overall in-cylinder cycle (from IC to EO). Table 2.3 lists the summary of the engine energy flow per cycle and efficiencies. The combustion efficiency (η_{comb}) is assumed unity so $\Phi_{comb} = \Phi_f$.

6) Describing combustion with Vibe functions

The double Vibe (or multiple Vibe) model provides an efficient way to model the combustion process in a diesel engine. With the determination of the Vibe parameters (in a double Vibe model m_1 , m_2 , b_1 , a , SOC , EOC and m_{fr}), the non-dimensional combustion rate (e.g. Figure 2.2) is found, from which – together with the fuel consumption – the combustion reaction rate (CRR , e.g. Figure 2.5) can be obtained. Using this – with heat of combustion value – the heat of combustion flow versus crank angle is obtained (e.g. Figure 2.6). In this research the most important in-cylinder parameters (e.g. p_{max} , T_{max} , engine efficiency) are used as benchmarks for finding the correct Vibe parameters. [Watson, 1980] used an empirical method to investigate the Vibe parameters (in fact single Vibe, so m_1 , m_2 , b_1 , a) as a function of engine operating parameters, but his research is limited to the truck engines.

Table 2.4 Summary of the double Vibe parameters range

Double Vibe parameter	Nominal value	Range
m_1	0.2	0.05 - 0.5
m_2	3	1.5 - 4.0
b_1	0.8	0.3 - 0.9
a	6.9078	3.9120 - 9.2103
(η_{comb})	(0.999)	(0.980 - 0.9999)
SOC	177	174 - 179
EOC	280	250 - 300
m_{fr}	1.0	0.7 - 1.2

In this section, the influence of parameters in a double Vibe model on the in-cylinder process is investigated systematically. The value ranges of the parameters are shown in Table 2.4. The values are the same as found in Table 2.1 but three additional parameters are added. Again, when a parameter is changed, the others are kept at their nominal value. The influence on the calculated in-cylinder pressure and temperature figures as a result of each varying parameter are shown, which will provide some guidelines for selecting the values of these parameters.

a). **Parameter m_1**

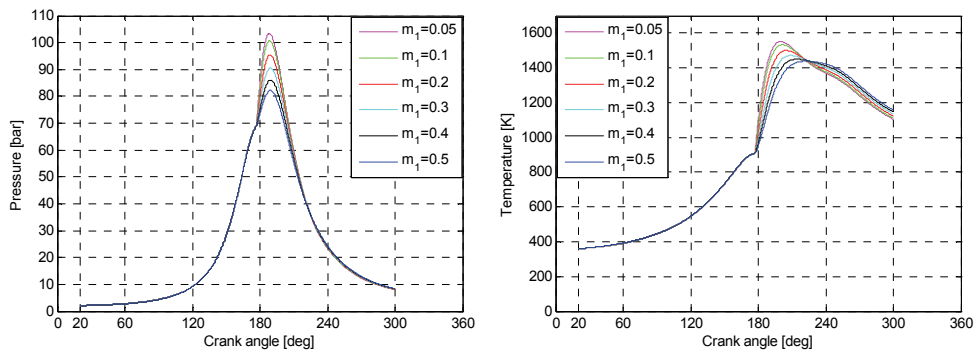


Figure 2.21 Parameter m_1

Parameters m_1 and m_2 are used to describe the ‘shape’ of the premix and the diffusive combustion respectively. With m_1 decreasing, the maximum pressure is increasing and the pressure in the late combustion period does not change significantly; the maximum temperature follows the same trend as the maximum pressure and necessarily occurs at an earlier crank angle, but the temperature during late combustion decreases (Figure 2.21).

b). **Parameter m_2**

As to m_2 , the pressure changes only slightly in the late combustion stage (Figure 2.22). Since the nominal value of b_2 is only 0.2, the proportion of diffusive combustion is quite small. When zooming in on the pressure around 240°, it turns out that the pressure is lower for larger m_2 values. With m_2 decreasing, the temperature initially increases when combustion starts but then decreases after a certain value of crank angle. This is caused by earlier heat release in the diffusive combustion stage with a smaller m_2 .

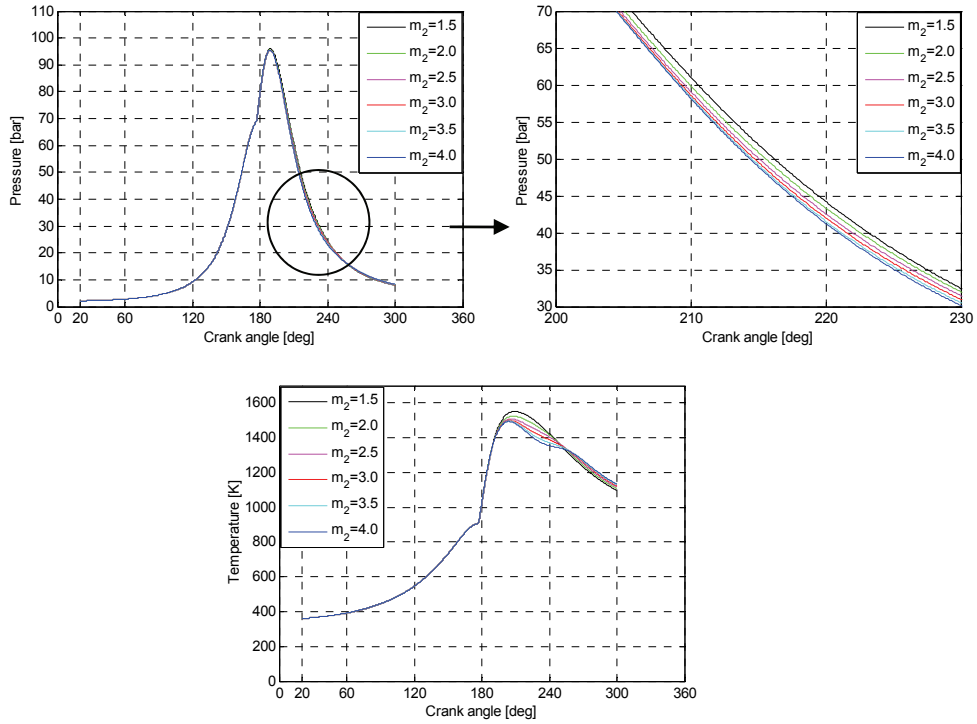


Figure 2.22 Parameter m_2

c). Parameter b_1

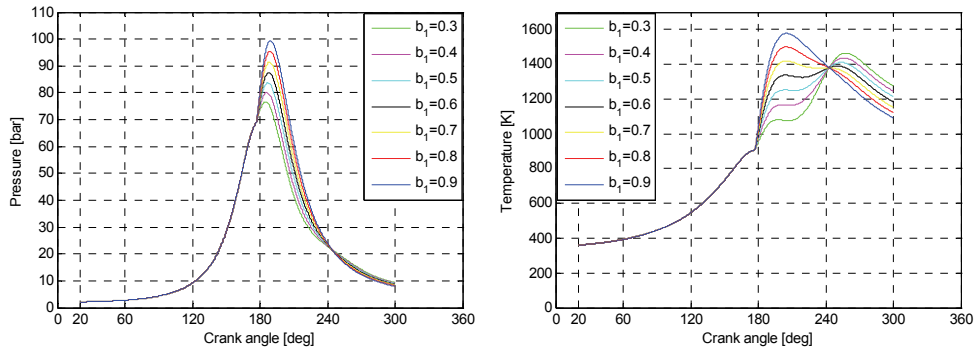


Figure 2.23 Parameter b_1

The parameters b_1 and b_2 ($b_2 = 1 - b_1$) specify the proportion of the premix and diffusive combustion stages as a fraction of the entire combustion. A crossing point emerges in the pressure and temperature (Figure 2.23), as a greater b_1 gives more heat

release in the premix combustion and less heat release in the diffusive combustion, and vice versa. This crossing point is also visible in Figure 2.3 (c).

d). Parameter a

Parameter a (in fact combustion efficiency η_{comb}) is influenced by many factors, e.g. the combustion chamber shape or the amount of intake air. As shown in Figure 2.24, the peak pressure and temperature increase with a (η_{comb}) whereas the temperature at exhaust open (EO) is higher for smaller a (η_{comb}) due to incomplete combustion. The maximum temperature also shifts to a later crank angle because a (η_{comb}) changes the shape of combustion rate and for lower values more fuel is burnt at later crank angles.

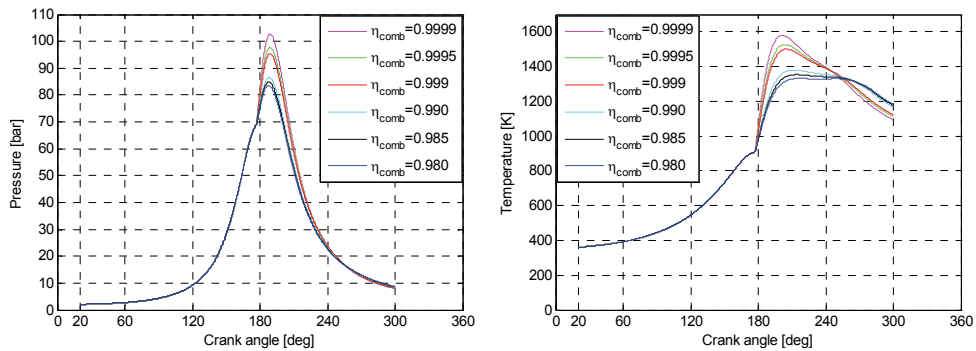


Figure 2.24 Parameter a (η_{comb})

e). Parameter SOC

SOC is defined as the start of injection including the ignition delay. The pressure and temperature figures are zoomed in separately in Figure 2.25. With earlier SOC the maximum pressure occurs earlier and the peak value is increasing, after which the pressure traces converge rapidly. The temperature behaves in the same way as the pressure around the peak value, but at around 220° the temperature trend changes inversely.

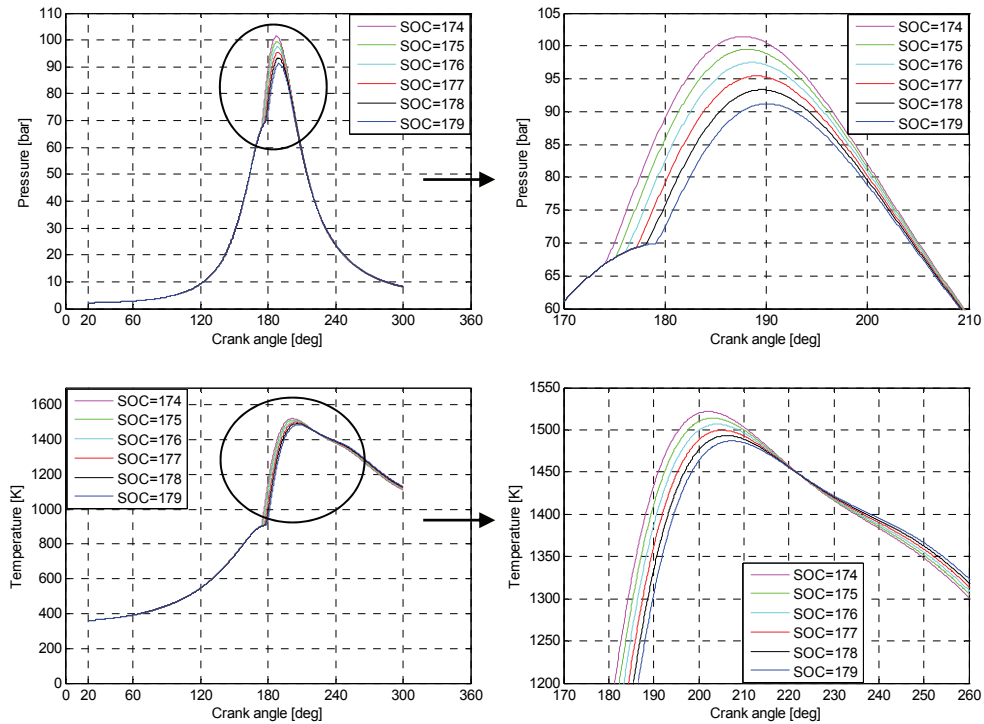


Figure 2.25 Parameter SOC

f). Parameter EOC

Since the difference between *SOC* and *EOC* indicates the duration of combustion, a smaller *EOC* value means shortening the combustion. From Figure 2.26, shortening the duration of combustion will result in an earlier and more pronounced increase in the peak pressure and temperature. Consequently, the parameters *EOC* and m_l have the strongest impact on maximum pressure. However, at point EO, the pressure and temperature are lower for a shorter combustion because the combustion terminates earlier. The selection of *EOC* should consider the engine type, and normally newer engine types (with common rail or other advanced injection technology) should have a shorter combustion time than older engines (such as the MAN engine used in this thesis). However, for extreme late Start of Injection as can be required to lower NO_x emissions, even modern engines could have (very) late combustion.

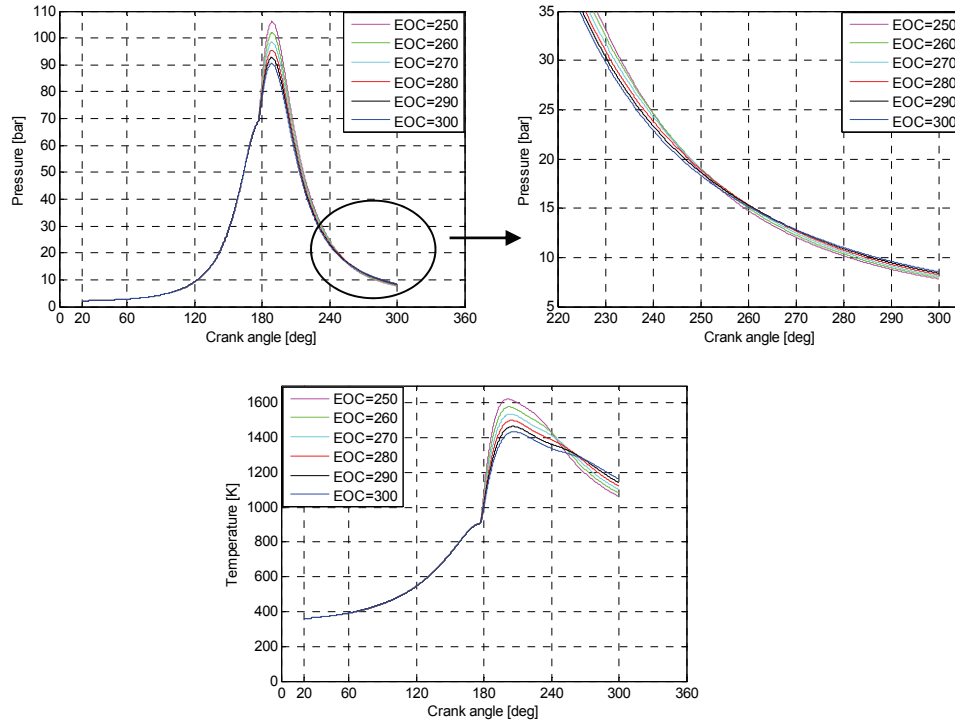


Figure 2.26 Parameter *EOC*

g). Parameter m_{fr}

The total mass of fuel burnt during combustion ($m_{f,0}$ in equation [2.16]) plays an important role in determining the heat release, but it is an extensive rather than an intensive parameter. In Figure 2.27, the m_{fr} is the ratio between fuel burnt in the simulation case and the nominal value. Since more fuel burnt under the same combustion shape produces more heat release, the pressure and temperature after *SOC* increase with larger m_{fr} value.

There are two ways to determine the total fuel burnt during combustion $m_{f,0}$. One way is to measure the fuel consumption per cycle at the engine test bed. The other way is to calculate it according to equation [2.34]. Air excess ratio (λ) can be estimated based on experience and the stoichiometric air-fuel ratio (σ) is known when the fuel type is given.

$$m_{f,0} = \frac{m_1 \cdot x_1}{\lambda \cdot \sigma} \quad [2.34]$$

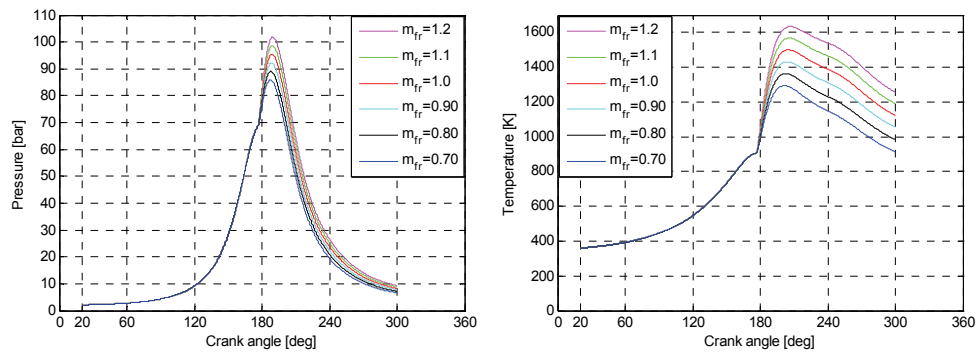


Figure 2.27 Parameter m_{fr}

2.2.5 Discussions

The in-cylinder process model gives the closed cycle simulation of a diesel engine, resulting in pressure, temperature, power, heat release as the most important outputs. Since the gas exchange is not included in the model it does not give an integral simulation of the full diesel engine cycle.

The single Vibe, double Vibe or the multiple Vibe models can be used to estimate the heat release rate in a diesel engine. They only give the approximate solution, but especially in the first analysis stages, the Vibe model provides a concise and convenient way to determine the heat release. However, in practice knowledge must be available how the parameters in the Vibe formula should be selected at part load operating conditions of engine.

2.3 Heat release calculation model

2.3.1 Introduction

Heat release rate (HRR) analysis in a diesel engine provides an efficient way to acquire combustion information. The HRR is defined as the rate at which the chemical energy of the fuel is released by the combustion process [Heywood, 1988].

Knowing the heat release, the in-cylinder process can be simulated on the basis of thermodynamic knowledge. As explained in the previous section, in such a model the temperature and pressure in the cylinder can be calculated based on the first law of thermodynamics and the gas law [Ding, 2009]. In contrast, if the in-cylinder pressure is measured from the engine test bed, an anti-causal simulation model – being the reverse of the ‘in-cylinder process model’ – can be used to reconstruct the temperature and the heat release rate [Ding, 2011b].

The main purpose of this section is to present the method to calculate the heat release rate during combustion in a diesel engine using this inverse in-cylinder process model based on measurement of three operating points and discuss the MATLAB/SIMULINK simulation results. All refinements that were taken into account in the process simulation are automatically incorporated in the inverse simulation including variation of the lower combustion value with temperature and the energy of the fuel entering the system.

2.3.2 Structure of the simulation model

Heat release rate can be defined in many different ways. The three main definitions used in this research are:

(a) Net Apparent Heat Release Rate (*NAHRR*):

$$NAHRR = \dot{Q}_{comb} - \dot{Q}_{loss} + \dot{E}_f = m \cdot c_v \cdot \frac{dT}{dt} + p \cdot \frac{dV}{dt} \quad [\text{J/s}] \quad [2.35]$$

(b) Gross Apparent Heat Release Rate (*GAHRR*):

$$GAHRR = \dot{Q}_{comb} + \dot{E}_f = m \cdot c_v \cdot \frac{dT}{dt} + p \cdot \frac{dV}{dt} + \dot{Q}_{loss} \quad [\text{J/s}] \quad [2.36]$$

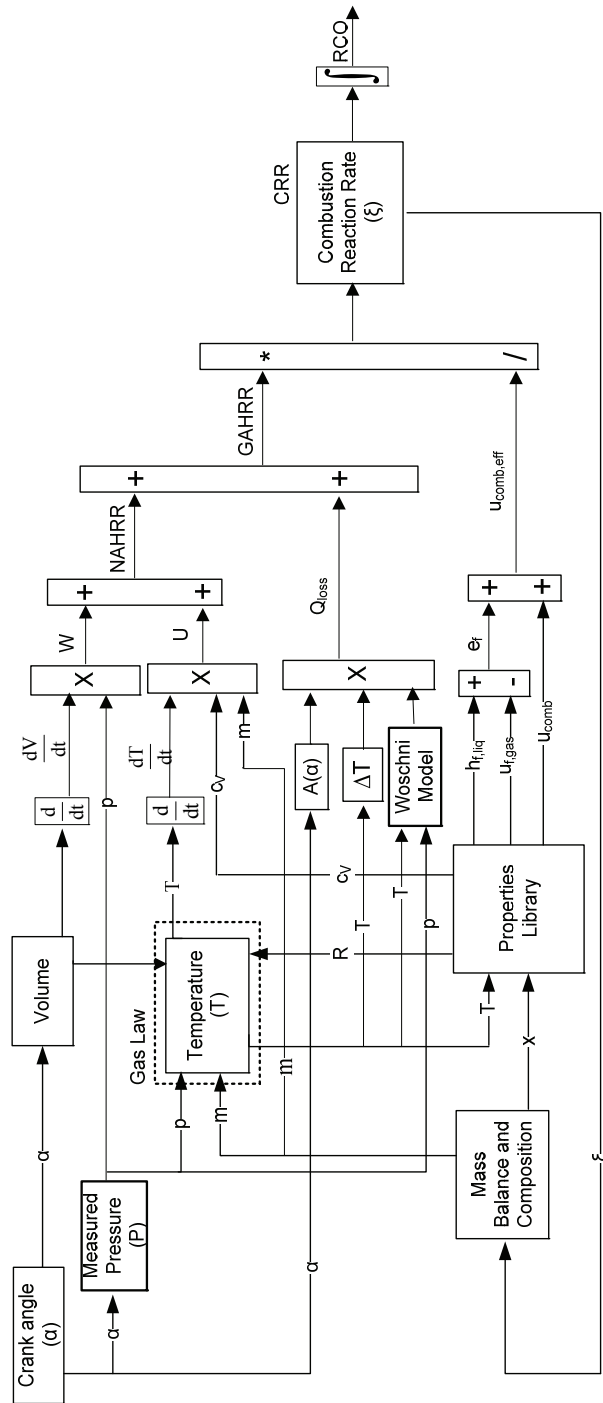


Figure 2.28 General block diagram of 'heat release calculation model'

(c) Combustion Reaction Rate (*CRR*):

$$CRR = \xi = \frac{m \cdot c_v \cdot \frac{dT}{dt} + p \cdot \frac{dV}{dt} + \dot{Q}_{loss}}{u_{comb} + e_f} \quad [\text{kg/s}] \quad [2.37]$$

NAHRR can directly be calculated from the pressure and temperature in the cylinder. *GAHRR* includes heat loss to the walls and indicates the heat produced by combustion correctly, but it is not possible to calculate it directly from measurements. Therefore the accuracy of *GAHRR* relies on the appropriate estimation model of the heat loss.

For the *CRR* the effective combustion value ($u_{eff} + e_f$) must be known including its dependency on temperature. Also the effect of ‘energy of fuel’ is included, for which it is assumed that the injection rate is equal to the evaporation rate of the fuel entering the system, the latter being assumed equal to the combustion rate.

Figure 2.28 illustrates the structure of the ‘heat release calculation model’, which shares many elements with the ‘in-cylinder process model’ but reverses the in- and output. The prime input of the model is the pressure and volume (in fact the crank angle) while the ultimate output is one of the definitions of heat release – Combustion Reaction Rate (*CRR*). Since *CRR* is calculated based on measured pressure it is heavily fluctuating, where the Reaction coordinate (*RCO*) – being the integral of the *CRR* – is a monotonous increasing function, suitable for analysis and curve fitting as most of the fluctuation are smoothed in the integration process. The submodels and elements of the ‘heat release calculation model’ have already been discussed in section 2.2.2.

2.3.3 Result and analysis

The results shown in this section are for three operating points measurements of cylinder 1 in the MAN 20/27 diesel engine (The general data of this engine have been shown in Table 2.2):

- (A) the nominal point: 1000 rpm, 100% power;
- (B) a point on the generator curve: 1000 rpm, 25% power;
- (C) a point on the propeller curve: 800 rpm, 50% power.

A specification and description of the major sensors in the test bed and the measured parameters are presented in Appendix VIII.

The fuel type used during the tests was ‘F76’ (a NATO standard DMA type of fuel). Since no sample of the fuel was sent to a laboratory, default property values based on previous tests were used for the simulations and heat release calculations. The properties of this fuel are listed in Table 2.5.

Table 2.5 Properties of ‘F76’ diesel fuel

Property	Value	Unit
Carbon mass fraction	0.865	[--]
Hydrogen mass fraction	0.133	[--]
Sulphur mass fraction	0.002	[--]
Density at 15°C	843	kg/m ³

The results can be compared with the results in section 2.2.3, which are based on a double Vibe heat release model. All the figures have a corresponding figure in section 2.2.3 (only the nominal point was calculated there). The comparison will show the feasibility and reliability of the simulation models.

1) State parameters

First, the four gas state parameters are shown in Figure 2.29 – Figure 2.32. The pressure signals in Figure 2.29 are derived from the measurement directly and the temperatures in Figure 2.30 are calculated on the basis of the ‘gas law’. At first sight it seems that the fluctuations in temperature are much fiercer than in pressure. Closer inspection reveals that the fluctuations relative to the instantaneous value are identical for pressure and temperature as expected from the gas law. The effect is a graphical effect since the order of magnitude of the temperatures is much larger relative to the

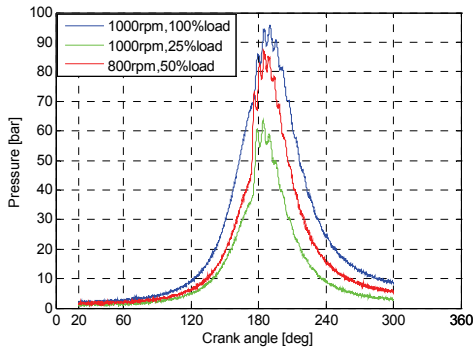


Figure 2.29 In-cylinder pressure

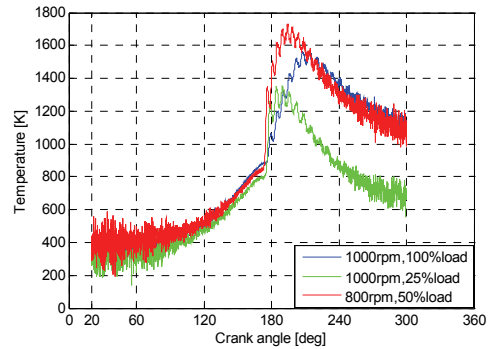


Figure 2.30 In-cylinder temperature

maximum (i.e. 400 K versus 1300 K) than for the pressures (i.e. 1 bar versus 90 bar). The differences between the three operating conditions are clearly revealed in these two figures. When calculating volume, the engine speed is assumed constant during one revolution. Then the cylinder volume is only a function of crank angle and the cylinder volumes plots shown in Figure 2.31 of the three cases are identical.

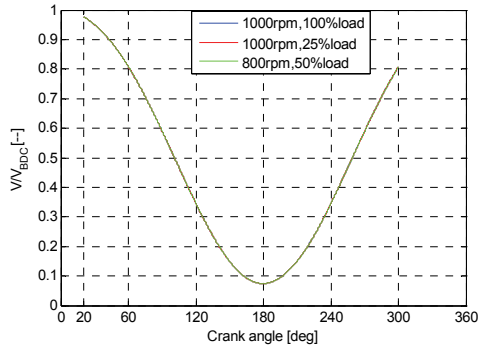


Figure 2.31 In-cylinder volume

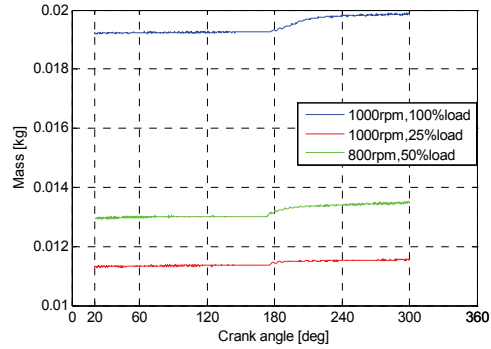


Figure 2.32 In-cylinder mass

2) Heat release analysis

When the reaction coordinate (RCO) is calculated (Figure 2.33 shows the normalized reaction coordinate, which means the ‘fuel burnt percentage’), the values at the beginning of the curves are larger than zero (discarding the measurement fluctuation) and near the end of the curves the values are much higher than unity (the part load lines – green and red – even go over 1.2). This last phenomenon would suggest there is more fuel burned than injected in the cylinder, and that more heat is produced than in the actual case. These effects could only partly be explained by a wrong choice of TDC shift (as presented in the next section). Another and better explanation is that the main cause is the start value of the RCO and, as this is the integral of CRR , the RCO is very sensitive to the start value. Therefore as a correction it was decided to give the RCO a vertical shift (Figure 2.34).

The jump in the RCO curve indicates the start of combustion and just before this jump, there is a short descending slope period, representing the slightly negative heat release due to fuel evaporation (Figure 2.35). The start of combustion (SOC) is defined in this thesis at the point where RCO starts to increase again, just before TDC. Therefore the RCO just before descending should be 0 to reveal that there is no fuel burnt at that time.

In the model, the correction in RCO is based on the fact that between 160 degree and 170 degree should be zero.

Although after shifting the RCO , the RCO after SOC is reasonable and can be used for curve fitting in the next section, the RCO before SOC – in particular at the beginning of the in-cylinder process – is negative, resulting in an endothermic process at the beginning of the cycle, giving unrealistic values. This could be caused by the heat loss estimated with the Woschni model as well as by the start value of RCO .

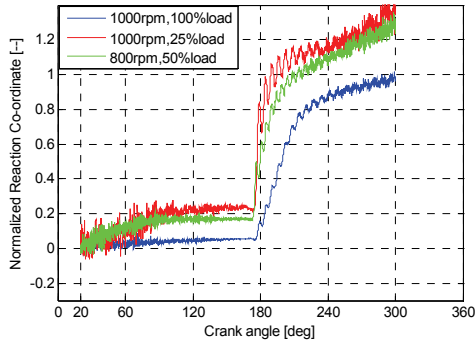


Figure 2.33 Reaction coordinate (original)

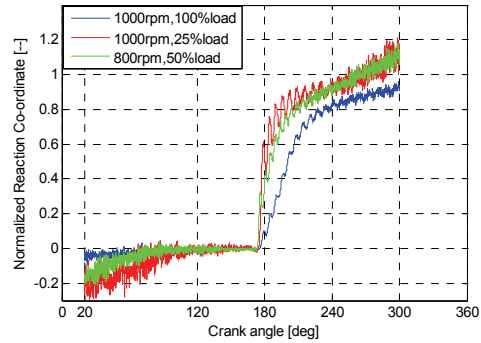


Figure 2.34 Reaction coordinate (corrected)

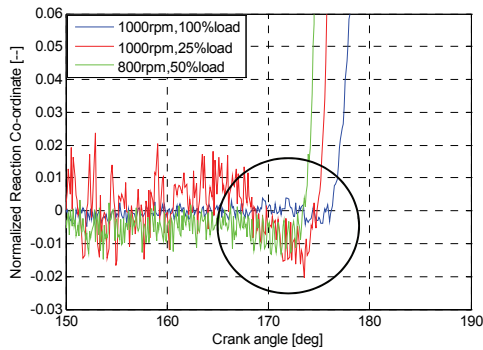


Figure 2.35 Zoom in reaction coordinate (corrected)

3) Top Dead Centre (TDC) shift effect on the heat release

In the in-cylinder pressure measurement, the accuracy of the TDC determination greatly affects the heat release calculation. In order to investigate the effect of a TDC

shift, the ‘in-cylinder process simulation model’ is used to produce an in-cylinder pressure signal, which is then used in the ‘heat release calculation model’ to (re) calculate the heat release, but the TDC is shifted with 0, +0.3, +0.5 and +1.0 degrees respectively.

Figure 2.36 – Figure 2.38 show the *RCO* for different TDC shifts. When shifting the TDC, the *RCO* attains values less than unity as shown in Figure 2.36. The second effect is during the compression (Figure 2.37). There is some heat input during compression when the TDC is shifted and again a larger TDC shift results in a more pronounced effect. The third effect is on the *SOC* according to the definition of the previous section (Figure 2.38). The combustion starts earlier when shifting the TDC and the dip in *RCO* just before *SOC* becomes more pronounced.

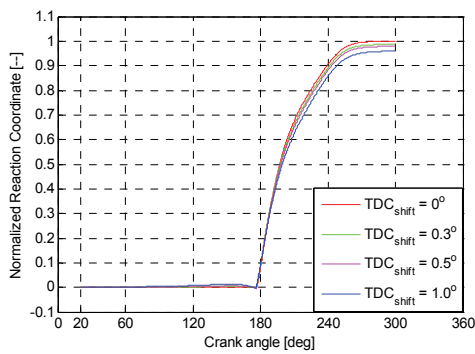


Figure 2.36 RCO with shifting TDC

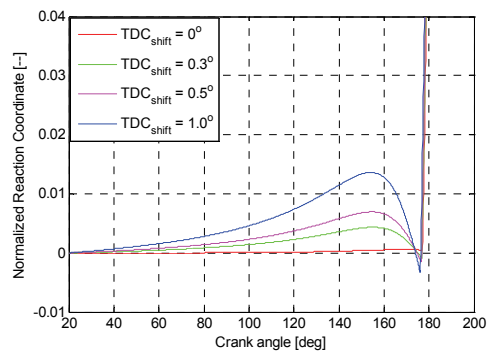


Figure 2.37 RCO with shifting TDC
(zoom in 1)

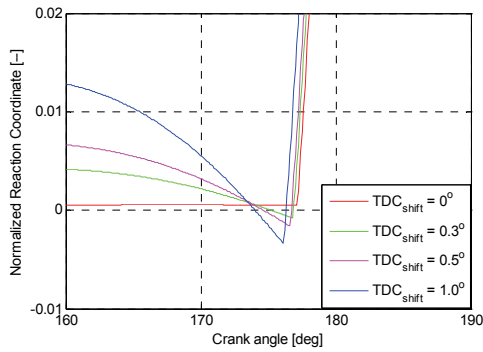


Figure 2.38 RCO with shifting TDC
(zoom in 2)

The deviation of the RCO reaching unity is however much larger than can be explained by a wrong TDC shift (see Figure 2.33 and Figure 2.34). Therefore the first effect will finally be corrected by changing the constant in Woschni's heat loss model, see a next section 2.3.3 5). The second effect was already largely corrected by the vertical shift of RCO .

The determination of TDC takes some effort and disturbs the engine measurement and therefore is not carried out before every measurement. The accuracy of the TDC is limited to a relative small range (normally it is unlikely to make 1 degree error in shifting TDC). Therefore it was decided to apply a constant TDC shift of 0.7 degree for all measurements.

4) Gas property parameters

Figure 2.39 illustrates the fresh air fraction in the cylinder. After revising the reaction coordinate, before SOC it remains constant and does not fluctuate too much ($x_I = 0.95$). From the point SOC it (obviously) decreases. When the engine is running at low load, the fresh air fraction decreases less and ends at a higher value (about 0.7). Figure 2.40 shows the e_f in equation [2.7]. This figure is consistent with Figure 2.14 in section 2.2.4.

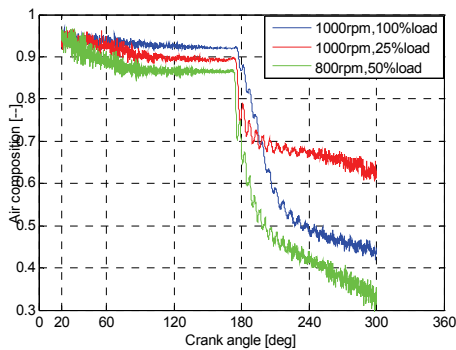


Figure 2.39 In-cylinder air fraction

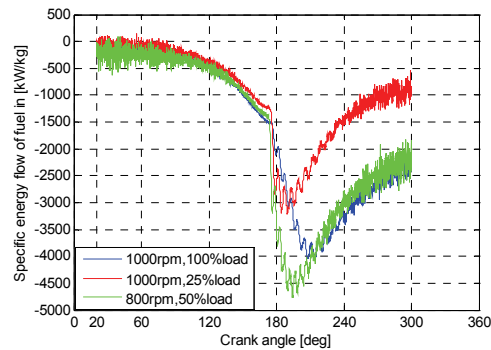
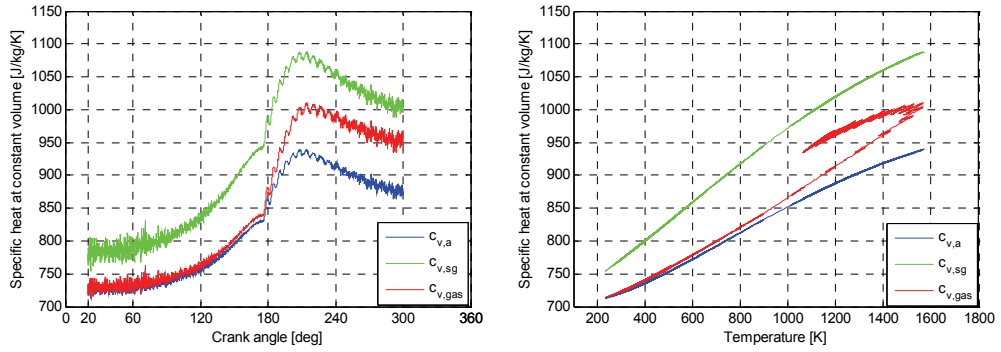


Figure 2.40 Specific energy of fuel

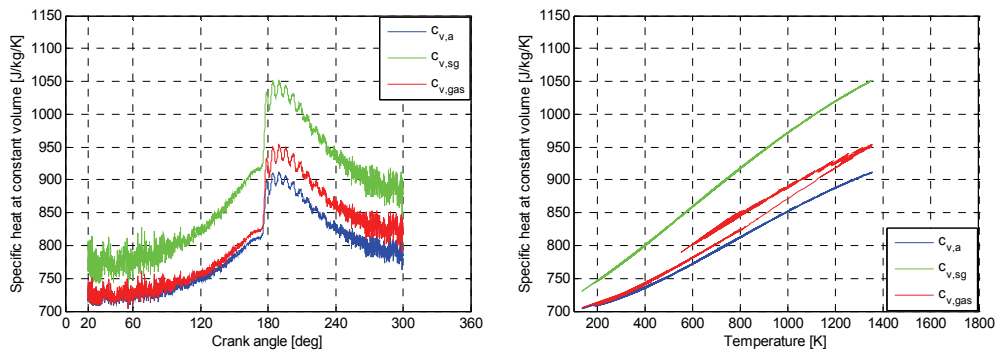
The c_v is illustrated in Figure 2.41 – Figure 2.43 for the three operating points. The c_v of air, stoichiometric gas and in-cylinder gas are displayed.



(a) versus crank angle

(b) versus temperature

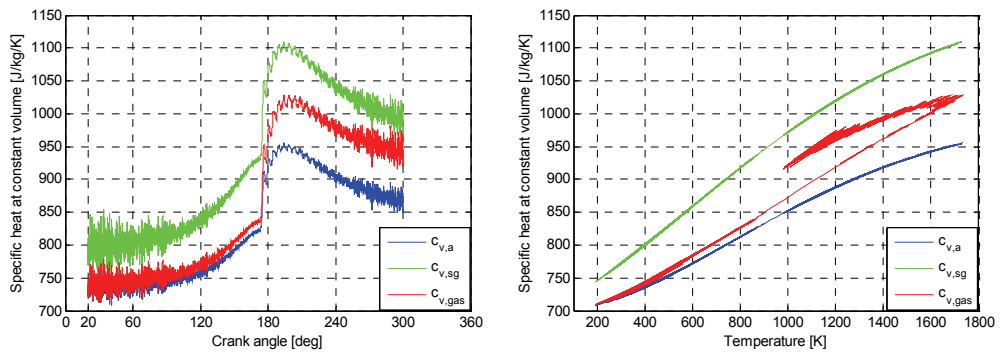
Figure 2.41 Specific heat at constant volume (c_v , 1000 rpm, 100% power)



(a) versus crank angle

(b) versus temperature

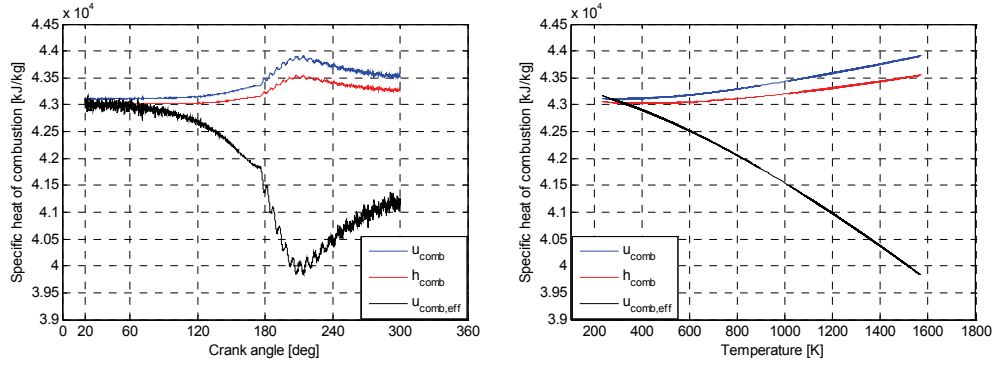
Figure 2.42 Specific heat at constant volume (c_v , 1000 rpm, 25% power)



(a) versus crank angle

(b) versus temperature

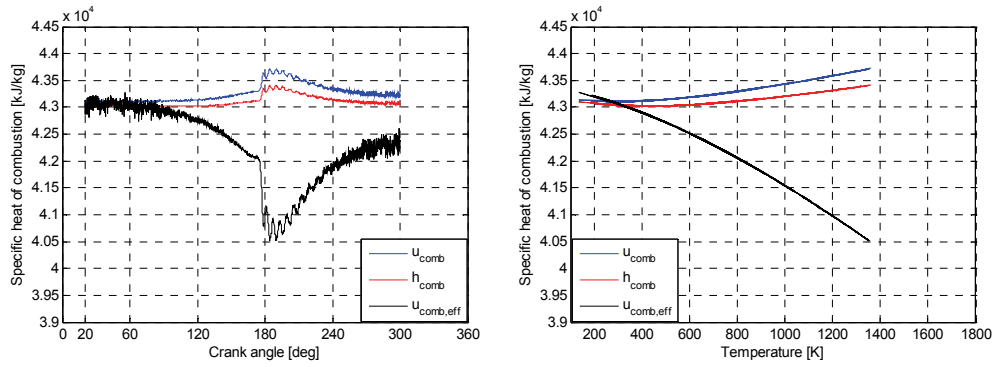
Figure 2.43 Specific heat at constant volume (c_v , 800 rpm, 50% power)



(a) versus crank angle

(b) versus temperature

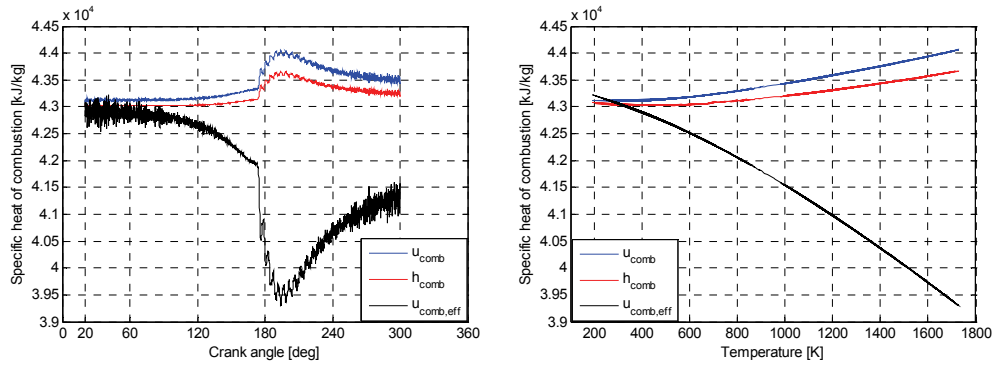
Figure 2.44 Heat of combustion (u_{comb} , 1000 rpm, 100% power)



(a) versus crank angle

(b) versus temperature

Figure 2.45 Heat of combustion (u_{comb} , 1000 rpm, 25% power)



(a) versus crank angle

(b) versus temperature

Figure 2.46 Heat of combustion (u_{comb} , 800 rpm, 50% power)

Figure 2.44 – Figure 2.46 show the ‘heat of combustion’ derived from equation [2.6]. As stated before, due to the closed system of in-cylinder process the internal energy should be used to calculate the ‘heat of combustion’ (u_{comb}). The ‘heat of combustion’ derived from enthalpy (h_{comb}) is also displayed in the figures, which is smaller than u_{comb} . Again the black curves in these three figures indicate the ‘effective heat of combustion’, which include e_f as part of heat loss for evaporation and heating the fuel before combustion.

5) Heat loss to the walls

Figure 2.47 shows the heat transfer coefficient versus crank angle, as calculated with Woschni’s model (equation [2.9]). The instantaneous heat loss flow is illustrated in Figure 2.48, in which the temperature of cylinder wall, piston crown and cylinder head are assumed the same as presented in section 2.2.4 4). There is some heat input (negative heat loss flow) at the beginning of compression, during the rest of the cycle the heat loss flow is positive. In part load, the heat loss during compression is close to zero, which means it is more or less an adiabatic process.

Theoretically, the normalized reaction coordinate should reach unity for complete combustion. However, this is not a fixed value but the result of a rather complex calculation and often is not reached. Other authors report the same phenomenon (i.e. that the normalized reaction co-ordinate did not arrive at unity ([He, 1990], [Hua, 1984] and [Lapuerta, 2000])). Figure 2.52 shows the percentage of the components of heat release (equal to the normalized reaction coordinate) for a turbocharged DI diesel engine in mid-load and mid-speed range from [Heywood, 1988]. The heat loss to the wall amounted to approximately 20% - 30% of total heat release (note that crevices heat loss is not considered in this model). As mentioned previously, the heat loss is derived from the empirical Woschni equations, resulting in uncertainty when calculating the reaction coordinate. Overrating or underrating the heat loss to the walls could lead to a final normalized reaction coordinate being above or below unity. C_l in equation [2.9] is directly proportional to the heat transfer coefficient. Therefore C_l is considered a varying parameter that can be used to bring the RCO to unity at different operating points. In Figure 2.47 and Figure 2.48, the C_l used is the original value of 130 (uncorrected) for all these three operating points. In the other case (corrected), C_l is set to 230, 70 and 20 for 1000 rpm at 100% power, 1000 rpm at 25% power and 800 rpm at 50% power respectively (Figure 2.49 – Figure 2.51). The latter will also be used

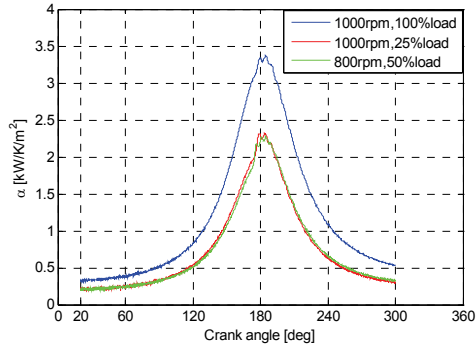


Figure 2.47 Heat transfer coefficient (uncorrected)

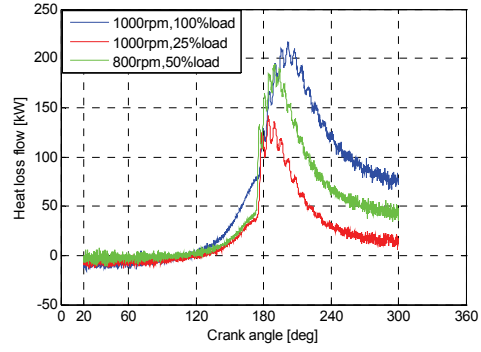


Figure 2.48 Instantaneous heat loss flow (uncorrected)

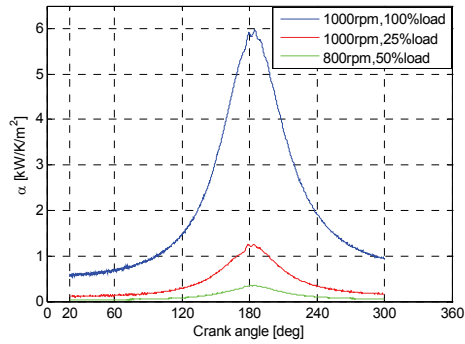


Figure 2.49 Heat transfer coefficient (corrected)

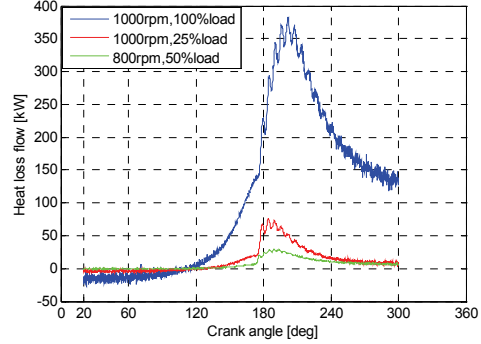


Figure 2.50 Instantaneous heat loss flow (corrected)

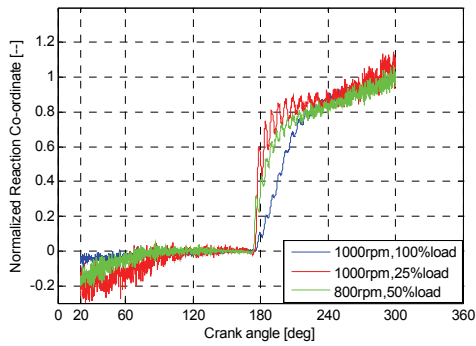


Figure 2.51 Reaction coordinate (shift) (corrected)

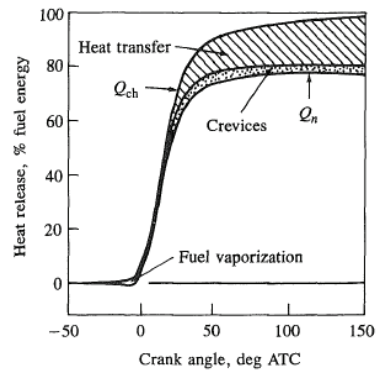


Figure 2.52 Heat release profile [Heywood, 1988]

in the simulation model when it is used for smoothing in a next section (i.e. the RCO arrives at unity at EOC).

6) *Engine performance*

Figure 2.53 shows the instantaneous indicated power. The figures of heat combustion flow, heat input flow and combustion reaction rate corresponding to Figure 2.5 – Figure 2.7 are not shown here since, due to the heavy fluctuation in the measured signal, it is hard to discern useful information.

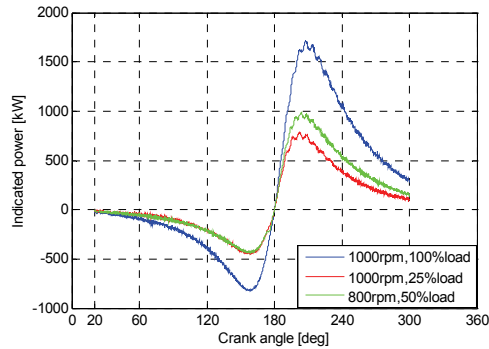


Figure 2.53 Instantaneous indicated power

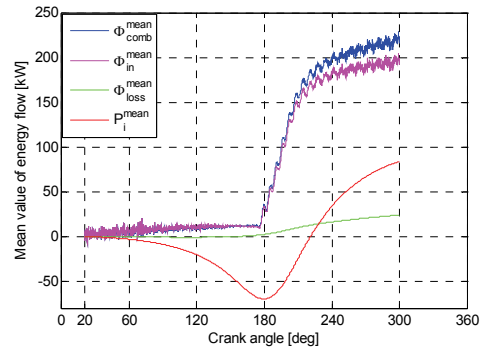


Figure 2.54 Summary of mean value of energy flow (1000 rpm, 100% power)

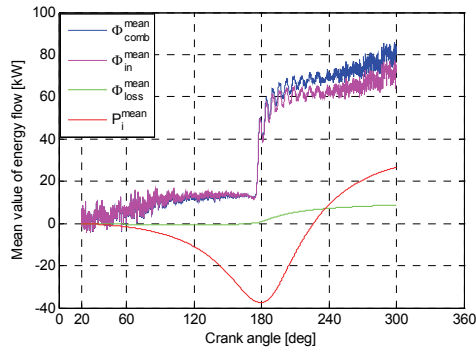


Figure 2.55 Summary of mean value of energy flow (1000 rpm, 25% power)

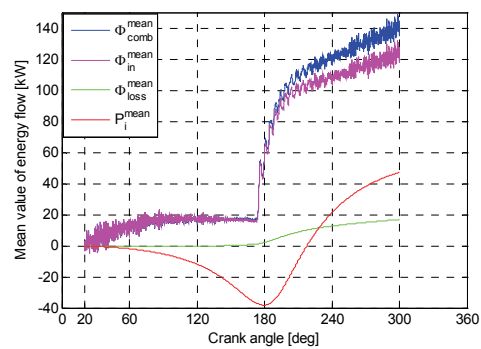


Figure 2.56 Summary of mean value of energy flow (800 rpm, 50% power)

Figure 2.54 – Figure 2.56 show the mean values of the indicated power, heat combustion flow, heat input flow and heat loss flow, which are calculated based on equation [2.30] – [2.33]. The end value of each one is the mean value of the overall

in-cylinder cycle (from IC to EO). Table 2.6 summarises the energy flow per cycle and the engine efficiencies of the three operating points. It is noted here again that η_{comb} is assumed to be unity so $\Phi_{comb} = \Phi_f$.

Table 2.6 Summary of energy flow and engine efficiency per cycle

Operating point	Φ_{comb} [kW]	Φ_i [kW]	Φ_{loss} [kW]	P_i [kW]	η_i [--]	η_{hl} [--]	η_{td} [--]
1000 rpm, 100% power	228.32	185.70	42.62	82.85	0.41	0.88	0.46
1000 rpm, 25% power	68.32	62.73	5.59	26.92	0.39	0.92	0.43
800 rpm, 50% power	111.68	109.08	7.85	49.49	0.44	0.98	0.46

2.3.4 Discussions

This heat release model as presented is an anti-causal simulation model that is derived from an in-cylinder process model and is used to reconstruct the *CRR*. Since there are integral and differential equations during simulation, it is important to choose a suitable numerical solution (a solver named ‘ode45’ in MATLAB/SIMULINK, which is based on an explicit Runge-Kutta (4,5) formula, the Dormand-Prince pair for non-stiff problem with medium accuracy, is used in this thesis) for ordinary differential equations to get a reliable outcome.

There are some uncertainties in the simulation model such as heat loss to the walls, the effect of measurement errors in TDC. The way to tackle these effects was discussed and practical solutions were found.

2.4 Smoothing of the in-cylinder pressure signals

2.4.1 Introduction

The pressure signal in the cylinder, as measured from engine test facilities, is very erratic due to the inherent character of the combustion process and in particular the location of the pressure transducer. If and how the pressure signal is smoothed will affect the subsequent heat release analysis. Mathematic algorithms can be used to smooth the pressure signals, such as a parabola curve fitting to determine the peak pressure or averaging a few points to one point in the trace. However, because these algorithms do not physically interpret the data, they introduce the risk of loss of information from the measurement. In this thesis, a new method will be presented using not only mathematic calculation but also thermodynamic knowledge as presented in [Ding, 2011]. The latter paper was taking up the idea of a multiple Vibe function as introduced in an earlier paper [Knobbe, 2001], extending the concept of a double Vibe function. As discussed in the previous sections a thermodynamic heat release model is used to calculate the combustion reaction coordinate based on the measured pressure, which will now be used for fitting a multiple Vibe function. These Vibe parameters are the input to a single zone cylinder process model to obtain a smooth pressure and temperature trace that potentially has a better quality than mathematically (up-front) smoothed signals.

The procedure of smoothing is:

- Separate the closed cycle pressure signal (between IC and EO) from the overall pressure trace.
- Take the average of 15 to 25 cycles (but refrain from smoothing at this stage).
- Apply a thermodynamic heat release analysis on the raw but averaged data to calculate the reaction coordinate. Since the reaction coordinate entails an integration of the signal this has already a smoothing effect. Also the reaction coordinate is monotonously increasing.
- Fit the reaction coordinate with a multiple Vibe model by curve fitting techniques, i.e. smooth the reaction rate.
- Calculate the pressure and temperature in the cylinder by simulating the cylinder process with the same thermodynamic elements as the heat release calculation and

with the fitted and smoothed combustion rate as input.

2.4.2 Averaging and direct mathematical smoothing of pressure trace

The pressure signal as measured in the cylinder is oscillating and varying from cycle to cycle. The oscillation of the pressure in the cylinder is partly caused by the combustion process. The fast combustion causes in-cylinder gas velocities and pressure fluctuations. Since combustion is stochastic these fluctuations will be random and can be smoothed by taking the mean of a number of cycles. Another important cause of fluctuations is the fact that the pressure transducer is installed in a channel to the cylinder, where reverberations spoil the pressure signal. These oscillations will not disappear after averaging over a number of cycles and must be smoothed in a different way.

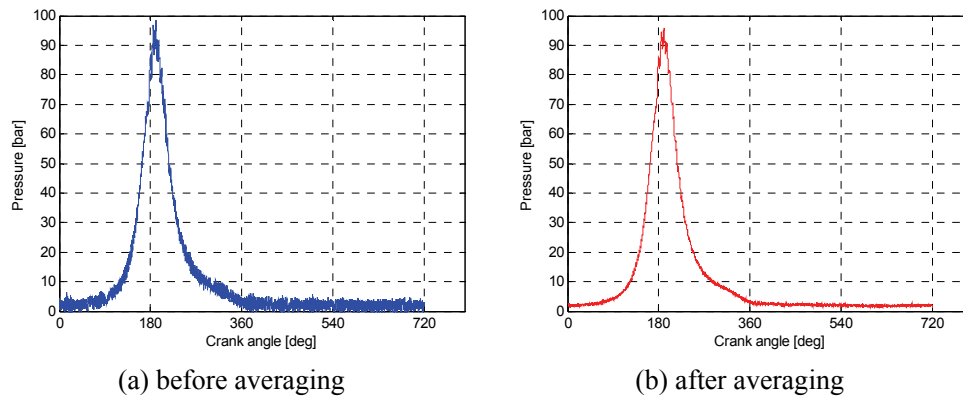


Figure 2.57 Averaging of the measured pressure signal

Figure 2.57 shows a comparison of the cylinder pressure signals before and after averaging (over 25 cycles for the engine running in the nominal point). It is obvious that the pressure signal after averaging is smoother than before averaging, but the oscillations due to the channel effect persist.

2.4.3 Indirect fitting of pressure signal based on multiple Vibe function

The normalized reaction coordinate X , which is the CRR integrated over time, is very

suitable for curve fitting since it is (contrary to the original pressure signal) a monotonous increasing function:

$$CRR = \xi = \frac{m \cdot c_v \cdot \frac{dT}{dt} + p \cdot \frac{dV}{dt} + \dot{Q}_{loss}}{u_{comb} + e_f} \quad \text{ref [2.37]}$$

$$X = \frac{RCO}{m_{f,0}} = \int_{SOC}^{EOC} \frac{\xi}{m_{f,0}} \cdot dt \quad [2.38]$$

The multiple Vibe function is expressed as:

$$X = \sum_{k=1}^n b_k \cdot X_k = \sum_{k=1}^n b_k \cdot \left(1 - e^{-a \cdot \tau^{m_k+1}}\right) \quad \text{ref [2.24]}$$

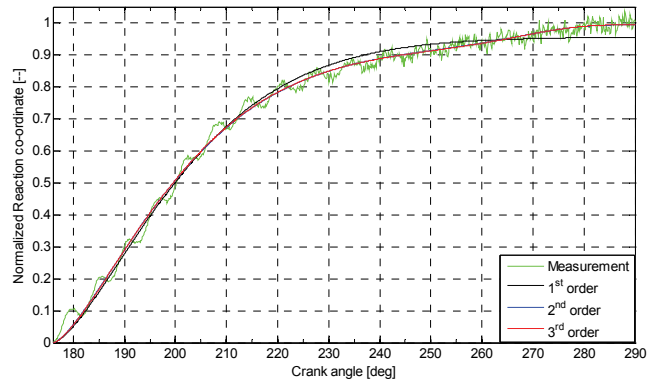
It is mentioned here again that each single Vibe function has its own form factor m_k and weight factor b_k but they share the same a and the same duration of combustion.

Combining equation [2.24] and equation [2.38] and assuming $m_{f,0}$ is known, X can be fitted with for instance a double Vibe function (but higher orders are investigated too). Since the reaction coordinate is a monotonous function this is expected to be more accurate than direct smoothing of the pressure trace.

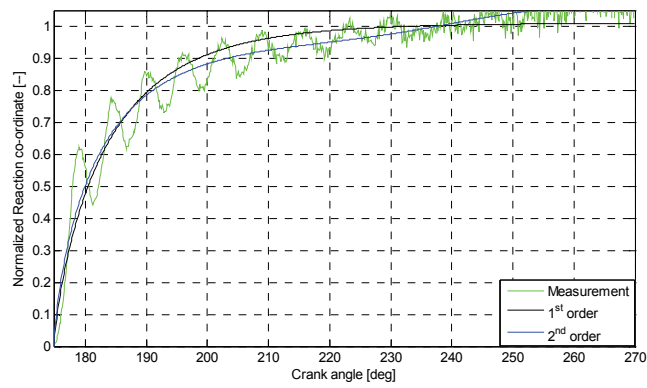
1) Use curve fitting techniques to obtain smoothed heat release

A fit is obtained using nonlinear least square fitting method, after setting fit options and fitting function (equation [2.24]), using the Curve Fitting Toolbox in MATLAB [MATLAB, 2009]. The theory of the method can be found in Appendix III. In the fitting process the abscissa ‘time’ and the ordinate ‘reaction coordinate’ are used in their non-dimensional form, which makes the procedure less complex and more efficient. Fitting of higher order Vibe functions is numerically sensitive to the start values of the parameters. Therefore the first order solution was used as start value for the second order and so forth.

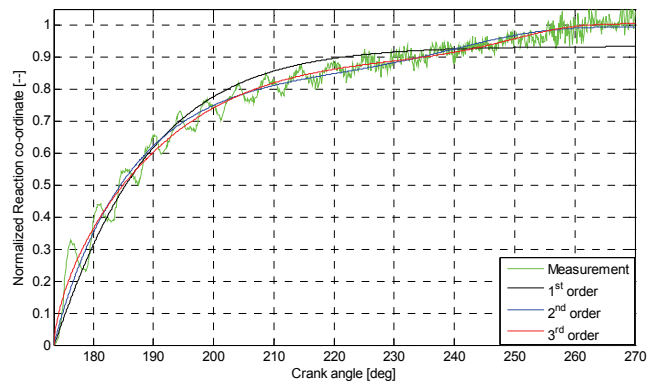
Pressure measurements of the three operating points used in the previous section are analysed as a proof of principle of the proposed smoothing method. As the MAN engine used is an older engine with direct injection using plunger pumps and relatively low injection pressure, it is to be expected that late combustion will occur in all three operating points.



(a) Operating point (A)



(b) Operating point (B)



(c) Operating point (c)

Figure 2.58 Fitting the reaction coordinate with multiple Vibe function

Figure 2.58 shows the fit results for the normalized reaction coordinate with different order of Vibe functions for the three operating points and Table 2.7 summarizes the fit parameters of these Vibe functions. Operating points (A) and (C) use third order Vibe functions as the highest order for fitting and operating point (B) uses second order, which depends on the freedom of sign of m in the first order Vibe function. This will be explained in details in next section.

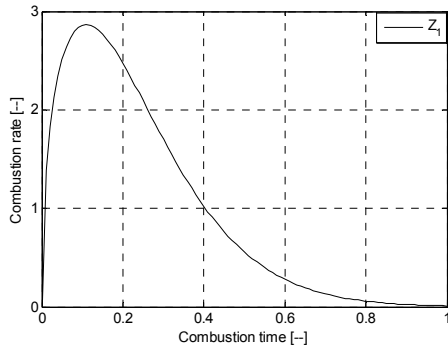
Other important parameters are SOC and EOC , which determine the interval over which ROC is smoothed. Determination of SOC has been explained in section 2.3.3, but EOC remains difficult to decide. In [He, 1988] some methods are presented to determine EOC but most of them are based on an experimental approach. In this research, EOC is estimated according to experience, and based on the fact that this is an older engine with presumably relatively late combustion. For operating point (A) it is set to 290 degree (just 10 degree before EO) and for operating point (B) and (C) it is set to 270 degree since combustion is ending faster at very low load.

Table 2.7 Vibe parameters for fit functions

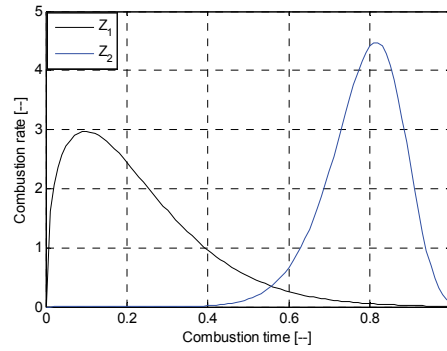
Operating point	Vibe Function	1		2		3	
		b_1	m_1	b_2	M	b_3	m_3
(A)	First order	0.956	0.423				
	Second order	0.928	0.383	0.067	8.981		
	Third order	0.957	0.398	0.069	8.974	-0.030	1.038
(B)	First order	1.01	-0.182				
	Second order	0.962	-0.234	0.100	4.899		
(C)	First order	0.934	0.051				
	Second order	0.867	-0.039	0.129	5.099		
	Third order	0.425	-0.303	0.104	7.981	0.477	0.317

Figure 2.59 shows contribution of each Vibe fitting function to the normalized combustion rate for the nominal operating point. The single Vibe function only gives premix combustion (Figure 2.59(a)) and a double Vibe function adds a late combustion component (Figure 2.59(b)). In the third order Vibe function (Figure 2.59(c)), there is one Vibe function for premix combustion ($m_1 = 0.398$) and one for late combustion ($m_2 = 8.974$). The third Vibe function is a diffusive combustion ($m_3 = 1.038$). It can be concluded here that for the nominal point, it is wise to use three orders Vibe functions

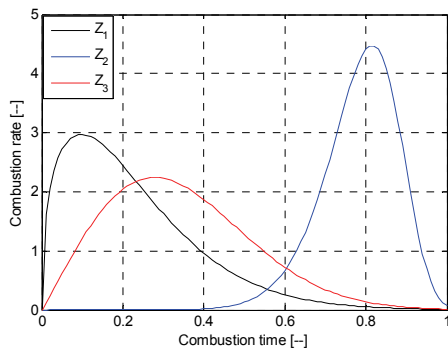
in order to capture both diffusive and late combustion (if late combustion is important for a specific engine).



(a) Single Vibe function



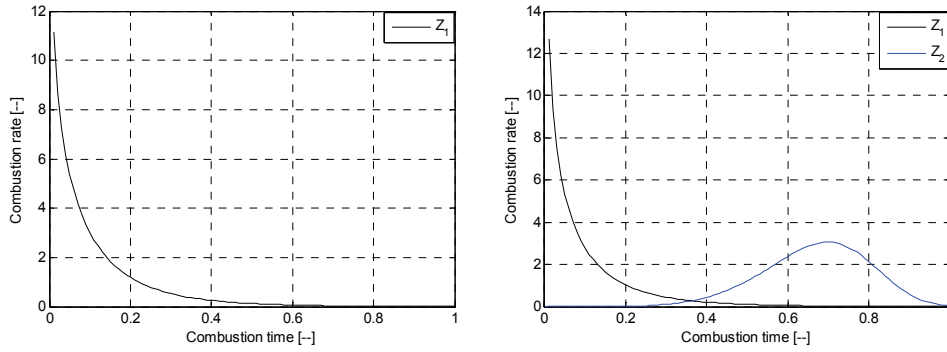
(b) Double Vibe function



(a) Triple Vibe function

Figure 2.59 Contribution of each Vibe fitting function to the normalized combustion rate (1000 rpm, 100% power)

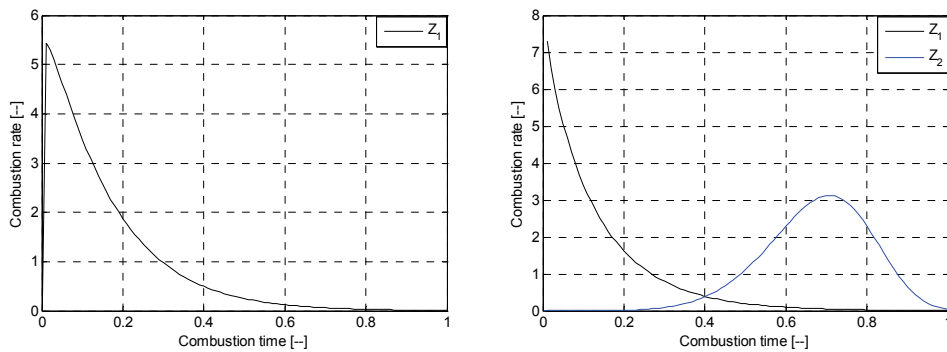
Figure 2.60 shows the contribution of each Vibe fitting function to the normalized combustion rate for the 1000 rpm, 25% power point. The single Vibe function only gives premix combustion (Figure 2.60(a)) but m_1 is negative ($m_1 = -0.182$) and a double Vibe function adds a late combustion component ($m_2 = 4.899$), but only occupying about 10% of the total combustion (Figure 2.60(b)). For part load, the diffusive combustion stage has almost disappeared. Therefore double Vibe functions can be used to describe the premix and late combustion stages.



(a) Single Vibe function

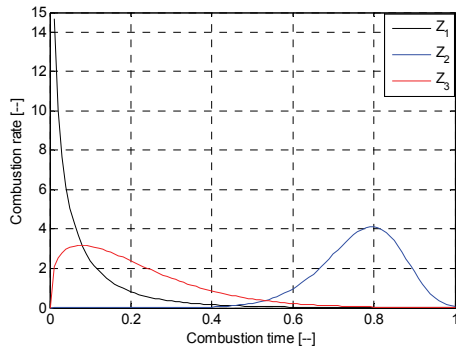
(b) Double Vibe function

Figure 2.60 Contribution of each Vibe fitting function to the normalized combustion rate (1000 rpm, 25% power)



(a) Single Vibe function

(b) Double Vibe function



(a) Triple Vibe function

Figure 2.61 Contribution of each Vibe fitting function to the normalized combustion rate (800 rpm, 50% power)

Figure 2.61 shows the contribution of each Vibe fitting function to the normalized combustion rate of 800 rpm, 50% power point. Like the 1000 rpm, 100% power point, the single Vibe function only gives premix combustion (Figure 2.61(a)) with a positive value ($m_1 = 0.051$). The second order Vibe function again adds a late combustion ($m_2 = 5.099$) with $b_1 = 0.129$, and the premix combustion parameter becomes negative to $m_1 = -0.01$. The third order Vibe function adds a premix combustion ($m_3 = 0.317$).

The late combustion for this cylinder (cylinder 1) is pronounced in particular for operating points (A) and (C). It seems to be not accidental since the same behaviour can be seen on the other three cylinders too. The phenomenon also showed up for cylinder 1 when the original hole position was used (having a shorter channel since it was located on the lower side of the cylinder head instead of on top). The smoothed heat release measurement of the other three cylinders and for cylinder 1 with its original hole position is presented in Appendix VII.

2) Restriction of fit parameters m_k and ' b_k '

The weight factor b_k can be both positive and negative to allow exothermic and endothermic processes during combustion. Originally the form factor m_k as presented in [Ding, 2011a] was only allowed to have positive values in order to give a realistic physical meaning: a negative m implies an infinite reaction rate at the start of combustion (Figure 2.62(a)) and more rapid combustion progress than in the case of positive m value (Figure 2.62(b)). Nevertheless when the engine runs in part load, an infinite reaction rate at the start of combustion improves the fitting of the relative step reaction coordinate at the start of combustion. The sign of m_k in the first order

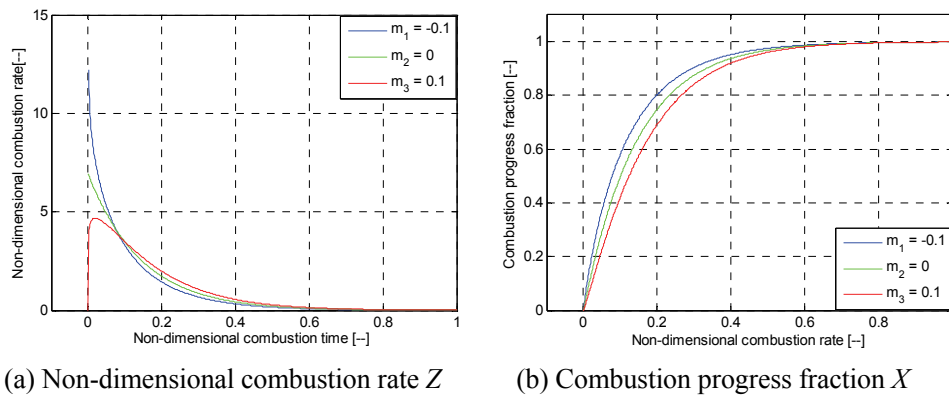


Figure 2.62 The combustion rate and progress for different m values

Vibe fit function is also a criterion to determine what order Vibe function as the highest will be applied in the curve fitting: if the sign is negative, i.e. the engine is running at very low load, a second order Vibe function is sufficient for a satisfactory fit; otherwise a third order Vibe function is required to fit more heat release during diffusive combustion. This phenomenon will be further explained in the next section.

3) *Fitting residual analysis*

After fitting the reaction coordinate from a measurement with multiple Vibe functions using the nonlinear least square method, it is necessary to evaluate the quality of the fit, which is presented in Appendix IV.

In this research, the number of measured points (n) of each fit is around 1000 (in the nominal point, $n = 951$) and the number of parameters to be fitted (k) is 2, 4 and 6 for first, second and third order fitting function respectively. Clearly the number of degrees of freedom ($u = n - k$) is approximately equal to n .

Table 2.8 lists the residual analysis of each fit functions for the three operating points. Contrary to Sum of Squared Errors (*SSE*, which is an absolute value), *R-square* is a relative value and therefore very useful for analysing the quality of fit. In short *R-squares* describes the proportion of variability in a data set that is accounted for by the statistical model. It is clear from Table 2.8 that for the same operating points a higher Vibe order results in a higher *R-square* value. The residual of the fourth order Vibe of operating point (A), the third order Vibe of operating point (B) and the third order Vibe of operating point (C) are also shown in the table. They do not show much improvement when compared to the next lower order function (e.g. the relative value of *R-Square*).

There are some other statistics, provided by MATLAB, by which the fit can be evaluated, e.g. Root Mean Squared Error (*RMSE*), Confidence and Prediction Bounds. However such a residual analysis is only based on mathematics. In the next section the smoothed results based on the multiple Vibe function will be compared with the raw data on the basis of some important engine running parameters to verify that the fitting method and results are not only statistically, but also physically reliable and therefore useful.

Table 2.8 Residual analysis of Vibe fitting functions

Operating point	Vibe Function	SSE	R-Square	DFE
(A)	First order	0.6824	0.9910	949
	Second order	0.3610	0.9952	947
	Third order	0.3601	0.9952	945
	Fourth order	0.3599	0.9952	943
(B)	First order	2.6303	0.9125	793
	Second order	1.8202	0.9395	791
	Third order	1.7666	0.9412	789
(C)	First order	2.4592	0.9486	1006
	Second order	0.9978	0.9791	1004
	Third order	0.8348	0.9825	1002
	Fourth order	0.8044	0.9832	1000

2.4.4 Smoothed result and analysis

1) Nominal speed, nominal load

Five important parameters are considered as criteria to evaluate the investigated smoothing methods: maximum pressure (p_{max}), maximum temperature (T_{max}), pressure at exhaust open (p_{EO}), temperature at exhaust open (T_{EO}) and indicated power (P_i) between IC and EO.

Figure 2.63 shows the smoothed pressure signals and heat release of the engine running at nominal load (operating point (A)), and, in Table 2.9, the five important parameters are compared for different order of Vibe functions. The maximum pressure is a measure of mechanical loading of the engine and its value is predicted highest for the second order Vibe function and lowest for the first order Vibe function. The maximum temperatures are important in view of certain emissions and the

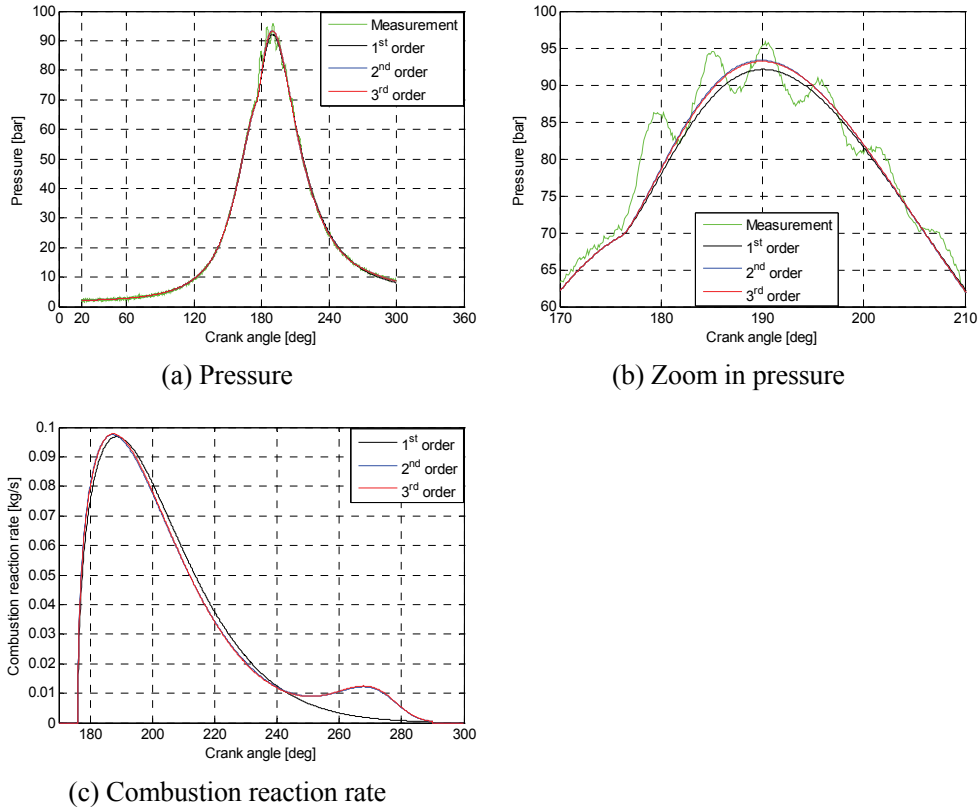


Figure 2.63 Smoothed pressure and combustion reaction rate (point A))

Table 2.9 Comparison results of different multiple Vibe functions (point A))

Signal	P_{max} (bar)	T_{max} (K)	P_{EO} (bar)	T_{EO} (K)	P_i (kW)
Raw data	95.865	1569.70	8.952	1159.98	83.590
First order	92.109	1522.54	8.165	1062.59	83.378
Second order	93.336	1511.84	8.607	1118.73	83.309
Third order	93.194	1513.58	8.614	1119.60	83.322

thermal loading of the engine. The three Vibe fitting functions all estimate the temperature around 50 K lower than the raw data. At EO, the value of p_{EO} and T_{EO} represent the last point of the in-cylinder process. This point is important since it defines the starting point of the gas exchange, in particular the blow down process. For the second and third order Vibe fitting functions the temperature T_{EO} is about 40 K too low but still very close to the measured data. The first order (single) Vibe function gives a much lower T_{EO} (about 97 K lower), which is caused by the lack of

late combustion in the fit. Note that the relative differences of p_{EO} and T_{EO} are the same since both are related by the gas law and the mass is constant. Last but not least, the indicated powers (P_i) between IC and EO change less than 1% when increasing the Vibe order during fitting.

2) *Nominal speed, part load (along generator law)*

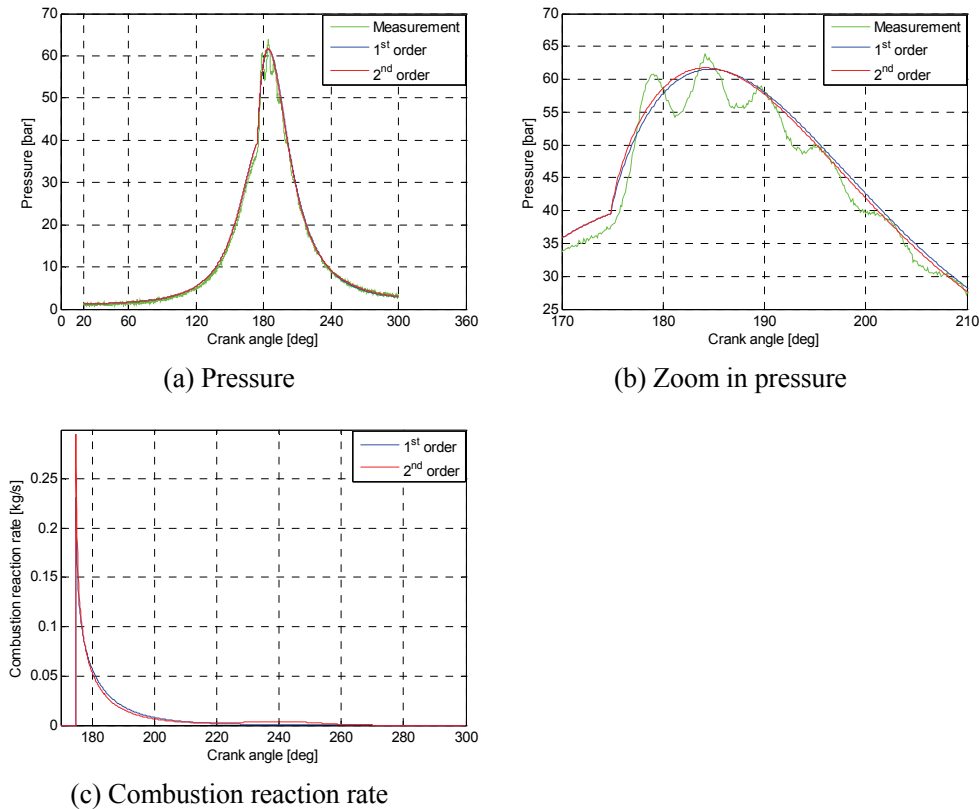


Figure 2.64 Smoothed pressure and combustion reaction rate (point B))

When the diesel engine runs in part load, the diffusive combustion almost disappears but the late combustion still persists (Figure 2.64(c) and Figure 2.65(c)). Figure 2.64 and Table 2.10 illustrate the smoothed pressure and smoothed CRR and the comparison of the results of different Vibe functions of the 1000 rpm, 25% power point (operating point (B)). Since negative values for m are allowed, the single Vibe function results in a reasonable pressure signal. The second order Vibe function adds late combustion. The peak pressures for first and second order are almost the same

and about 2 bar lower than the measured data. But the peak temperatures are around 7 K and 14 K lower than measured respectively. The pressure and temperature at EO of the second order are high but lower than the measured raw data, where the single Vibe is too low, which is caused by adding the late combustion. The differences in indicated power are close to the measured value for both (about 1 kW lower).

Table 2.10 Comparison results of different multiple Vibe functions (point (B))

Signal	P_{max} (bar)	T_{max} (K)	P_{EO} (bar)	T_{EO} (K)	P_i (kW)
Raw data	63.802	1354.13	3.191	711.31	26.592
First order	61.528	1347.43	2.842	638.34	25.169
Second order	61.734	1340.10	3.000	673.47	25.339

3) *Reduced speed, part load (along propeller law)*

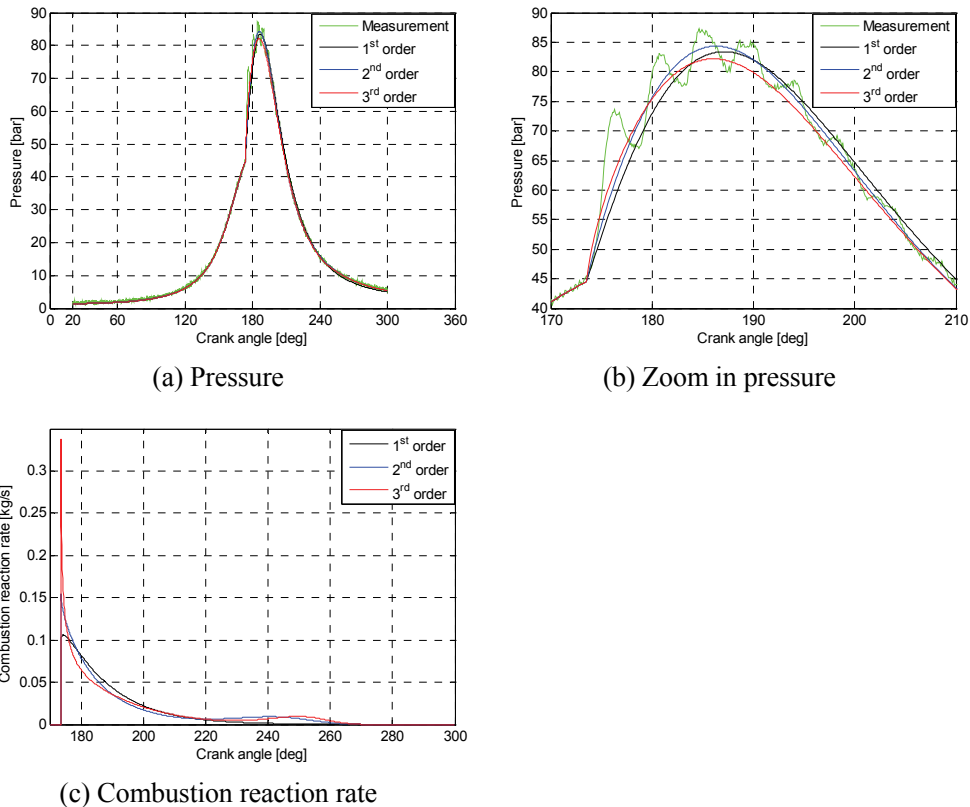


Figure 2.65 Smoothed pressure and combustion reaction rate (point (C))

This case is for the engine running at lower speed (800 rpm) and along the propeller line (50% power) (operating point (C)). Figure 2.65 and Table 2.11 illustrate the smoothed pressure and smoothed *CRR* and the comparison of the results for different order of Vibe functions. The second order gives highest peak pressure but lower peak temperature than the first order, and the third order gives the lowest peak pressure and peak temperature. As for the pressure and temperature at EO, the third order fit results in a highest value but still lower than measured. The indicated power is for both about 2 kW higher than measured.

Table 2.11 Comparison results of different multiple Vibe functions (point (C))

Signal	P_{max} (bar)	T_{max} (K)	P_{EO} (bar)	T_{EO} (K)	P_i (kW)
Raw data	87.269	1729.32	5.715	1095.27	46.962
First order	83.400	1699.58	5.046	977.43	48.258
Second order	84.325	1675.27	5.454	1054.54	48.436
Third order	82.185	1641.24	5.471	1058.18	47.699

2.4.5 Discussions

The smoothing method presented in this section gives good results. Especially for ill located pressure measured facilities [Knobbe, 2001], this method has great potential. But the main advantage lies in the fact that in a natural way a characterization of the combustion is provided in terms of the weighted contributions of a number of Vibe functions. The curve fitting method uses a nonlinear least-square fitting theory, which is sensitive to start points and type of iteration. It requires some experience in numerical analysis and knowledge of diesel engine combustion in order to get good results.

Chapter 3

Parameters for Finite Stage Cylinder Process Model

3.1 Introduction

The combustion process of a diesel engine can be investigated using both a simulation and an experimental approach. Nowadays with the development of advanced experimental methods and computer technology, the combustion phenomena can be described accurately and precisely. Nevertheless the in-cylinder combustion process of diesel engine not always needs a very detailed model, for example, for the research of integration of diesel engines in a ship propulsion system what is required is an adequate mean value description of the changes of the combustion and the effect on cylinder work as well as the air supply to the cylinder (i.e. interaction with the turbocharger system) under various operational conditions [Stapersma, 2001]. The Seiliger process then is a suitable method to calculate the in-cylinder process and together with a suitable gas exchange model [Schulten, 2003] a complete 'Mean Value First Principle (MVFP)' model can be developed that does not require an integration of differential equations for the core cylinder model. The MVFP model is not primarily intended for engine development but is used for system studies of engine users, such as the shipping and dredging industry.

Using the parameters defined in the Seiliger process it is possible to parameterize the in-cylinder process, both the net combustion heat and the heat loss during compression and expansion. The heat loss during combustion as well as incomplete combustion must be modelled separately. In particular the parameters describing the net combustion heat release are used in a mean value simulation model to give a global description of the combustion process. Determining a model for these combustion parameters is critical to the mean value simulation model and the present model as given in [Schulten, 2005] needs improvement.

Two approaches are used to research the Seiliger parameters: experimental and theoretical. For the experimental approach, measurements at a MAN 4L20/27 test bed of the Netherlands Defence Academy (NLDA) in Den Helder were carried out. The in-cylinder pressure measurement is transformed to a Seiliger process definition on the basis of equivalence criteria to uniquely determine the Seiliger parameters. Then the dependency of Seiliger parameters on engine operational parameters is obtained and the behaviour of the Seiliger parameters in relation to the engine running condition is researched. As to the theoretical approach, the commonly used heat

release model based on Vibe functions is implemented in a single zone closed cylinder process simulation. The results are also transformed to Seiliger parameters using the same equivalence criteria and then the Vibe driven cylinder simulation is compared with the Seiliger approximation. Exploring the interrelation between Vibe and Seiliger parameters provides an efficient way to understand the effect of combustion shape as expressed with multiple Vibe models on the basic engine thermodynamics as expressed by the Seiliger parameters and thus acquire a more global understanding of the effect of combustion changes on engine efficiency.

In this chapter, the theory of a *basic* Seiliger process is presented, which, by adding an isothermal combustion stage, goes back to the original cycle [Seiliger, 1922] and was improved by [Stapersma, 2009a]. However this thesis presents a new extension of the Seiliger model to enable modelling of very late combustion even better, called *advanced* Seiliger process. After introducing the definition of the *basic* and *advanced* Seiliger process models a systematic investigation of the Seiliger parameters and their effects on in-cylinder process is carried out. The most important part in this chapter is how to fit the measured engine cycle to the Seiliger process. Several combinations of equivalence criteria are used to make this transformation and set up the applicable systems of equations for the Seiliger parameters. A Newton-Raphson iteration method then is applied to find the solutions of these systems of equations. Finally in this chapter the developed method is tested on an artificial engine, i.e. a Vibe driven single zone cylinder process simulation and the relation of the resulting Seiliger parameters with the original Vibe parameters is investigated.

3.2 Theory of Advanced Seiliger Process

The Seiliger process was originally published by [Seiliger, 1922] (Figure 3.1) He used five stages (1-2, 2-3, 3-4, 4-5 and 5-6) to describe the closed cylinder process and four stages (6-7, 7-1, 1-0 and 0-1) to model blow down and gas exchange separately. Note that the combustion is represented by 3 of the 5 stages of the overall in-cylinder process: stage 2-3 (iso-volumetric combustion), 3-4 (isobaric combustion) and 4-5 (isothermal combustion). Nowadays the Seiliger cycle mostly used is restricted to two combustion stages (the so called dual combustion cycle see a.o [Klein Woud, 2002]). However [Stapersma, 2002a], refer to (Figure 3.2), returned to the original 3-stage combustion to define the *basic* Seiliger process, in order to be able to represent the main features of diesel engine combustion, i.e. pre-mix, diffusive and late combustion. In addition the compression and expansion stages 1-2 and 5-6 – which normally (following original Seiliger) are taken adiabatic – were both changed into polytropic processes in [Stapersma, 2009a]. This allows for some heat loss from the working medium to the wall during compression and expansion, resulting in lower work during these stages. Also note that both Seiliger and Stapersma allow the point where compression starts and expansion ends to be at a different volume, to be able to model earlier opening of the exhaust valve and later closing of inlet valve. The gas exchange – that takes place in the stages 6-7, 7-1, 1-0 and 0-1 in the original [Seiliger, 1922] version – was replaced in [Schulten, 2003] by a model using a mean value approach as developed in [Stapersma, 2002b].

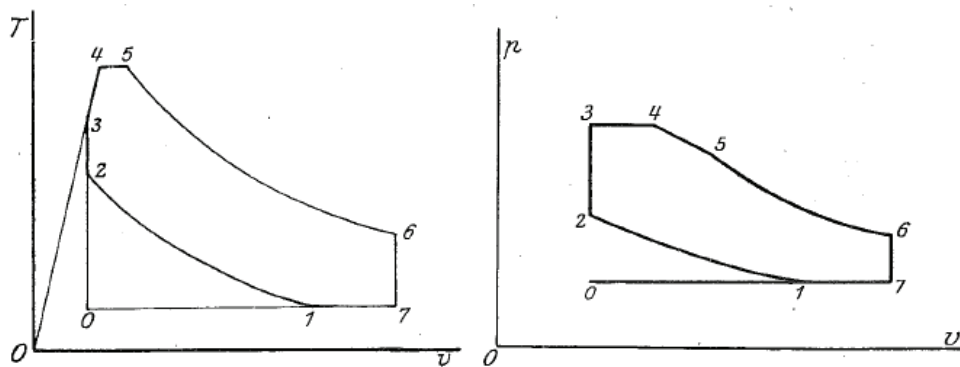


Figure 3.1 Original Seiliger process definition [Seiliger, 1922]

Nevertheless when *very* late combustion is present there could be net heat input during stage 5-6. Therefore in the *advanced* Seiliger process model, as defined in this thesis, the polytropic (expansion) stage 5-6 now represents both heat loss and heat input from combustion.

3.2.1 Definition of basic and advanced Seiliger process of closed cycle

Figure 3.2 shows the six-point *basic* and *advanced* Seiliger process model. The station points between these stages are designated 1 to 6 for the *basic* Seiliger process based on [Stapersma, 2002a] and 1 to 6' for the *advanced* Seiliger process. The stages can be described as follows:

- 1-2: polytropic compression, indicating net heat loss;
- 2-3: isovolumetric combustion;
- 3-4: isobaric combustion and expansion;
- 4-5: isothermal combustion and expansion;
- 5-6: polytropic expansion indicating net heat loss, used when there is no combustion in this stage;
- 5-6': polytropic expansion indicating the net heat input caused by combustion.

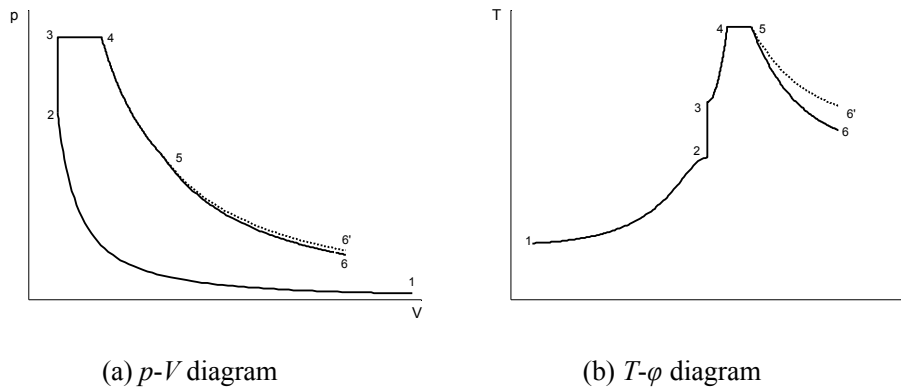


Figure 3.2 six-point Seiliger process definition

Cycle 1-6 is the *basic* Seiliger process and point 6 is the polytropic process terminal point due to heat loss during expansion, and, in this case, the state parameters are based on point 6 (only heat loss).

Cycle 1-6' is the *advanced* Seiliger process and assumes there is combustion during stage 5-6, the state parameters after expansion are based on point 6' which is the outcome of net heat input during expansion. The only difference between cycle 1-6 and cycle 1-6' (i.e. *basic* Seiliger process and *advanced* Seiliger process) is whether there is combustion in the last stage, which can be introduced by selecting the appropriate value of the exponent (n_{exp}). Note that if the heat loss to the walls in stage 5-6' needs to be determined in the *advanced* Seiliger process, it can be modelled either by comparison with the *basic* Seiliger process (by choosing another n_{exp}), or using the same method to determine the heat loss to the wall directly as used in the other combustion stages (using e.g. a Woschni heat loss model).

The *basic* and *advanced* Seiliger process can be described by a finite number of parameters, that – together with the initial condition (trapped condition) and the properties of the working medium – fully specify the process.

Table 3.1 Seiliger process definition and parameters

Seiliger stage	Seiliger definition	Parameter definition	Seiliger parameters
1-2	$\frac{p_2}{p_1} = r_c^{n_{comp}}$	$\frac{V_1}{V_2} = r_c$	r_c, n_{comp}
2-3	$\frac{V_2}{V_3} = 1$	$\frac{p_3}{p_2} = a$	a
3-4	$\frac{p_4}{p_3} = 1$	$\frac{V_4}{V_3} = b$	b
4-5	$\frac{T_5}{T_4} = 1$	$\frac{V_5}{V_4} = c$	c
5-6 (5-6')	$\frac{p_6}{p_5} = r_e^{n_{exp}}$	$\frac{V_5}{V_6} = r_e$	r_e, n_{exp}

Table 3.1 gives the definition of the Seiligers stages as well as the definition of the Seiliger parameters for the different stages. Among these parameters a, b, c are the 'shape' parameters for the net combustion heat, n_{comp} models the heat loss during compression. The parameter n_{exp} models the net heat input in the *advanced* Seiliger

process but the same parameter is used to model the heat loss during expansion in the *basic* Seiliger process, like n_{comp} in stage 1-2.

The other two parameters r_c and r_e can be determined by the geometrical volumes (equation [3.1] and [3.2]). Since V_1 is fixed by the inlet valve timing, r_c is fixed by ratio of V_1 and V_2 ($V_2 = V_{TDC}$ in the definition of the Seiliger process). The same holds for r_e which is fixed by V_6 , determined by the exhaust valve timing, and the product of b , c and r_{26} . The parameter r_{26} is defined in equation [3.2] as the ratio of V_2 and V_6 (equation [3.3]). These volumes are assumed to be geometrically fixed (equation [3.4] – [3.6]) in [Stapersma 2009a].

$$r_c = \frac{V_1}{V_2} \quad [3.1]$$

$$r_e = \frac{V_5}{V_6} = \frac{V_2 \cdot b \cdot c}{V_6} = b \cdot c \cdot r_{26} \quad [3.2]$$

$$r_{26} = \frac{V_2}{V_6} \quad [3.3]$$

$$V_1 = V_{IC} \quad [3.4]$$

$$V_2 = V_{TDC} \quad [3.5]$$

$$V_6 = V_{EO} \quad [3.6]$$

With $V_{IC} = V(\alpha_1)$,

$$V_{EO} = V(\alpha_6),$$

$$V_{TDC} = V(180^\circ),$$

$$\alpha_1 = IO,$$

$$\alpha_6 = EO.$$

Then the V_{IC} , V_{EO} and V_{TDC} can be calculated using the volumetric relation as given in equation [2.2]:

$$V(\alpha) = A_b \cdot L_s \cdot \left[\frac{1}{\varepsilon - 1} + \frac{1}{2} \cdot \left\{ (1 + \cos \alpha) + \frac{1}{\lambda_{CR}} \left(1 - \sqrt{1 - \lambda_{CR}^2 \cdot \sin^2 \alpha} \right) \right\} \right] \quad \text{Ref [2.2]}$$

However, as valve opening and closing also influence the process, IO and EO might be considered as indicative values only. To investigate late (or early) start of

combustion in this thesis r_c is used as variable, by varying V_2 . Also V_6 is made variable by bringing in a new parameter ΔEO allowing variation of the duration of the expansion. The effect of these two variations will be investigated in section 3.2.3.

3.2.2 Modeling the in-cylinder process with Seiliger model

The MAN 4L 20/27 engine is used to investigate the possibilities to approximate the in-cylinder process with the Seiliger model. The general data of the engine are presented in Table 2.2. The full load and maximum speed define the nominal point used in the following simulation and analysis.

1) Determine the initial condition

The initial condition of the Seiliger process (point 1) is the trapped condition at inlet valve close (IC). The pressure and temperature (p_1 and T_1) can be approximated by the measured pressure and temperature in the inlet receiver. Trapped pressure p_1 in a nominal operating point is approximately equal to p_{IR} :

$$p_1 \approx p_{IR} = 2.085 \text{ bar} \quad [3.7]$$

The trapped temperature T_1 is assumed to be induction temperature (T_{ind}) that can be calculated considering the heat pick up during the air intake:

$$T_{ind} = T_c + \varepsilon_{INL} \cdot (T_{INL} - T_c) \quad [3.8]$$

The parameter ε_{INL} and T_{INL} are estimated using an experimental equation [Zinner, 1980] $\varepsilon_{INL} = 1/6$, metal temperature $T_{INL} = 513 \text{ K}$ and $T_c = T_{IR} = 315.8 \text{ K}$ (measured). In the nominal operating point this gives:

$$\begin{aligned} T_1 &= 315.8 + \frac{1}{6}(513 - 315.8) \\ &= 348.7 \text{ K} \end{aligned} \quad [3.9]$$

The volume at trapped condition is:

$$V_1 = V_{IC} \quad \text{Ref [3.4]}$$

The mass at trapped condition can be calculated using the gas law:

$$m_1 = \frac{p_1 \cdot V_1}{R_1 \cdot T_1} \quad [3.10]$$

2) *First estimate of Seiliger parameters*

The initial values for the Seiliger parameters are selected here based on modelling and measurement experience and will serve as a base value for the systematic investigation of Seiliger parameters.

The parameters defining the combustion ‘shape’ and heat loss during compression and expansion for the combustion stages (for *basic* three and for *advanced* four) are selected as follows:

Table 3.2 Selection of Seiliger parameters

Seiliger Parameter	Basic Seiliger process with three combustion stages	Advanced Seiliger process with four combustion stages
<i>a</i>	1.4	1.4
<i>B</i>	1.4	1.4
<i>C</i>	2	1.5
<i>n_{exp}</i>	1.31	1.27
<i>n_{comp}</i>	1.36	1.36
<i>r_c</i>	<i>V₁/V_{TDC}</i>	<i>V₁/V_{TDC}</i>
<i>ΔEO</i>	0	0

The parameter *a*, *b*, *n_{comp}*, *r_c* and *ΔEO* are selected the same in these two Seiliger process. As stated before, *n_{exp}* is different to indicate heat loss and net heat input in *basic* and *advance* Seiliger process respectively. In order to distinguish these two processes unambiguously, *c* is set to be smaller (1.5 instead of 2.0) in the *advanced* Seiliger process, which is reasonable because some heat input from stage 4-5’ is then moved to stage 5-6’ to represent very late combustion.

When determining *n_{comp}* and *n_{exp}*, the actual isentropic coefficient (*γ*) should be considered:

$$\gamma = \frac{c_p}{c_v} \quad [3.11]$$

Since *γ* is the ratio of the two specific heats, that are both functions of temperature and composition, *γ* also is a function of temperature and composition, albeit weaker. Therefore the mean value of *γ* during compression and expansion is different for different operating points and the compression exponent and expansion exponent

should be determined on the basis of isentropic coefficient γ , for which a polytropic factor is used.

The polytropic factor is derived in [Stapersma, 2011(e)] and reproduced in Appendix V, for compression:

$$\eta_{pol,comp} = \frac{\gamma - 1}{n_{comp} - 1} \quad [3.12]$$

Only when $n_{comp} < \gamma$, $\eta_{pol,comp} > 1$, the polytropic compression process will give net heat loss.

The polytropic factor for expansion is defined in an inversed way:

$$\eta_{pol,exp} = \frac{n_{exp} - 1}{\gamma - 1} \quad [3.13]$$

Then in this case, when $n_{exp} > \gamma$, $\eta_{pol,exp} > 1$, the polytropic expansion process has a net heat loss. However, when $n_{exp} < \gamma$, $\eta_{pol,exp} < 1$, the polytropic expansion process has a net heat input and the heat source must be included in the heat input originating from combustion.

3) Determine the state parameters at the stations

After selecting the Seiliger parameters and the initial conditions, the state parameters in the six station points can be calculated on the basis of the Seiliger definition and the gas law. Two state parameters V and p (or T for stage 4-5) of each stage can be calculated according to Table 3.1 and finally T (or p for stage 4-5) can be calculated using the gas law when mass m is determined. In the original Seiliger process model the mass was assumed to be constant. However, the fuel injected into cylinder increases the mass slightly, which will be taken into account in the Seiliger models applied here. The fuel injected per cycle into a cylinder is divided into the three or four combustion stages in the process i.e. stage 2-3, 3-4, 4-5 and, if applicable, 5-6. The fuel mass of each part is calculated based on the 'heat input ratio'. Generally for stage i to j :

$$m_f^{ij} = m_f^{cyc} \cdot q_{ratio}^{ij} \quad \text{and} \quad q_{ratio}^{ij} = \frac{q_{ij}}{q_{in}} \quad [3.14]$$

With $i = 1,2,3,4,5$ and $j = i + 1$.

The mass of the Seiliger station point j can be calculated from the previous point i :

$$m_j = m_i + m_f^{ij} \quad [3.15]$$

For $i = 1$, $q_{12} = 0$, at least for combustion, so $m_2 = m_1$ and $x_2 = x_1$. Introducing the stoichiometric air/fuel ratio (σ), the air fraction in these points is:

$$x_j = \frac{m_i \cdot x_i - m_f^{ij} \cdot \sigma}{m_i + m_f^{ij}} \quad [3.16]$$

4) Determine the state parameters during the stages

Now the state parameters p , T , m and V of the six station points have been obtained, but to make sure the Seiliger process model describes the closed cycle reliably, the process between the two station points should be described correctly as well.

First an array of crank angles is set up for the closed cycle between IC and $(EO+\Delta EO)$:

$$\alpha_{ref} = [\alpha_{IC} \ \alpha_{EO+\Delta EO}] \quad [3.17]$$

The associated volume array can be calculated based on equation [2.2]:

$$V_{ref} = [V_{IC} \ V_{EO+\Delta EO}] \quad [3.18]$$

Then the corresponding volume of the six station points is retrieved in order to determine the crank angle of these station points α_1 to α_6 .

A factor for the crank angle increase for each stage (f_{ij}) is introduced to set the number of steps between two station points (e.g. if f_{ij} is 0.01 there are 101 points for the stage ij). In addition, the increase of mass and composition uses the factor f as well, which means that the mass and composition are assumed to increase linearly with the crank angle during a stage. The calculation of pressure and temperature for each stage follows:

- 1) In stage 1-2 and 5-6, the pressure is calculated based on the polytropic process and the temperature is then calculated on the basis of the gas law.
- 2) In stage 2-3 and 3-4, the pressure is calculated using factor f since crank angle or pressure are constant in these two stages respectively and the temperature is obtained according to the gas law.

3) In stage 4-5, the temperature is calculated using factor f since temperature is constant in this stage and the pressure is calculated with the gas law.

Table 3.3 illustrates the procedure of the state parameter calculation for each Seiliger process stage. It must be noted that in Table 3.3, the vectors (e.g. \overline{V}_{12} , \overline{p}_{12} etc.) are used to represent one state parameter between two station points, including the start,

Table 3.3 State parameter calculation procedure for the Seiliger process

Seiliger stage	1-2	2-3
	$\overline{\alpha}_{12} = \alpha_1 + \overline{f}_{12} \cdot (\alpha_2 - \alpha_1)$ $\overline{V}_{12} = V(\overline{\alpha}_{12})$ $\overline{m}_{12} = m_1 + \overline{f}_{12} \cdot (m_2 - m_1)$ $\overline{x}_{12} = x_1 + \overline{f}_{12} \cdot (x_2 - x_1)$ $\overline{R}_{12} = R_{air} \cdot \overline{x}_{12} + R_{sg} \cdot (1 - \overline{x}_{12})$ $\overline{p}_{12} = p_1 \cdot \left(\frac{V_1}{\overline{V}_{12}} \right)^{n_{comp}}$ $\overline{T}_{12} = \frac{(\overline{p}_{12}) \cdot (\overline{V}_{12})}{(\overline{m}_{12}) \cdot (\overline{R}_{12})}$	$\overline{\alpha}_{23} = \alpha_2 + \overline{f}_{23} \cdot (\alpha_3 - \alpha_2)$ $\overline{V}_{23} = V(\overline{\alpha}_{23})$ $\overline{m}_{23} = m_2 + \overline{f}_{23} \cdot (m_3 - m_2)$ $\overline{x}_{23} = x_2 + \overline{f}_{23} \cdot (x_3 - x_2)$ $\overline{R}_{23} = R_{air} \cdot \overline{x}_{23} + R_{sg} \cdot (1 - \overline{x}_{23})$ $\overline{p}_{23} = p_2 + \overline{f}_{23} \cdot (p_3 - p_2)$ $\overline{T}_{23} = \frac{(\overline{p}_{23}) \cdot (\overline{V}_{23})}{(\overline{m}_{23}) \cdot (\overline{R}_{23})}$
Seiliger stage	3-4	4-5
	$\overline{\alpha}_{34} = \alpha_3 + \overline{f}_{34} \cdot (\alpha_4 - \alpha_3)$ $\overline{V}_{34} = V(\overline{\alpha}_{34})$ $\overline{m}_{34} = m_3 + \overline{f}_{34} \cdot (m_4 - m_3)$ $\overline{x}_{34} = x_3 + \overline{f}_{34} \cdot (x_4 - x_3)$ $\overline{R}_{34} = R_{air} \cdot \overline{x}_{34} + R_{sg} \cdot (1 - \overline{x}_{34})$ $\overline{p}_{34} = p_3 + \overline{f}_{34} \cdot (p_4 - p_3)$ $\overline{T}_{34} = \frac{(\overline{p}_{34}) \cdot (\overline{V}_{34})}{(\overline{m}_{34}) \cdot (\overline{R}_{34})}$	$\overline{\alpha}_{45} = \alpha_4 + \overline{f}_{45} \cdot (\alpha_5 - \alpha_4)$ $\overline{V}_{45} = V(\overline{\alpha}_{45})$ $\overline{m}_{45} = m_4 + \overline{f}_{45} \cdot (m_5 - m_4)$ $\overline{x}_{45} = x_4 + \overline{f}_{45} \cdot (x_5 - x_4)$ $\overline{R}_{45} = R_{air} \cdot \overline{x}_{45} + R_{sg} \cdot (1 - \overline{x}_{45})$ $\overline{T}_{45} = T_4 + \overline{f}_{45} \cdot (p_5 - p_4)$ $(\overline{p}_{45}) = \frac{(\overline{m}_{45}) \cdot (\overline{R}_{45}) \cdot (\overline{T}_{45})}{(\overline{V}_{45})}$

Seiliger stage	5-6
	$\overline{\alpha}_{56} = \alpha_5 + \overline{f}_{56} \cdot (\alpha_6 - \alpha_5)$ $\overline{V}_{56} = V(\overline{\alpha}_{56})$ $\overline{m}_{56} = m_5 + \overline{f}_{56} \cdot (m_6 - m_5)$ $\overline{x}_{56} = x_5 + \overline{f}_{56} \cdot (x_6 - x_5)$ $\overline{R}_{56} = R_{air} \cdot \overline{x}_{56} + R_{sg} \cdot (1 - \overline{x}_{56})$ $\overline{p}_{56} = p_5 \cdot \left(\frac{V_5}{\overline{V}_{56}} \right)^{n_{exp}}$ $\overline{T}_{56} = \frac{(\overline{p}_{56})_{\bullet} \times (\overline{V}_{56})_{\bullet}}{(\overline{m}_{56})_{\bullet} \times (\overline{R}_{56})_{\bullet}}$

end and all intermediate points. The symbol (e.g. $(\overline{p}_{12})_{\bullet}, (\overline{m}_{12})_{\bullet}$) indicates that the elements of the vector are pointwise calculated.

Entropy is a function of pressure, temperature and composition and it is calculated using the ‘Properties Library’, as presented in Appendix II.

Figure 3.3 to Figure 3.8 show the pressure, temperature and entropy in cylinder in different forms. Figure 3.3 and Figure 3.4 are crank angle dependent diagrams, from which the definition of Seiliger process can clearly be seen. Figure 3.5 is a p - V diagram with abscissa V/V_{TDC} instead of volume. When the pressure and volume are taken as the logarithm, the curves of the 5 stages will be straight lines, see Figure 3.6. Note that here the polytropic exponents are constant, and the slopes of line 1-2, line 5-6 increase with increasing temperature according to Appendix V, and even if the polytropic factors in equation [3.12] and [3.13] are constant, the lines become also curved. The slopes of line 2-3, 3-4, 4-5 are 0, infinite, zero and unity respectively. Figure 3.7 and Figure 3.8 show the entropy diagram, from which it is easy to grasp the information of the heat input. In particular for stage 5’-6’ and 5-6, the net heat input and heat loss can be seen separately in the T - S diagram.

Furthermore using the mean properties parameters of the gas, the work, heat input, internal energy and enthalpy, etc. of each stage can be calculated. Therefore the cycle performance of the engine is known.

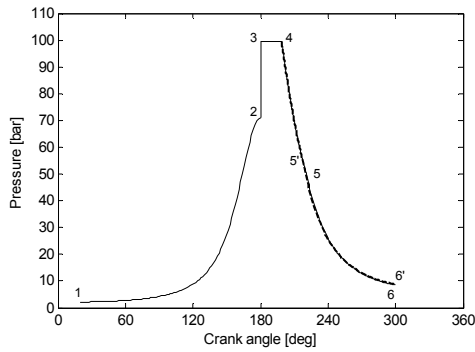


Figure 3.3 Seiliger process $p-\phi$ diagram

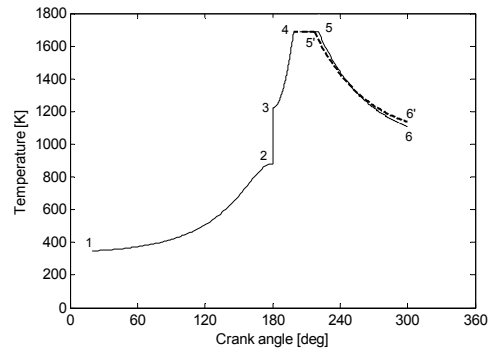


Figure 3.4 Seiliger process $T-\phi$ diagram

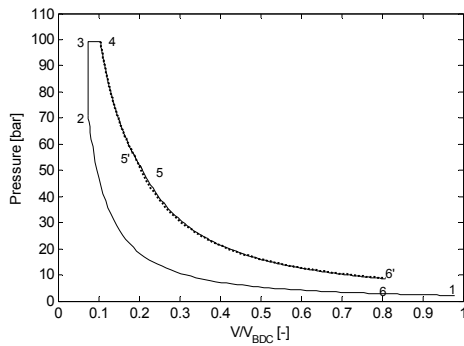


Figure 3.5 Seiliger process $p-V$ diagram

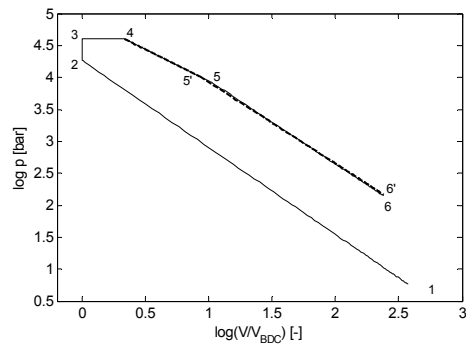


Figure 3.6 Seiliger process $\log(p-V)$ diagram

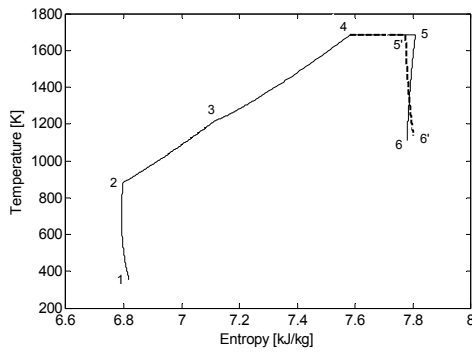


Figure 3.7 Seiliger process $T-s$ diagram

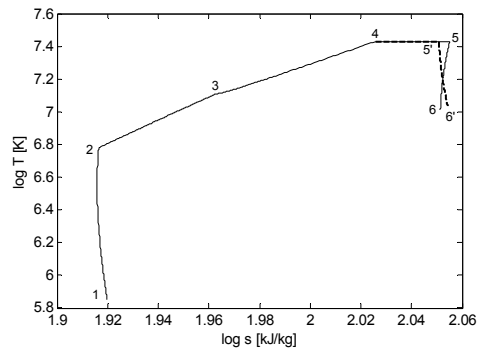


Figure 3.8 Seiliger process $\log(T-s)$ diagram

3.2.3 Systematic investigation of the influence of Seiliger parameters on the in-cylinder process

The Seiliger process provides a simple way to model the closed cycle of a diesel engine. However, Seiliger parameters need to be determined to describe the process correctly. For a real diesel engine, the Seiliger parameters can be determined from measurement by using equivalence criteria.

In this section, a systematic variation of the Seiliger combustion parameters is carried out. Table 3.4 shows the values of the Seiliger parameters used in the investigation. During the variations, only one parameter is changed at a time, while the others are kept at their base value. Another approach would be to change many elementary parameters at the same time while keeping constant other derived quantities – such as maximum pressure or temperature, or even more complex derived quantities, such as heat, work, air excess ratio. This type of analysis can be found in [Stapersma, 2003a]. However the purpose here is to get a clear picture of the elementary parameter variations.

Since the processes 5-6 and 5-6' both represent a polytropic expansion and the only difference is the exponent n_{exp} and $n_{exp,hl}$, the influence of these two parameters is the same. Therefore only variations of the parameter n_{exp} are carried out in this section (i.e. n_{exp} plays both net heat input and heat loss roles in the Seiliger process, depending on the chosen value). Also the virtual process 5-6' will not be plotted in these figures to avoid ambiguity.

Table 3.4 The values of Seiliger parameters used in the investigation

Seiliger Parameter	Base Value	Range
a	1.4	1.0 - 2.0
b	1.4	1.0 - 2.0
c	2	1.0 - 3.5
n_{comp}	1.36	1.30 - 1.40
r_c	V_1/V_{TDC}	$(0.9 - 1.0) \times V_1/V_{TDC}$
ΔEO	0	-10 - 15*
n_{exp}	1.31	1.27 - 1.37

* A negative sign of ΔEO means the exhaust valve opens earlier and a positive sign means the exhaust valve opens later.

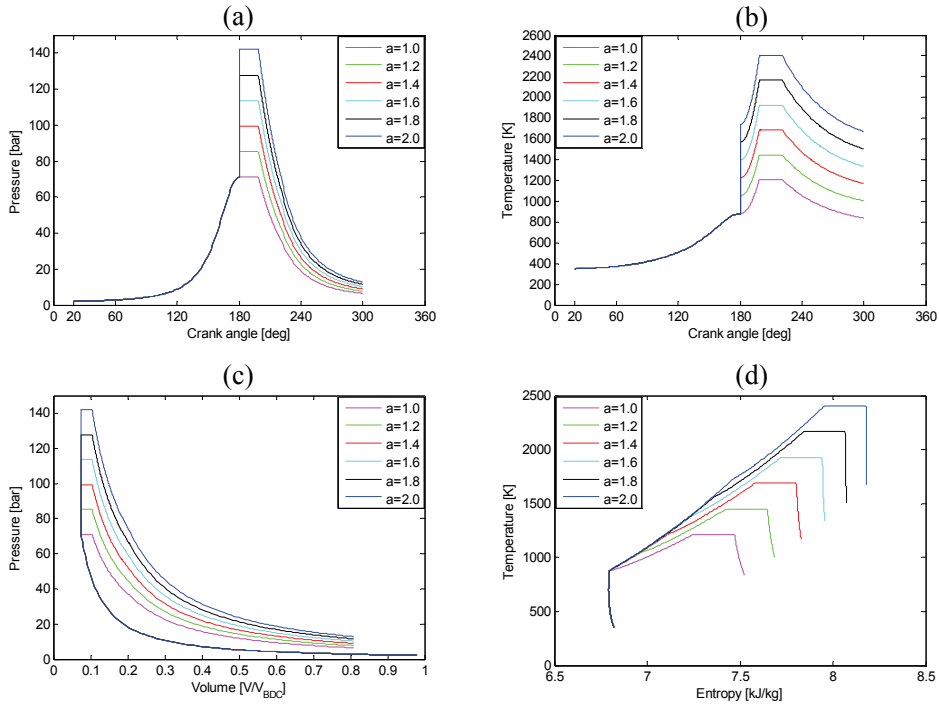


Figure 3.9 Influence of parameter a to in-cylinder process

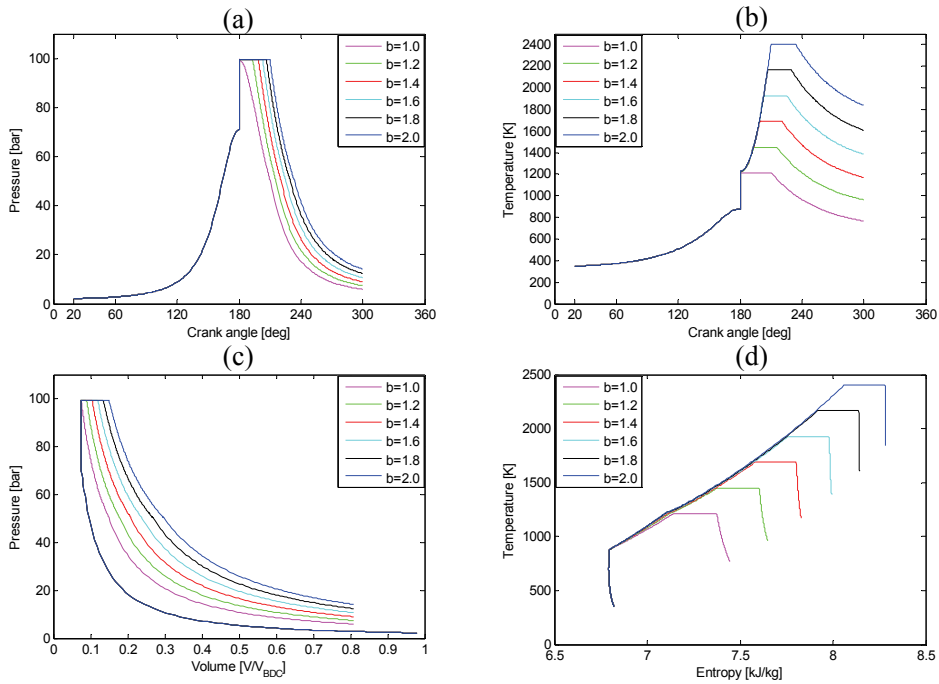


Figure 3.10 Influence of parameter b to in-cylinder process

In Figure 3.9, the maximum pressure as well as the maximum temperature is rising with increasing a . Obviously Seiliger parameter a has a great effect on p_{max} and T_{max} .

When parameter b rises, the peak pressures in point 3 remains the same (Figure 3.10 (a) and (c)). The temperature however rises from point 3 onward and the maximum temperature is considerably higher with increasing b (Figure 3.10 (d)). Another difference between T_{max} in Figure 3.9 (b) and Figure 3.10 (b) is that the T_{max} occurs at the same crank angle in Figure 3.9 (b) but is retarded when b increases in Figure 3.10 (b).

Parameter c only has an impact on the last stage of the Seiliger process (Figure 3.11). The pressure and temperature at EO increase with larger c values. Remember that the p_{EO} and T_{EO} are the prime input of the gas exchange model and ultimately determine the turbine inlet temperature of the turbocharger.

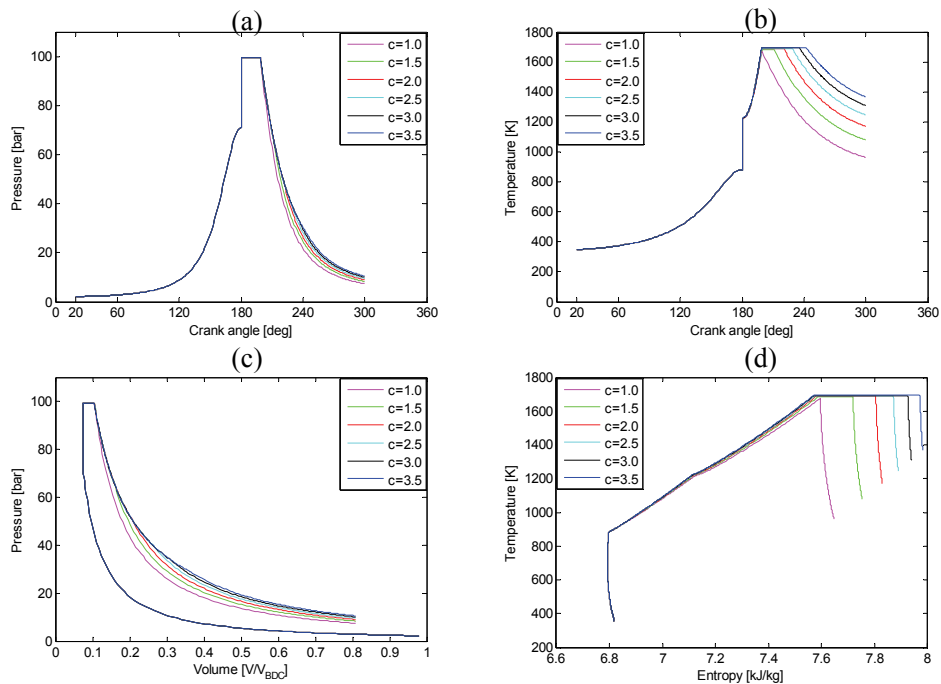


Figure 3.11 Influence of parameter c to in-cylinder process

The parameter n_{exp} plays a role in stage 5-6 and also determines the state parameters at EO point. According to Figure 3.12, the process from point 1 to point 5 does not change with varying n_{exp} but the change occurs from point 5 until point 6 (the EO

point). With larger n_{exp} values the pressure and temperature at EO decrease, see Figure 3.12 (a) – (e). In Figure 3.12 (f) the slope of the T-s curve in stage 5-6 indicates whether the process is exothermic or endothermic. If parameter n_{exp} is used to indicate heat loss during polytropic expansion, the slope of the T-s curve should be positive. If there is combustion occurring during that stage and the net heat flow is positive, the slope of the T-s curve should be negative.

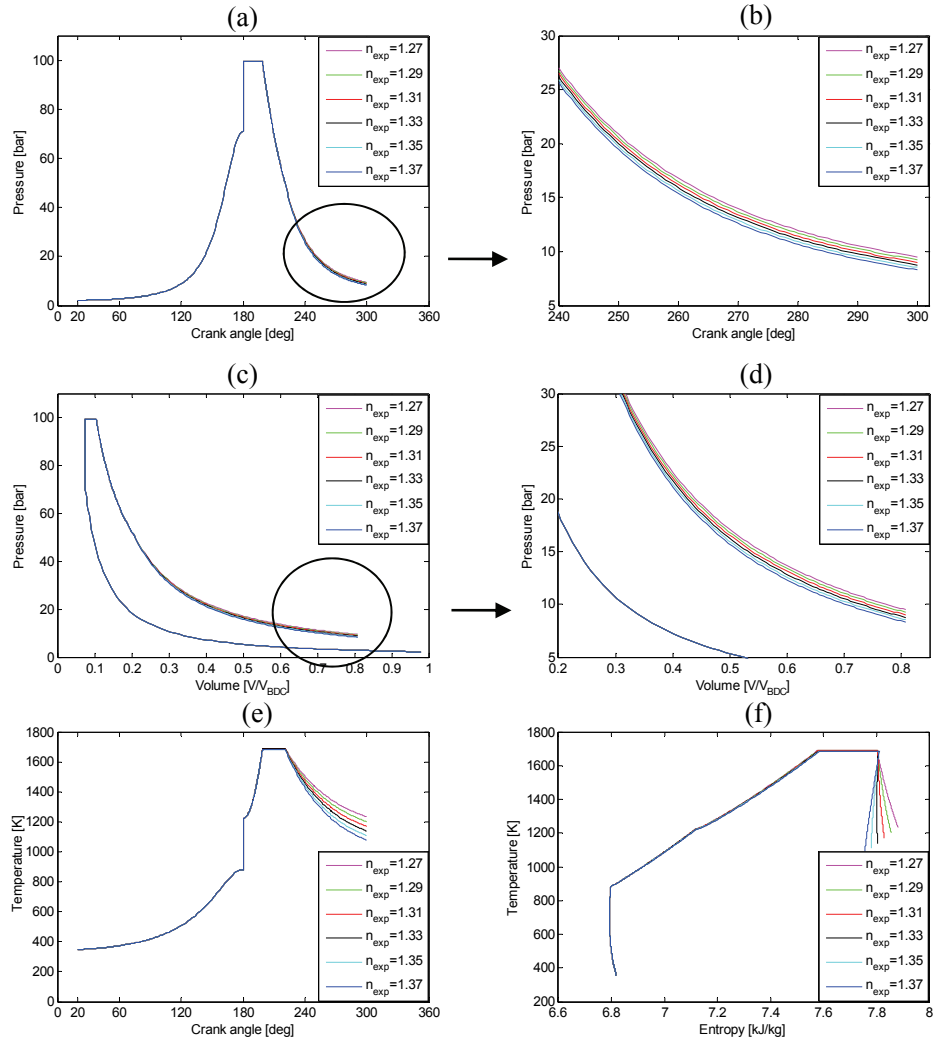


Figure 3.12 Influence of parameter n_{exp} to in-cylinder process

As shown in Figure 3.13, when n_{comp} increases, p_2 and T_2 are both increasing. The parameters p_2 and T_2 , i.e. the start condition of combustion, will affect all the stages of

Seiliger process. It can also be noted that in Figure 3.13 (d) when n_{comp} increases, the polytropic compression process changes from heat input to heat loss. In a measured engine the beginning of the compression will imply heat input (from the hot wall) but as soon as the gas temperature rises above the cylinder wall temperature, this will change to a heat loss to the wall. Since heat loss dominates, n_{comp} must be selected such that stage 1-2 represents a heat loss process.

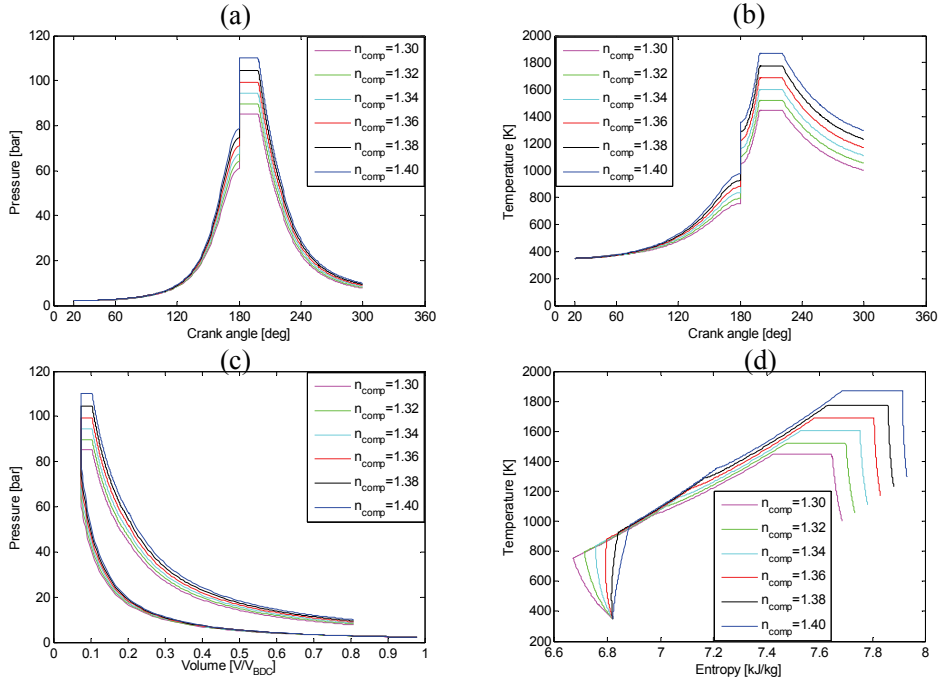


Figure 3.13 Influence of parameter n_{comp} to in-cylinder process

Parameter r_c is normally a constant in the Seiliger process, but it can be used to model late (or early) start of combustion by varying V_2 (it can also be varied by choosing different IC). Here one case where the start of combustion (SOC) is considered earlier is investigated to see the effect of this parameter. Figure 3.14 show the influence of parameter r_c on the in-cylinder process. Parameter r_c also has an effect on the SOC condition (point 2) not only through p_2 and T_2 (Figure 3.14 (a) – (d)) but also V_2 (Figure 3.14 (f)). The peak pressure and temperature both increase with larger r_c value but the relative increase of p_{max} is much larger than T_{max} (Figure 3.14 (a) – (f)). When r_c decreases from V_1/V_{TDC} , the temperature after T_2 first goes down and then rises up to T_3 along with an irregular change of T - s during stage 2-3 (Figure 3.14 (h)). From these figures it is concluded that r_c affects stage 5-6 only slightly because V_6 is fixed

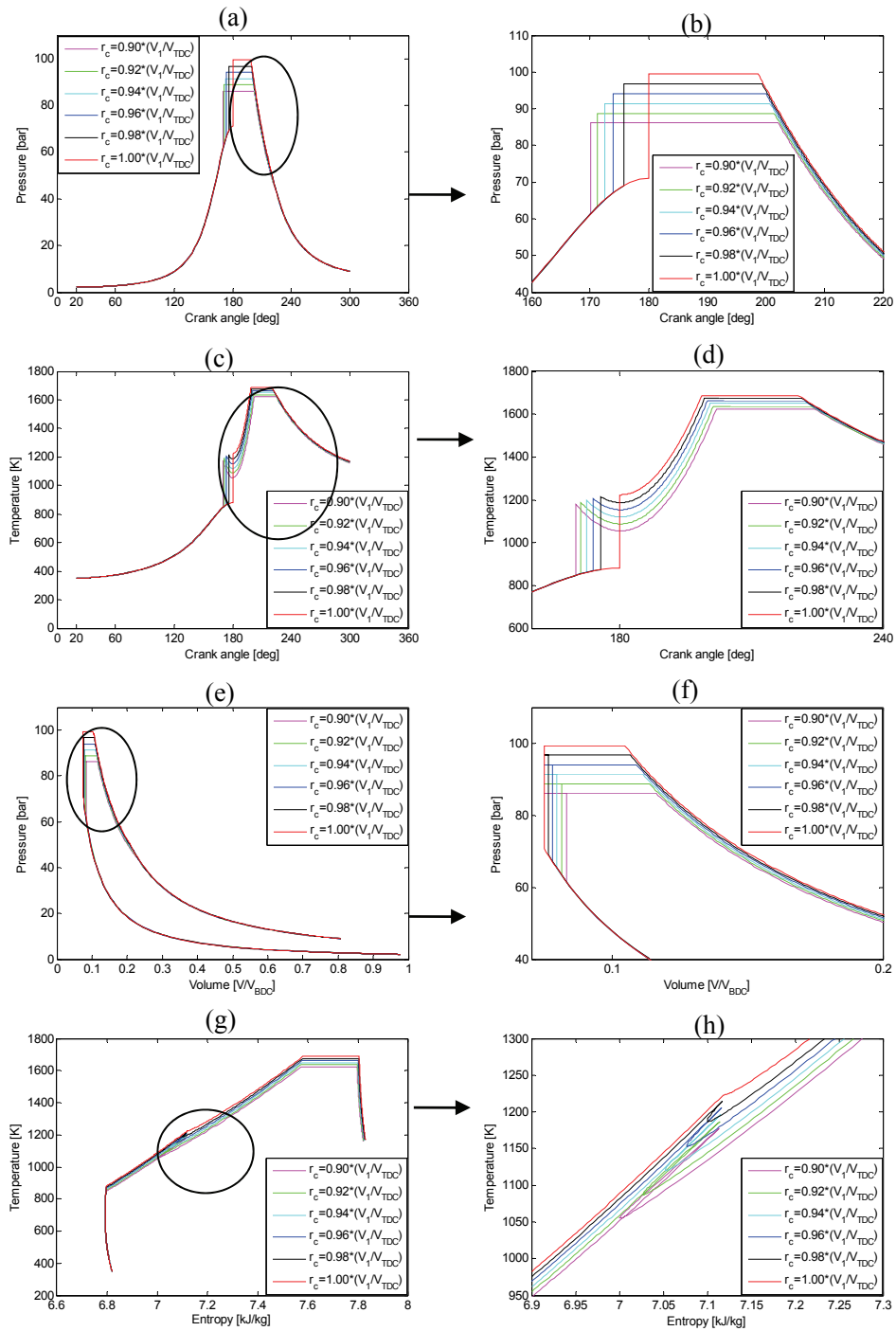


Figure 3.14 Influence of parameter r_c to in-cylinder process

by $\Delta EO = 0$ and V_5 increases with decreasing r_c resulting in a lower r_e but p_5 and T_5 both decrease.

Figure 3.15 shows the influence of Seiliger parameter ΔEO on the in-cylinder process. ΔEO is used to virtually delay or advance the exhaust valve opening timing in order to vary the duration of the expansion. It is obvious that from point 1 to point 5 there is no change, as shown in Figure 3.15, and the curves are overlapping in stage 5-6 except for the final part. Although ΔEO affects the in-cylinder process hardly, it has influence on the work per cycle and will change T_{EO} and p_{EO} .

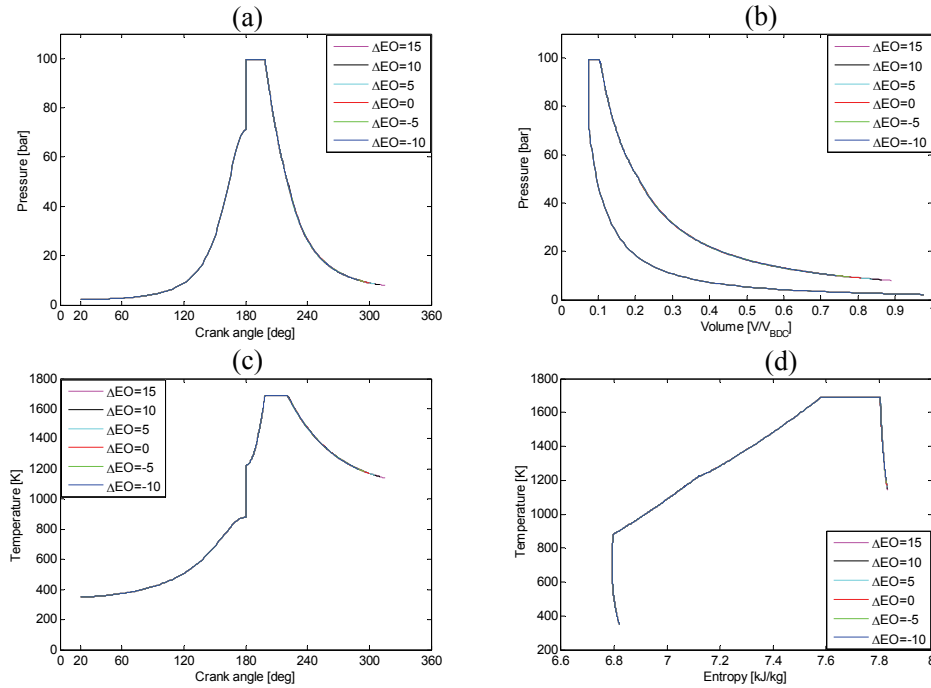


Figure 3.15 Influence of parameter r_e (ΔEO) to in-cylinder process

According to the parametric representation of the combustion in the Seiliger process, parameter a can be loosely associated with the premix combustion while parameters b , c and n_{exp} play the role of the diffusive and late combustion, in particular parameter n_{exp} represents the *very* late combustion.

There are some special cases of the *advanced* Seiliger process model. If n_{exp} indicates a heat loss process, the *advanced* model becomes the *basic* six-point Seiliger process. If, in addition, $c = 1$, the *basic* Seiliger process becomes the ordinary 5-point dual Seiliger

process. If $a = 1$ and $c = 1$, the cycle will reduce to the ideal 4-point ‘Diesel’ process. And if $a = 1$ and $b = 1$, the cycle will reduce to the ideal 4-point ‘Otto’ process.

Table 3.5 summarizes the Seiliger parameters for different numbers of finite combustion stages. It is noted that the difference of *basic* and *advanced* Seiliger process is whether there is combustion in stage 5-6, i.e. the parameter n_{exp} indicates a heat *loss* process or a net heat *input* process. It is obvious from Table 3.5 that in all the *advanced* Seiliger process, n_{exp} is a combustion parameter to indicate a very late combustion, and in the *basic* Seiliger process, n_{exp} is not included in the combustion parameters but only determines the heat loss during expansion. The numbers in the bracket mean the total stages of the closed cycle. For the *basic* Seiliger process, the difference between this number and the combustion stages is two, meaning two heat loss processes (during compression and expansion respectively). For advanced Seiliger process, the difference is only one.

- (1) One combustion stage: only one parameter is used to describe the combustion. If only b is used, the cycle is a ‘Diesel’ process; if only a is used, the cycle is an ‘Otto’ process. The other two cases – only combustion at constant temperature or combustion only during expansion – are very unlikely to occur in a measured engine cycle.
- (2) Two combustion stages: now there are six cases, three for the *basic* Seiliger process and three for the *advanced* process. The case of using parameters a and b for the two combustion stages is the standard ‘dual’ combustion cycle, as presented in [Klein Woud, 2002] and [Moran, 2003].
- (3) Three combustion stages: there is one case corresponding to the *basic* Seiliger process, which is the Seiliger process as presented in [Stapersma, 2002a]. The other three cases are based on the *advanced* Seiliger process.
- (4) Four combustion stages: there is only one possibility, corresponding to the *advanced* Seiliger process including four combustion stages.

When the Seiliger process is fitted to a measured engine cycle, the combustion stages could be selected on the basis of engine type, engine running condition, etc. On the other hand, the number of finite combustion stages (in fact the number of Seiliger parameters) determine the number of features that can be made equal for the measured cycle and the Seiliger model cycle, i.e. the equivalence criteria that will be introduced in the next chapter.

Table 3.5 Summary of finite combustion stages

Combustion stages	Basic Seiliger process			Advanced Seiliger process		
	1	a (3)*	b (3)	c (3)	n_e (2)	
2	a, b (4)	a, c (4)	b, c (4)	a, n_e (3)	b, n_e (3)	c, n_e (3)
3	a, b, c (5)			a, b, n_e (4)	a, c, n_e (4)	b, c, n_e (4)
4				a, b, c, n_e (5)		

* the number in the bracket means total stages of in-cylinder process

3.3 Fitting measured engine cycle with Seiliger process

The Seiliger process provides an efficient and simple way to describe the engine closed cycle. On the one hand the Seiliger process can be used to model the in-cylinder process when the Seiliger parameters are known. On the other hand the Seiliger process, or rather some Seiliger parameters can be used to fit the measured engine cycle when equivalence criteria are established. Then the trend of the Seiliger parameters as a function of the engine load and speed can be investigated and the combustion process over the whole engine operating range can be characterized in terms of the Seiliger parameters.

3.3.1 Determine equivalence criteria and suitable Seiliger parameters

In order to fit the Seiliger process to the real diesel engine cycle, equivalence criteria must be selected first, as these are the objectives of the fit, and then their relation with the Seiliger parameters must be established. Equivalence criteria relate the Seiliger process to the measured engine parameters that are deemed important. Therefore they should be selected to cover the engine performance as fully as possible. Table 3.6 lists the equivalence criteria of the engine closed-cycle performance along with their (subjective) significance level.

Table 3.6 Equivalence criterion

p_{max}	****
T_{max}	*
Q_{in}	****
W_i	****
T_{EO}	***

W_i, Q_{in} – Work and heat input are the main indicator of the engine output. Their ratio is the efficiency of cycle, which is the most important parameter to evaluate the engine performance. Therefore they are at the highest (the fourth) significance level.

p_{max} – Maximum pressure represents the mechanical load of the engine. For example in crankshaft, connecting rod and cylinder head strength calculation, p_{max} is very

important to determine the maximum stresses caused by the cylinder process. Therefore it is at the fourth significance level as well.

T_{EO} – Temperature at exhaust valve opens is the last point of in-cylinder process and defines the starting point of gas exchange process, in particular the blow down process. As such it determines for a large part the temperature of the gas that enters the turbine, which has a strong impact on the performance of turbine. Therefore it is at a relative high (the third) significance level. In addition, the pressure at EO point can also be considered as a criterion. Since p_{EO} and T_{EO} are both related by gas law and mass is constant, only one of them is used as equivalence criterion.

T_{max} – Maximum temperature represents the thermal load of the engine. However, it occurs during such a short time that it hardly affects wall temperature but it may affect emissions. It is put at the lowest significance level.

The maximum pressure is expressed according to the Seiliger process definition:

$$p_{max} = p_1 \cdot r_c^{n_{comp}} \cdot a \quad [3.19]$$

The maximum temperature can be expressed in equation [3.20] when the mass addition is neglected (otherwise the gas law should be used to calculate the T_{max}):

$$T_{max} = T_1 \cdot r_c^{n_{comp}-1} \cdot a \cdot b \quad [3.20]$$

The temperature at EO is expressed in equation [3.21], again the mass addition is neglected. The parameter r_{26} is a non-dimensional volume ratio defined in equation [3.3]:

$$\begin{aligned} T_{EO} &= \frac{T_5}{r_e^{n_{exp}-1}} \\ &= T_1 \cdot r_c^{n_{comp}-1} \cdot a \cdot b \cdot \left(\frac{V_6}{b \cdot c \cdot V_2} \right)^{1-n_{exp}} \\ &= T_1 \cdot r_c^{n_{comp}-1} \cdot a \cdot b \cdot \left(b \cdot c \cdot \frac{V_2}{r_6} \right)^{n_{exp}-1} \\ &= T_1 \cdot r_c^{n_{comp}-1} \cdot a \cdot b^{n_{exp}} \cdot c^{n_{exp}-1} \cdot r_{26}^{n_{exp}-1} \end{aligned} \quad [3.21]$$

The specific net heat input for the three stages of combustion based on *basic* Seiliger process is:

$$\begin{aligned}
 q_{in} &= q_{23} + q_{34} + q_{45} \\
 &= c_{v,23} \cdot T_1 \cdot r_c^{n_{comp}-1} \cdot (a-1) + c_{v,34} \cdot T_1 \cdot \gamma \cdot r_c^{n_{comp}-1} \cdot a \cdot (b-1) \\
 &\quad + c_{v,45} \cdot T_1 \cdot (\gamma-1) \cdot r_c^{n_{comp}-1} \cdot a \cdot b \cdot \ln c
 \end{aligned} \tag{3.22}$$

If there is combustion during last stage 5-6 (the *advanced* Seiliger process), the specific net heat input is:

$$\begin{aligned}
 q_{in} &= q_{23} + q_{34} + q_{45} + q_{56} \\
 &= c_{v,23} \cdot T_1 \cdot r_c^{n_{comp}-1} \cdot (a-1) + c_{v,34} \cdot T_1 \cdot \gamma \cdot r_c^{n_{comp}-1} \cdot a \cdot (b-1) \\
 &\quad + c_{v,45} \cdot T_1 \cdot (\gamma-1) \cdot r_c^{n_{comp}-1} \cdot a \cdot b \cdot \ln c \\
 &\quad + c_{v,56} \cdot T_1 \cdot \left(1 - \frac{\gamma-1}{n_{exp}-1}\right) \cdot r_c^{n_{comp}-1} \cdot a \cdot b \cdot \left(1 - b^{n_{exp}-1} \cdot c^{n_{exp}-1} \cdot r_{26}^{n_{exp}-1}\right)
 \end{aligned} \tag{3.23}$$

It is noted here that the *net* heat input in the Seiliger process (q_{in}) has *no* relation to heat loss to the walls (refer to section 2.3). Therefore the correction of the Woschni heat loss model (refer to section 2.3.3.5) is not necessary in the Seiliger fit models. However, the equivalence criteria of the Seiliger fit are all taken directly from chapter 2, so in this chapter, the correction of the Woschni model is included, but in chapter 4 it is not considered anymore when analysing all the measurements.

The specific work of the closed cycle based on the Seiliger process definition is:

$$\begin{aligned}
 w_i &= w_{12} + w_{34} + w_{45} + w_{56} \\
 &= -c_{v,12} \cdot T_1 \cdot \frac{\gamma-1}{n_{comp}-1} \left(1 - r_c^{n_{comp}-1}\right) + c_{v,34} \cdot T_1 \cdot (\gamma-1) \cdot r_c^{n_{comp}-1} \cdot a \cdot (b-1) \\
 &\quad + c_{v,45} \cdot T_1 \cdot (\gamma-1) \cdot r_c^{n_{comp}-1} \cdot a \cdot b \cdot \ln c \\
 &\quad + c_{v,56} \cdot T_1 \cdot \frac{\gamma-1}{n_{exp}-1} \cdot r_c^{n_{comp}-1} \cdot a \cdot b \cdot \left(1 - b^{n_{exp}-1} \cdot c^{n_{exp}-1} \cdot r_{26}^{n_{exp}-1}\right)
 \end{aligned} \tag{3.24}$$

When expressing the equivalence criteria as functions of the Seiliger parameters (equation [3.19] – [3.24]), some parameters can be assumed constant since their influence is not significant or they do not change too much with engine running condition (e.g. gas properties c_v , γ). Nevertheless in a time domain simulation environment, the gas properties can be calculated based on the (mean) temperature in the different Seiliger stages.

Some parameters have a complex implication on the equivalence criteria and they cannot be determined in a straightforward manner for varying engine running conditions (i.e. a , b and c). Six Seiliger parameters, which have been introduced in the last section, are listed in Table 3.7 along with a rating representing the significance level of the corresponding parameter.

Table 3.7 Seiliger parameters

a	ΔΔΔΔ
b	ΔΔΔΔ
c	ΔΔΔΔ
n_{comp}	Δ
r_c	Δ
n_{exp}	ΔΔΔ
ΔEO	ΔΔ

Firstly, Seiliger parameters a , b and c represent the main part of the combustion process and thus are the most important (fourth significance level). The expansion exponent n_{exp} also indicates the combustion process of stage 5-6 but it only supplies a small amount of very late combustion and in most cases only represents the heat loss during expansion. So, it is set at the third significance level. The virtual shift of the angle at which the exhaust opens, ΔEO , is set at the second significance level due to its effect only on work and hardly on the other equivalence criteria. Parameter n_{comp} can be determined according to experience and does not vary much with engine working condition. Parameter r_c is geometrically determined and would be constant (although it has been considered to make r_c variable in order to simulate late start of combustion). These two parameters are set at the lowest significance level.

3.3.2 Numerical method implementation and calculation procedure

After selecting equivalence criteria and Seiliger parameters, a system of equations can be determined on the basis of equation [3.19] – [3.24]. Since in most cases the system of equations is non-linear, a numerical root finding method (i.e. Bisection method, Secant method, Newton-Raphson method, etc.) needs to be used. When more variables (Seiliger parameters) are chosen, the system of equivalence criteria becomes

a multi-variable function and the Newton-Raphson method is a suitable way to find the roots of the system of equations.

First the Newton-Raphson method applied for a single variable function is briefly introduced. If the initial estimate of the root is x_n , a tangent can be extended from the point $[x_n, f(x_n)]$. The point where this tangent crosses the x-axis represents an improved estimate of the root. The first derivative $f'(x_n)$ is equivalent to the slope of the tangent and can be derived on the basis of a geometrical interpretation (Figure 3.16) and an iteration scheme is constructed:

$$f'(x_n) = \frac{f(x_n) - 0}{x_n - x_{n+1}} \quad [3.25]$$

Then

$$x_{n+1} = x_n - \frac{f(x_n)}{f'(x_n)} \quad [3.26]$$

While $|x_{n+1} - x_n| \leq \textit{tolerance}$, the x_{n+1} can be considered to be the root of function $f(x)$.

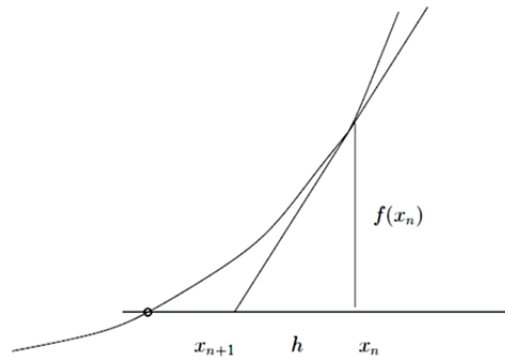


Figure 3.16 Graphical description of Newton-Raphson method [Otto, 2005]

Furthermore, the Newton-Raphson method can be used to acquire the solution for a multi-variable function, $\mathbf{f}(\mathbf{x})$. If the zero was considered to occur at $\mathbf{x} = \mathbf{x}^*$, where \mathbf{x}^* is a vector, then the Taylor series for multi-variable function is applied. If \mathbf{x}_n is assumed to be the current estimation of the functions and $\mathbf{x}_{n+1} = \mathbf{x}_n + \mathbf{h}$, due to the demand that $\mathbf{f}(\mathbf{x}^*) = \mathbf{0}$, the Taylor series is acquired:

$$\mathbf{f}(\mathbf{x})|_{\mathbf{x}=\mathbf{x}_{n+1}} = \mathbf{f}(\mathbf{x}_n + \mathbf{h}) = \mathbf{f}(\mathbf{x}_n) + \nabla \mathbf{f}|_{\mathbf{x}_n} \cdot \mathbf{h} + o(|\mathbf{h}|^2) = \mathbf{0} \quad [3.27]$$

If $o(|\mathbf{h}|^2)$ is assumed small enough to neglect, equation 3.26 becomes:

$$\mathbf{f}(\mathbf{x}_n) = -\nabla \mathbf{f}|_{\mathbf{x}_n} \cdot \mathbf{h} \quad [3.28]$$

When $-\nabla \mathbf{f}|_{\mathbf{x}_n}$ is replaced by matrix \mathbf{A} :

$$\mathbf{h} = -\mathbf{A}^{-1} \cdot \mathbf{f}(\mathbf{x}_n) \quad [3.29]$$

$$\mathbf{A} = \begin{bmatrix} \frac{\partial f_1}{\partial x_1} & \frac{\partial f_1}{\partial x_2} & \dots & \frac{\partial f_1}{\partial x_n} \\ \frac{\partial f_2}{\partial x_1} & \frac{\partial f_2}{\partial x_2} & \dots & \frac{\partial f_2}{\partial x_n} \\ \vdots & \vdots & \ddots & \vdots \\ \frac{\partial f_n}{\partial x_1} & \frac{\partial f_n}{\partial x_2} & \dots & \frac{\partial f_n}{\partial x_n} \end{bmatrix} \text{ and } \mathbf{f}(\mathbf{x}) = \begin{bmatrix} f_1(x_1, x_2, \dots, x_n) \\ f_2(x_1, x_2, \dots, x_n) \\ \vdots \\ f_n(x_1, x_2, \dots, x_n) \end{bmatrix} \quad [3.30]$$

Finally the next estimate of \mathbf{x}_{n+1} is obtained and used as the initial value of the next iteration and the iteration is terminated when the stop criteria are met.

The Newton-Raphson multi-variable root finding method is applied to find the solution for the fitting of the (real) engine equivalence values by means of varying Seiliger process parameters. The case with five equivalence criteria as functions of five variables (Seiliger parameters) is taken as an example. The differences between the calculated result from the equivalence criteria functions of the Seiliger process and the measured engine cycle are the functions for which the zero has to be found:

$$f_1(x_1, x_2, x_3, x_4, x_5) = q_{in} - q_{in,th} \quad [3.31]$$

$$f_2(x_1, x_2, x_3, x_4, x_5) = w_i - w_{i,th} \quad [3.32]$$

$$f_3(x_1, x_2, x_3, x_4, x_5) = p_2 - p_{max} \quad [3.33]$$

$$f_4(x_1, x_2, x_3, x_4, x_5) = T_4 - T_{\max} \quad [3.34]$$

$$f_5(x_1, x_2, x_3, x_4, x_5) = T_6 - T_{\text{end}} \quad [3.35]$$

The five functions are set to a column vector as **func**:

$$\mathbf{func} = [f_1, f_2, f_3, f_4, f_5] \quad [3.36]$$

A matrix **PDE** then is set to solve the derivatives:

$$\mathbf{PDE} = \begin{bmatrix} \frac{\partial f_1}{\partial x_1} & \dots & \frac{\partial f_1}{\partial x_5} \\ \vdots & \ddots & \vdots \\ \frac{\partial f_5}{\partial x_1} & \dots & \frac{\partial f_5}{\partial x_5} \end{bmatrix} \quad [3.37]$$

$$\mathbf{Vect} = -\mathbf{PDE} \backslash \mathbf{func} \quad [3.38]$$

Vect is the increment or decrement of the root that is obtained from the previous step:

$$x_i = x_i + \mathbf{Vect}(i) \quad i = 1, 2, 3, 4, 5 \quad [3.39]$$

The partial derivatives of the elements in matrix **PDE** are obtained with numerical analysis rather than with an analytical method. The latter is impossible because some parameters in equivalence criteria functions (equation [3.19] – [3.24]) are interdependent, e.g. in equation [3.24], $c_{v,34}$ is determined by T_3 , T_4 and the air fraction in stage 3-4, all of which are also influenced by parameters a and b . Therefore a numerical method is used to avoid this problem.

Variable x_i is changed one percent and then the partial derivatives are obtained relying on the local linearity.

$$\Delta x_i = 0.01x_i \quad i = 1, 2, 3, 4, 5 \quad [3.40]$$

$$\frac{\partial f_i}{\partial x_j} = \frac{f(x_j + \Delta x_j, \dots) - f(x_j, \dots)}{\Delta x_j} \quad i = 1, 2, 3, 4, 5; \quad j = 1, 2, 3, 4, 5 \quad [3.41]$$

3.3.3 Fit versions with three Seiliger parameters

Among the equivalence criteria and Seiliger parameters, a number of equivalence criteria can be selected and then a choice of appropriate Seiliger parameters is made, or vice versa, refer to table 3.28 for an overview. Note that the number of them must be equal in order to solve the system of equations. First the simplest version – three Seiliger parameters – is introduced. In these fit versions, the three most significant Seiliger parameters a , b and c are set as variables and three equivalence criteria are selected to derive the system of equations to find the solutions for the corresponding a , b and c .

1) V3-1 (Equivalence criteria: p_{max} , T_{max} and Q_{in} ; Seiliger parameters: a , b and c)

In this version the equivalence criteria are p_{max} , Q_{in} and T_{max} , to be fitted with Seiliger parameters a , b and c . As to the other Seiliger parameters, n_{comp} , r_c and ΔEO (refer Table 3.28), they are set to the base value presented in section 3.3.2 (also in Table 3.10). The expansion exponent n_{exp} is set to be constant and the $\eta_{pol,exp}$ in equation [3.13] is used to restrict the value of n_{exp} to indicate heat loss process, i.e. there is no combustion in stage 5-6, so it is the *basic* Seiliger process.

In this fit version **V3-1** the indicated work W_i is not an equivalence criterion resulting in a cycle efficiency of the Seiliger process that is not necessarily equal to the measured engine cycle. The system of equations between equivalence criteria and Seiliger parameters of **V3-1** on the basis of the advanced Seiliger process definition are as follows:

$$p_{max} = p_1 \cdot r_c^{n_{comp}} \cdot a = \boxed{M_1 \cdot a} \quad [3.42]$$

$$T_{max} = T_1 \cdot r_c^{n_{comp}-1} \cdot a \cdot b = \boxed{M_2 \cdot a \cdot b} \quad [3.43]$$

$$\begin{aligned} q_{in} &= q_{23} + q_{34} + q_{45} \\ &= c_v \cdot T_1 \cdot r_c^{n_{comp}-1} \cdot (a-1) + c_v \cdot T_1 \cdot \gamma \cdot r_c^{n_{comp}-1} \cdot a \cdot (b-1) \\ &\quad + c_v \cdot T_1 \cdot (\gamma-1) \cdot r_c^{n_{comp}-1} \cdot a \cdot b \cdot \ln(c) \\ &= \boxed{M_3 \cdot (a - a \cdot b \cdot \ln(c)) + M_3 \cdot \gamma \cdot (a \cdot b - a + a \cdot b \cdot \ln(c)) - M_3} \end{aligned} \quad [3.44]$$

In equation [3.42] – [3.44], the constants (M_1 , M_2 and M_3) can be obtained from the constant Seiliger parameters n_{comp} , r_c , ΔEO , n_{exp} and the gas properties. This set of

three equations is relative simple to solve using the elimination method. However the universal Newton-Raphson method is applied to find the roots of the equations and the numerical calculation converges as expected. In this version, n_{comp} and n_{exp} are both set to be constant and the limiting of the values is based on $\eta_{pol,comp}$ and $\eta_{pol,exp}$ respectively. If $\eta_{pol,comp}$ and $\eta_{pol,exp}$ are both larger than unity, the n_{comp} and n_{exp} can be accepted. Otherwise the exponents are adjusted until these demands are met.

The stop criteria of the iteration in the Newton-Raphson method are:

$$|p_3 - p_{max}| \leq 1\text{bar}, |T_4 - T_{max}| \leq 1\text{K}, |Q_{in,Seiliger} - Q_{in,measured}| \leq 10 \text{ J} \quad [3.45]$$

The three measured engine operating points defined in Section 2.3.3 are also used to investigate the Seiliger fit version. These points were: (A) the nominal point: 1000 rpm, 100% power; (B) a point along the generator curve: 1000 rpm, 25% power; (C) a point along the propeller curve: 800 rpm, 50% power. Table 3.8 lists the values of equivalence criteria from smoothed measurement.

Table 3.8 The equivalence criteria of smoothed measurement

	p_{max}	T_{max}	Q_{in}	W_i	T_{EO}
point (A)	93.19 bar	1513.58 K	21.52 kJ	10.01 kJ	1119.60 K
point (B)	61.73 bar	1340.10 K	5.71 kJ	3.05 kJ	673.47 K
point (C)	82.19 bar	1641.24 K	14.23 kJ	7.16 kJ	1058.18 K

Table 3.9 lists the γ value of Seiliger fit version **V3-I** together with the selected polytropic exponents and resulting polytropic factors.

Table 3.9 Selection of polytropic exponents of the three operation points

	γ_{comp}	n_{comp}	$\eta_{pol,comp}$	γ_{exp}	n_{exp}	$\eta_{pol,exp}$
point (A)	1.368	1.360	1.022	1.294	1.31	1.054
point (B)	1.370	1.360	1.028	1.329	1.33	1.003
point (C)	1.370	1.360	1.028	1.300	1.31	1.033

In Table 3.10 and Table 3.11, the results of the Seiliger parameters after fitting to the measured cycle are illustrated together with the error analysis of the equivalence criteria used in this version and the absolute and relative difference of unused equivalence criteria. Table 3.11 summarizes the heat input ratio of different Seiliger stages of **V3-I**. Figure 3.17 – Figure 3.19 show the comparison of the **V3-I** fit results with the raw and the smoothed measurements. For the three operating points, the

indicated work W_i of point (A) and (C) are both about 3.6% larger than measured but point (B) is about 2.0% smaller. T_{EO} of the Seiliger fit is around 4.5% – 6.5% smaller than measured for all three points.

Table 3.10 Results of Seiliger fit version V3-1

Seiliger Parameter	Value	EC*	Relative Error (%)	Difference ^{&} Absolute	Relative	
Constant	n_{comp}	1.36				
	r_c	13.1073				
	ΔEO	0				
(A)	Variable	a	1.3129	p_{max}	0	
		b	1.3362	T_{max}	$4.831 * 10^{-5}$	
		c	2.6250	Q_{in}	$8.465 * 10^{-5}$	
	Constant	n_{exp}	1.31	W_i		363.213 J 3.63%
				T_{EO}		-52.428 K -4.68%
(B)	Variable	a	1.5281	p_{max}	0	
		b	1.0444	T_{max}	$9.791 * 10^{-5}$	
		c	1.1408	Q_{in}	$4.012 * 10^{-4}$	
	Constant	n_{exp}	1.33	W_i		-63.571 J -2.09%
				T_{EO}		-40.692 K -6.04%
(C)	Variable	a	1.7842	p_{max}	0	
		b	1.1088	T_{max}	$3.838 * 10^{-5}$	
		c	1.9272	Q_{in}	$6.958 * 10^{-5}$	
	Constant	n_{exp}	1.31	W_i		257.624 J 3.60%
				T_{EO}		-65.759 K -6.21%

* EC here means Equivalence Criteria

& the difference is the equivalence criteria of Seiliger fit minus smoothed measurement

Table 3.11 Heat input ratio of V3-1

	$Q_{23,ratio}$	$Q_{34,ratio}$	$Q_{45,ratio}$
point (A)	0.2080	0.4076	0.3844
point (B)	0.7639	0.1343	0.1019
point (C)	0.5300	0.1813	0.2887

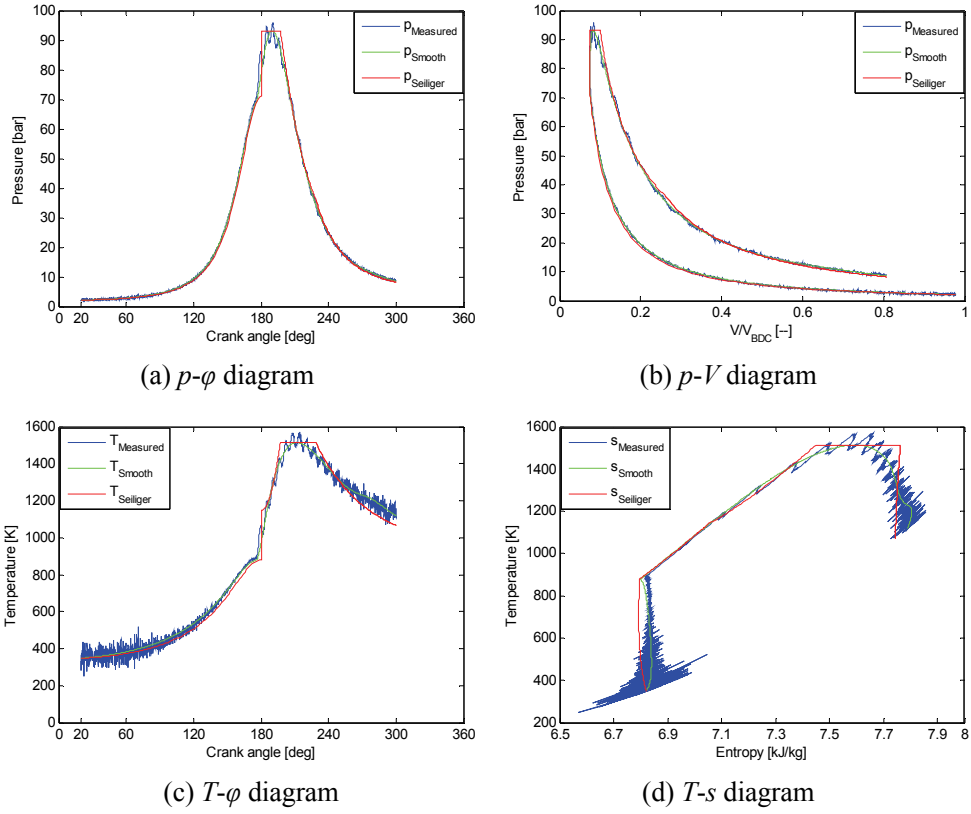
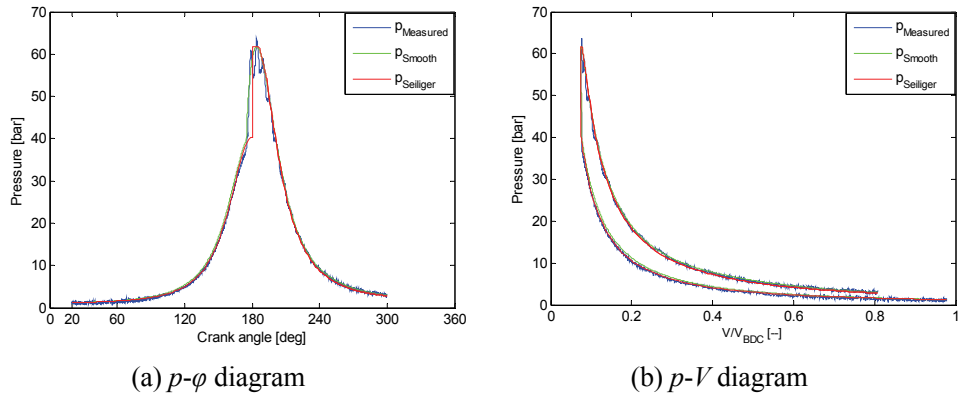


Figure 3.17 Comparison of Seiliger fit ($V3-I$) with raw and smoothed measurement (point (A))



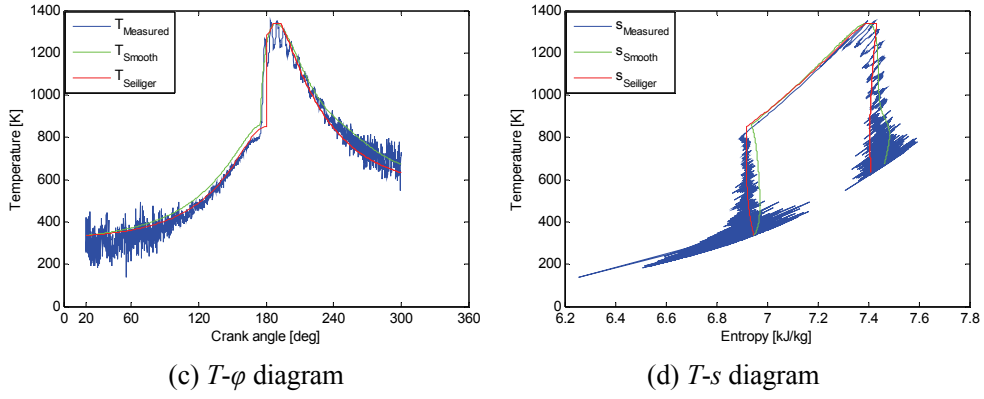


Figure 3.18 Comparison of Seiliger fit ($V3-I$) with raw and smoothed measurement (point (B))

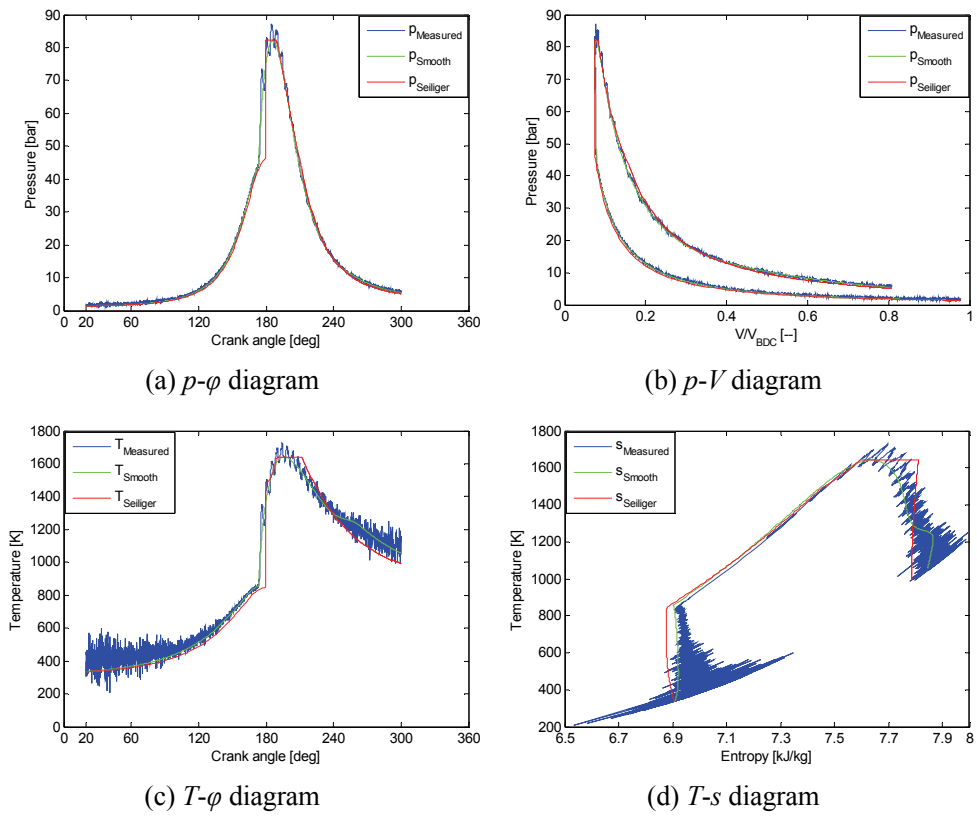


Figure 3.19 Comparison of Seiliger fit ($V3-I$) with raw and smoothed measurement (point (C))

V3-1 is a simple fit version as a , b and c can also be directly calculated by equation [3.42] – [3.44] respectively. This is one of the reasons why most earlier research of Seiliger parameters in the mean value diesel engine model was based on **V3-1**.

The main drawback of this version is that the cycle efficiency is not consistent with the measured cycle. However due to the simple calculation with no need of iteration it provides an efficient way to investigate the effect of Seiliger parameters.

2) V3-2 (Equivalence criteria: p_{max} , Q_{in} and W_i ; Seiliger parameters: a , b and c)

In this version the equivalence criteria are the most significant three: p_{max} , Q_{in} and W_i , along with Seiliger parameters a , b and c (refer Table 3.28). The other Seiliger parameters are selected to be the same as in **V3-1**. Due to the inclusion of indicated work W_i in this version the theoretical engine efficiency is now equal to that of the measured engine. The system of equations between equivalence criteria and Seiliger parameters of **V3-2** according to Seiliger process definition can be expressed based on equation [3.19], [3.22] and [3.24].

The first two equations are the same as **V3-1** and the third one on w_i is more complicated, in fact the system cannot be solved explicitly anymore. The Newton-Raphson method is applied to find the roots of the equations and the numerical calculation is converging. The stop criteria for the iteration are:

$$\begin{aligned} |p_3 - p_{max}| &\leq 1 \text{ bar}, |Q_{in,Seiliger} - Q_{in,measured}| \leq 10 \text{ J} \\ \text{and } |W_{i,Seiliger} - W_{i,measured}| &\leq 10 \text{ J} \end{aligned} \quad [3.46]$$

The fit results and error analysis are shown in Table 3.12, Table 3.13 and Figure 3.20 – Figure 3.22. The parameter a is the same as for **V3-1** because a is the only variable influencing p_{max} . Because in the equivalence criteria T_{max} is replaced by W_i , the parameter b of all the three points is smaller than in **V3-1**. In point (B) the value of b is smaller than unity, which would indicate that during stage 3-4, the heat input of the (combustion) process is changing into a heat loss (Figure 3.21(d)). This is of course impossible but the numerical method finds this solution anyway, albeit that it is outside the initially allowed range of the roots. The ‘unrealistic’ b is accepted in this fit version but in the **V4** Seiliger fit version this issue will be considered in more detail and a way will be presented to avoid these ‘unrealistic’ b values. The constant parameter n_{exp} of point (B), initially was set to be 1.34 instead of 1.33 (i.e. the heat loss during stage 5-6 is -278.30 J instead of -25.06 J), but in that case the iteration is

not converging. This is caused by the sensitivity of the equivalence criterion W_i for n_{exp} .

The unused equivalence criteria T_{EO} and T_{max} are also presented in Table 3.12. The T_{EO} for all three operating points is approximately 2% – 4% lower than measured. The T_{max} of the three points is around 5% – 10% lower than the smoothed data. Nevertheless in the Seiliger process T_{max} is maintained for a longer time than in the real case, where it occurs only during a very short time. Therefore, it is reasonable to regard T_{max} in Seiliger process as the mean value of the temperature in the real cycle during the period corresponding to Seiliger stage 3-4, and a lower value is acceptable.

Table 3.12 Results of Seiliger fit version V3-2

Seiliger Parameter		Value	EC*	Relative Error (%)	Difference ^{&}		
					Absolute	Relative	
Constant	n_{comp}	1.36					
	r_c	13.1073					
	ΔEO	0					
(A)	Variable	a	1.3129	p_{max}	0		
		b	1.2598	W_i	$2.270 \cdot 10^{-2}$		
		c	3.5710	Q_{in}	$1.954 \cdot 10^{-2}$		
	Constant	n_{exp}	1.31	T_{EO}		-29.439 K	-2.63%
				T_{max}		-82.192 K	-5.43%
(B)	Variable	a	1.5281	p_{max}	0		
		b	0.9725	W_i	0.1733		
		c	1.5521	Q_{in}	0.1698		
	Constant	n_{exp}	1.33	T_{EO}		-20.172 K	-3.00%
				T_{max}		-88.342 K	-6.59%
(C)	Variable	a	1.7842	p_{max}	$2.209 \cdot 10^{-14}$		
		b	1.0103	W_i	$1.471 \cdot 10^{-2}$		
		c	3.0848	Q_{in}	$2.091 \cdot 10^{-2}$		
	Constant	n_{exp}	1.31	T_{EO}		-36.577 K	-3.46%
				T_{max}		-138.293 K	-8.43%

* EC here means Equivalence Criterion

& the difference is the equivalence criteria of Seiliger fit minus smoothed measurement

Table 3.13 Heat input ratio of *V3-2*

	$Q_{23,ratio}$	$Q_{34,ratio}$	$Q_{45,ratio}$
point (A)	0.2080	0.3132	0.4788
point (B)	0.7642	-0.0815	0.3173
point (C)	0.5300	0.0172	0.4528

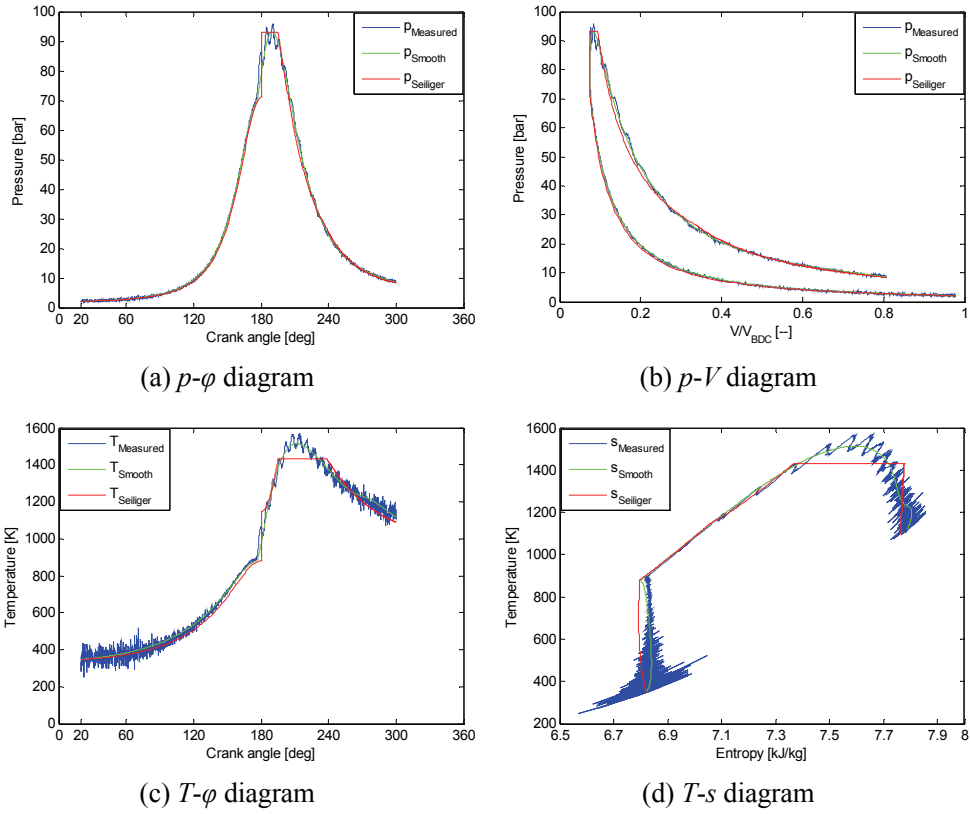


Figure 3.20 Comparison of Seiliger fit (*V3-2*) with raw and smooth measurement (point (A))

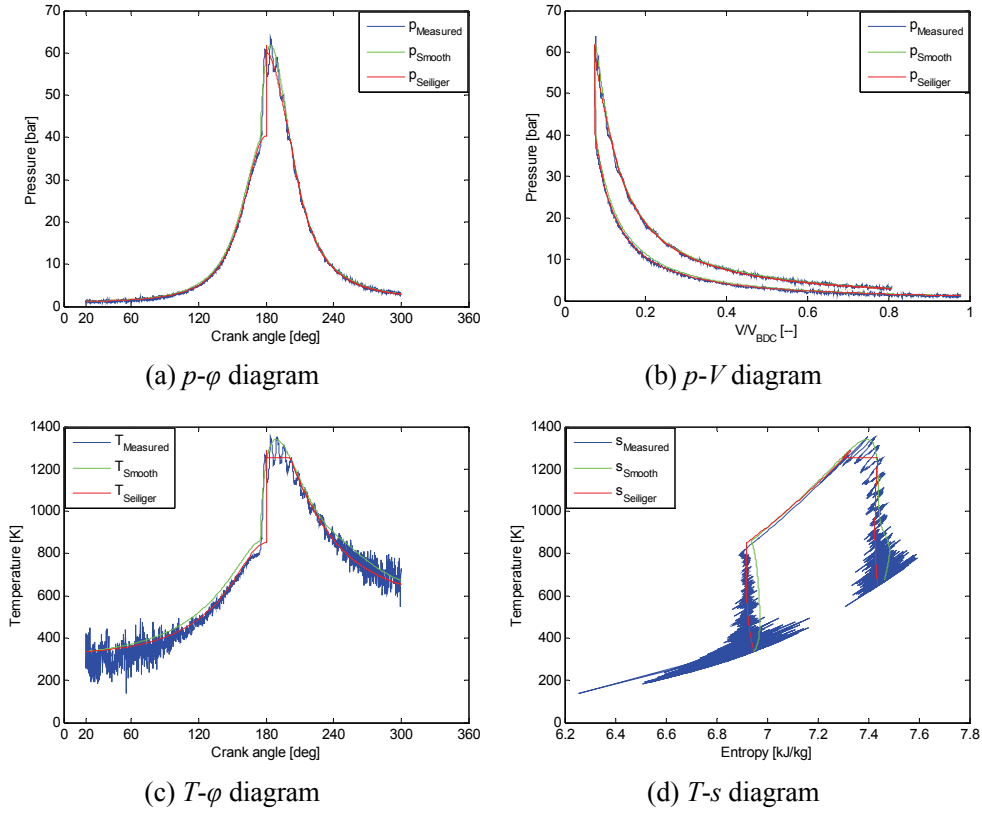
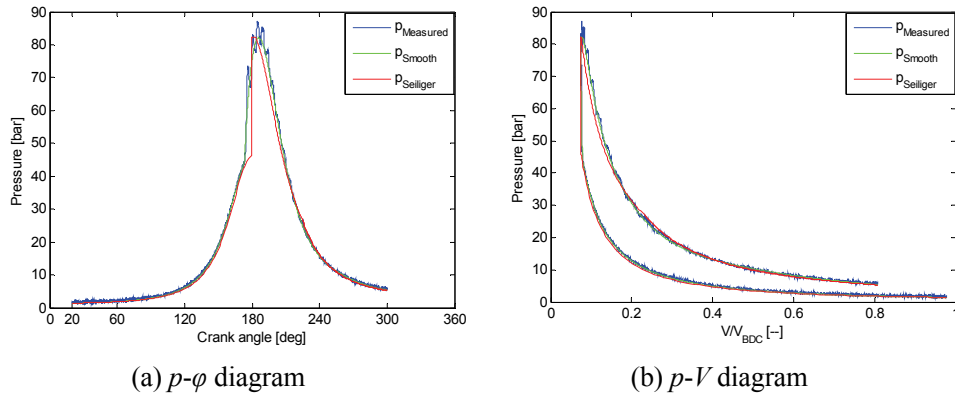


Figure 3.21 Comparison of Seiliger fit (V3-2) with raw and smooth measurement (point B)



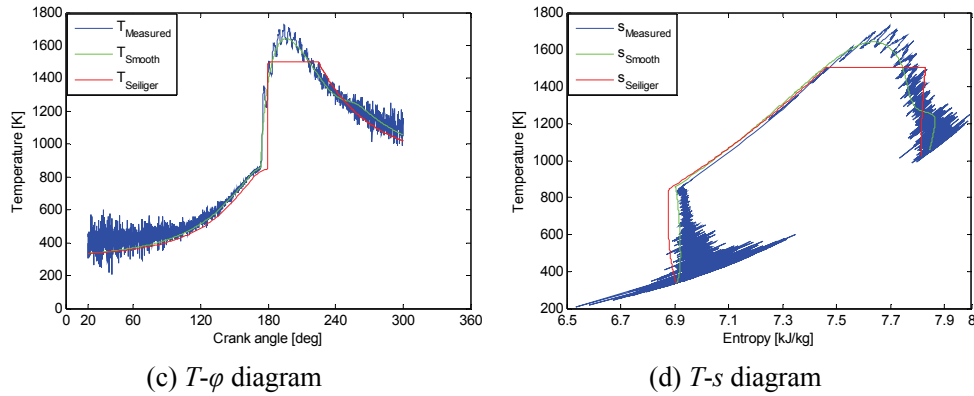


Figure 3.22 Comparison of Seiliger fit ($V3-2$) with raw and smooth measurement (point (C))

In order to avoid the ‘unrealistic’ $b < 1$ in $V3-2$ at part load, a new fit version $V3-2-1$ is introduced, which is derived from version $V3-2$. However, it is limited to two equivalence criteria W_i and Q_{in} and also only two Seiliger parameter a and c as variables, together with $b = 1$. $V3-2-1$ is only applied in cases where $b < 1$, and because this only occurs when the engine runs in part load p_{max} is eliminated from the equivalence criteria. The numerical calculation is converging and the stop criteria are the same as $V3-2$ except obviously for p_{max} .

Table 3.14 Results of Seiliger fit version $V3-2-1$

Seiliger Parameter	Value	EC*	Difference ^{&}			
			Relative Error (%)	Absolute	Relative	
Constant	n_{comp}	1.36				
	r_c	13.1073				
	ΔEO	0				
	b	1				
(B)	Variable	a	1.4926	W_i	$5.972 \cdot 10^{-2}$	
		c	1.4913	Q_{in}	$3.978 \cdot 10^{-2}$	
	Constant	n_{exp}	1.33	p_{max}	-1.434 bar	-2.32%
				T_{EO}	-20.169 K	-3.00%
				T_{max}	-83.339 K	-6.22%

* EC here means Equivalence Criterion

& the difference is the equivalence criteria of Seiliger fit minus smoothed measurement

Table 3.15 Heat input ratio of *V3-2-1*

	$Q_{23, \text{ratio}}$	$Q_{34, \text{ratio}}$	$Q_{45, \text{ratio}}$
point (B)	0.7105	0	0.2895

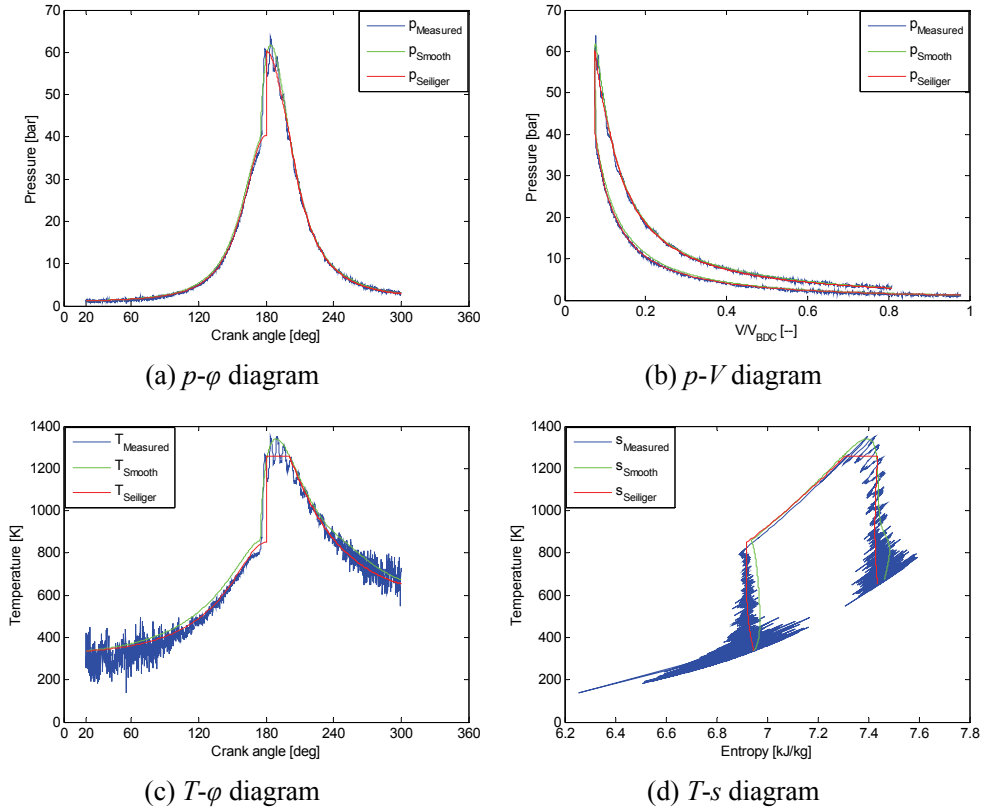

Figure 3.23 Comparison of Seiliger fit (*V3-2-1*) with raw and smooth measurement (point (B))

Table 3.14, Table 3.15 and Figure 3.23 illustrate the fit result of *V3-2-1* for point (B). Compared with the results of *V3-2*, parameter a and c are both smaller since b increased from 0.9725 to 1, resulting in an increase of the heat input during stage 3-4 and – since Q_{in} is still an equivalence criterion – the heat input during 2-3 and 4-5 must decrease. The unused equivalence criterion T_{EO} does not change because n_{exp} (which has the strongest effect on T_{EO}) remains the same. Along with the decrease of parameter a , also p_{max} is decreasing and about 2.32% lower than measured. T_{max} is higher than in *V3-2* but still about 6.22% lower than measured.

Summarising, **V3-2** uses the most significant equivalence criteria and most significant parameters to fit the Seiliger process to the measured cycle. Among others, the engine efficiency found through the Seiliger process now is consistent with measurements, which is often the most important requirement to be considered. However during fitting an unexpected error occurred where parameter b became smaller than unity at some part load operating points. Therefore **V3-2-1** was introduced to set b to 1 and use only the equivalence criteria W_i and Q_{in} to fit Seiliger parameters a and c .

3.3.4 Fit versions with four Seiliger parameters

In order to fit more equivalence criteria of a measured engine cycle with a Seiliger process, Seiliger fit versions with four variable parameters are introduced, with which there are many combinations of Seiliger parameters to fit the equivalence criteria, refer to table 3.28 for an overview. However, it was found that in some cases the system of equations on the basis of the equivalence criteria did not converge when using the Newton-Raphson method, suggesting that there may be no roots. The four Seiliger parameters fit versions **V4-1** to **V4-4**, which are based on the *basic* Seiliger process definition (i.e. there are three combustion phases, stage 2-3, stage 3-4 and stage 4-5), are sorted by commonality of the equivalence criteria. The other two versions **V4-5** and **V4-6**, which are based on the *advanced* Seiliger process (i.e. there are four combustion phases, stage 2-3, stage 3-4, stage 4-5 and stage 5-6), are presented in another section. The equivalence criteria, p_{max} , Q_{in} and W_i are in all **V4** versions, combined with either T_{EO} or T_{max} . As to the Seiliger parameters, the combustion shape parameters a , b and c are selected in all **V4** versions, combined with ΔEO or n_{exp} where the latter can either indicate heat loss (**V4-3 and V4-4**) or combustion (**V4-5 and V4-6**).

Since n_{comp} and r_c are parameters of stage 1-2, they affect all the following stages (presented in section 3.2.3, see Figure 3.13 and Figure 3.14), which makes the fit function sensitive and the numerical solution of the system of equations will easily diverge. Also they can only vary in a relative narrow range. Therefore these two parameters are not considered to be variables of choice in the **V4** versions.

1) V4-1 and V4-3 (Equivalence criteria: p_{max} , W_i , Q_{in} and T_{EO})

The equivalence criteria are p_{max} , Q_{in} and W_i and T_{EO} in the versions **V4-1** and **V4-3** and the Seiliger parameters to fulfil these objectives are selected to be (Table 3.28):

V4-1 – a , b , c and ΔEO ;

V4-3 – a , b , c and n_{exp} (n_{exp} modelling heat loss during 5-6).

The equations of equivalence criteria p_{max} and Q_{in} of the two versions are the same as in **V3-1** and **V3-2** (based on equation [3.19] and [3.22]). The other two equations (based on equation [3.21] and [3.24]) of equivalence criteria W_i and T_{EO} are the same but with different variables (Seiliger parameters).

Again it is impossible to solve the system of equations directly. Therefore the Newton-Raphson numerical method is used again to solve the system of equations. During iteration, the system of equations for **V4-3** is converging but for **V4-1** it is not converging. The stop criteria for the iteration are:

$$|p_3 - p_{max}| \leq 1 \text{ bar}, |Q_{in,Seiliger} - Q_{in,measured}| \leq 10 \text{ J}, |W_{i,Seiliger} - W_{i,measured}| \leq 10 \text{ J}$$

$$\text{and } |T_6 - T_{end}| \leq 1 \text{ K} \quad [3.47]$$

The fit results and analysis of **V4-3** is shown in Table 3.16, Table 3.17 and Figure 3.24 – Figure 3.26. Parameter a is the same as in the **V3** versions. Compared to **V3-1**, where T_{max} was explicitly used as an equivalence criterion, parameter b in **V4-3** is smaller, which results in T_{max} being considerably lower than measured. Especially in operating point (B), b is smaller than 1 and even smaller than it was in **V3-2**. As to the other fitting parameters n_{exp} it can be concluded from the fitting result of the three points that $n_{exp} < \gamma$, which means the expansion process is an exothermic process rather than endothermic process. However for this case stage 5-6 is assumed to be a heat loss and consequently the heat Q_{56} is not included in the total heat input originating from combustion. The percentage Q_{56} of Q_{in} (and thus the error in heat input) is 1.068%, 2.885% and 1.395% for the three operation points respectively.

The unused equivalence criterion T_{max} is lower than measured for the three operating points and for point (B) and (C), the relative difference is more than 10%.

Table 3.16 Results of Seiliger fit version V4-3

Seiliger Parameter		Value	EC*	Relative Error (%)	Difference ^{&}		
					Absolute	Relative	
Constant	n_{comp}	1.36					
	r_c	13.1073					
	ΔEO	0					
(A)	Variable	a	1.3129	p_{max}	0		
		b	1.2473	W_i	$3.001 \cdot 10^{-2}$		
		c	3.7657	Q_{in}	$2.694 \cdot 10^{-2}$		
		n_{exp}	1.2827	T_{EO}	$2.086 \cdot 10^{-2}$		
				T_{max}		-95.585 K	-6.32%
(B)	Variable	a	1.5281	p_{max}	0		
		b	0.9204	W_i	0.1251		
		c	1.9962	Q_{in}	0.1347		
		n_{exp}	1.3197	T_{EO}	$4.363 \cdot 10^{-2}$		
				T_{max}		-152.650 K	-11.39%
(C)	Variable	a	1.7842	p_{max}	0		
		b	0.9910	W_i	$1.649 \cdot 10^{-2}$		
		c	3.4150	Q_{in}	$4.067 \cdot 10^{-2}$		
		n_{exp}	1.2857	T_{EO}	$1.240 \cdot 10^{-2}$		
				T_{max}		-165.568 K	-10.09%

* EC here means Equivalence Criterion

& the difference is the equivalence criteria of Seiliger fit minus smoothed measurement

Table 3.17 Heat input ratio of V4-3

	$Q_{23,ratio}$	$Q_{34,ratio}$	$Q_{45,ratio}$
point (A)	0.2080	0.2996	0.4924
point (B)	0.7640	-0.2294	0.4654
point (C)	0.5300	-0.0124	0.4825

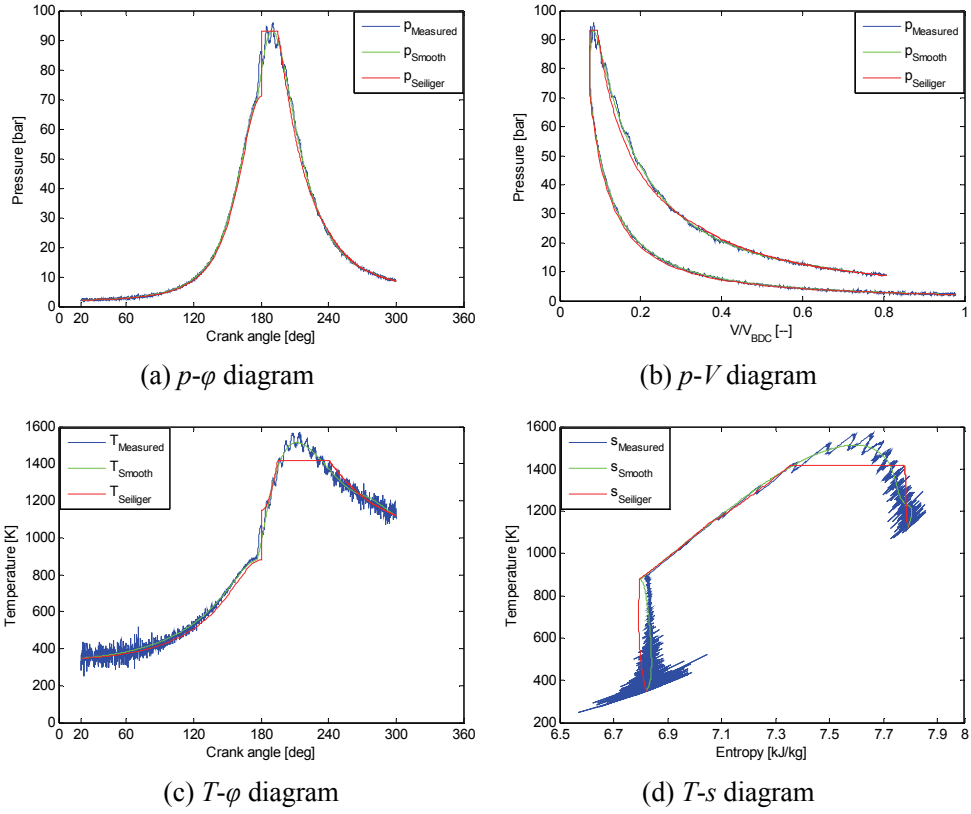
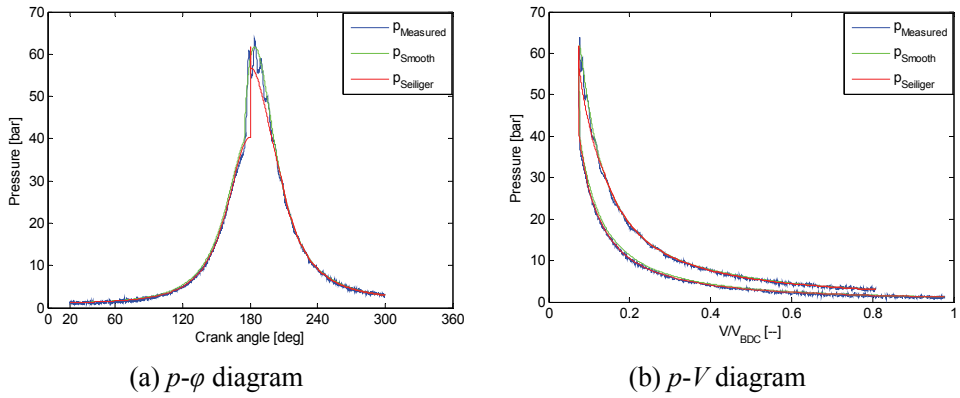
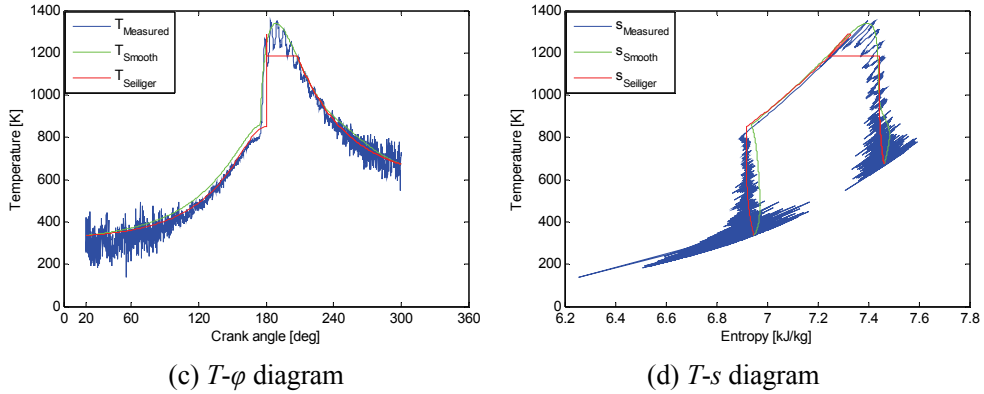
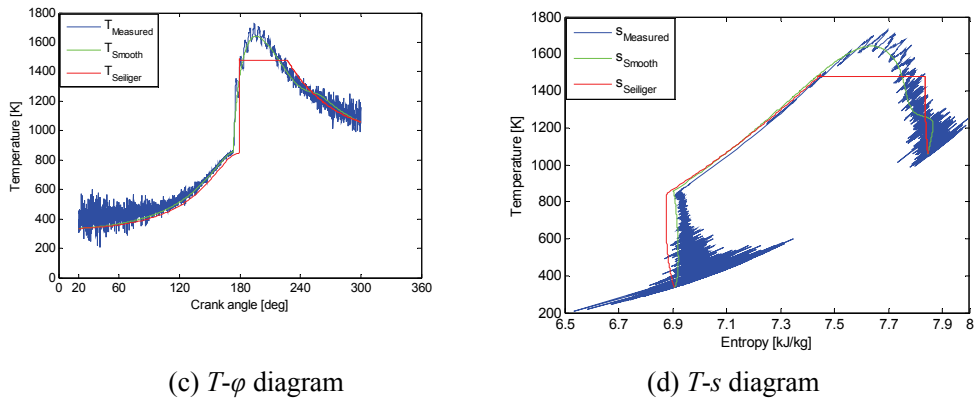
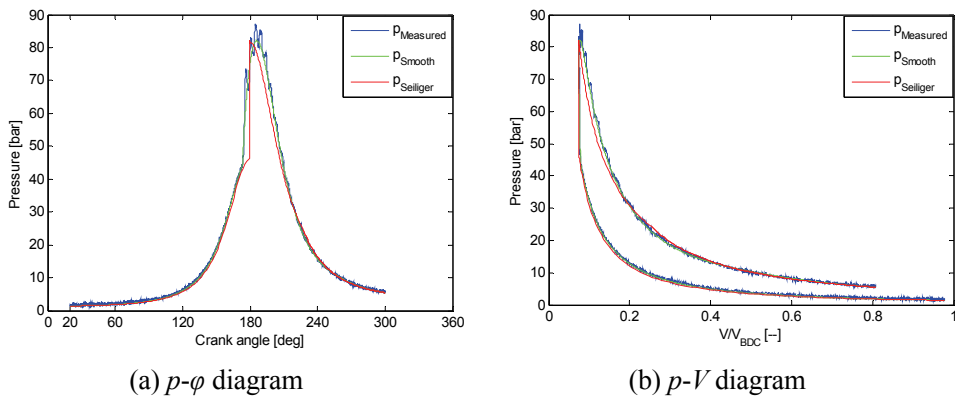


Figure 3.24 Comparison of Seiliger fit (V4-3) with raw and smooth measurement (point A)





(c) $T-\phi$ diagram (d) $T-s$ diagram
Figure 3.25 Comparison of Seiliger fit (V4-3) with raw and smooth measurement (point (B))



(c) $T-\phi$ diagram (d) $T-s$ diagram
Figure 3.26 Comparison of Seiliger fit (V4-3) with raw and smooth measurement (point (C))

Like *V3-2-1*, a new fit version *V4-3-1* is introduced, which is the derived version from *V4-3* using three equivalence criteria W_i , Q_{in} and T_{EO} and three Seiliger parameter a , c and n_{exp} as variables together with $b = 1$. The Newton-Raphson numerical method is used to solve the system and the stop criteria are the same as *V4-3* except that p_{max} is removed.

Table 3.18, Table 3.19 and Figure 3.27 – Figure 3.28 illustrate the fit results of *V4-3-1* for point (B) and (C). Compared to the results of *V4-3*, parameter a and c are both decreasing and n_{exp} does not change. Together with the decrease of parameter a , also p_{max} is decreasing and is 7.56% and 0.72% lower than for the measured engine cycle for these two operating points respectively. The unused equivalence criterion T_{max} is higher than it was in *V4-3* but still around 10% lower than it in the measured engine cycle.

Table 3.18 Results of Seiliger fit version *V4-3-1*

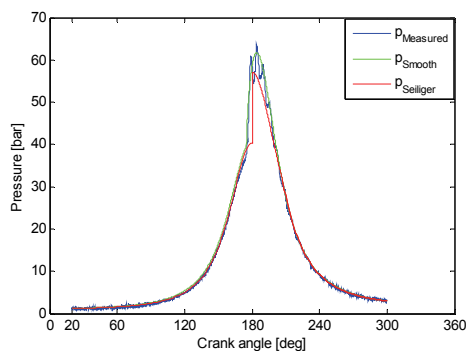
Seiliger Parameter	Value	EC*	Relative Error (%)	Difference ^{&}		
				Absolute	Relative	
Constant	n_{comp}	1.36				
	r_c	13.1073				
	b	1				
	ΔEO	0				
(B)	Variable	a	1.4125	W_i	$5.133 \cdot 10^{-2}$	
		c	1.8159	Q_{in}	$5.673 \cdot 10^{-2}$	
		n_{exp}	1.3195	T_{EO}	$6.261 \cdot 10^{-3}$	
					p_{max}	-4.669 bar -7.56%
					T_{max}	-148.635 K -11.09%
	(C)	Variable	a	1.7714	W_i	$4.946 \cdot 10^{-3}$
c			3.3630	Q_{in}	$6.079 \cdot 10^{-2}$	
n_{exp}			1.2858	T_{EO}	$2.875 \cdot 10^{-3}$	
					p_{max}	-0.590 bar -0.72%
					T_{max}	-163.110 K -9.94%

* EC here means Equivalence Criterion

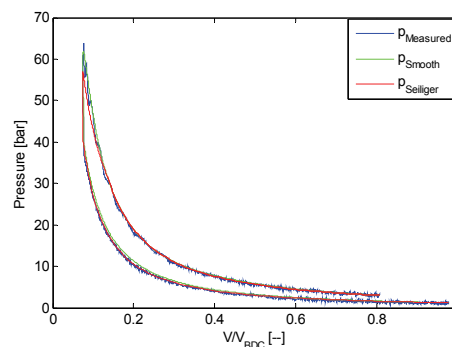
& the difference is the equivalence criteria of Seiliger fit minus smoothed measurement

Table 3.19 Heat input ratio of *V4-3-1*

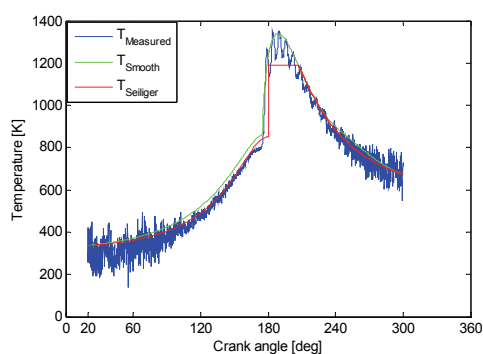
	$Q_{23, ratio}$	$Q_{34, ratio}$	$Q_{45, ratio}$
point (B)	0.5901	0.0005	0.4093
point (C)	0.5208	0	0.4792



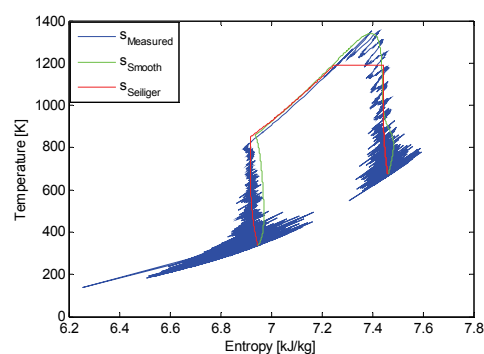
(a) p - ϕ diagram



(b) p - V diagram



(c) T - ϕ diagram



(d) T - s diagram

Figure 3.27 Comparison of Seiliger fit (*V4-3-1*) with raw and smooth measurement (point (B))

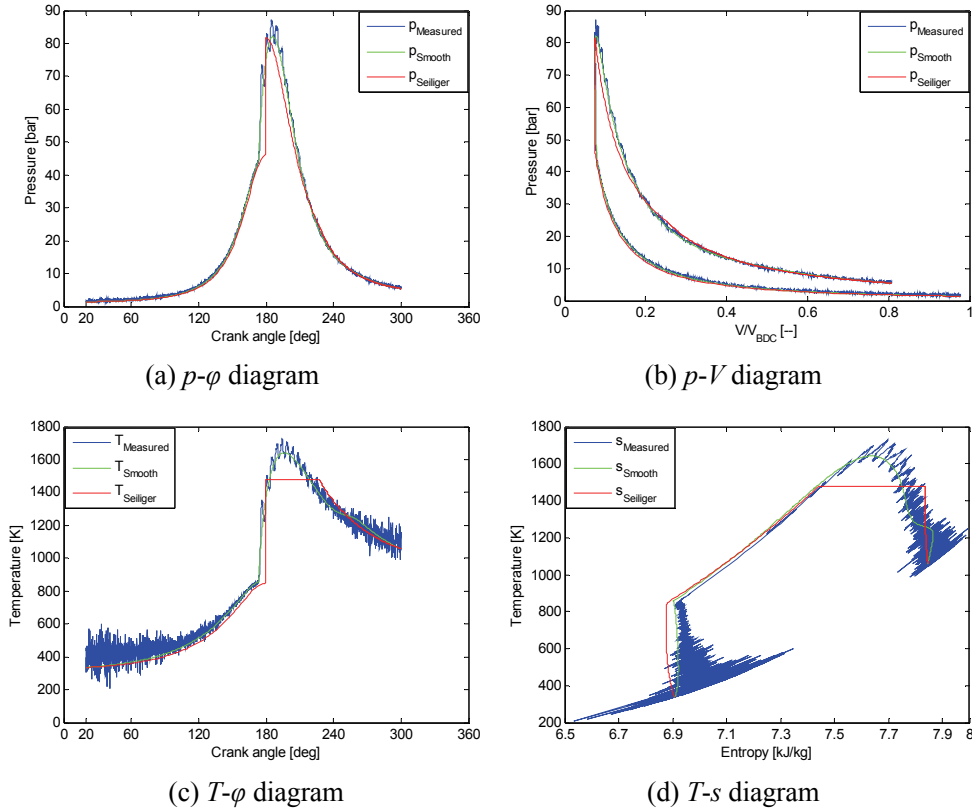


Figure 3.28 Comparison of Seiliger fit (*V4-3-1*) with raw and smooth measurement (point C))

V4-1 and *V4-3* use as the equivalence criteria p_{max} , W_i , Q_{in} (having the highest significance), in conjunction with T_{EO} . The shortcoming of these two versions is that when T_{EO} is selected as an equivalence criterion rather than T_{max} , the system of equations becomes more complicated, and the iteration to find a solution with the Newton-Raphson method is likely to diverge (*V4-1* is one example). In Appendix VI, the investigation of diverging in Newton-Raphson numerical method is carried out. Although the iteration calculation of *V4-3* is converging, the fit result of n_{exp} is not in accordance with the definition of the basic Seiliger process (Q_{56} should be negative instead of positive from the fitting).

2) V4-2 and V4-4 (Equivalence criteria: p_{max} , W_i , Q_{in} and T_{max})

The equivalence criteria in the V4-2 and V4-4 versions are p_{max} , Q_{in} and W_i again but now in conjunction with T_{max} and the following Seiliger parameters are selected (refer Table 3.28):

V4-2 – a , b , c and ΔEO ;

V4-4 – a , b , c and n_{exp} (intended to express a heat loss during 5-6)..

The equations of the equivalence criteria p_{max} , T_{max} and Q_{in} of these two versions (based on equation [3.19], [3.20] and [3.22]) are the same as in V3-1. The other equations (based on equation [3.24]) of equivalence criterion W_i are the same but with different variables.

Again it is impossible to solve the system of equations directly. The numerical iteration for the two versions are both converging. The stop criteria of the iteration are:

$$|p_3 - p_{max}| \leq 1 \text{ bar}, |Q_{in,Seiliger} - Q_{in,measured}| \leq 10 \text{ J}, |W_{i,Seiliger} - W_{i,measured}| \leq 10 \text{ J}$$

$$\text{and } |T_4 - T_{max}| \leq 1 \text{ K} \quad [3.48]$$

Table 3.20, Table 3.21 and Figure 3.29 – Figure 3.31 illustrate the fit results of V4-2. The Seiliger parameters a , b and c are the same as in V3-1 because p_{max} , T_{max} and Q_{in} are based on the same functions and the same variables. Parameter ΔEO is calculated based on the work W_i (equation [3.24]). The result of ΔEO for operating point (A) and (C) are both negative (i.e. making the exhaust valve virtually open earlier) but for operating point (B) is positive (i.e. making the exhaust valve virtually open later).

The unused equivalence criterion T_{EO} is 2% – 7% smaller for the three operating points than for the measured engine cycle.

Table 3.20 Heat input ratio of V4-2

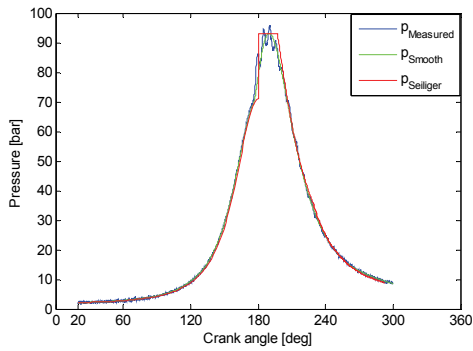
	$Q_{23,ratio}$	$Q_{34,ratio}$	$Q_{45,ratio}$
point (A)	0.2080	0.4085	0.3836
point (B)	0.7639	0.1342	0.1020
point (C)	0.5300	0.1813	0.2887

Table 3.21 Results of Seiliger fit version V4-2

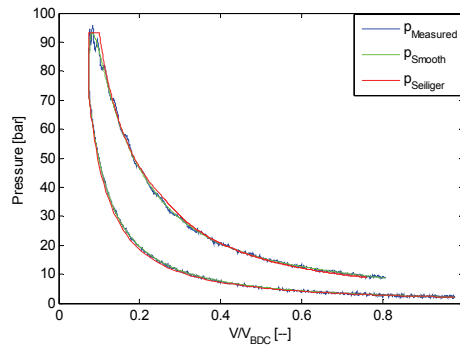
Seiliger Parameter	Value	EC*	Relative Error (%)	Difference ^{&}		
				Absolute	Relative	
Constant	n_{comp}	1.36				
	r_c	13.1073				
(A)	Variable	a	1.3129	p_{max}	0	
		b	1.3369	W_i	$1.694 \cdot 10^{-2}$	
		c	2.6184	Q_{in}	$1.278 \cdot 10^{-2}$	
		ΔEO	-7.1924	T_{max}	$5.251 \cdot 10^{-2}$	
	Constant	n_{exp}	1.31	T_{EO}		-32.651 K -2.92%
(B)	Variable	a	1.5281	p_{max}	0	
		b	1.0445	W_i	$3.210 \cdot 10^{-2}$	
		c	1.1409	Q_{in}	$2.643 \cdot 10^{-2}$	
		ΔEO	4.0637	T_{max}	$5.865 \cdot 10^{-3}$	
	Constant	n_{exp}	1.33	T_{EO}		-47.000 K -6.98%
(C)	Variable	a	1.7842	p_{max}	0	
		b	1.1090	W_i	$3.971 \cdot 10^{-2}$	
		c	1.9270	Q_{in}	$3.506 \cdot 10^{-2}$	
		ΔEO	-8.0139	T_{max}	$1.727 \cdot 10^{-2}$	
	Constant	n_{exp}	1.31	T_{EO}		-44.760 K -4.23%

* EC here means Equivalence Criterion

& the difference is the equivalence criteria of Seiliger fit minus smoothed measurement



(a) p - ϕ diagram



(b) p - V diagram

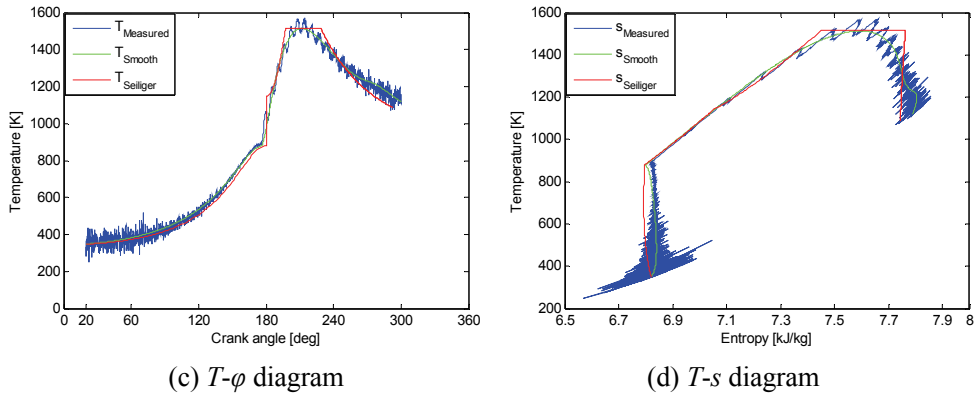


Figure 3.29 Comparison of Seiliger fit (V4-2) with raw and smooth measurement (point (A))

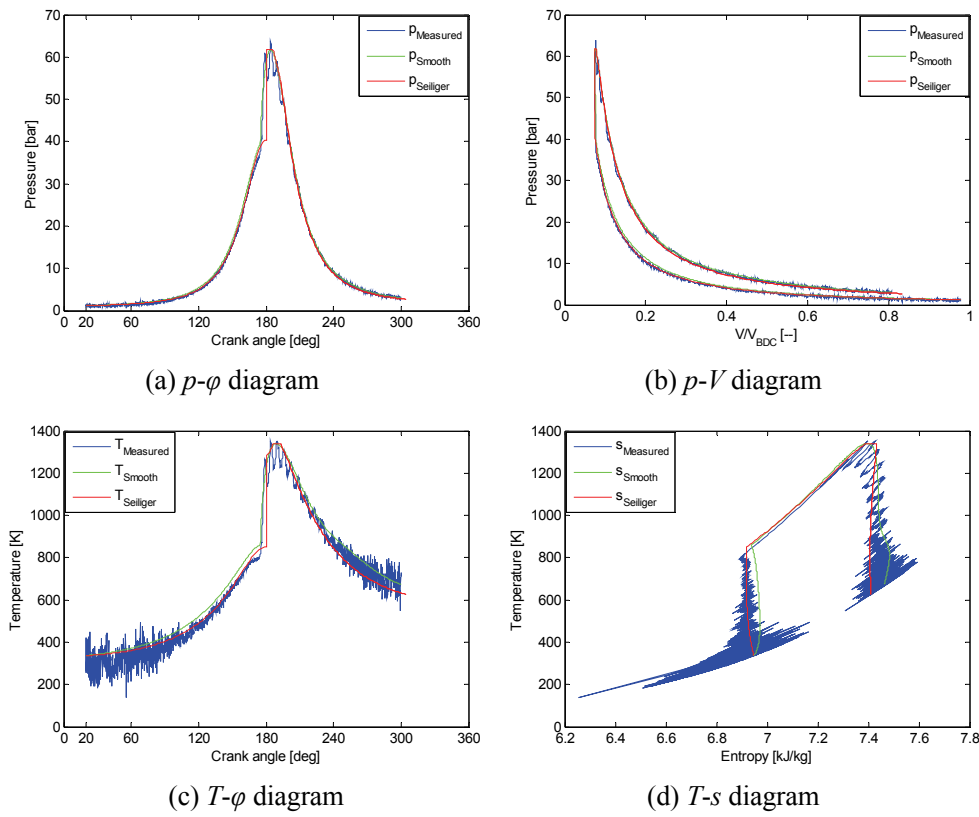


Figure 3.30 Comparison of Seiliger fit (V4-2) with raw and smooth measurement (point (B))

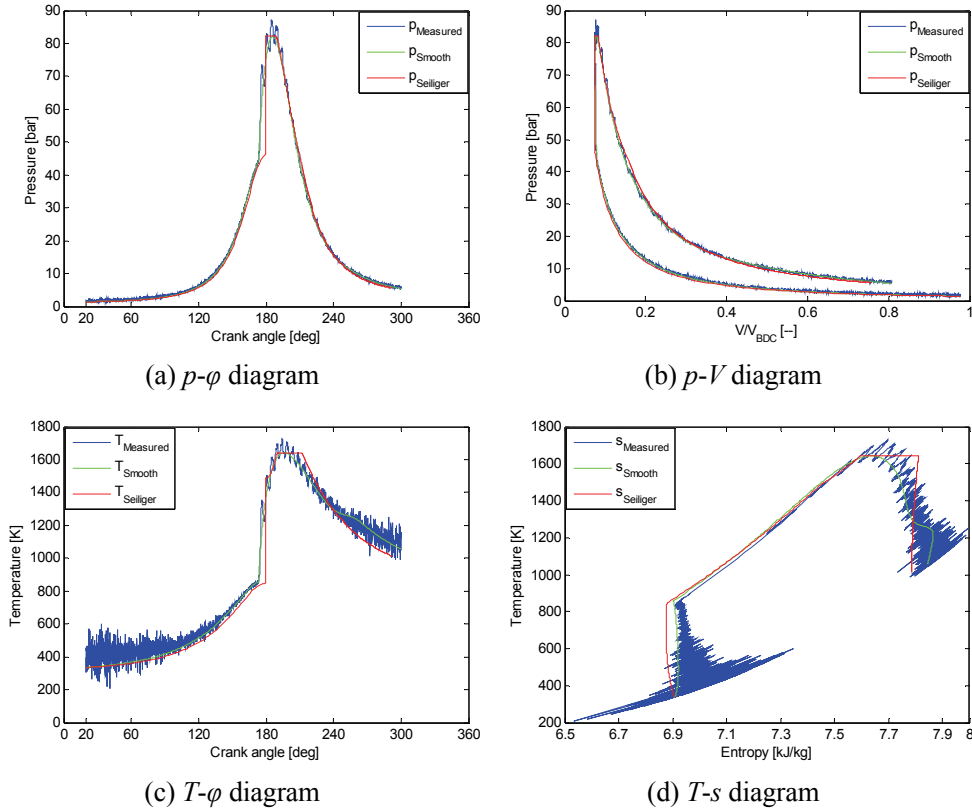


Figure 3.31 Comparison of Seiliger fit ($V4-2$) with raw and smooth measurement (point (C))

Table 3.22, Table 3.23 and Figure 3.32 – Figure 3.34 illustrate the fit result for $V4-4$. The Seiliger parameters a , b and c are the same as in $V3-1$ and $V4-4$ due to the fact that p_{max} , T_{max} and Q_{in} are determined with the same functions. Parameter n_{exp} is calculated based on the work W_i (equation [3.24]). The value of n_{exp} (intended to express a heat loss) for all the three points is larger than the isentropic coefficient (γ), indicating a heat loss process. The heat loss is relative high, especially for operating point (A) and (C), see Figure 3.33 (d) and Figure 3.34(d).

The unused equivalence criterion T_{EO} for all three operating points is more than 10% smaller than in the measured engine cycle. Compared to the unused equivalence criterion T_{EO} in $V4-2$, the relative difference is much larger in $V4-4$.

Table 3.22 Results of Seiliger fit version *V4-4*

Seiliger Parameter		Value	EC*	Relative Error (%)	Difference ^{&}		
					Absolute	Relative	
Constant	n_{comp}	1.36					
	r_c	13.1073					
	ΔEO	0					
(A)	Variable	a	1.3129	p_{max}	0		
		b	1.3362	W_i	$4.246 \cdot 10^{-3}$		
		c	2.6249	Q_{in}	$2.894 \cdot 10^{-3}$		
		n_{exp}	1.3960	T_{max}	$2.208 \cdot 10^{-3}$		
				T_{EO}		-150.988 K	-13.49%
(B)	Variable	a	1.5281	p_{max}	0		
		b	1.0445	W_i	$6.903 \cdot 10^{-2}$		
		c	1.1409	Q_{in}	$2.643 \cdot 10^{-2}$		
		n_{exp}	1.3303	T_{max}	$5.865 \cdot 10^{-3}$		
				T_{EO}		-26.896 K	-3.99%
(C)	Variable	a	1.7842	p_{max}	0		
		b	1.1090	W_i	$4.199 \cdot 10^{-2}$		
		c	1.9270	Q_{in}	$3.506 \cdot 10^{-2}$		
		n_{exp}	1.3541	T_{max}	$1.727 \cdot 10^{-3}$		
				T_{EO}		-134.066 K	-12.67%

* EC here means Equivalence Criterion

& the difference is the equivalence criteria of Seiliger fit minus smoothed measurement

Table 3.23 Heat input ratio of *V4-4*

	$Q_{23,ratio}$	$Q_{34,ratio}$	$Q_{45,ratio}$
point (A)	0.2080	0.4076	0.3844
point (B)	0.7639	0.1342	0.1020
point (C)	0.5300	0.1813	0.2887

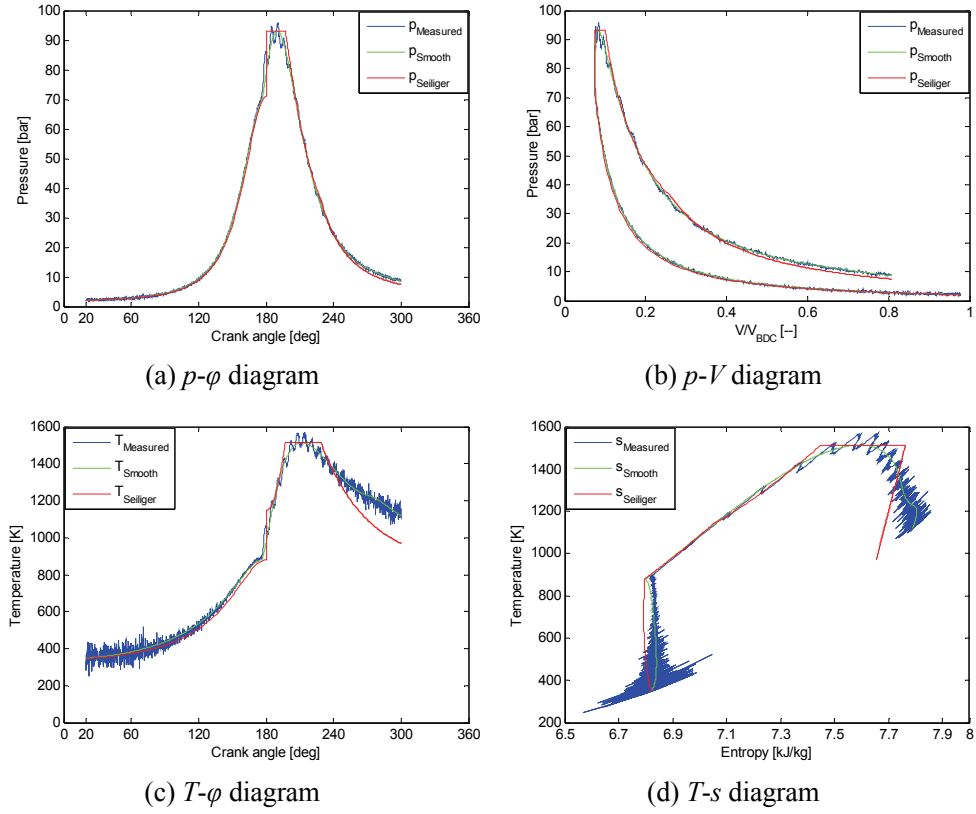
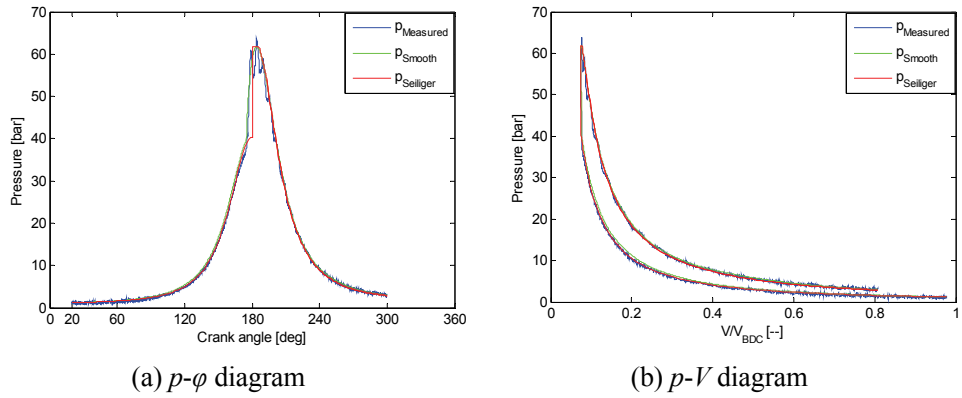
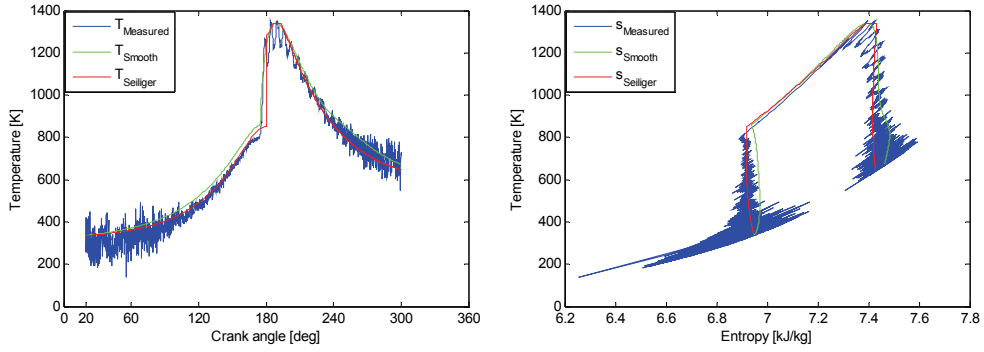


Figure 3.32 Comparison of Seiliger fit (V4-4) with raw and smooth measurement (point A))

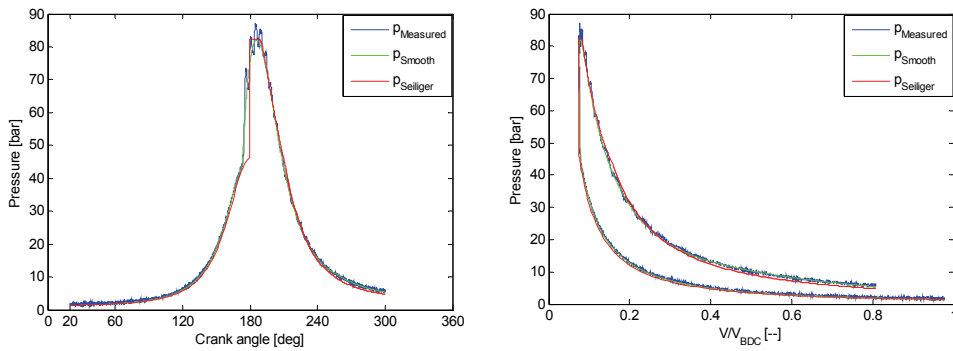




(c) $T-\phi$ diagram

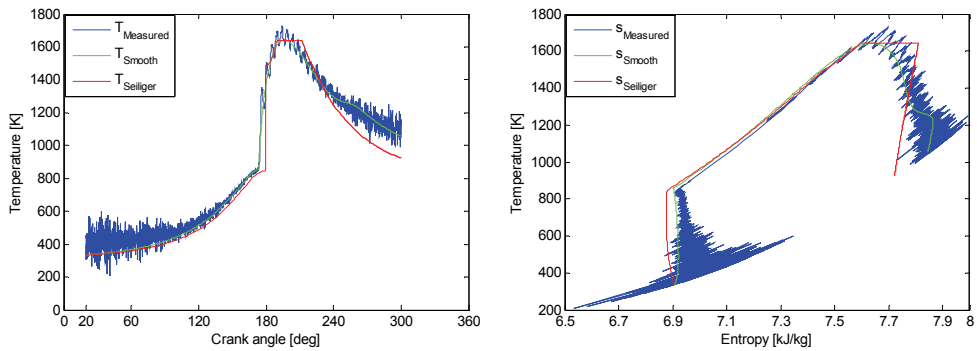
(d) $T-s$ diagram

Figure 3.33 Comparison of Seiliger fit (V4-4) with raw and smooth measurement (point (B))



(a) $p-\phi$ diagram

(b) $p-V$ diagram



(c) $T-\phi$ diagram

(d) $T-s$ diagram

Figure 3.34 Comparison of Seiliger fit (V4-4) with raw and smooth measurement (point (C))

Since two parameters a and b can be determined by two separate equations using equivalence criteria p_{max} and T_{max} , **V4-2** and **V4-4** are both converging. In **V4-2**, the fit result of ΔEO is negative in operating point (A) and (C). In **V4-4** the n_{exp} is appropriate and indicates heat loss during stage 5-6, albeit that the resulting heat loss looks somewhat high.

3) V4-5 and V4-6 (Seiliger parameters: a , b , c and n_{exp})

In Seiliger fit versions **V4-1** – **V4-4**, it was assumed that there is no combustion in stage 5-6, so only heat loss is expected to happen in stage 5-6. Therefore in the equivalence criterion Q_{in} , the heat Q_{56} is excluded. However, if there is *very* late combustion, some heat could be released during stage 5-6. In order to describe the heat input process, the *advanced* Seiliger process is defined to consist of four stages of combustion: stage 2-3, stage 3-4, stage 4-5 and stage 5-6. Stage 5-6 uses a different value for the polytropic exponent n_{exp} such that it has heat input, which has been explained in section 3.2.

Seiliger fit versions **V4-5** and **V4-6** are based on the advanced, but still six-point Seiliger process. The Seiliger parameters are the same: a , b , c and n_{exp} and the equivalence criteria are selected to be (refer Table 3.28):

V4-5 – p_{max} , W_i , Q_{in} and T_{EO} (same as **V4-1** and **V4-3**);

V4-6 – p_{max} , W_i , Q_{in} and T_{max} (same as **V4-2** and **V4-4**).

Note that due to the four staged combustion in **V4-5** and **V4-6**, one of the equivalence criteria Q_{in} is based on equation [3.23] instead of equation [3.22]. The system of equations of **V4-5** is based on equation [3.19], [3.21], [3.23] and [3.24], and **V4-6** is based on equation [3.19], [3.20], [3.23] and [3.24].

The system of equations for **V4-6** is numerically converging but **V4-5** does not converge. The stop criteria for the iteration are:

$$\begin{aligned} \mathbf{V4-5:} \quad & |p_3 - p_{max}| \leq 1 \text{ bar}, |Q_{in,Seiliger} - Q_{in,measured}| \leq 10 \text{ J}, \\ & \text{and } |W_{i,Seiliger} - W_{i,measured}| \leq 10 \text{ J}, |T_6 - T_{end}| \leq 1 \text{ K} \end{aligned} \quad [3.49]$$

$$\begin{aligned} \mathbf{V4-6:} \quad & |p_3 - p_{max}| \leq 1 \text{ bar}, |Q_{in,Seiliger} - Q_{in,measured}| \leq 10 \text{ J}, \\ & \text{and } |W_{i,Seiliger} - W_{i,measured}| \leq 10 \text{ J}, |T_4 - T_{max}| \leq 1 \text{ K} \end{aligned} \quad [3.50]$$

Table 3.24 Results of Seiliger fit version *V4-6*

Seiliger Parameter		Value	EC*	Relative Error (%)	Difference ^{&}		
					Absolute	Relative	
Constant	n_{comp}	1.36					
	r_c	13.1073					
	ΔEO	0					
(A)	Variable	a	1.3129	p_{max}	0		
		b	1.3362	W_i	$5.190 \cdot 10^{-2}$		
		c	1.3014	Q_{in}	$2.114 \cdot 10^{-3}$		
		n_{exp}	1.1671	T_{max}	$5.715 \cdot 10^{-6}$		
				T_{EO}		-14.546 K	-1.30%
(B)	Variable	a	1.5281	p_{max}	0		
		b	1.0445	W_i	$2.377 \cdot 10^{-2}$		
		c	1.0996	Q_{in}	$2.016 \cdot 10^{-2}$		
		n_{exp}	1.3185	T_{max}	$6.077 \cdot 10^{-3}$		
				T_{EO}		-17.851 K	-2.65%
(C)	Variable	a	1.7842	p_{max}	0		
		b	1.1088	W_i	0.1049		
		c	1.2284	Q_{in}	$7.014 \cdot 10^{-2}$		
		n_{exp}	1.2170	T_{max}	$8.475 \cdot 10^{-4}$		
				T_{EO}		-17.648 K	-1.67%

* EC here means Equivalence Criterion

& the difference is the equivalence criteria of Seiliger fit minus smoothed measurement

Table 3.25 Heat input ratio of *V4-6*

	$Q_{23, ratio}$	$Q_{34, ratio}$	$Q_{45, ratio}$	$Q_{56, ratio}$
point (A)	0.2080	0.4076	0.1042	0.2802
point (B)	0.7638	0.1343	0.0734	0.0285
point (C)	0.5300	0.1814	0.0917	0.1968

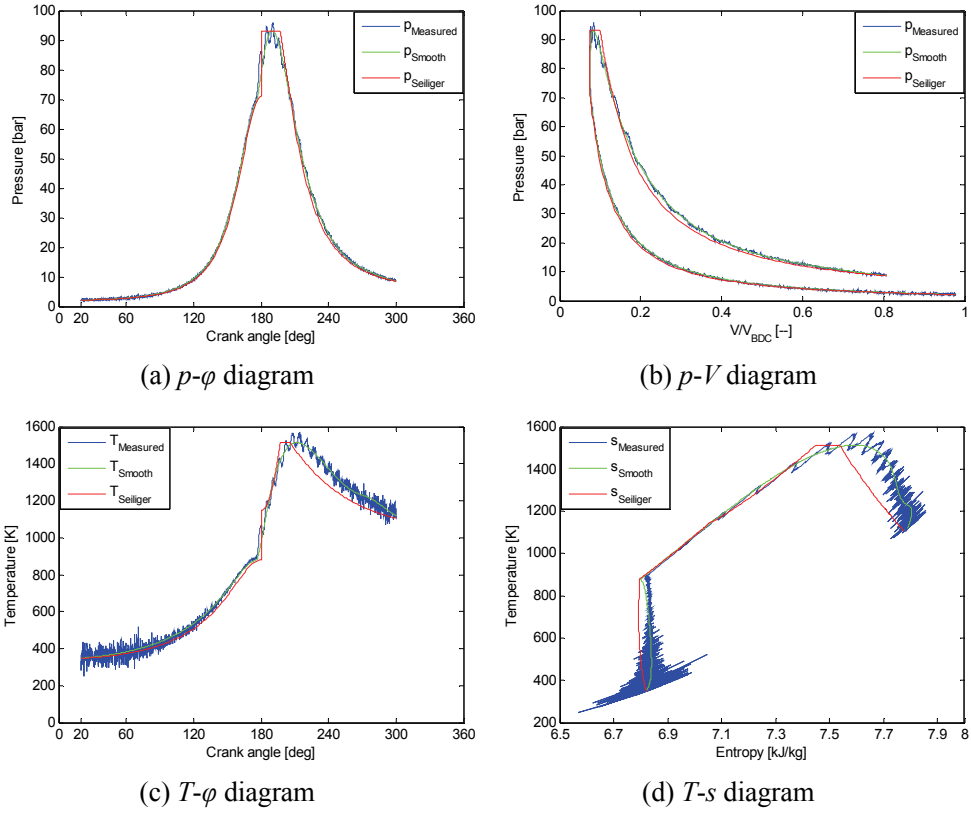
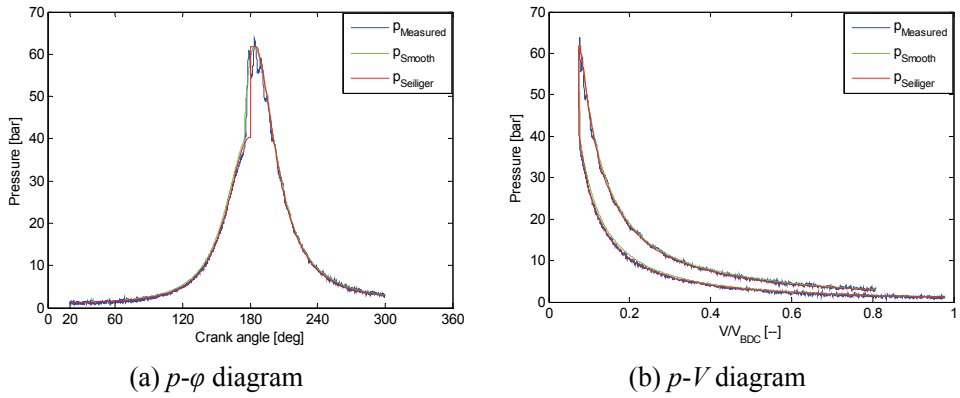
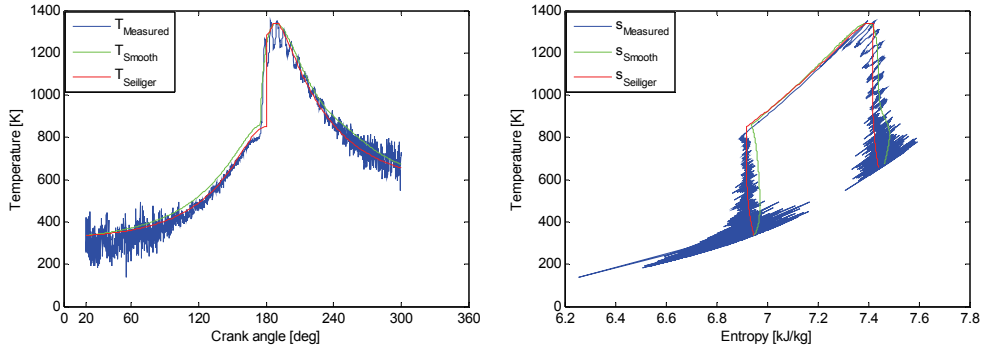


Figure 3.35 Comparison of Seiliger fit (V4-6) with raw and smooth measurement (point (A))

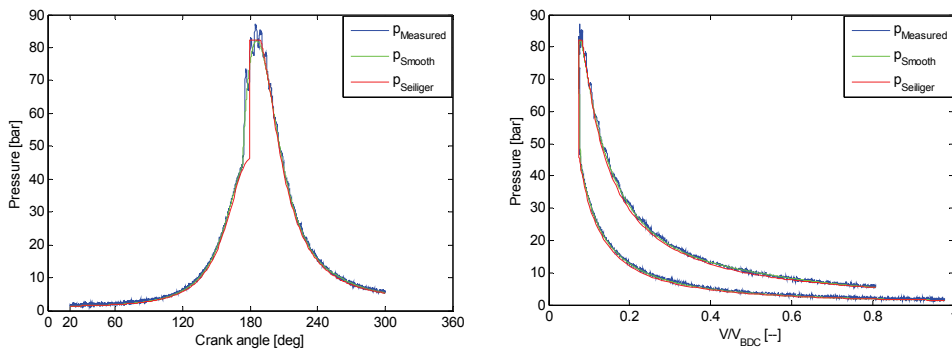




(c) $T-\phi$ diagram

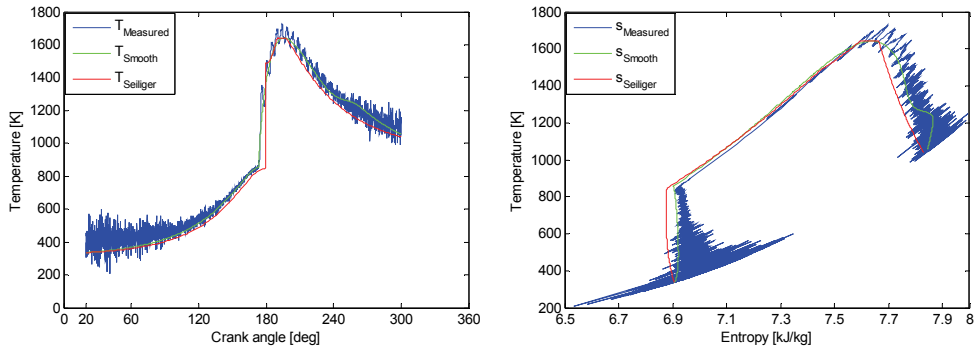
(d) $T-s$ diagram

Figure 3.36 Comparison of Seiliger fit (V4-6) with raw and smooth measurement (point (B))



(a) $p-\phi$ diagram

(b) $p-V$ diagram



(c) $T-\phi$ diagram

(d) $T-s$ diagram

Figure 3.37 Comparison of Seiliger fit (V4-6) with raw and smooth measurement (point (C))

Table 3.24 and Figure 3.35 – Figure 3.37 illustrate the fit results for **V4-6**. The Seiliger parameters a and b are the same as in **V3-1**, **V4-2** and **V4-4**. As for parameter c and n_{exp} , for operating point (A) and (C): parameter c is for both decreasing when compared with the c value in **V4-1** – **V4-4**, and parameters n_{exp} are much smaller than the isentropic exponent meaning that there is much net heat input during stage 5-6. Table 3.25 summarises the heat input ratios of the different Seiliger stages of **V4-6**. $Q_{56,ratio}$ of operating point (A) and (C) are 28.0% and 19.7% and $Q_{45,ratio}$ are only 10.4% and 9.2% respectively. This means the heat input during late combustion shifts to a much later phase and becomes ‘very late combustion’. For operating point (B), c is also very closed to unity and n_{exp} is smaller than, but close to, the isentropic coefficient (γ). $Q_{56,ratio}$ of operating point (B) is about 2.9% which indicates less very late combustion when the engine is running at part load.

The unused equivalence criterion T_{EO} of the three operation points are all smaller than in the measured engine cycle and the relative difference is small (less than 3% of the three points).

V4-5 and **V4-6** are the Seiliger process fit versions on the basis of the *advanced* Seiliger process definition (four combustion stages in Seiliger process), in which there is some heat input expected during stage 5-6. In terms of the fit results, **V4-5** is not converging which could be caused by the fact that, besides equation [3.19], the other three equations all include three variables (b , c and n_{exp}) and the relationship among them are complicated. **V4-6** is converging and the fit results are reasonable that for the aged engine, there very late combustion in heavy load (operating point (A) and (C)) and less in part load (operating point (B)).

3.3.5 Fit versions with five Seiliger parameters

In this ultimate case the five important equivalence criteria p_{max} , Q_{in} and W_i , T_{EO} and T_{max} are all selected and the Seiliger parameters to achieve these are chosen as a , b , c , n_{exp} and ΔEO . **V5-1** is based on the *basic* Seiliger process, i.e. parameter n_{exp} for stage 5-6 is chosen such that heat loss is implied. **V5-2** is based on *advanced* Seiliger process, i.e. parameter n_{exp} for stage 5-6 is chosen such that heat input is implied (refer Table 3.28 for an overview).

The system of equations of **V5-1** is based on equation [3.19] [3.22] and [3.24], and **V5-2** is based on equation [3.19] – [3.21], [3.23] and [3.24].

The Newton-Raphson numerical method is used to solve the system of equations in the SIMULINK environment. During iteration, the system of equations of **V5-1** is converging but for **V5-2** is not converging. The stop criteria of the iteration setting in Newton-Raphson method are:

$$|p_3 - p_{max}| \leq 1\text{bar}, |Q_{in,Seiliger} - Q_{in,measured}| \leq 10\text{J}, |W_{i,Seiliger} - W_{i,measured}| \leq 10\text{J},$$

$$|T_6 - T_{end}| \leq 1\text{K}, |T_4 - T_{max}| \leq 1\text{K} \quad [3.51]$$

Table 3.26 Results of Seiliger fit version **V5-1**

Seiliger Parameter	Value	EC*	Difference ^{&}		
			Relative Error (%)	Absolute Relative	
Constant	n_{comp}	1.36			
	r_c	13.1073			
(A)	Variable	a	1.3129	p_{max}	0
		b	1.3362	W_i	$2.467 \cdot 10^{-2}$
		c	2.6206	Q_{in}	$8.676 \cdot 10^{-3}$
		n_{exp}	1.2860	T_{max}	$4.972 \cdot 10^{-2}$
		ΔEO	-8.8408	T_{EO}	$4.782 \cdot 10^{-2}$
(B)	Variable	a	1.5281	p_{max}	0
		b	1.0444	W_i	$1.334 \cdot 10^{-2}$
		c	1.1412	Q_{in}	$2.539 \cdot 10^{-2}$
		n_{exp}	1.3175	T_{max}	$4.674 \cdot 10^{-3}$
		ΔEO	-4.9636	T_{EO}	$1.521 \cdot 10^{-2}$
(C)	Variable	A	1.7842	p_{max}	0
		B	1.1086	W_i	$3.846 \cdot 10^{-2}$
		C	1.9291	Q_{in}	$3.400 \cdot 10^{-2}$
		n_{exp}	1.2878	T_{max}	$1.389 \cdot 10^{-2}$
		ΔEO	-11.2313	T_{EO}	$1.212 \cdot 10^{-2}$

* EC here means Equivalence Criterion

& the difference is the equivalence criteria of Seiliger fit minus smoothed measurement

Table 3.27 Heat input ratio of *V5-1*

	$Q_{23,ratio}$	$Q_{34,ratio}$	$Q_{45,ratio}$
point (A)	0.2080	0.4083	0.3838
point (B)	0.7639	0.1342	0.1020
point (C)	0.5300	0.1813	0.2887

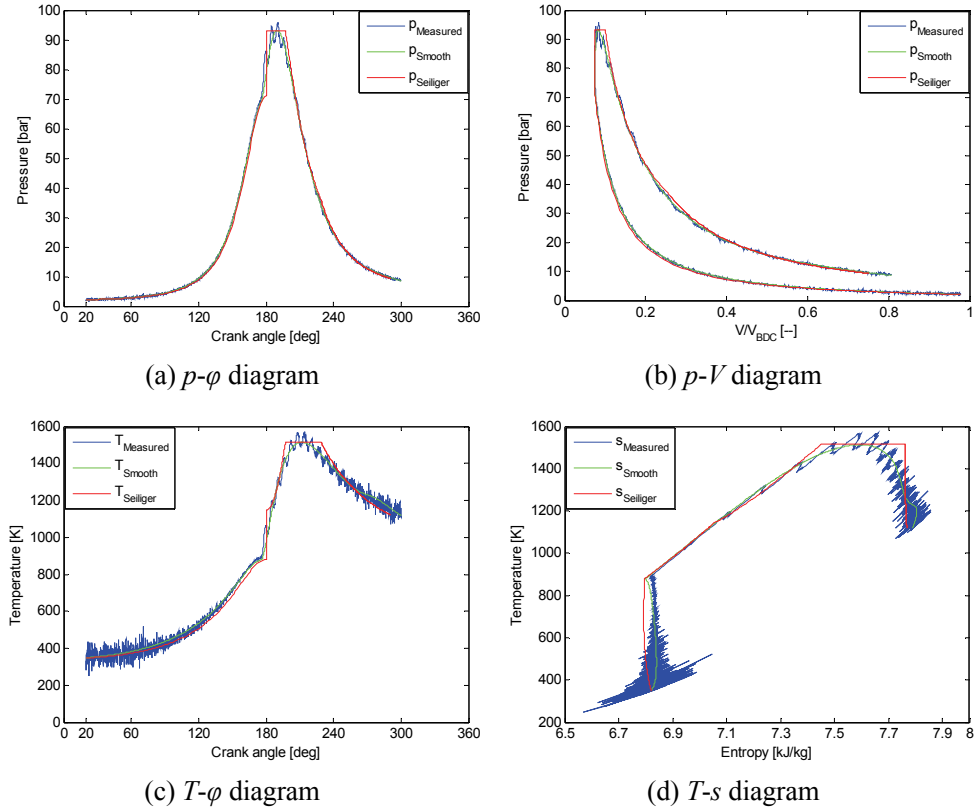


Figure 3.38 Comparison of Seiliger fit (*V5-1*) with raw and smooth measurement (point (A))

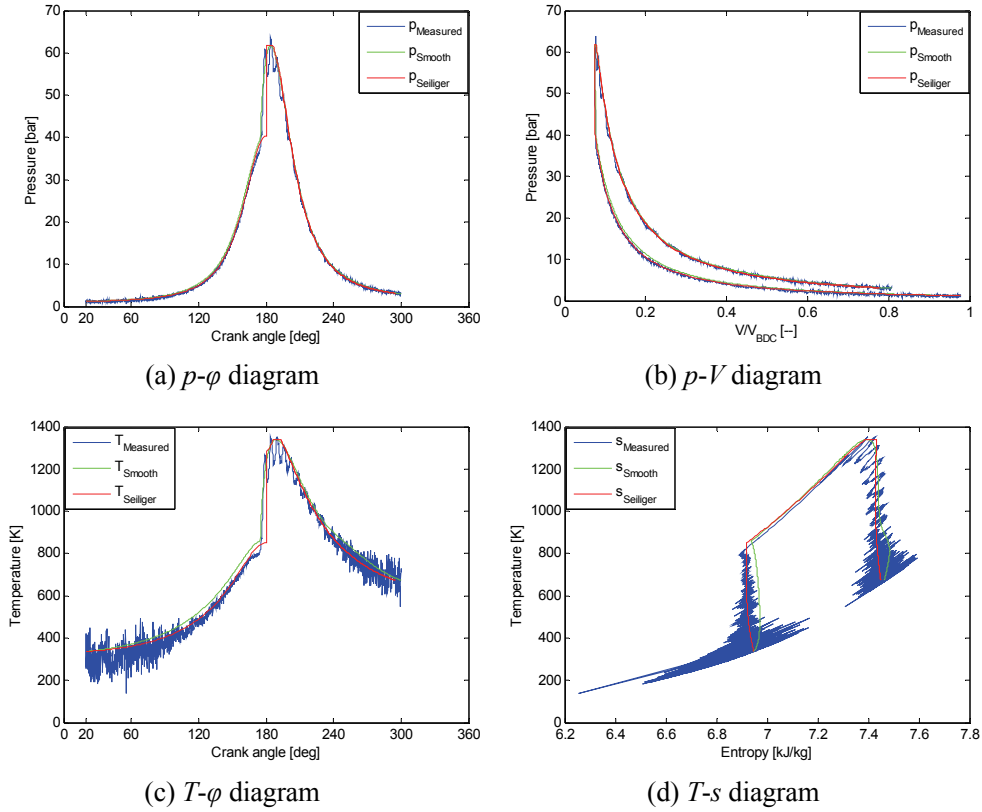
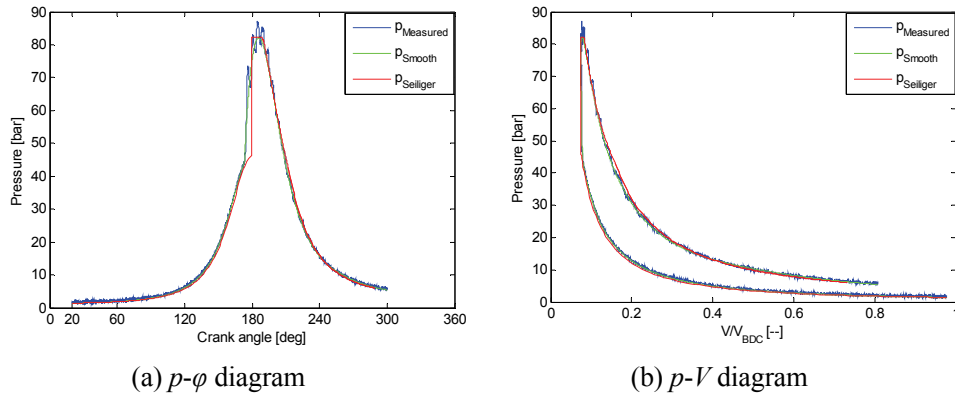


Figure 3.39 Comparison of Seiliger fit (*V5-I*) with raw and smooth measurement (point (B))



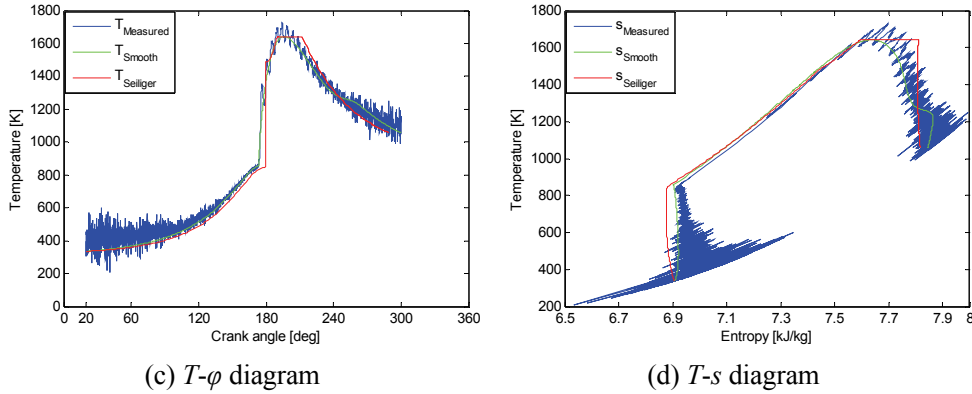


Figure 3.40 Comparison of Seiliger fit (*V5-I*) with raw and smooth measurement (point C))

Table 3.26, Table 3.27 and Figure 3.38 – Figure 3.40 illustrate the fit results for *V5-I*. The Seiliger parameters a , and b are the same as in *V3-I*, *V4-2*, *V4-4* and *V4-6*. Parameter n_{exp} of the three points are all smaller than isentropic coefficient (γ) meaning that there is some heat input during stage 5-6 which should not be the case. Parameter ΔEO of the three operating points are all smaller than 0, which means the exhaust valve is virtually opened earlier than in reality.

3.3.6 Summary and comparison of Seiliger fit versions

Table 3.28 summarises all the Seiliger fit versions. The numbers of equivalence criterion and Seiliger parameters must be equal to the number of equations (or degrees of freedom). The number of combustion stages (refer Table 3.5) are not equal to the equation number for some fit versions but cannot be larger than it. For example, in fit version *V3-I*, the three Seiliger parameters (a , b , c) are all combustion shape parameters, so the number of combustion stages is equal to number of equations; in fit version *V4-3*, one of the Seiliger parameters n_{exp} is not a combustion shape parameter resulting in number of combustion stages smaller than the number of equations. The latter can be compared with *V4-6*, although they use the same equivalence criteria and the same Seiliger parameters as variables, due to different combustion stages, the meaning of n_{exp} is different in these two version resulting in different equation used for the calculation of q_{in} (equation [3.22] vs. [3.23]).

Since equation [3.20] is simpler than equation [3.21], it can be conclude that *V4-I*,

V4-3 and V4-5 tend to be diverging than V4-2, V4-4 and V4-6 respectively. The cause and results of diverging problem based on graphical solution for the algebraic equations has been presented in Appendix VI. On the other hand, the Seiliger parameters n_{comp} and r_c could be used in these equivalence criterion equations as variables but they appear in the equations [3.19] – [3.24] in many positions, therefore these approaches also tend to be diverging. They are varied in a relative small range, so in all the Seiliger fit versions, they are set to be constant.

Table 3.28 Summary of Seiliger fit versions

Fit version	Equivalence criterion	Seiliger parameter	Nr of Equations	Combustion stages
V3-1	p_{max}, T_{max}, Q_{in}	a, b, c	3	3
V3-2	p_{max}, W_i, Q_{in}	a, b, c	3	3
V3-2-1	W_i, Q_{in}	a, c	2	2
V4-1	$p_{max}, W_i, Q_{in}, T_{EO}$	$a, b, c, \Delta EO$	4	3
V4-2	$p_{max}, W_i, Q_{in}, T_{max}$	$a, b, c, \Delta EO$	4	3
V4-3	$p_{max}, W_i, Q_{in}, T_{EO}$	a, b, c, n_{exp}	4	3
V4-3-1	W_i, Q_{in}, T_{EO}	a, c, n_{exp}	3	2
V4-4	$p_{max}, W_i, Q_{in}, T_{max}$	a, b, c, n_{exp}	4	3
V4-5	$p_{max}, W_i, Q_{in}, T_{EO}$	a, b, c, n_{exp}	4	4
V4-6	$p_{max}, W_i, Q_{in}, T_{max}$	a, b, c, n_{exp}	4	4
V5-1	$p_{max}, W_i, Q_{in}, T_{max}, T_{EO}$	$a, b, c, n_{exp}, \Delta EO$	5	3
V5-2	$p_{max}, W_i, Q_{in}, T_{max}, T_{EO}$	$a, b, c, n_{exp}, \Delta EO$	5	4

The Seiliger fit results of all the investigated fit versions for the three operating points are listed in Table 3.30 –Table 3.32. The text in grey indicates an unexpected fit result. Table 3.29 compares the advantages and disadvantages of the fit versions. In the last column of Table 3.29 the (subjective) ratings of the fit versions are listed, A – good, B – moderate, C – poor. V3-2-1, V4-4 and V4-6 are the favourites according to the analysis in Table 3.29.

Table 3.29 Comparison of Seiliger fit versions results

Fit version	Advantage	Disadvantages	Subjective rating
V3-1	The simplest fit version and equations can be solved in a simple way.	The theoretical engine efficiency in not fitted.	C

Fit version	Advantage	Disadvantages	Subjective rating
V3-2	Also a simple fit version. The most important three equivalence criteria (p_{max} , W_i , Q_{in}) are fitted	The fit value b is smaller than unity in operating point (B).	B
V3-2-1		Not real a new version and only used when $b < 1$ in V3-2. b is set to 1. p_{max} is no longer an equivalence criterion.	A
V4-1		not converging	N/A
V4-2		The fit results of ΔEO in operating point (A) and (C) are negative.	B
V4-3		1) The fit result of n_{exp} wrongly indicates heat input in all operating points; 2) The fit value b is smaller than 1 in operating point (B) and (C).	B
V4-3-1		Not real new version and only used when $b < 1$ in V4-3. b is set to 1. The fit results of n_{exp} wrongly indicate heat input process in all operating points.	B
V4-4	All the values of fit parameters are reasonable.	The difference in unused equivalence criterion T_{EO} between fit and real cycle are large for operating point (A) and (C)	A
V4-5		Not converging	N/A

Fit version	Advantage	Disadvantages	Subjective rating
<i>V4-6</i>	On the basis of <i>advanced</i> Seiliger process and considers four combustion stages.		A
<i>V5-1</i>	The five important equivalence criteria are all in this version.	The fit results of ΔEO in operating point (A) and (C) are negative.	B
<i>V5-2</i>		Not converging	N/A

Fit version	Converge	a	b	c	n_{exp}	η_{exp}	ΔEO	n_{comp}	η_{comp}	r_c	P_{max}	W_i	Q_{in}	T_{EO}	T_{max}
V3-1	√	1.313	1.336	2.625	1.31	1.054	0	1.36	1.022	13.10	0	3.63%	0	-4.68%	0
V3-2	√	1.313	1.260	3.571	1.31	1.054	0	1.36	1.022	13.10	0	0	0	-2.63%	-5.43%
V3-2-1	√	same as V3-2													
V4-1	×	not converging													
V4-2	√	1.313	1.337	2.618	1.31	1.054	-7.19	1.36	1.022	13.10	0	0	0	-2.92%	0
V4-3	√	1.313	1.247	3.766	1.283	0.915	0	1.36	1.022	13.10	0	0	0	0	-6.32%
V4-3-1	√	same as V4-3													
V4-4	√	1.313	1.336	2.625	1.396	1.411	0	1.36	1.022	13.10	0	0	0	-13.49%	0
V4-5	×	not converging													
V4-6	√	1.313	1.336	1.301	1.167	0.408	0	1.36	1.022	13.10	0	0	0	-1.30%	0
V5-1	√	1.313	1.336	2.621	1.286	0.986	-8.84	1.36	1.022	13.10	0	0	0	0	0
V5-2	×	not converging													

Table 3.30 Summary of fitting results of Seiliger fit versions of point (A)

Fit version	Converge	a	b	c	n_{exp}	η_{exp}	ΔEO	n_{comp}	η_{comp}	r_c	P_{max}	W_i	Q_{in}	T_{EO}	T_{max}
V3-1	√	1.528	1.044	1.141	1.33	1.003	0	1.36	1.028	13.10	0	-2.09%	0	-6.04%	0
V3-2	√	1.528	0.973	1.552	1.33	1.003	0	1.36	1.028	13.10	0	0	0	-3.00%	-6.59%
V3-2-1	√	1.493	1	1.491	1.33	1.003	0	1.36	1.028	13.10	-2.32%	0	0	-3.00%	-6.22%
V4-1	×									not converging					
V4-2	√	1.528	1.045	1.141	1.33	1.003	4.06	1.36	1.028	13.10	0	0	0	-6.98%	0
V4-3	√	1.528	0.920	1.996	1.320	0.983	0	1.36	1.028	13.10	0	0	0	0	-11.39%
V4-3-1	√	1.413	1	1.816	1.320	0.982	0	1.36	1.028	13.10	-7.56%	0	0	0	-11.09%
V4-4	√	1.528	1.045	1.141	1.330	1.026		1.36	1.028	13.10	0	0	0	-3.99%	0
V4-5	×									not converging					
V4-6	√	1.528	1.045	1.100	1.319	0.974		1.36	1.028	13.10	0	0	0	0	-2.65%
V5-1	√	1.528	1.044	1.141	1.318	0.990	-4.96	1.36	1.028	13.10	0	0	0	0	0
V5-2	×									not converging					

Table 3.31 Summary of fitting results of Seiliger fit versions of point (B)

Fit version	Converge	a	b	c	n_{exp}	η_{exp}	ΔEO	n_{comp}	η_{comp}	r_c	P_{max}	W_i	Q_{in}	T_{EO}	T_{max}
V3-1	√	1.784	1.109	1.927	1.31	1.033	0	1.36	1.028	13.10	0	3.60%	0	-6.21%	0
V3-2	√	1.784	1.010	3.085	1.31	1.033	0	1.36	1.028	13.10	0	0	0	-3.46%	-8.43%
V3-2-1	√	same as V3-2													
V4-1	×	not converging													
V4-2	√	1.784	1.109	1.927	1.31	1.033	-8.01	1.36	1.028	13.10	0	0	0	-4.23%	0
V4-3	√	1.784	0.991	3.415	1.286	0.972	0	1.36	1.028	13.10	0	0	0	0	-10.09%
V4-3-1	√	1.771	1	3.363	1.286	0.973	0	1.36	1.028	13.10	-0.72%	0	0	0	-9.94%
V4-4	×	1.784	1.109	1.927	1.354	1.187	0	1.36	1.028	13.10	0	0	0	-12.67%	0
V4-5	√	not converging													
V4-6	√	1.784	1.109	1.228	1.217	0.634	0	1.36	1.028	13.10	0	0	0	-1.67%	0
V5-1	√	1.784	1.109	1.929	1.288	0.991	-11.23	1.36	1.028	13.10	0	0	0	0	0
V5-2	×	not converging													

Table 3.32 Summary of results of Seiliger fit versions of point (C)

3.4 Comparison of Seiliger process with Vibe heat release model

The Seiliger process model and the Vibe model both contain a set of parameters to specify the combustion and cylinder process. In particular for the Seiliger process this requires a clear definition of the equivalence criteria between real cylinder process and the Seiliger model. Using the double Vibe model as the basis of the ‘in-cylinder process model’ – as presented in Chapter 2 – the in-cylinder pressure, temperature, work, heat input, etc, can be obtained. The output can be used to determine the Seiliger parameters on the basis of the Seiliger process fit versions. Here the simplest but efficient fit version *V3-1* and the fit version based on *advanced* Seiliger process *V4-6* are used. In this way the relation between the two sets of parameters, i.e. the Seiliger parameters and the Vibe parameters can be investigated, for full load and part load operating conditions of the engine. The investigation based on *V3-1* has been published in [Ding, 2010].

Table 3.33 lists the base values and the range of the double Vibe parameters used in the ‘in-cylinder process model’. According to the discussion in section 2.2.3, Vibe parameter a and m_{fr} can be constant, so in this section they are set to their respective base value in all cases. Figure 3.41 shows the $p-\phi$ and $T-\phi$ diagram of the Seiliger process fit, found with fit version *V3-1* and based on a double Vibe model with the base values from Table 3.33.

Table 3.33 The values of double Vibe parameters used in the comparison

Double Vibe Parameter	Base Value	Range
m_1	0.1	0.01 – 0.6
m_2	3	1.0 – 7.0
b_1	0.7	0.1 – 0.9
SOC	176	160 – 190
EOC	260	240 - 300
a	6.908	
m_{fr}	1	

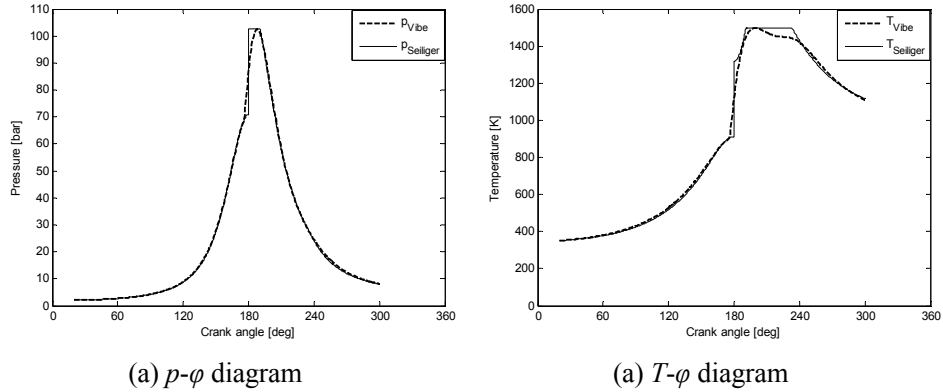


Figure 3.41 Comparison of Seiliger process and double Vibe model

3.4.1 Seiliger process model based on $V3-1$ fit version

1) Comparison of Vibe parameter m_1 and Seiliger parameters ($V3-1$)

The shape factor m_1 in a double Vibe model represents the premix combustion stage. With larger values of m_1 , Seiliger parameter a becomes smaller (Figure 3.42 (a)) and b larger (Figure 3.42(b)). A larger a value in the Seiliger process corresponds to a larger heat release during premix combustion while for b a larger value corresponds to less premix combustion. Also a decreasing parameter a obviously corresponds to a decreasing peak pressure. The product $a*b$ is proportional to the maximum (peak) temperature, and is almost constant in this case (Figure 3.42(d)).

Although hardly visible, $a*b$ and thus T_{max} has a minimum for $m_1 = 0.28$, which can be traced down to the fact that for that value the peak temperature caused by the second Vibe function in the later part of the heat release (occurring at around 240° in Figure 3.41(b)) becomes higher than the peak temperature caused by the first Vibe function. The effect can also be seen as a slight change of slope of b at $m_1 = 0.28$ in Figure 3.42(b). The Seiliger parameter c increases first with increasing m_1 , to provide more diffusive combustion (Figure 3.42(c)). However, parameter b also plays an important role in diffusive combustion. The slight but noticeable change in slope of b then causes c to decrease rather abruptly.

The product of $b*c$ is, in terms of the Seiliger process, equal to the duration of the combustion, or rather the volume change during combustion. For values of m_1 higher

than 0.28 the duration of combustion becomes almost constant. So the subtle shift from premix to diffusive combustion caused by an increase of m_1 in terms of Vibe is translated in an abruptly different combination of changes in b and c in terms of Seiliger.

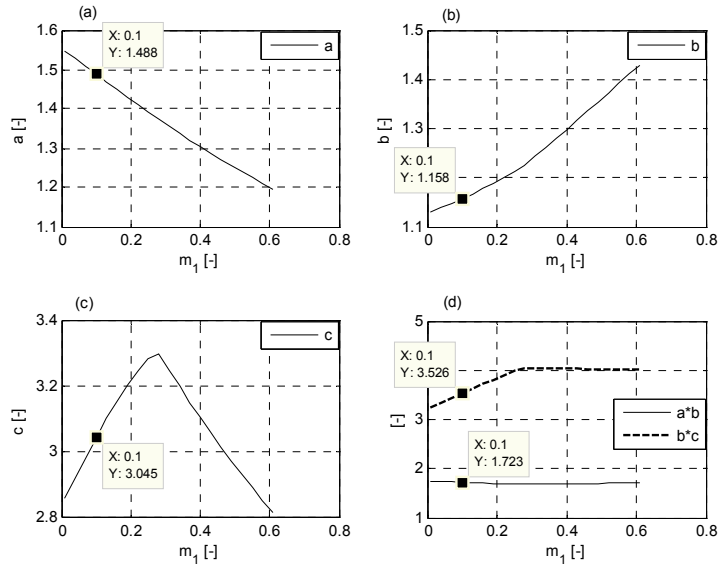


Figure 3.42 Seiliger parameters (V3-1) vs. variation of Vibe parameter m_1

2) Comparison of Vibe parameter m_2 and Seiliger parameters (V3-1)

The parameter m_2 is set to a relative wide range of values and it is obvious that from around $m_2 = 4$, the three Seiliger parameters remain constant. Before that point, a and b both decrease steeply with increasing m_2 (Figure 3.43(a) and (b)), while parameter c increases steeply (Figure 3.43(c)). Parameter c corresponds to the intensity of the diffusive combustion. The duration of the combustion $b \cdot c$ also increases up to $m_2 = 4$ and remains constant from then onward (Figure 3.43(d)). In the same figure the maximum temperature, characterized by $a \cdot b$, hardly changes.

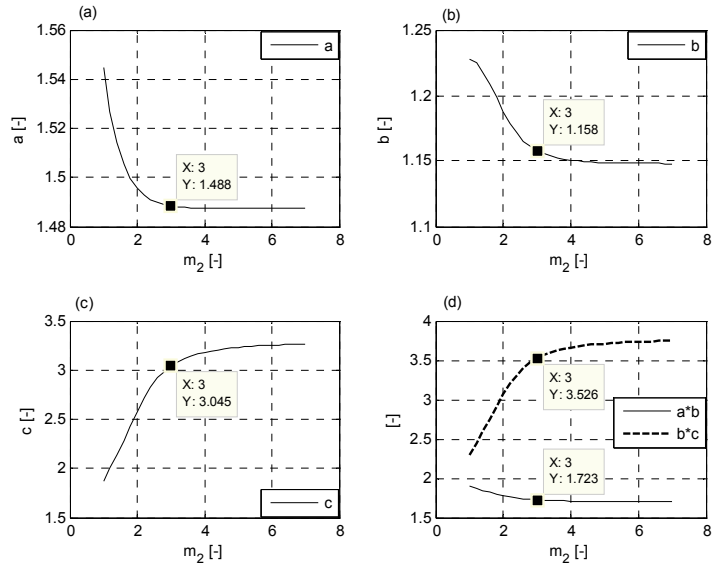


Figure 3.43 Seiliger parameters (V3-1) vs. variation of Vibe parameter m_2

3) Comparison of Vibe parameter b_1 and Seiliger parameters (V3-1)

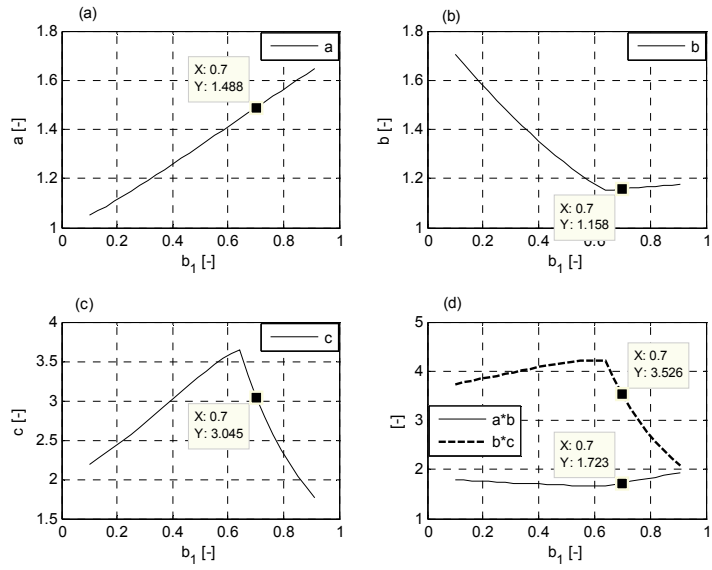


Figure 3.44 Seiliger parameters (V3-1) vs. variation of Vibe parameter b_1

Weight factor b_l indicates the percentage of premixed combustion. So Seiliger parameter a increases with increasing b_l (Figure 3.44(a)) and Seiliger parameter b decreases with increasing b_l (Figure 3.44(b)). But for $b_l > 0.64$, parameter b remains constant, while at that point c changes abruptly from increasing to decreasing (Figure 3.44(c)). Also the combustion duration b^*c becomes shorter, as can be seen in Figure 3.44(d). The cause again seems to be the hardly noticeable minimum of T_{max} as expressed by the product $a*b$, Figure 3.44(d). Again it can be shown that at $b_l = 0.64$ the peak temperature caused by the second Vibe function in the later part of the heat release becomes higher then the peak temperature caused by the first Vibe function.

4) Comparison of Vibe parameter SOC and Seiliger parameters (V3-1)

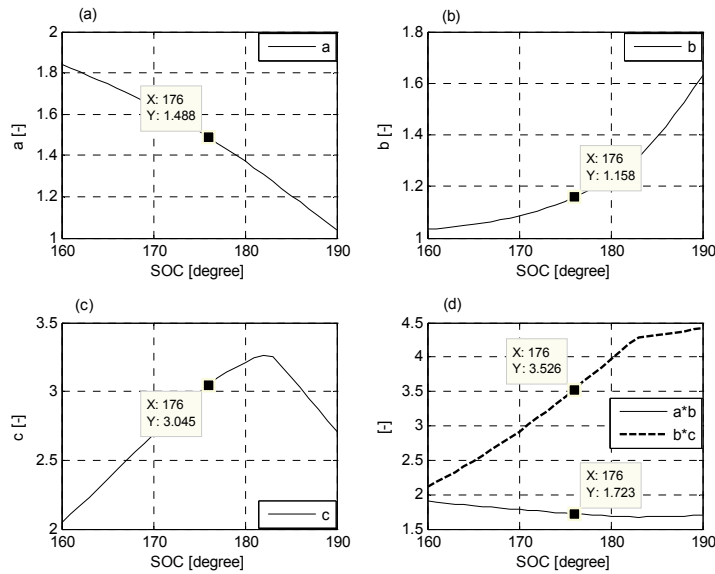


Figure 3.45 Seiliger parameters (V3-1) vs. variation of Vibe parameter SOC

The base value of start of combustion (SOC) is set to 176° (4° before TDC). Parameter a decreases to almost unity when SOC is retarded (Figure 3.45(a)). Parameter b again shows the opposite trend (Figure 3.45(b)). Thus an (very) early start of combustion makes the pressure increase very sharp (large values of a while $b = 1$, i.e. ‘Otto like’) and late start of combustion gives a very low peak pressure ($a = 1$ while b becomes larger, i.e. ‘Diesel like’). A later SOC not only decreases the peak pressure but also reduces the maximum temperature as expressed by $a*b$ in Figure

3.45(d). Parameter c first increases but from $SOC = 184^\circ$, it sharply decreases (Figure 3.45(c)). The explanation is the same as before, i.e. a change of order in the first and second Vibe temperature peak, at $SOC = 184^\circ$.

Although the shape of the Vibe heat release remains the same, it shifts to a later crank angle segment and therefore finishes later. In the Seiliger representation (where combustion starts at TDC by definition) this is reflected in a longer duration of the combustion $b*c$, Figure 3.45(d).

5) Comparison of Vibe parameter EOC and Seiliger parameters (V3-1)

The duration of combustion ($\Delta\alpha_{comb}$) is a parameter in Vibe function. However when SOC and EOC are fixed, $\Delta\alpha_{comb}$ is the difference between them. Therefore in this thesis, EOC is used to investigate the duration of combustion. Since the length of premixed combustion becomes longer when EOC increases, parameter a is decreasing (Figure 3.46(a)) resulting in a lower peak pressure. EOC has a minor impact on b (Figure 3.46(b): b increased slightly from around 1.14 to 1.17). Enlarging combustion duration time causes late combustion, so c increases with rising EOC (Figure 3.46(c)) and thus the duration $b*c$ also increases (Figure 3.46 (d)).

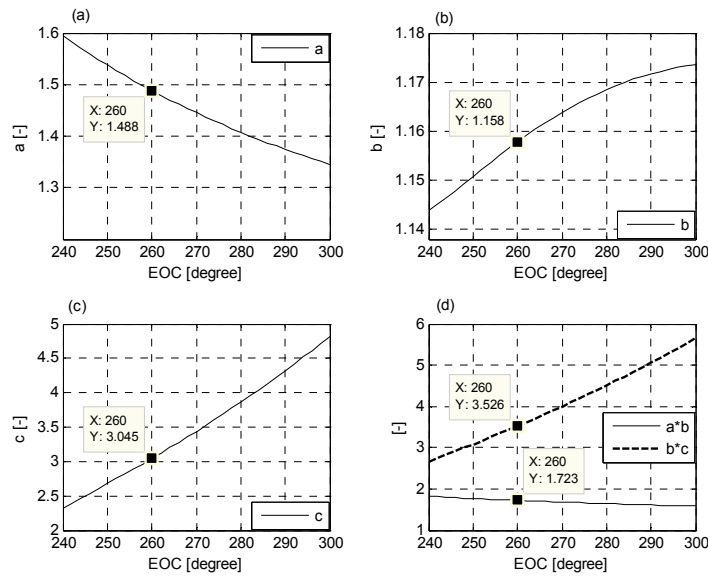


Figure 3.46 Seiliger parameters (V3-1) vs. variation of Vibe parameter EOC

In order to show what happens in cases where one of the Seiliger parameters (most often parameter c) changes abruptly, the cylinder process for the transition point $b_I = 0.64$ is shown in Figure 3.47. In particular the Figure 3.47(b) shows the second temperature peak becoming as high as the first temperature peak and this causes, after mapping to a Seiliger cycle, the parameter c to abruptly change direction in Figure 3.44(c). Of course this cause by an extreme Vibe combustion shape that probably will not occur in real engines, at least when the fuel injection is operating without failures.

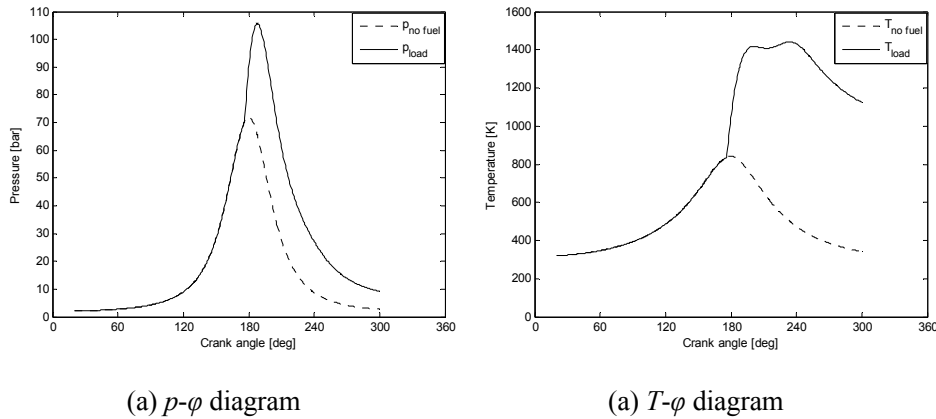


Figure 3.47 Double Vibe driven cylinder process: basic values but $b_I = 0.64$

3.4.2 Seiliger process model based on V4-6 fit version

In this section, the Seiliger fit version used is the *V4-6*, which is based on the advanced Seiliger process with four combustion stages. As discussed in section 3.3.6, the a and b are the same as in the V3-1 version. Therefore only the comparison of Vibe parameters and Seiliger parameters c , $b*c$ and n_{exp} is investigated in this section, and the comparison of a , b and $a*b$ for each Vibe parameters can be found in section 3.4.1 and Figure 3.42 – Figure 3.46. In order to investigate whether the expansion exponent n_{exp} appropriately indicates the heat input to the process, the polytropic factor η_{exp} is shown in the figures below.

1) Comparison of Vibe parameter m_I and Seiliger parameters (V4-6)

Figure 3.48 shows the comparison of Vibe parameter m_I and Seiliger parameters c and n_{exp} , also $b*c$ and η_{exp} . Compared with Figure 3.42(c), the trend of c fitted with

V4-6 is the same as V3-I, also the point, where the second peak temperature becomes the highest ($m_1 = 0.28$) is the same (Figure 3.48(a)). But for the same m_1 , c is smaller in V4-6, which means some heat input in stage 4-5 is moved to the stage 5-6. n_{exp} increases first, then at $m_1 = 0.28$ abruptly decreased caused by noticeable change of c . η_{exp} follows the same trend as n_{exp} with values that are smaller than unity indicating the heat input during stage 5-6 (Figure 3.48(d)).

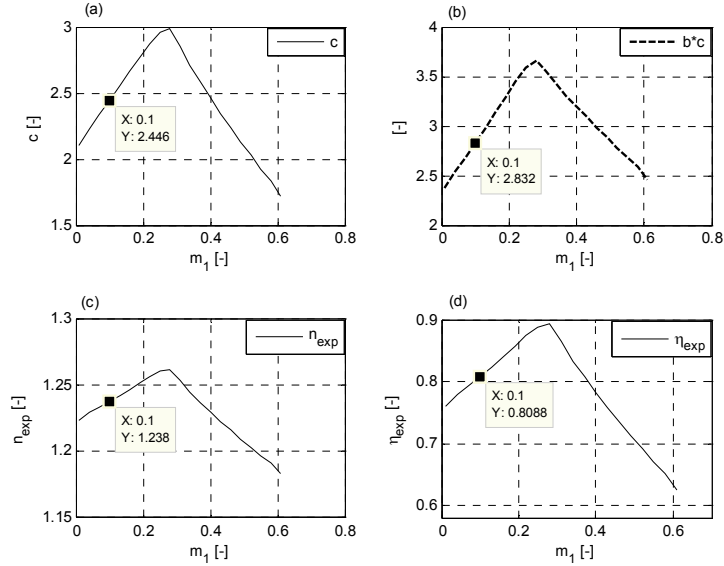


Figure 3.48 Seiliger parameters (V4-6) vs. variation of Vibe parameter m_1

2) Comparison of Vibe parameter m_2 and Seiliger parameters (V4-6)

Since parameter m_2 indicates the diffusive and late combustion in the Vibe model, when the Seiliger fit version V4-6 is used adding a very late combustion stage, the parameter m_2 is sensitive to parameter c and n_{exp} . Therefore, c and n_{exp} change remarkably with m_2 . Parameter c increases in the beginning and at around $m_2 = 2.8$, decreases rapidly, then at about $m_2 = 5$, the value goes below 1 indicating heat loss during stage 4-5 (Figure 3.49 (a)). n_{exp} and η_{exp} are both decreasing with rising m_2 so it is proved that a large m_2 value results in more heat input occurring in very late combustion stage.

It is mentioned that when the value m_2 rises to about 5.5, the fit equations of V4-6 cannot find solutions for the Seiliger parameters. Since the other Vibe parameters are

kept at the basic value, when m_2 rises to 5.5, only extreme engine running conditions, which could not happen in the measured engine cycle, could lead to cases where no Seiliger parameters can be fitted. Compared with *V3-1*, version *V4-6* has more variables to fit and more complicated equations, and therefore it cannot fit some extreme running condition case like *V3-1*.

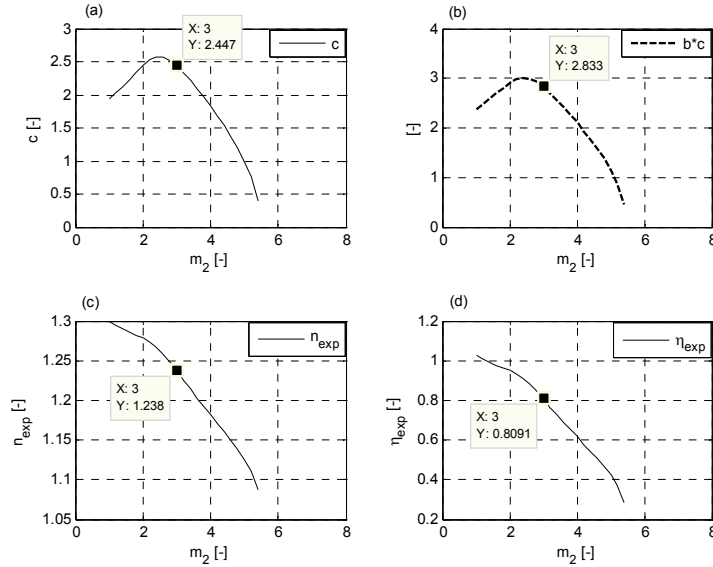


Figure 3.49 Seiliger parameters (*V4-6*) vs. variation of Vibe parameter m_2

3) Comparison of Vibe parameter b_1 and Seiliger parameters (*V4-6*)

Like m_2 , although the range of b_1 is set to be 0.1 – 0.9 (refer Table 3.33), only for $b_1 = 0.55$ the iteration is converging. With b_1 rising, parameter c firstly increases and then decreases at $b_1 = 0.64$ (Figure 3.50 (a)). This is the same effect, caused by the second peak in temperature, as explained in Figure 3.47. When m_2 increases, n_{exp} and η_{exp} are increasing but from $b_1 = 0.64$ the curves become less steep (Figure 3.50 (c) and (d)). η_{exp} finally almost arrives at unity when $b_1 = 0.64$, implying that stage 5-6 is almost isentropic process if the diffusive combustion is very short.

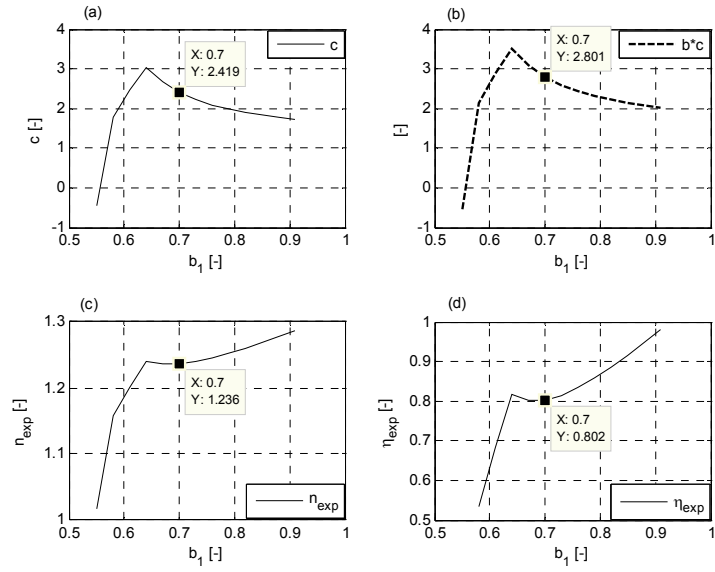


Figure 3.50 Seiliger parameters (V4-6) vs. variation of Vibe parameter b_1

4) Comparison of Vibe parameter SOC and Seiliger parameters (V4-6)

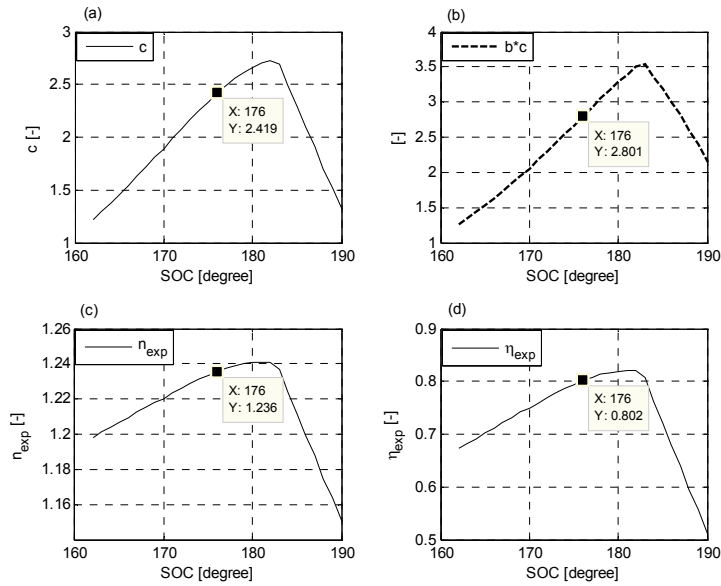


Figure 3.51 Seiliger parameters (V4-6) vs. variation of Vibe parameter SOC

When the start of combustion is late, the parameters c and n_{exp} both first increase and then start to decrease at about $SOC = 184^\circ$ (Figure 3.51 (a) and (c)), which is the same point as in V3-1 (Figure 3.45 (c)). From Figure 3.45 (d), η_{exp} is below unity for the whole range of SOC meaning that in all cases during stage 5-6 there is net heat input.

5) Comparison of Vibe parameter EOC and Seiliger parameters (V4-6)

When EOC is increasing, the duration of combustion is extended. In Figure 3.52 (a), when EOC increases, parameter c increases a little for the first 10° , then decreases slightly until $EOC = 274^\circ$. Since the iteration stops converging at $EOC = 276^\circ$, the last two points of EOC seem out of range. But from about $EOC = 272^\circ$, parameter c becomes smaller than unity, meaning heat loss occurring in (combustion!) stage 4-5 instead of heat input. n_{exp} decreases with larger EOC , and, also in the last two points of the EOC variation, n_{exp} changes abruptly (Figure 3.52 (c)). η_{exp} in the beginning is larger than unity, indicating the heat loss during stage 5-6, but at about $EOC = 247^\circ$, it becomes smaller than unity.

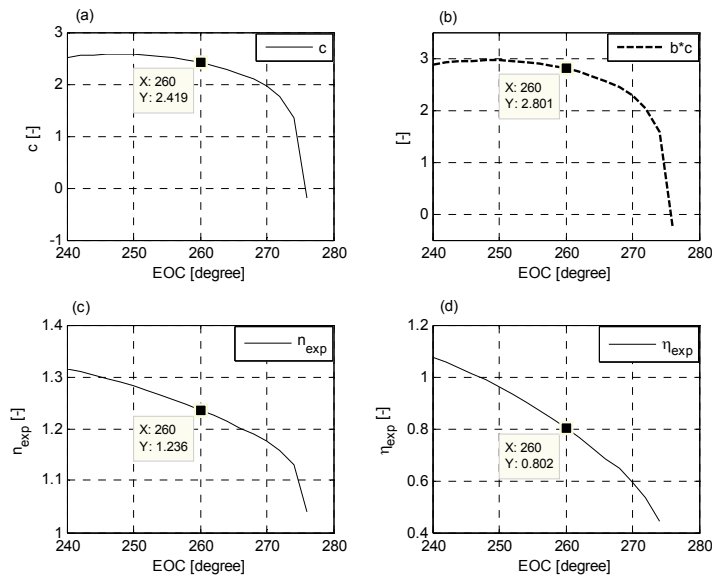


Figure 3.52 Seiliger parameters (V4-6) vs. variation of Vibe parameter EOC

3.4.3 Summary

This section compares two manners to characterise the combustion process in a diesel engine: the Seiliger process model and the Vibe model. They were compared to investigate the influence of the double Vibe parameters on the Seiliger parameters.

The systematic research of the three (*V3-1*) and four (*V4-6*) Seiliger combustion parameters leads to the conclusion that a wide variety of Vibe combustion shapes can be mapped adequately to the three (or four) Seiliger combustion parameters. Even when under extreme conditions the latent second temperature peak becomes the larger one, the Seiliger parameters still react in a very sensitive way.

V4-6 Seiliger fit version presents more Seiliger parameters (four instead of three in *V3-1* fit version) to give more combustion stages. However, due to more complicated equations of equivalence criteria, for some extreme engine running condition points, the iteration is not converging. Nonetheless, the advanced Seiliger process, as presented in this thesis, can also be used to characterise the combustion process at least as good as the basic Seiliger process. Furthermore, a Seiliger process description can achieve the same goal as a Vibe heat release model in characterizing the combustion of diesel engines.

Chapter 4

Using Measurements to Characterise Combustion

4.1 Introduction

In Chapter 3, the fit of the real engine cycle with a Seiliger process was presented in three representative operating points (nominal point, nominal speed and 25% power, low speed and 50% power). The differences of the Seiliger parameters coming out of several fit procedures for the three operating points were compared and their global behaviour as function of power and speed could be seen. However, to fully characterize the combustion process using a Seiliger model, the dependency of the Seiliger parameters on the engine running conditions (e.g. power output, engine speed) over the full operational range of the engine should be investigated. In this chapter, the behaviour of the Seiliger parameters over the full operational range of the MAN 4L20/27 diesel engine for cylinder 1 is shown based on one extensive series of measurements.

4.2 Flow chart of the simulation procedure

First, the flow chart of the overall simulation procedure is shown in Figure 4.1. The simulation procedure involves 5 main models: 1) heat release calculation model; 2) Vibe combustion fit model; 3) in-cylinder process simulation model; 4) Seiliger fit model and 5) Seiliger process model. The prime input of the procedure is the measured in-cylinder pressure signals and the output is the Seiliger parameters. The complete procedure will briefly be summarised here.

The ‘heat release calculation’ model (presented in Chapter 2) uses the measured data, primarily the in cylinder pressure signals, to calculate the reaction rate according to the ‘first law of thermodynamics’ and the temperature in cylinder based on the ‘gas law’. The combustion reaction rate (CRR), which is in fact the output of the ‘heat release calculation’ model, is integrated to get the monotonous increasing and smoother reaction co-ordinate (RCO) and then the RCO may be corrected to fit the gross heat input (section 2.3)¹. The ‘combustion fit model’ (section 2.4) makes use of multiple Vibe functions. The multiple Vibe parameters fitted with the ‘combustion fit model’ are then the input of the ‘in-cylinder process simulation model’, where the major in-cylinder parameters can be obtained (section 2.2). Then the Seiliger parameters (presented in Chapter 3) are determined on the basis of a chosen combination of equivalence criteria between Seiliger process and real engine. The Seiliger parameters are calculated from the ‘Seiliger fit model’ (section 3.3). This iteration method uses the equivalence parameters that are calculated by the ‘Seiliger process model’ (section 3.2). Then finally the cylinder performance is expressed in the Seiliger parameters. These parameters characterize the cylinder process and in particular the combustion shape.

With the simulation procedure, the Seiliger parameters can be calculated for one operational point. After obtaining the Seiliger parameters for all measured points over the engine operational map, their trend as function of the engine operating condition can be presented.

¹ As presented in section 3.3.1, the heat loss to the walls is not necessary for the Seiliger fit. Therefore the correction of the Woschni model is not considered in this chapter.

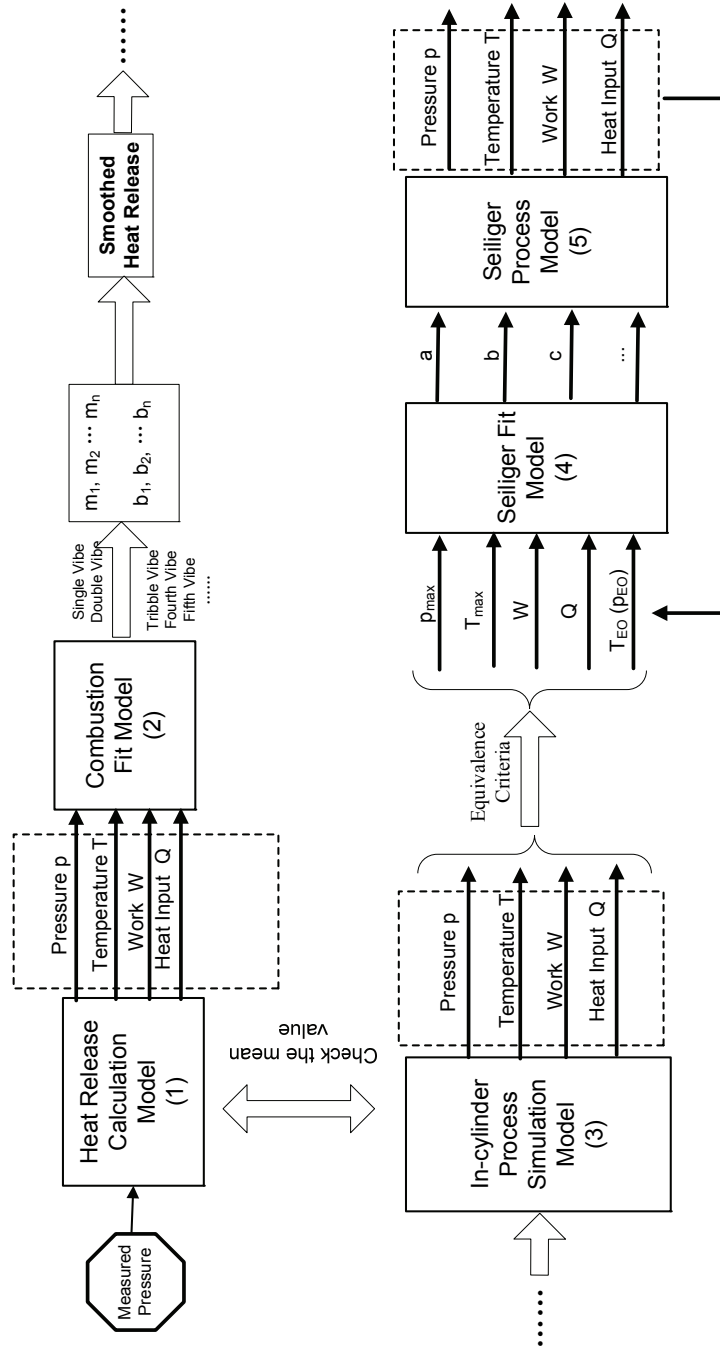


Figure 4.1 The flow chart of the overall simulation procedure

4.3 The map of measured series

Four series of measurements were carried out with the MAN 4L20/27 engine at the NLDA test facility. Figure 4.2 – Figure 4.5 show the map of measured points in terms of engine speed and indicated power for the four series.

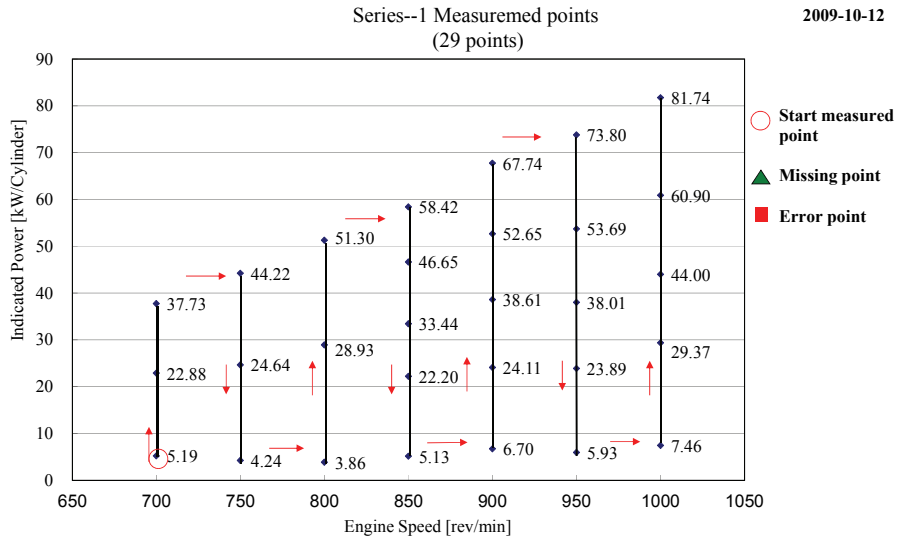


Figure 4.2 Map of measured points: Series I

In the measurement Series I, 29 engine operating points were measured (Figure 4.2). The engine was running between 700 rpm and 1000 rpm and the measurement was carried out with increments of 50 rpm. Three points were taken at engine speeds 700 rpm – 800 rpm and five points for engine speeds 850 rpm – 1000 rpm. The measurement of the overall series was started at the lowest load point at the lowest engine speed (700 rpm). In order to get the engine running points as much as possible thermodynamically stable, the operating points at constant speeds were traversed alternatively up and down, as indicated by the arrows.

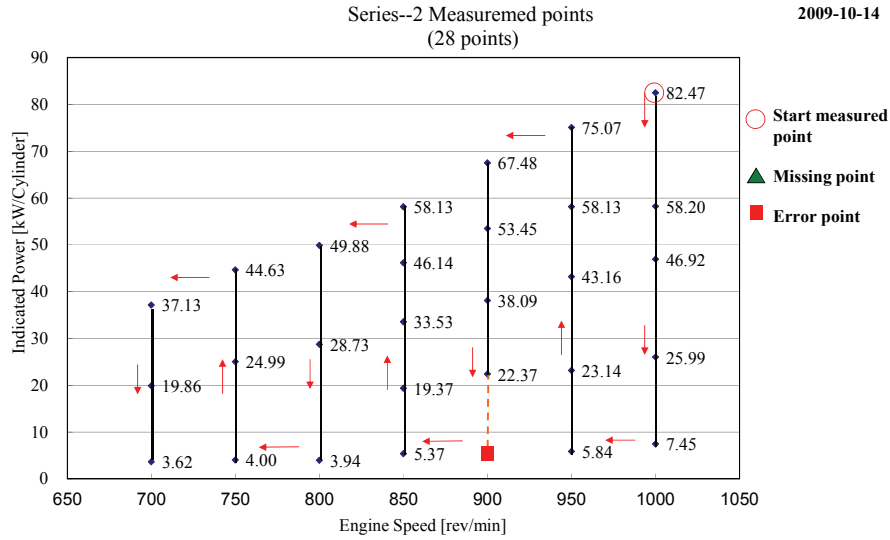


Figure 4.3 Map of measured points: Series II

The measurement Series II was carried out in almost the same points as for Series 1 but with a different starting point and traversing direction (Figure 4.3). Some measurement errors became apparent after calculation and analysis in the lowest load point at an engine speed 900 rpm and this point is removed from the series.

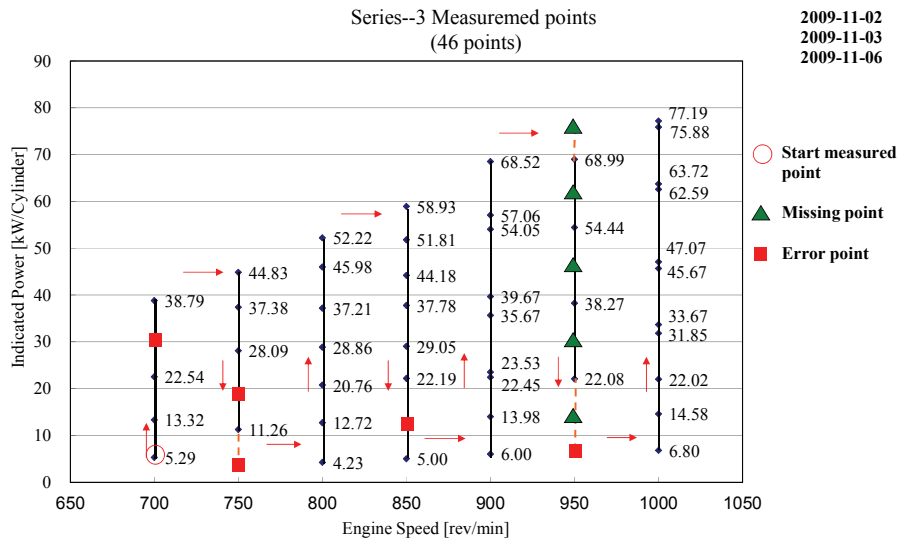


Figure 4.4 Map of Measured points: Series III

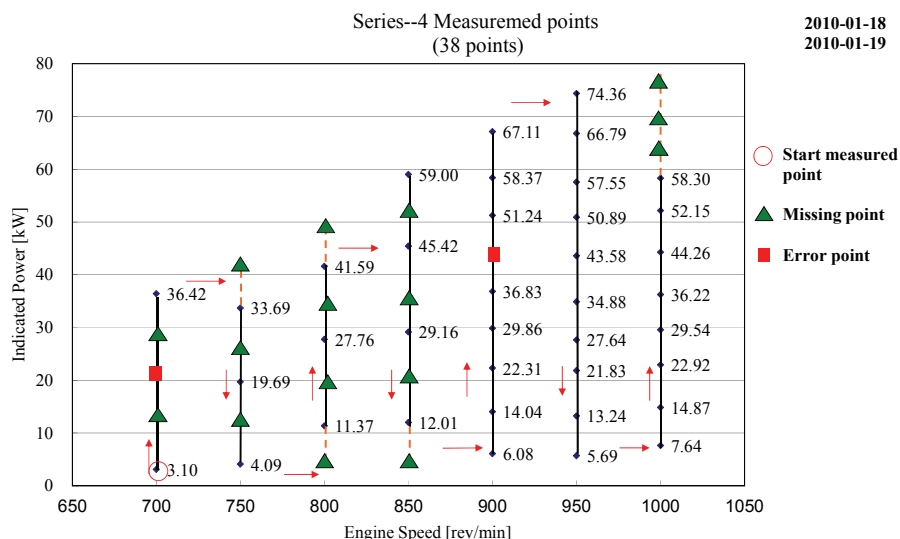


Figure 4.5 Map of measured points: Series IV

Figure 4.4 and Figure 4.5 show the measured points map for Series III and Series IV. It was the intention to take 56 measured points in both series but some unexpected and unpredictable failures of the test set-up occurred during the measurement. Therefore five intended point in Series III and sixteen intended points in Series IV are missing. Also five measured points in Series III and two measured points in Series IV gave no results because of errors that became apparent after calculation and analysis.

Among the four series measurement, Series I and II both were completed in one day. Since there were more measured points planned in Series III and IV, they were expected to be measured over two days. But for Series III, during the measurement the torque meter broke down on the first day with the consequence that no effective power could be measured. This is the reason why this series ultimately was carried out in three days. Also some adjacent points were very close to each other, in particular for engine speeds of 900 rpm and 1000 rpm. Although there are only 28 points measurements in Series II, they are all relatively reliable and evenly spaced. Therefore the following illustration and explanation of results are on the basis of Series II. The results of the other series are similar to this series and in due time they will be presented in a full internal report for later reference.

4.4 Result of Seiliger parameter a

Table 4.1 Summary of values of Seiliger parameters

	a	b	c	n_{exp}	ΔEO
<i>V3-1</i>	Value 1	Value 1	Value 1	Value 1	Value 1
<i>V3-2</i>	Value 1	Value 2	Value 2	Value 1	Value 1
<i>V3-2-1</i>	Value 2	Value 3	Value 3	Value 1	Value 1
<i>V4-1</i>	Not converging				
<i>V4-2</i>	Value 1	Value 1	Value 1	Value 1	Value 2
<i>V4-3</i>	Value 1	Value 4	Value 4	Value 2	Value 1
<i>V4-3-1</i>	Value 3	Value 5	Value 5	Value 3	Value 1
<i>V4-4</i>	Value 1	Value 1	Value 1	Value 4	Value 1
<i>V4-5</i>	Not converging				
<i>V4-6</i>	Value 1	Value 1	Value 6	Value 5	Value 1
<i>V5-1</i>	Value 1	Value 1	Value 1	Value 6	Value 3
<i>V5-2</i>	Not converging				

For all Seiliger parameters Table 4.1 lists the fit versions in which they are used, sorted according to the different values of the equivalence criteria introduced in Chapter 3.

Seiliger parameter a indicates the premixed combustion phase. A large value of a is associated with more premixed combustion. Figure 4.6 – Figure 4.8 show the trend of a as function of power (indicated power P_i rather than effective power P_e) at different engine speeds. At each engine speed, the value of a increases in at low load and reaches a maximum, then decreases going to higher load (but for low engine speed 700 rpm and 750 rpm there is no deflection due to relative low power output). As to the effect of engine speed on the Seiliger parameter a , it can be observed that for a certain load point parameter a is lower for higher engine speed.

There are three different sets of values for a appearing in the Seiliger process fit versions:

Value 1: *V3-1*, *V3-2*, *V4-2*, *V4-3*, *V4-4*, *V4-6*, *V5-1*

Value 2: *V3-2-1*

Value 3: *V4-3-1*

Since *V3-2-1* and *V4-3-1* are only applied when the Seiliger parameter *b* becomes smaller than unity in *V3-1* and *V4-3* respectively, the *a* in Figure 4.7 and Figure 4.8 are equal to value 1 at higher loads. But in part load, parameter *a* really gets value 2 and value 3 and both decrease fast at low load. At very low load (the lowest load point for each engine speed) the values go below unity. This implies that the elimination of the unrealistic heat input of stage 3-4 in Seiliger process by increasing parameter *b* from a value $b < 1$ to $b = 1$ is mostly compensated by a decreasing heat input in stage 1-2 (The black and blue dashed lines in the Figure 4.7 and Figure 4.8 indicate the boundary lines where parameter *b* becomes smaller than unity). The result must inevitably be that all combustion shifts to late combustion (parameter *c*) at low load, at least for this engine.

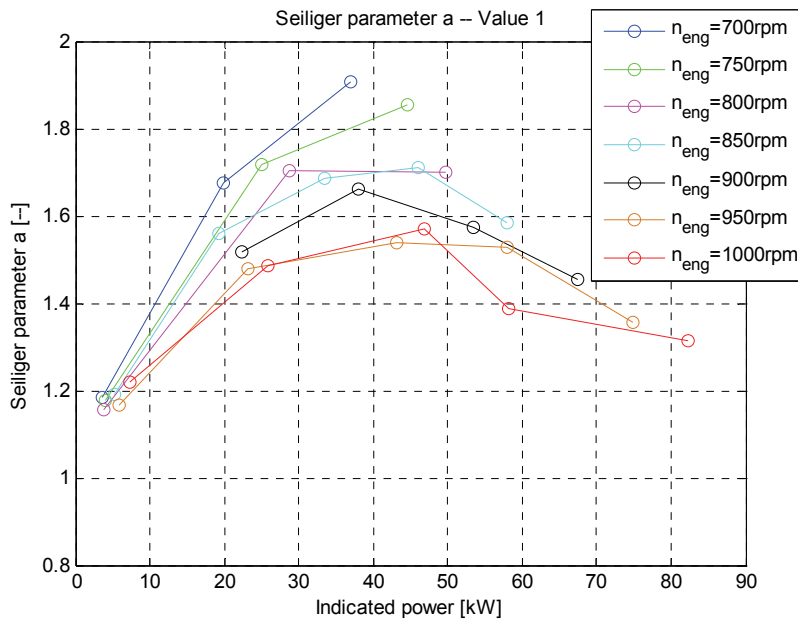


Figure 4.6 Result of Seiliger parameter *a* (value 1)

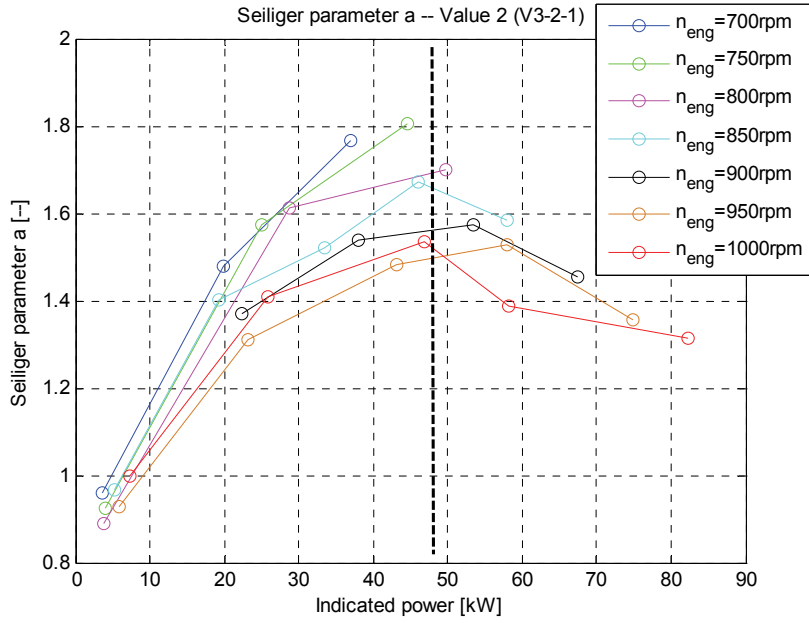


Figure 4.7 Result of Seiliger parameter a (value 2)

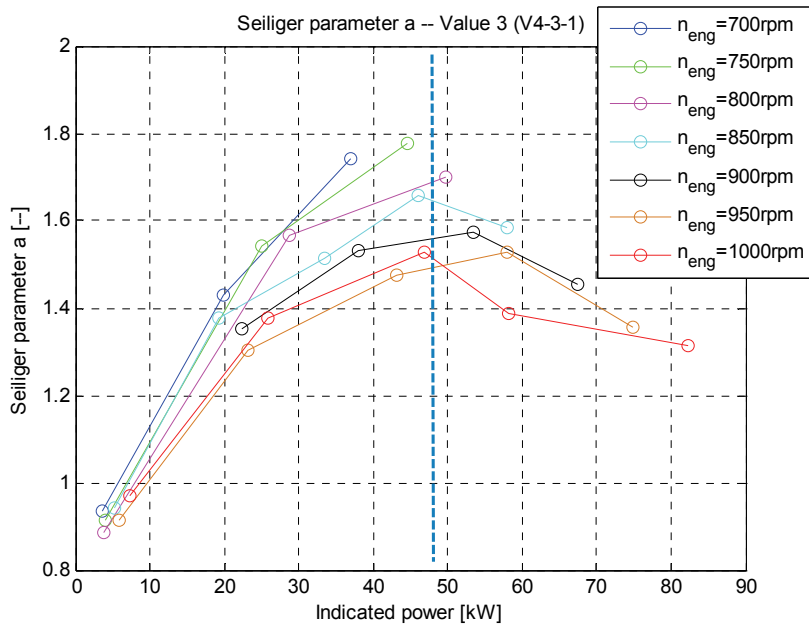


Figure 4.8 Result of Seiliger parameter a (value 3)

4.5 Result of Seiliger parameter b

Seiliger parameter b indicates the diffusive combustion phase. A large value of b is associated with more heat input during the diffusive combustion (stage 3-4 in Seiliger process), which generally is beneficial for engine efficiency. Figure 4.9 – Figure 4.13 show the tendency of b as function of indicated power for different engine speeds. There are five different sets of values of b appearing in the Seiliger fit versions:

Value 1: *V3-1, V4-2, V4-4, V4-6, V5-1*

Value 2: *V3-2*

Value 3: *V3-2-1*

Value 4: *V4-3*

Value 5: *V4-3-1*

In all the versions where parameter b has value 1, since T_{max} is one of the equivalence criteria, according to equation [3.20] it can be concluded that parameter b is always larger than unity. At a certain engine speed, b goes up with increasing load. The engine speed seems to have less effect on b , i.e. there is hardly any difference for different engine speeds at the same load, at least for this engine.

Value 2 and value 4 exclude the T_{max} as equivalence criterion, i.e. the T_{max} in these Seiliger fit versions are lower than in the real engine cycle so for the same operating point, these values for parameter b are smaller than value 1. In particular in part load (below 50 kW), b becomes even smaller than unity, which means the heat input changes to heat loss during stage 3-4, which of course is unrealistic. From this point of view, fit versions *V3-2* and *V4-3* are poor.

In order to avoid parameter b becoming smaller than unity, the ‘reduced’ fit versions *V3-2-1* and *V4-3-1* were applied, however only at part load from the point where $b < 1$. This is a discontinuous change that is of course not attractive. Value 3 and value 5 of b both become unity in part load. The black and blue dashed lines in the figures indicate the boundary lines where parameter b becomes smaller than unity.

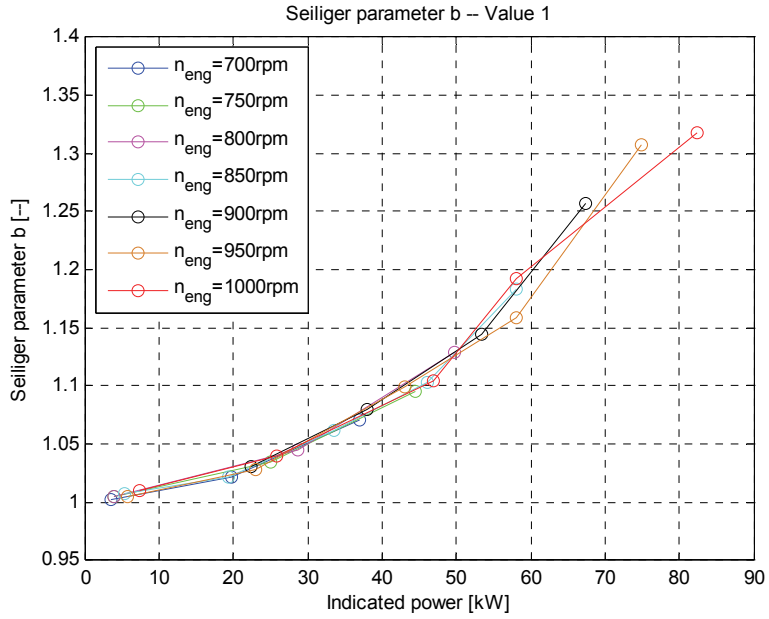


Figure 4.9 Result of Seiliger parameter b (value 1)

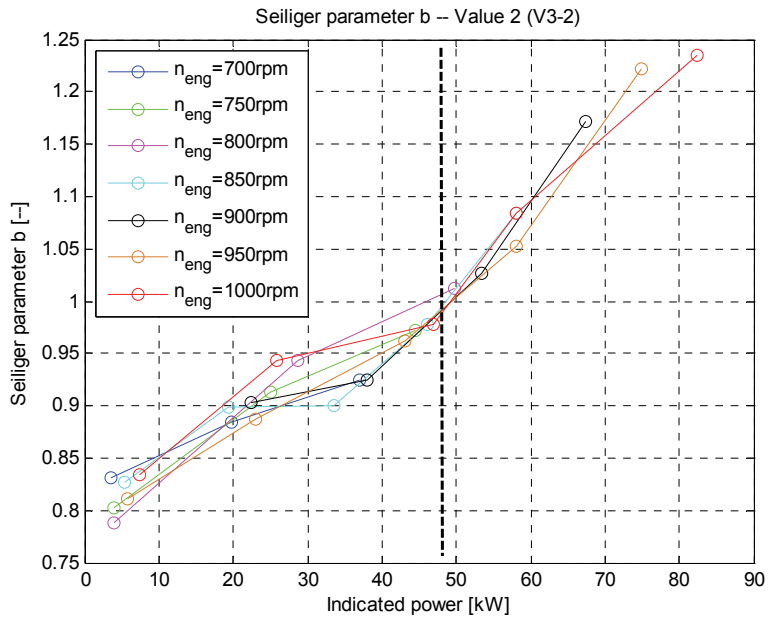


Figure 4.10 Result of Seiliger parameter b (value 2)

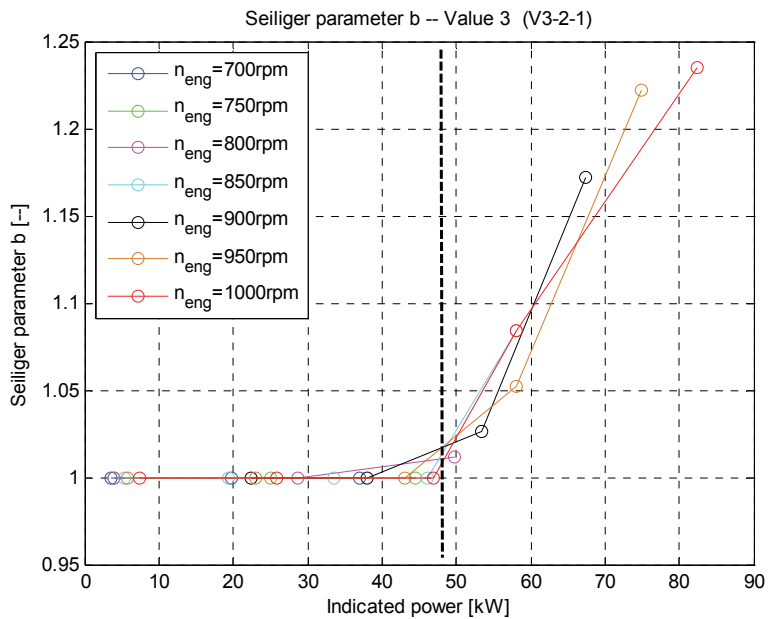


Figure 4.11 Result of Seiliger parameter b (value 3)

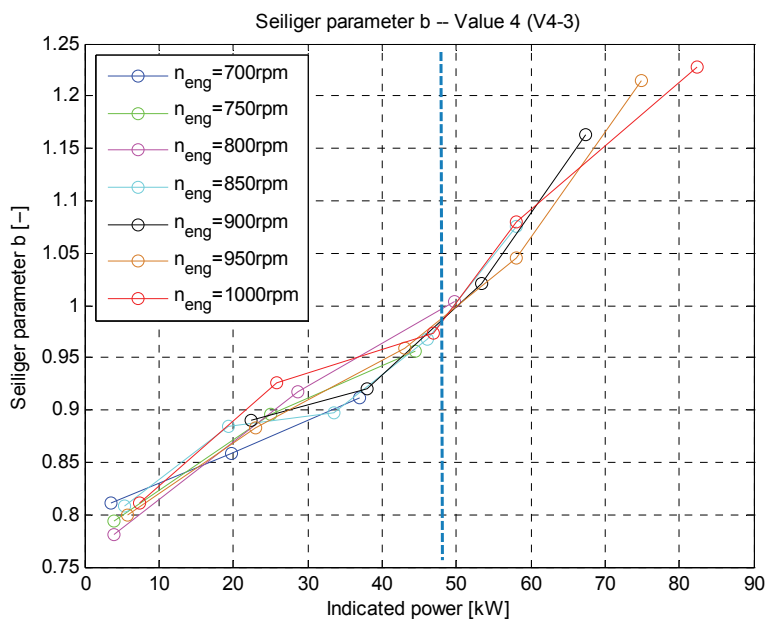


Figure 4.12 Result of Seiliger parameter b (value 4)

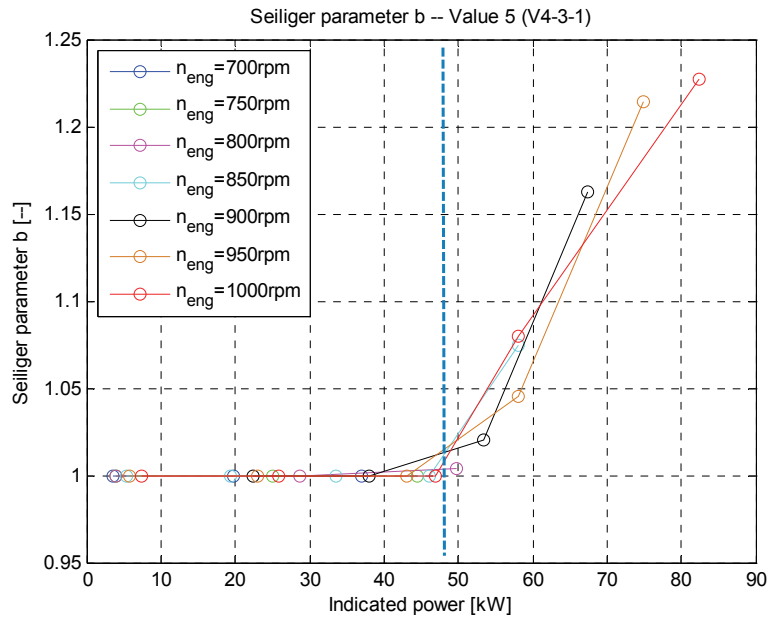


Figure 4.13 Result of Seiliger parameter b (value 5)

4.6 Result of Seiliger parameter c

Seiliger parameter c indicates the diffusive and late combustion process. A large value of c is associated with more combustion occurring in a late stage, which generally is not beneficial to engine efficiency and harmful in view of the possible unburned hydrocarbon emissions. Figure 4.14 – Figure 4.19 show the tendency of c as function of indicated power at different engine speeds. There are six different sets of values for c appearing in the Seiliger fit versions:

Value 1: *V3-1, V4-2, V4-4, V5-1*

Value 2: *V3-2*

Value 3: *V3-2-1*

Value 4: *V4-3*

Value 5: *V4-3-1*

Value6: *V4-6*

According to value 1 parameter c is rising with increasing load at a certain engine speed and the engine speed seems to have a minor effect on c .

The tendencies of value 2, value 3, value 4 and value 5 are difficult to describe due to the irregular and chaotic results. Same as for Seiliger parameter b , value 3 and value 5 are the extended versions of value 2 and value 4 respectively at low load. Therefore when value 3 is compared with value 2 and value 5 with value 4, the values only in the part load are somewhat lower. Again the black and blue dashed lines in the figures are used to indicate the boundary lines where parameter b becomes smaller than unity.

Value 6 is valid for the new *advanced* Seiliger process fit version and the values are rather low, which means the heat input during stage 4-5 is very low. However together with the result of n_{exp} (discussed in section 4.7), it can be said that in *V4-6*, the heat input during stage 4-5 moves to stage 5-6, also in some part load points. In some operating points at very low load the heat input changes into heat loss (c is smaller than unity), which of course is unrealistic.

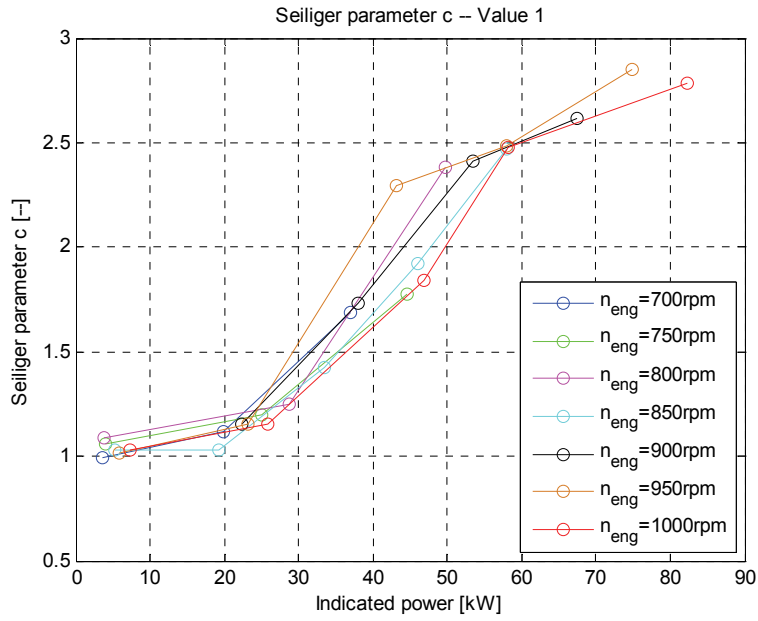


Figure 4.14 Result of Seiliger parameter c (value 1)

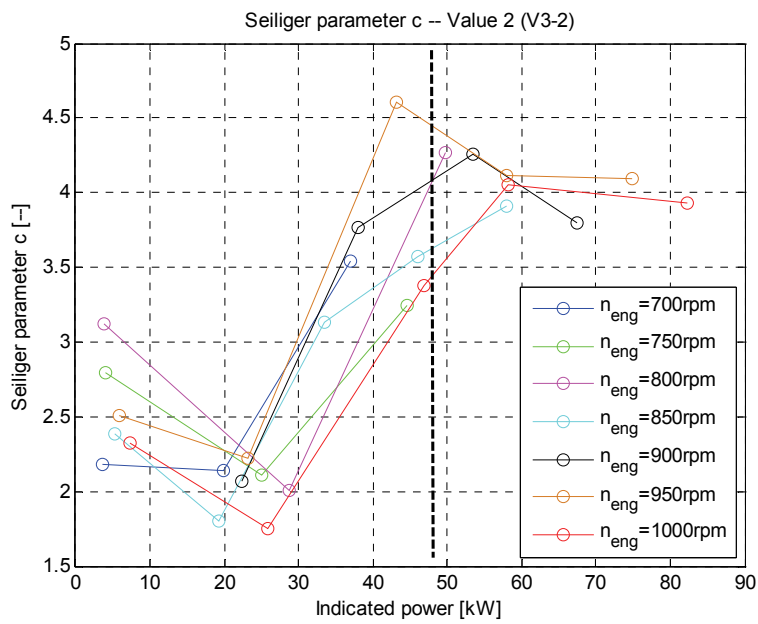


Figure 4.15 Result of Seiliger parameter c (value 2)

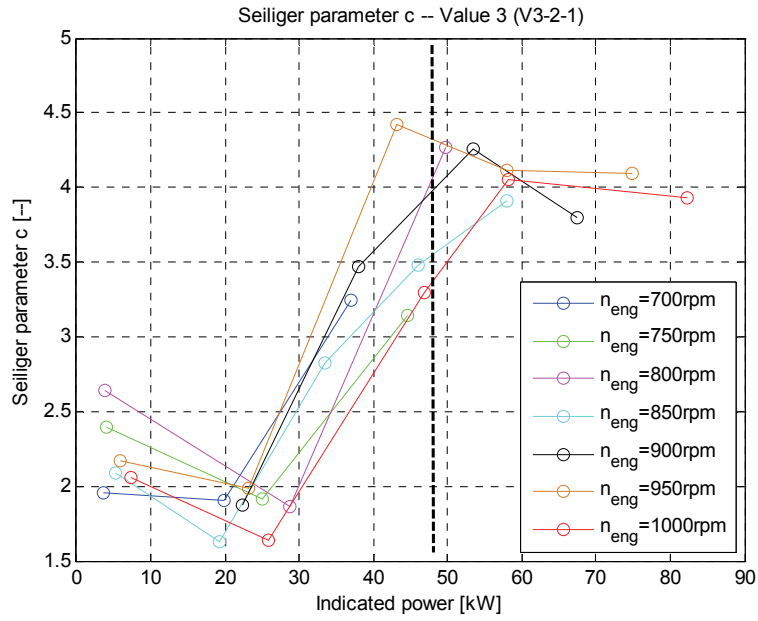


Figure 4.16 Result of Seiliger parameter c (value 3)

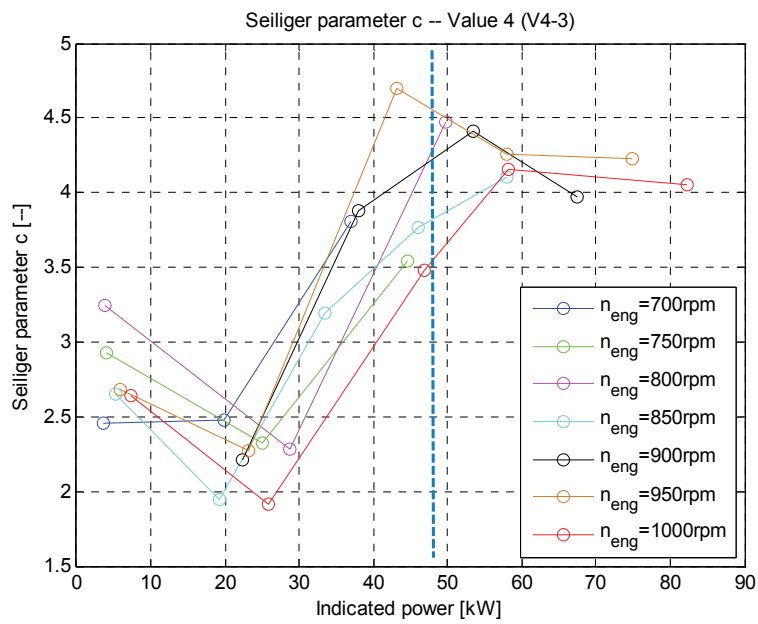


Figure 4.17 Result of Seiliger parameter c (value 4)

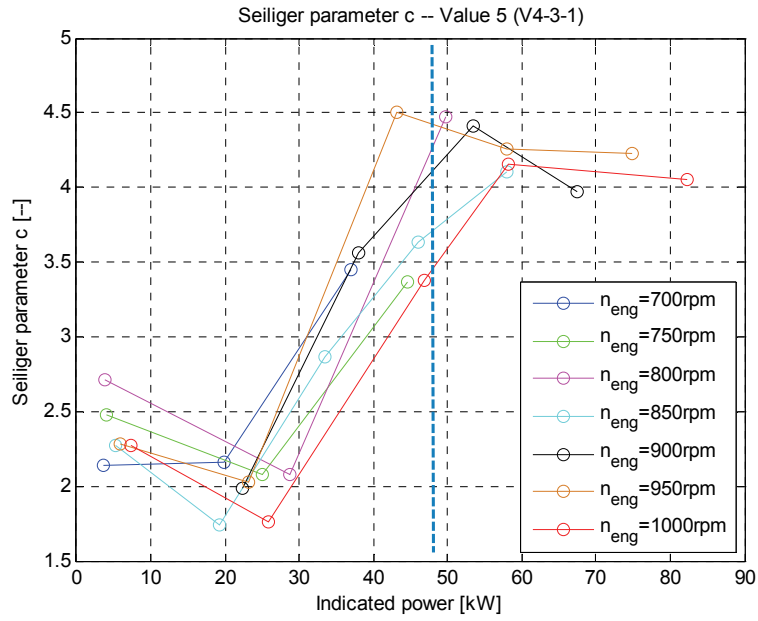


Figure 4.18 Result of Seiliger parameter c (value 5)

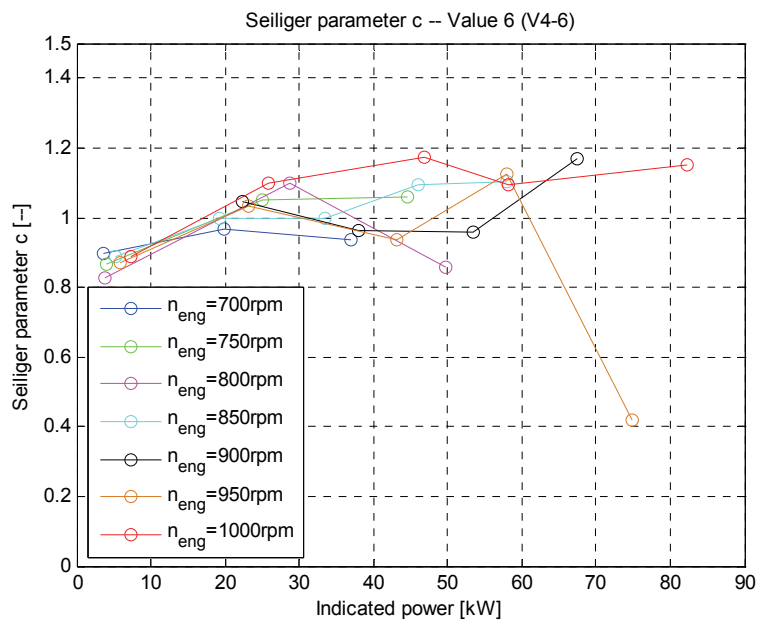


Figure 4.19 Result of Seiliger parameter c (value 6)

4.7 Result of Seiliger parameter n_{exp}

Seiliger parameter n_{exp} indicates net heat input during stage 5-6 due to *very* late combustion, or is used to describe the heat loss during stage 5-6. The determination of these parameters can be sorted in three categories:

- (1) n_{exp} is a *fixed constant* and *larger than the isentropic factor γ* . The parameter indicates the heat loss during expansion stage 5-6. In fact this is a defining feature of the *basic* Seiliger process (value 1).
- (2) n_{exp} is a *variable* and *equal to or larger than the isentropic factor γ* . The parameter again is expected to indicate a heat loss during expansion stage 5-6 but the values are depending on the Seiliger fitting procedure. Again this is a defining feature of the *basic* Seiliger process (value 2, value 3, value 4 and value 6).
- (3) n_{exp} is a *variable*. *The parameter* is expected to indicate a heat input during expansion stage 5-6. In fact this is the defining feature of the *advanced* Seiliger process (value 5).

The polytropic factor η_{exp} , which has been introduced in Appendix V, can be used to distinguish the effect of n_{exp} : from the polytropic factor it is immediately clear whether the process involves heat input or heat loss. Figure 4.20 – Figure 4.34 show the tendency of n_{exp} and η_{exp} as function of indicated power for different engine speeds. There are six different sets of values for n_{exp} in the Seiliger fit versions:

Value 1: *V3-1, V3-2, V3-2-1, V4-2*

Value 2: *V4-3*

Value 3: *V4-3-1*

Value 4: *V4-4*

Value 5 *V4-6*

Value 6: *V5-1*

Value 1 represents the constant settings in the Seiliger process (Figure 4.20). The versions in value 1 are all cases *with heat loss during expansion* so η_{exp} must be larger than unity to represent the heat loss (Figure 4.21 –Figure 4.24). However in *V3-2* and *V3-2-1* (Figure 4.22 and Figure 4.23), η_{exp} is smaller than unity at some part load operating points to indicate heat input during expansion. It is impossible to set correct value of n_{exp} at these operating points since when $\eta_{exp} > 1$ the Seiliger fit is diverging

when using Newton-Raphson method. It can conclude n_{exp} is sensitive to the numerical root finding.

It should be noted that Seiliger parameter n_{exp} is the setting value and polytropic factor η_{exp} is only used to verify the effect of n_{exp} . If η_{exp} is set to be constant this can easily result in numerical difficulties in the model, because γ is dependent on temperature.

The parameter values according to value 2, value 3 and value 6 are the result of a Seiliger fitting procedure and all η_{exp} turn out to be smaller than unity (Figure 4.26, Figure 4.28 and Figure 4.34). This should not be the case since the Seiliger fit versions for these three values are based on the *basic* Seiliger process, in which no combustion during stage 5-6 is foreseen. The values for the polytropic factor η_{exp} are not far from unity (value 2 and value 3 lie above 0.95 and value 7 is above 0.97). This still means that there is a small amount of heat input in stage 5-6 (and therefore in principle wrong) that is not included in equivalence criterion Q_{in} .

The polytropic factor η_{exp} according to value 4 is larger than unity over the whole range indicating heat loss, but for high loads, the values are very large ($\eta_{exp} = 1.43$ for the nominal point), which could be an indication that the heat loss is overrated.

Value 5 is applicable to the *advanced* Seiliger process definition. Whatever of value n_{exp} coming from the Seiliger fit, the heat, even if it is a heat loss, is included in the equivalence criterion Q_{in} . For value 5 in Figure 4.31, all the values of η_{exp} in Figure 4.32 are smaller than unity indicating heat input. With decreasing load η_{exp} goes down rapidly, in this case meaning more heat input, so very late combustion. Compared to Figure 4.19, the heat input in **V4-6** moves from stage 4-5 to stage 5-6 resulting in a decreased value of c and a low value of η_{exp} . In particular at high load, the heat input percentage is very high, as already found in section 3.4.3 3) for the selected three operational points. It can be concluded that the heat input observed during stage 5-6 is a *very* late combustion that could occur in an aged diesel engine, e.g. the MAN 20/27 diesel engine used in this thesis.

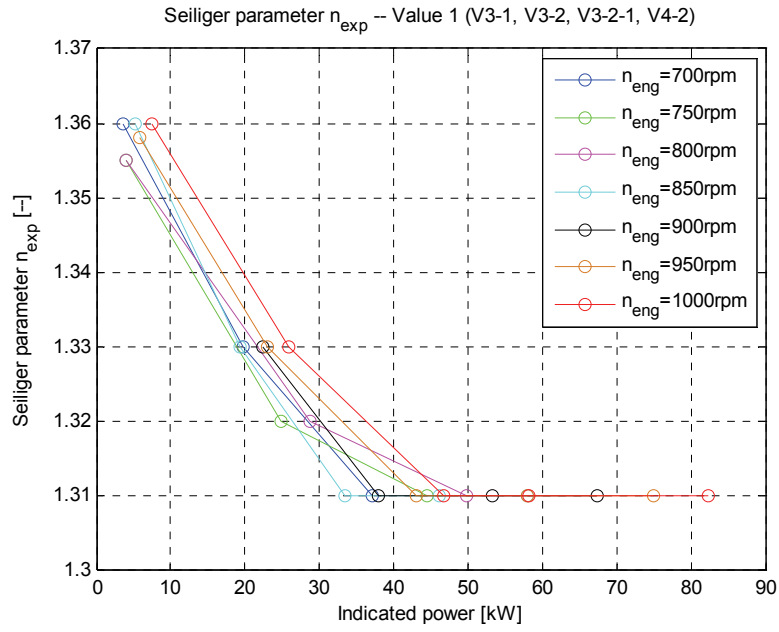


Figure 4.20 Result of Seiliger parameter n_{exp} (value 1)

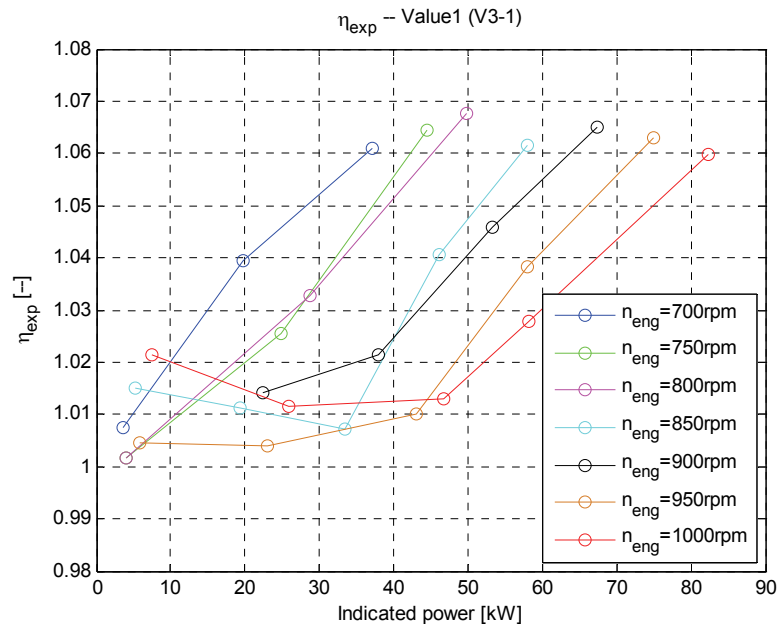


Figure 4.21 Result of η_{exp} (value 1(V3-1))

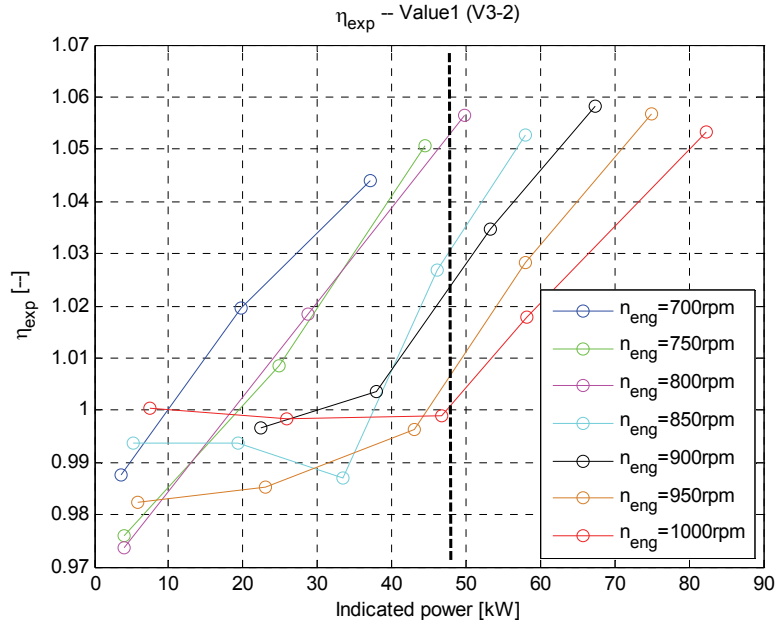


Figure 4.22 Result of η_{exp} (value 1(V3-2))

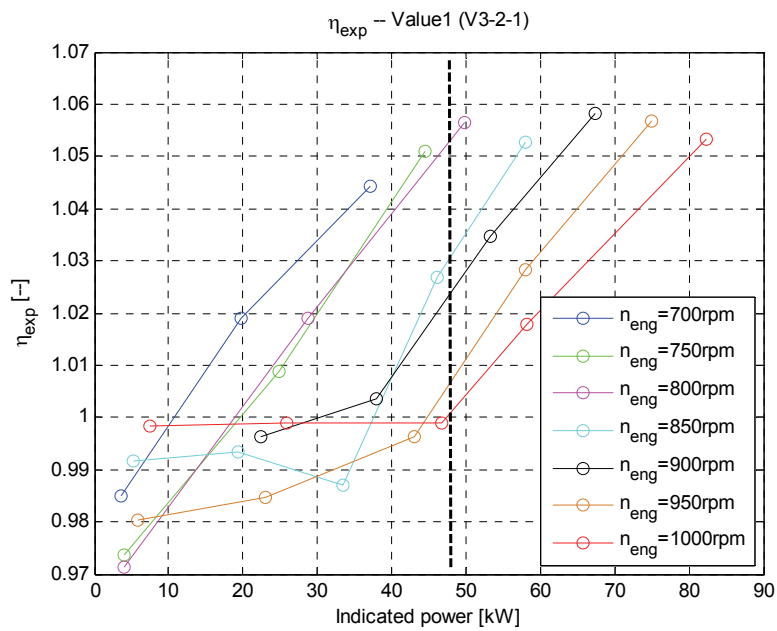


Figure 4.23 Result of η_{exp} (value 1(V3-2-1))

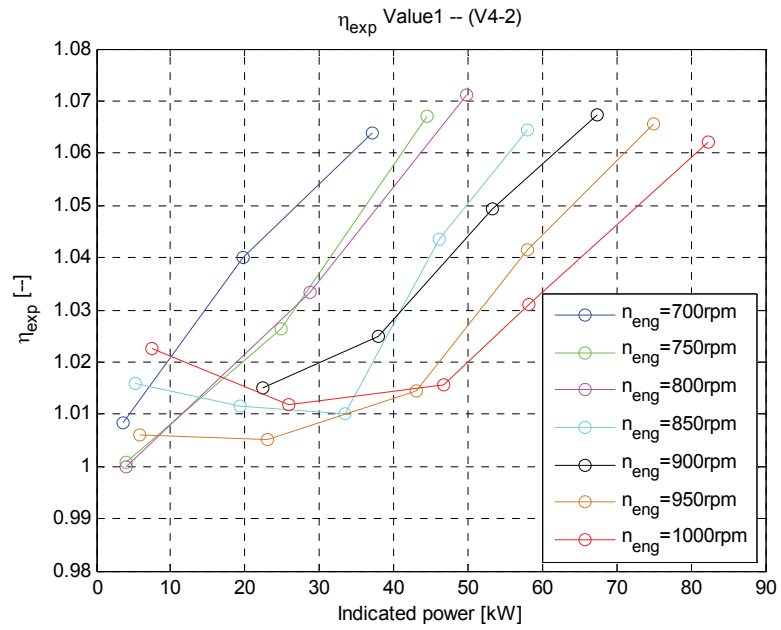


Figure 4.24 Result of η_{exp} (value 1(V4-2))

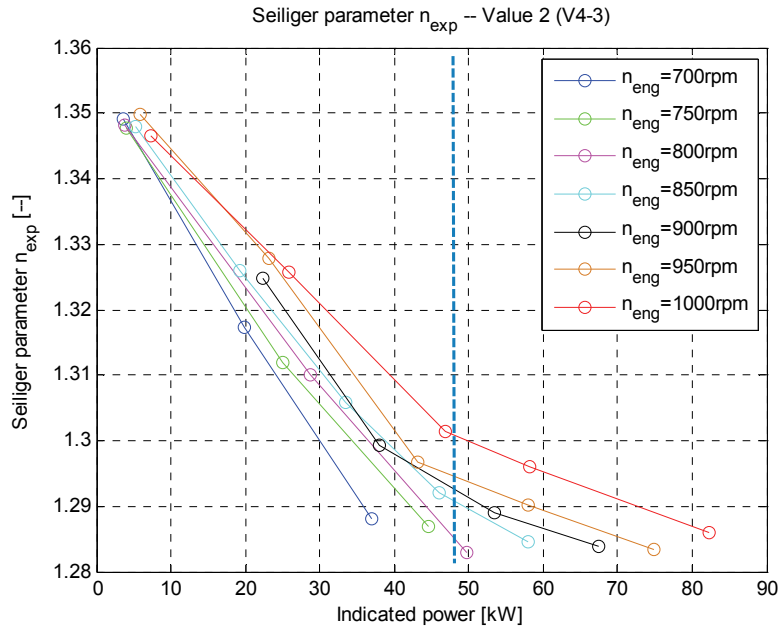


Figure 4.25 Result of Seiliger parameter n_{exp} (value 2)

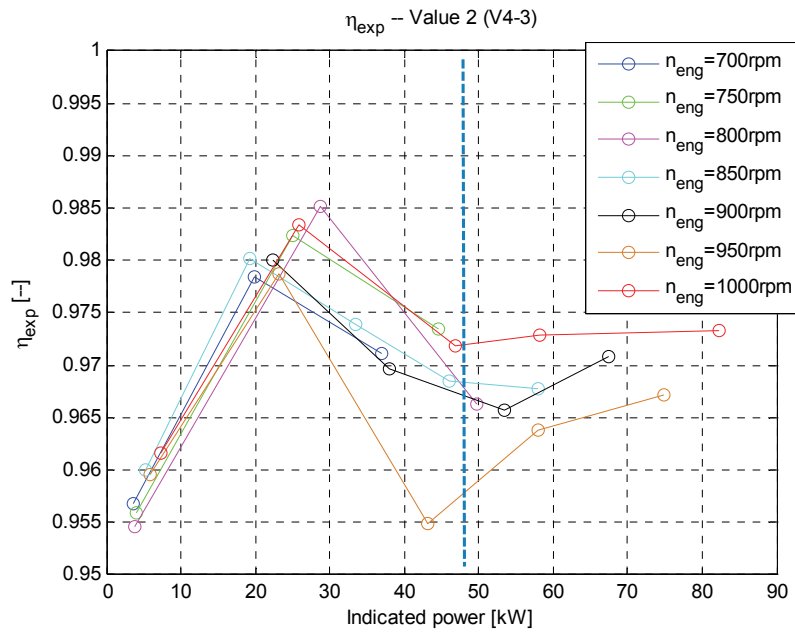


Figure 4.26 Result of η_{exp} (value 2)

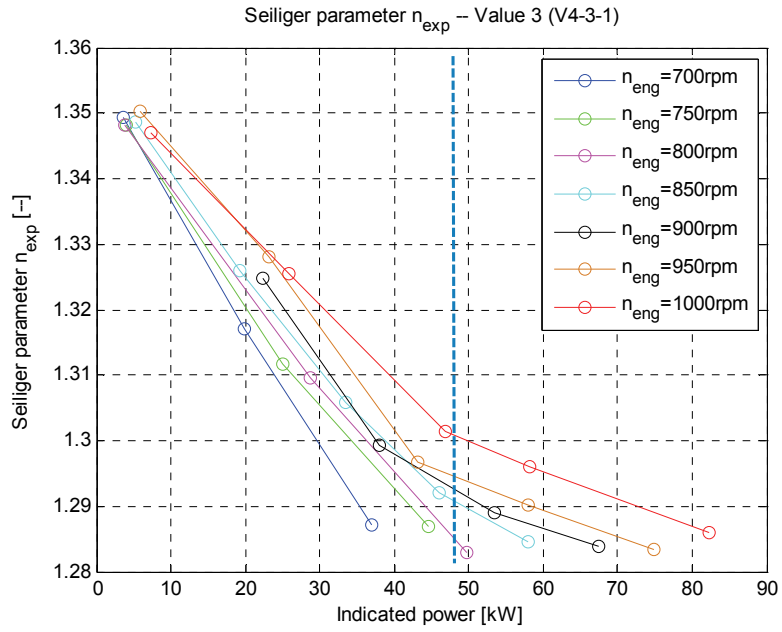


Figure 4.27 Result of Seiliger parameter n_{exp} (value 3)

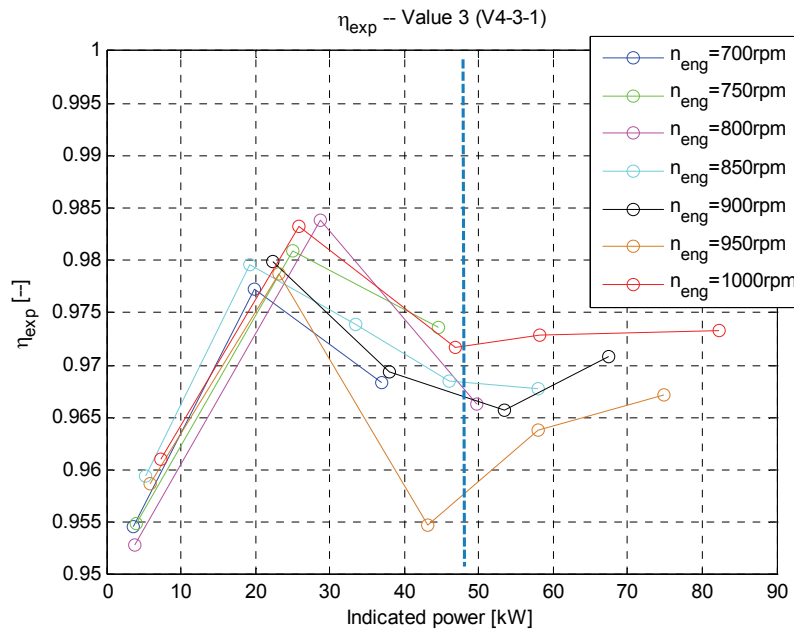


Figure 4.28 Result of η_{exp} (value 3)

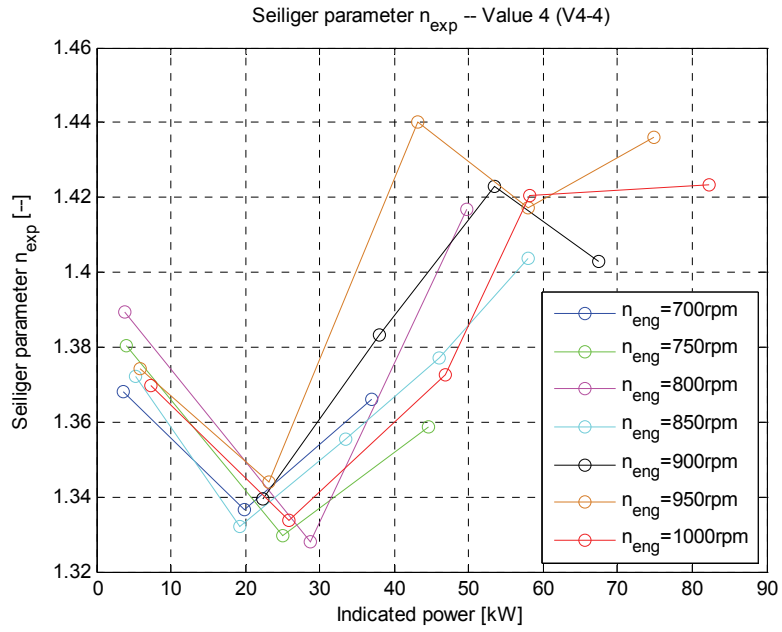


Figure 4.29 Result of Seiliger parameter n_{exp} (value 4)

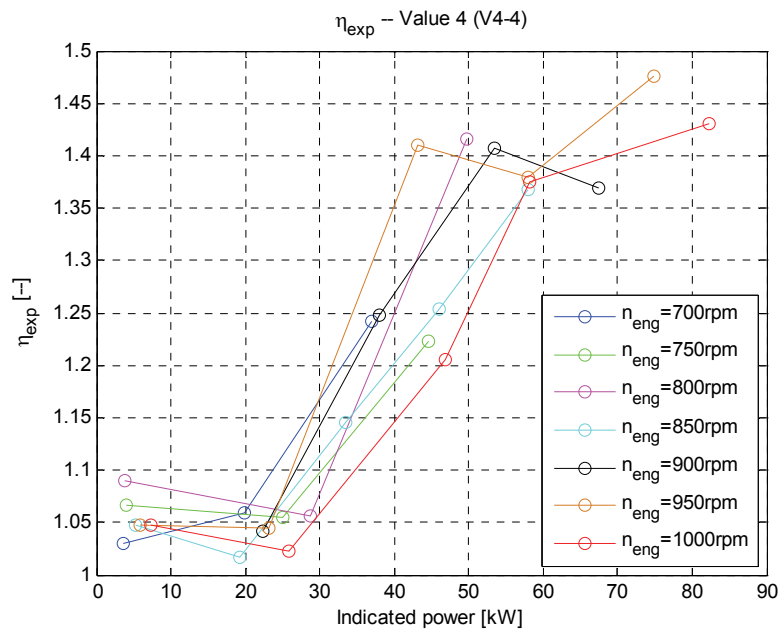


Figure 4.30 Result of η_{exp} (value 4)

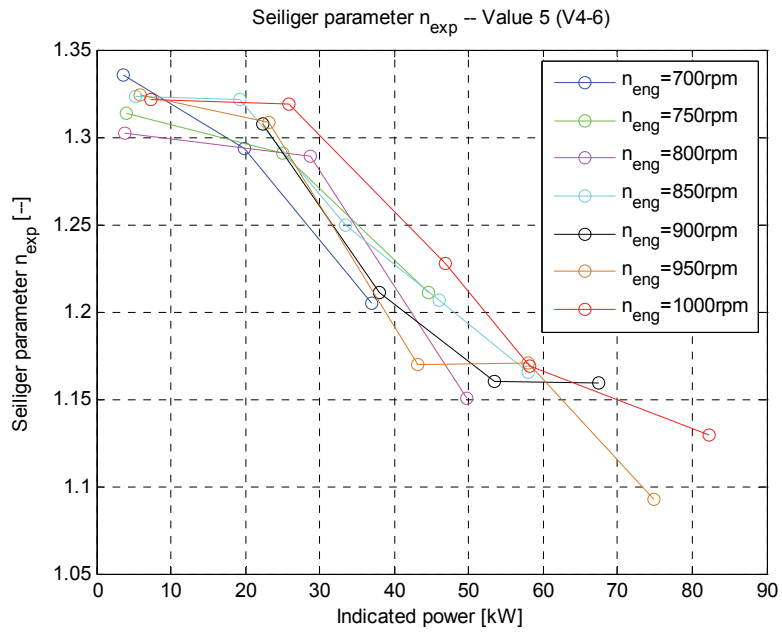


Figure 4.31 Result of Seiliger parameter n_{exp} (value 5)

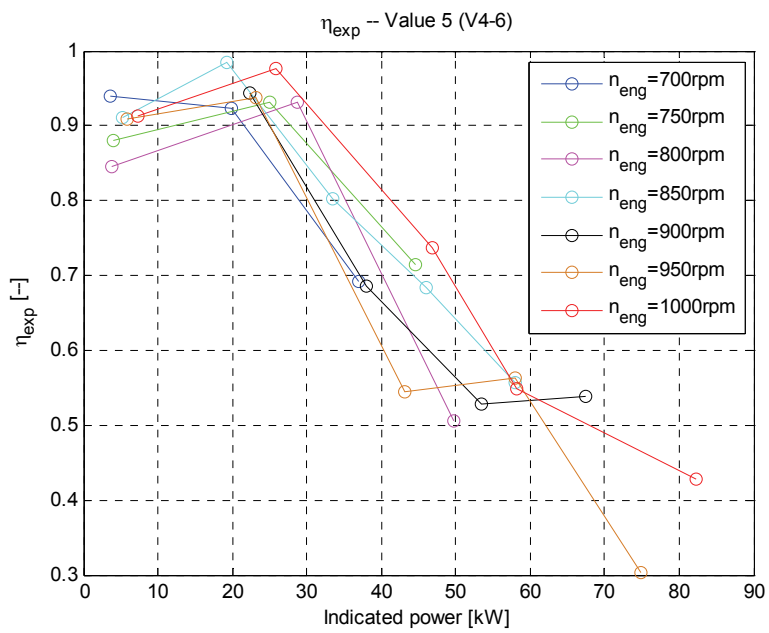


Figure 4.32 Result of η_{exp} (value 5)

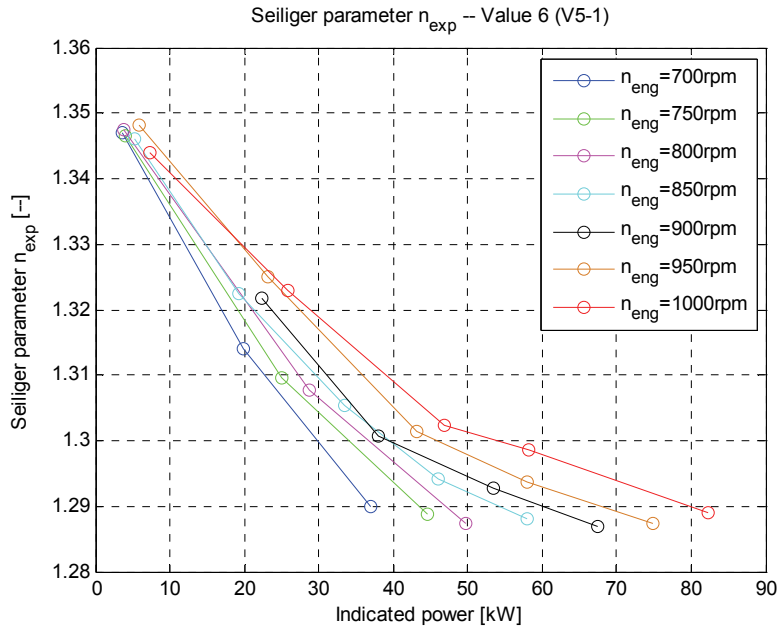


Figure 4.33 Result of Seiliger parameter n_{exp} (value 6)

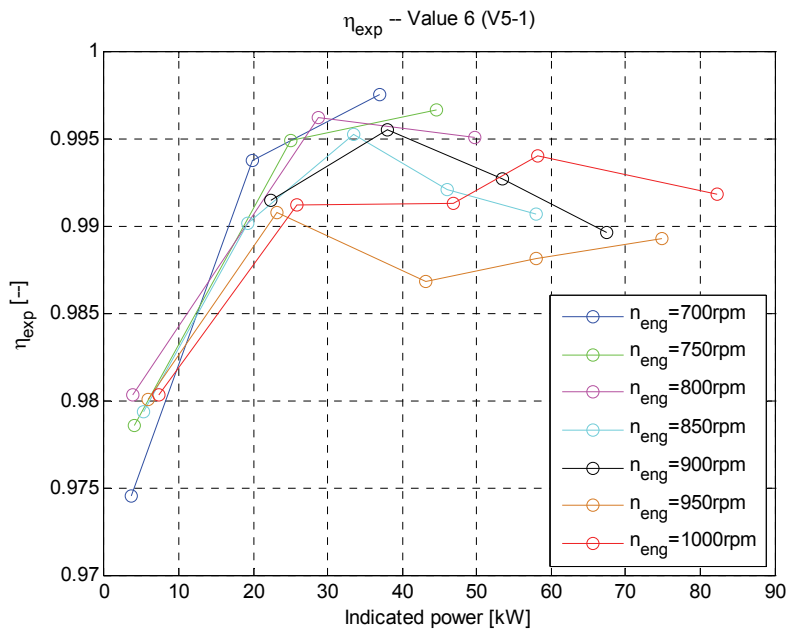


Figure 4.34 Result of η_{exp} (value 6)

4.8 Result of Seiliger parameter ΔEO

Seiliger parameter ΔEO is used to allow variation of the duration of the expansion. A later (or earlier) timing of the exhaust valve opening mainly changes the work and temperature at the moment of exhaust valve opening. There are three sets of values of ΔEO in all the Seiliger fit versions:

Value1: *V3-1, V3-2, V3-2-1, V4-3, V4-3-1, V4-4, V4-6* ($\Delta EO = 0$).

Value2: *V4-2*

Value3: *V5-1*

Value 1 of ΔEO is zero, indicating that there is no extension of the expansion. Value 2 and value 3 are both chaotic and the values are all negative and tend to shorten the expansion. This is a further reason that this parameter has the lowest priority among the Seiliger parameters.

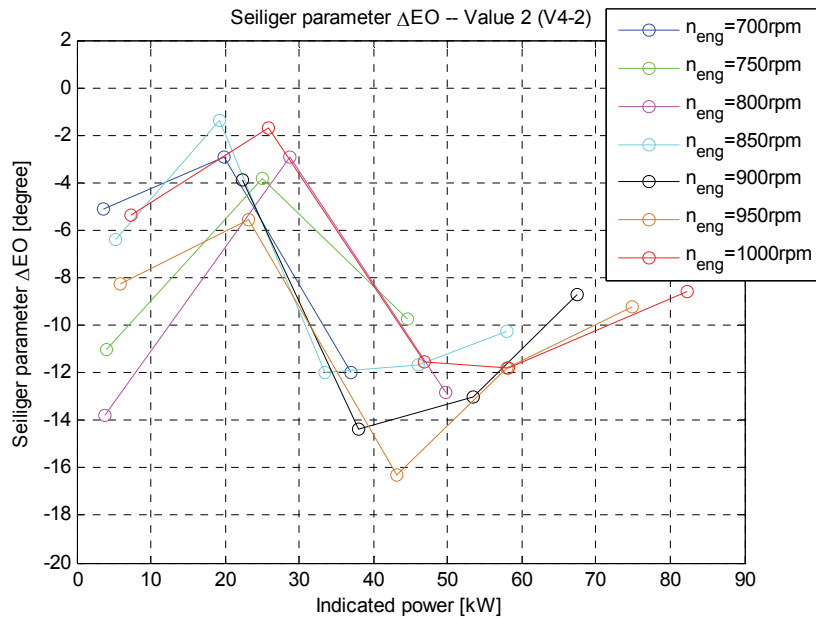


Figure 4.35 Result of Seiliger parameter ΔEO (value 2)

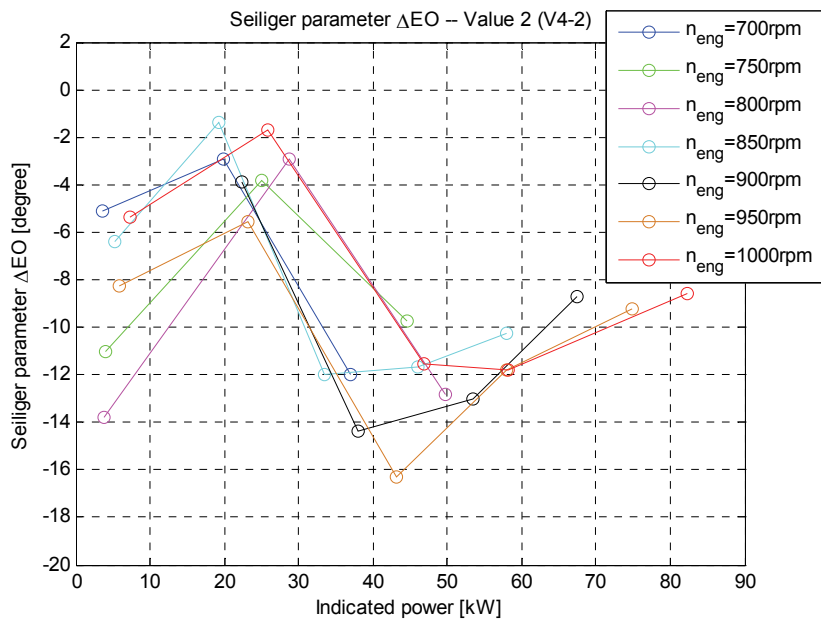


Figure 4.36 Result of Seiliger parameter ΔEO (value 3)

4.9 Non-used equivalence criteria

(1) Indicated work W_i

The indicated work W_i is the only non-used equivalence criterion in **V3-1**. Figure 4.37 shows the error of W_i in **V3-1**. Except for the lowest power operating point at 750 rpm, 800 rpm and 900 rpm, the errors are all below 10% (a positive value of the error means that W_i in the Seiliger fit is larger than obtained from the smoothed measurement).

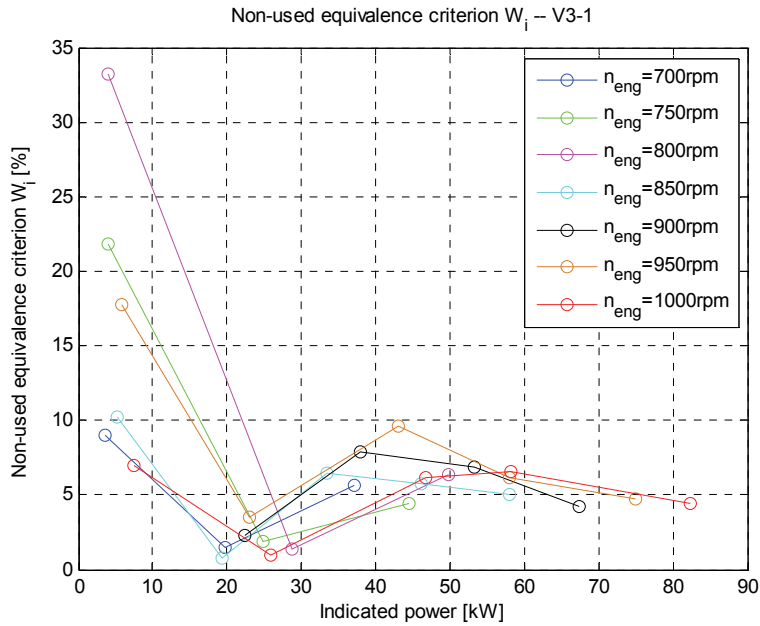


Figure 4.37 Non-used equivalence criterion W_i (**V3-1**)

(2) Peak pressure p_{max}

Figure 4.38 and Figure 4.39 show the errors of p_{max} in **V3-2-1** and **V4-3-1** respectively. Since these two versions are used only when $b < 1$ in **V3-2** and **V4-3**, the errors at high load are zero. At part load the errors become large with decreasing power. Again the black and blue dashed lines in the figures are used to indicate the boundary lines where parameter b becomes smaller than unity.

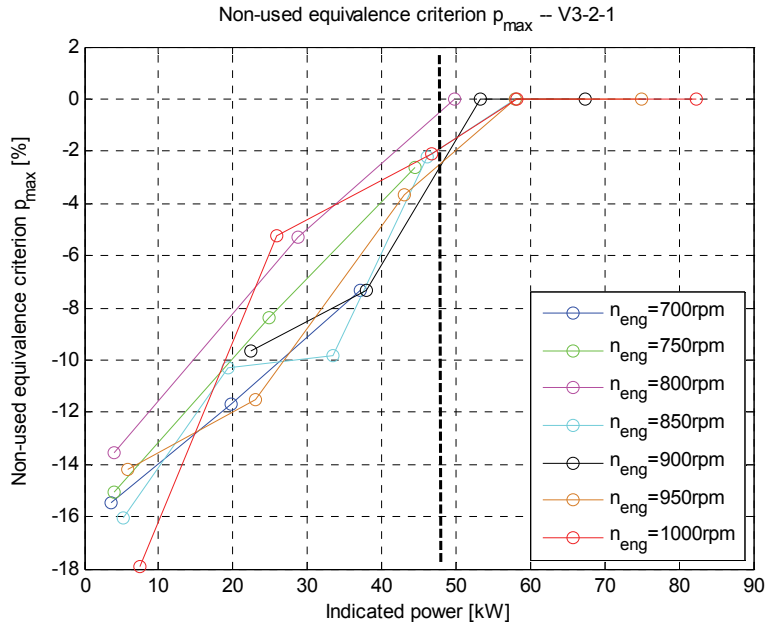


Figure 4.38 Non-used equivalence criterion p_{max} (V3-2-1)

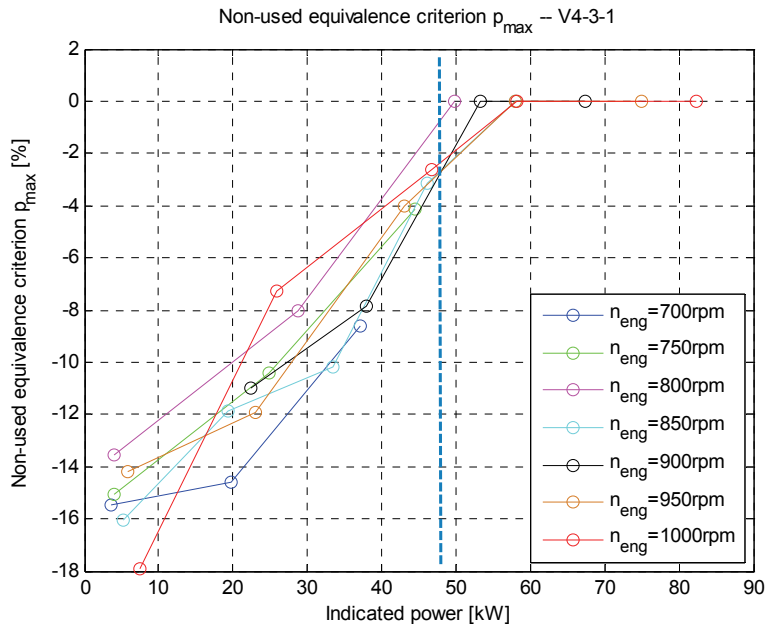


Figure 4.39 Non-used equivalence criterion p_{max} (V4-3-1)

(3) Peak temperature T_{max}

Figure 4.40 –Figure 4.43 show the errors of T_{max} in *V3-2*, *V3-2-1*, *V4-3* and *V4-3-1* respectively. In *V3-2* and *V4-3*, the errors go down and then up with power decreasing within 10%. In *V3-2-1* and *V4-3-1*, the errors are the same as *V3-2* and *V4-3* in part load, but in at high load the errors become larger for the same operating point. Again the black and blue dashed lines in the figures are used to indicate the boundary lines where parameter b becomes smaller than unity.

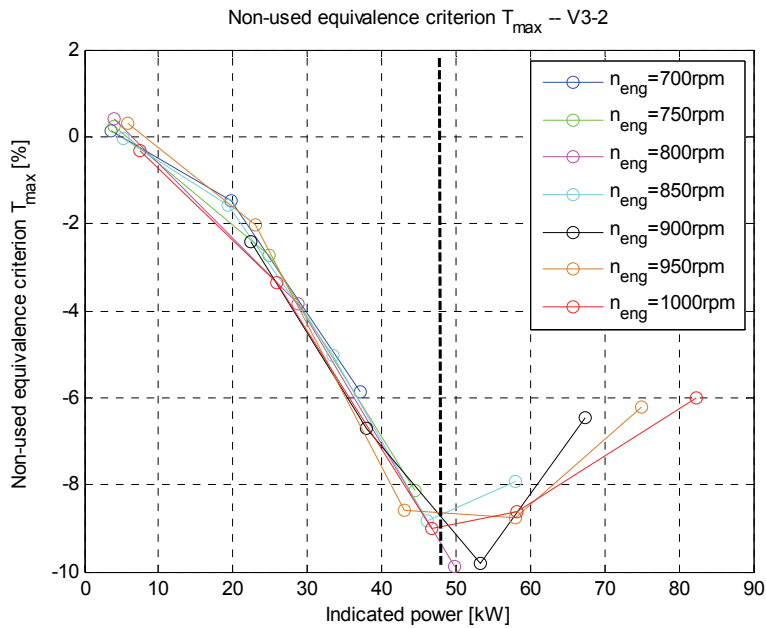


Figure 4.40 Non-used equivalence criterion T_{max} (*V3-2*)

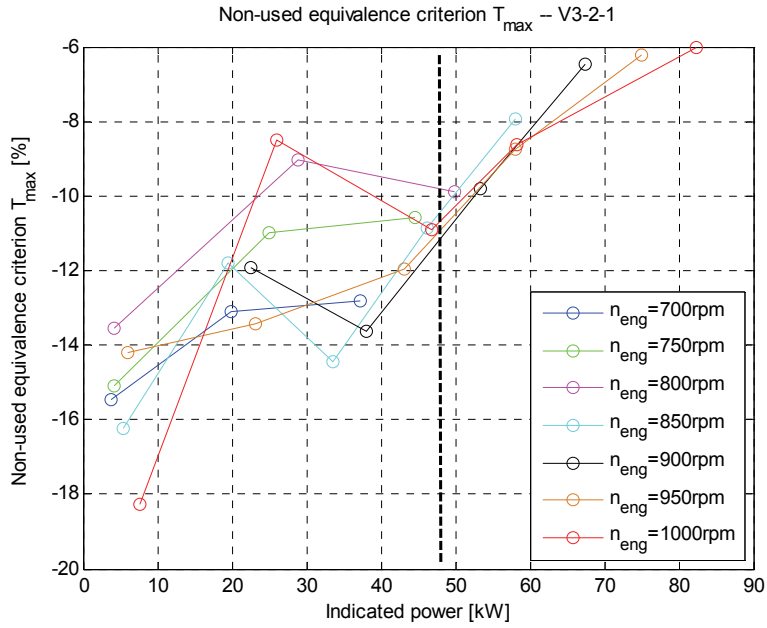


Figure 4.41 Non-used equivalence criterion T_{max} (V3-2-1)

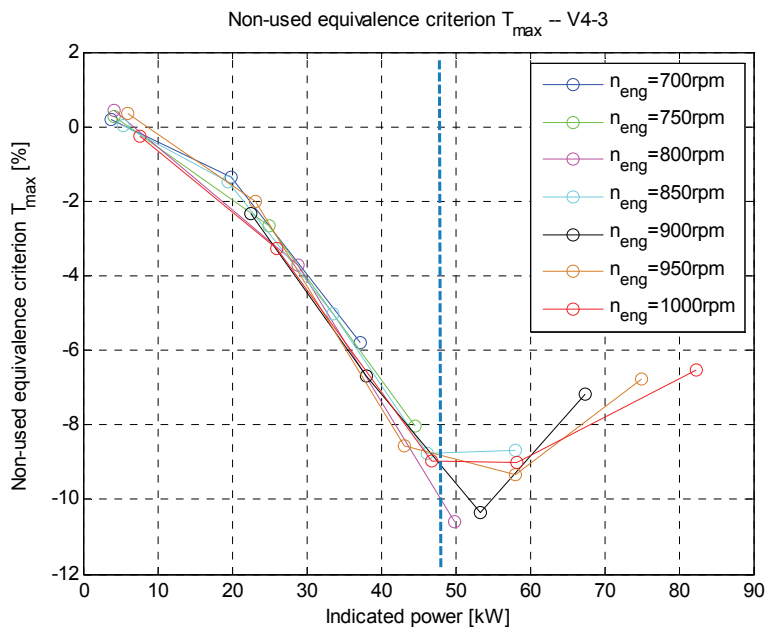


Figure 4.42 Non-used equivalence criterion T_{max} (V4-3)

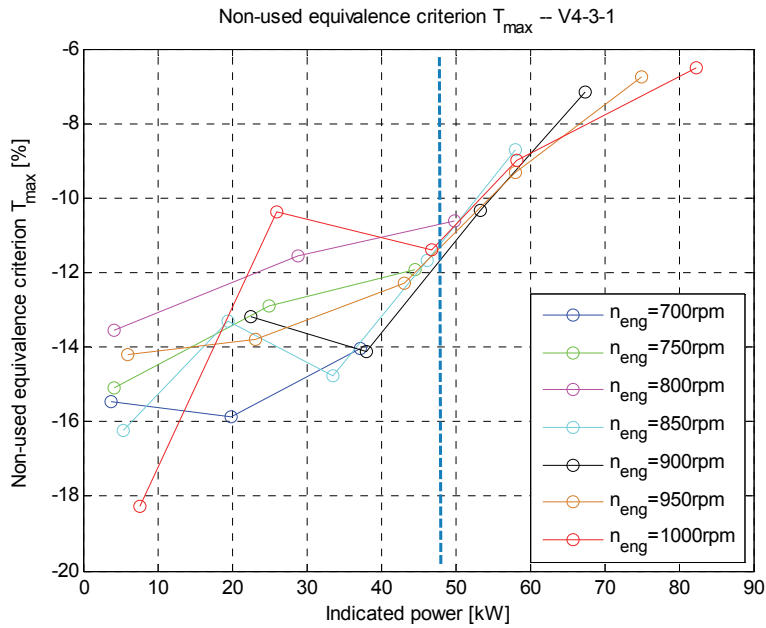


Figure 4.43 Non-used equivalence criterion T_{max} (V4-3-1)

(4) Temperature at point where exhaust is opening T_{EO}

Figure 4.44 – Figure 4.49 show the errors of T_{EO} in V3-1, V3-2, V3-2-1, V4-2, V4-4 and V4-6 respectively. In V4-4 (Figure 4.48), the errors are relative high (more than 15%) in particular at high load. In V3-1, the errors at some operating points are larger than 5%. The errors in the other versions are all within 5%. Again the black line in the figures is used to indicate the boundary lines where parameter b becomes smaller than unity.

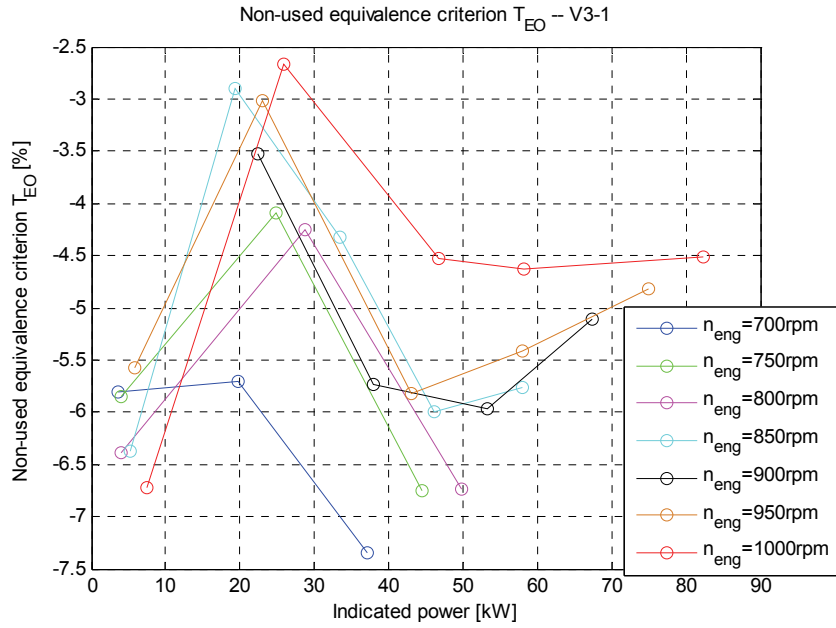


Figure 4.44 Non-used equivalence criterion T_{EO} (V3-1)

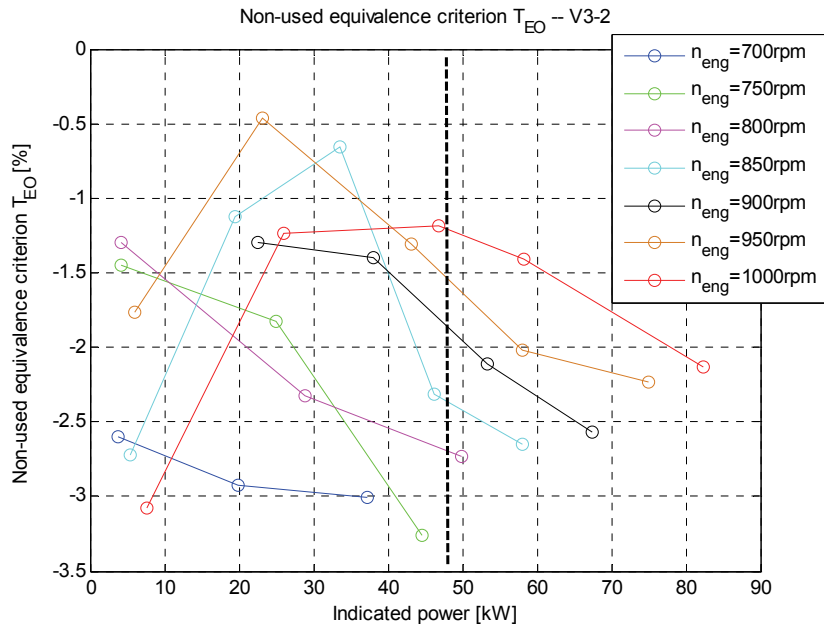


Figure 4.45 Non-used equivalence criterion T_{EO} (V3-2)

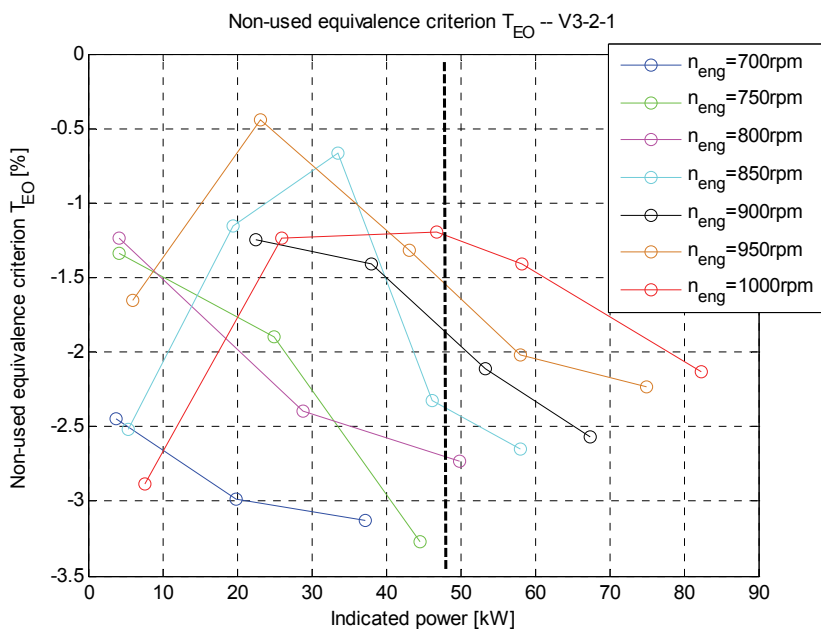


Figure 4.46 Non-used equivalence criterion T_{EO} (V3-2-1)

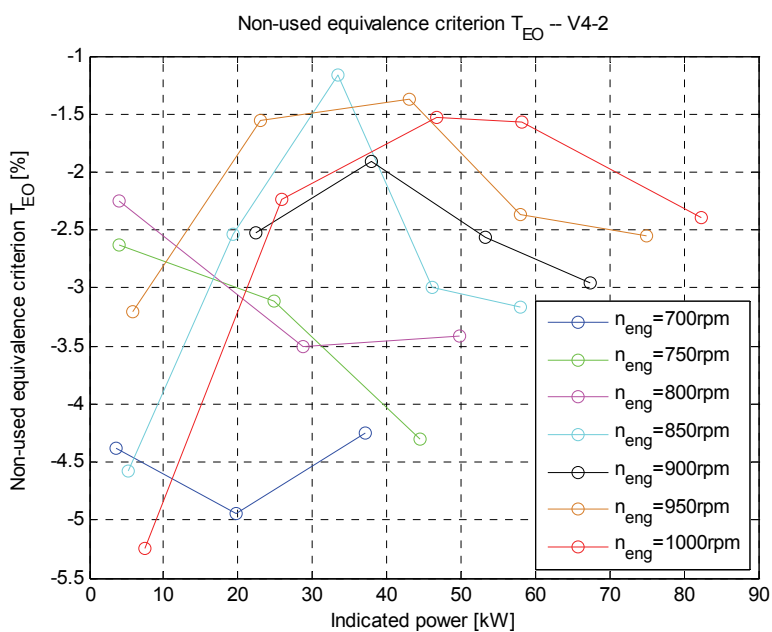


Figure 4.47 Non-used equivalence criterion T_{EO} (V4-2)

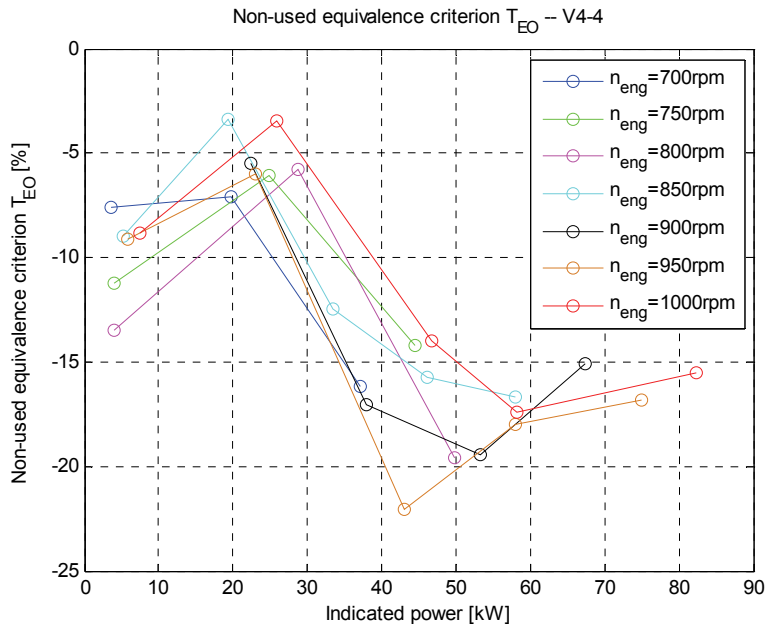


Figure 4.48 Non-used equivalence criterion T_{EO} (V4-4)

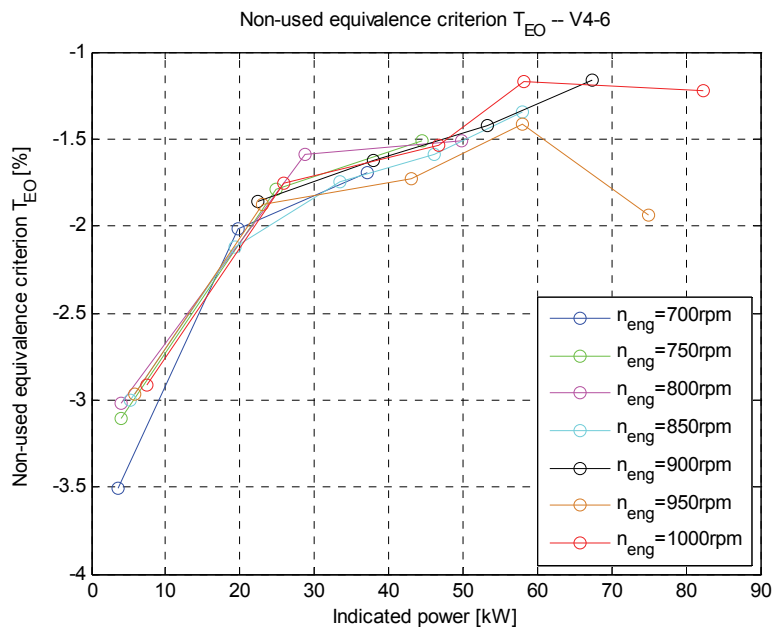


Figure 4.49 Non-used equivalence criterion T_{EO} (V4-6)

4.10 Summary

The tendency of the Seiliger parameters for the different fit versions – as function of engine load and speed – are investigated in this chapter. The fit values of the Seiliger parameters are sorted into sets where the fit results were similar.

The trends of Seiliger parameters a and b are unambiguous, but at low load, value 2 and value 3 of a and value 2 and value 4 of b become smaller than unity. Parameter c is relatively chaotic and it is difficult to discern a trend. However in the ‘DE B4’ simulation model, the heat input during stage 4-5 and thus parameter c is calculated after modelling the heat input during stage 2-3 and 3-4 on the basis of models for parameters a and b , given the total input heat as determined by the fuel allowing for incomplete combustion and an estimate of the heat loss.

As to parameter n_{exp} the polytropic factor (η_{exp}) could be introduced to restrict its value. But in the Seiliger fit versions it is impossible to restrict the polytropic factor since it is essentially an output of the whole procedure. The results are sometimes (value 2, value 3 and value 6) not correct, i.e. indicating heat input when heat loss is expected and vice versa.

The Seiliger parameter ΔEO comes always out at negative values and shows erratic behaviour.

Table 4.2 compares the fit Seiliger parameters for different fit versions, from which the drawbacks of some Seiliger fit versions can be concluded.

There are two versions with a value smaller than unity, i.e. $V3-2-1$ and $V4-3-1$, but these two versions are extensions (in fact only used at part load) from $V3-2$ and $V4-3$ respectively, introduced to avoid b values smaller than unity in part load. But when the parameter b is set to unity, parameter a in turn drops below unity, proving that both premixed and diffusive combustion, at least for the MAN 20/27 engine, tend to disappear at low load in favour of the late and *very* late combustion.

The latter is proven since there is one version where even parameter c drops below unity at very low load, $V4-6$, and combustion shifts to very late combustion in stage 5-6. However all the fit values for c in this version are in a relative small range: all between 0.8 and 1.0 (except one point in 950 rpm which looks like an outlier).

As for n_{exp} , first – in *V3-1*, *V3-2* and *V3-2-1* – this parameter is set to be constant such that heat loss occurs during stage 5-6. The polytropic factor η_{exp} can be used to judge whether the n_{exp} is appropriately set. Then in *V4-2*, *V4-3*, *V4-3-1*, *V4-4* and *V5-1*, the n_{exp} should also indicate heat loss during expansion. However, only in *V4-4* there is heat loss. Last but not least, *V4-6* – which is based on the *advanced* Seiliger process definition – uses n_{exp} as a variable in the fitting procedure. The results are satisfactory in the sense that there is heat input during expansion stage 5-6 as expected.

There are two versions where ΔEO is variable, i.e. *V4-2* and *V5-1*. All the fit values of ΔEO appear to be negative indicating shorter total expansion. A change of the exhaust opening is not realistic since the timing of the opening of the valve is a geometric parameter. It was however introduced to see whether it could give a better fit.

Table 4.2 Comparison of Seiliger parameters in Seiliger fit versions

	<i>a</i>	<i>b</i>	<i>c</i>	n_{exp}	η_{exp}		ΔEO
					<i>Expect</i>	<i>Result</i>	
<i>V3-1</i>				fixed	> 1	> 1	0
<i>V3-2</i>		≤ 1		fixed	> 1	> 1	0
<i>V3-2-1</i>	≤ 1			fixed	> 1	> 1	0
<i>V4-2</i>				fixed	> 1	> 1	≤ 0
<i>V4-3</i>		≤ 1		variable	≥ 1	≤ 1	0
<i>V4-3-1</i>	≤ 1			variable	≥ 1	≤ 1	0
<i>V4-4</i>				variable	> 1	> 1	0
<i>V4-6</i>			≤ 1	variable	< 1	< 1	0
<i>V5-1</i>				variable	≥ 1	≤ 1	≤ 0

In combination with section 3.3.1 and section 3.3.6, the Seiliger fit versions can be evaluated on three aspects:

- 1) Priority of equivalence criteria;
- 2) Seiliger parameters fit results;
- 3) The unused equivalence criteria.

Table 4.3 lists the scores for each fit version in these three aspects. ‘A’ is good, ‘B’ is moderate and ‘C’ is poor.

Since ‘priority of equivalence criteria and parameters’ is a subjective selection and always is done before the fit procedure, it has less weight in the evaluation of the

Seiliger fit versions. As to the ‘Unused equivalence criteria’, although it is critical for the engine performance, only a few performance parameters can be restricted. On the other hand, in order to model the Seiliger parameters in the ‘DE B4’ model using engine measurement, good and realistic fitting results are important. Therefore the rating of different ‘Fitting Seiliger parameters result’ should be considered firstly. Besides the simplest version *V3-1*, *V4-4* and *V4-6* could be the favourite for the further research, at least for this MAN 20/27 engine.

Table 4.3 The evaluation of Seiliger fit versions

	Priority of equivalence criteria and parameters	Fitting Seiliger parameters result	Unused equivalence criteria
<i>V3-1</i>	C	A	B
<i>V3-2</i>	A	C	A
<i>V3-2-1</i>	A	C	A
<i>V4-1</i>	B	N/A	N/A
<i>V4-2</i>	B	C	A
<i>V4-3</i>	A	C	A
<i>V4-3-1</i>	A	C	A
<i>V4-4</i>	B	B	C
<i>V4-5</i>	A	N/A	N/A
<i>V4-6</i>	B	B	A
<i>V5_1</i>	B	C	A
<i>V5-2</i>	A	N/A	N/A

Chapter 5

Conclusions and Recommendations

5.1 Summary of thesis work

Characterizing combustion of diesel engines investigates not only the instantaneous combustion phenomena at a certain operating point, but also the change of the combustion process under variable engine operating conditions. Both experimental and theoretical methods were used in this thesis to investigate the combustion process using finite cylinder process models.

In Chapter 2 the ‘heat release calculation model’, as built in MATLAB/SIMULINK, uses the same elements as the ‘in-cylinder process simulation’ model but in a reversed way: it is in fact an anti-causal simulation model. On the basis of the physical principles the state parameters (smoothed pressure, temperature, mass, volume), engine performance parameters (heat input, heat release rate, power output, etc.) were calculated from the model using the engine in-cylinder pressure, fuel consumption measurements and engine parameters. Some sub-models – such as the ‘property library’, the ‘heat loss to the walls’ etc. – were also built in the SIMULINK environment. The gas in the cylinder is assumed to consist of dry air and stoichiometric gas, and the properties are calculated in the ‘properties library’. The specific heat and heat of combustion are a function of temperature and composition in the simulation model instead of constants, making the model more correct. The main application of the model in this thesis is to calculate the reaction coordinate, which is a monotonous increasing function of crank angle. The reaction coordinate has been used in a new smoothing method based on a multiple Vibe heat release model to reconstruct the in-cylinder pressure signals. The smoothed pressure and temperature traces potentially have a better quality than mathematically (up-front) smoothed signals.

The definition of the basic and advanced Seiliger process model is given in Chapter 3, after which the possible finite combustion stage cylinder process models are summarized based on these two kinds of Seiliger process. A systematic investigation of Seiliger parameters was carried out to show their influences on the Seiliger process stages and the overall cycle. The most important part in this chapter is to present unambiguous ways to fit a measured engine cycle to a Seiliger process. Several combinations of equivalence criteria are proposed as requirements for this fit and the applicable systems of equations for the Seiliger parameters were set up. A

MATLAB/Simulink model was taken from the mean value first principle diesel engine model developed at TU Delft / NLDA (DE B4). The combination of equivalence criteria and Seiliger parameters led to a total of twelve fit versions, where nine versions are based on a basic Seiliger process with three combustion stages and three versions are based on an advanced Seiliger process with four combustion stages. In three versions the numerical iteration to find the solutions did not converge when using a Newton-Raphson method. The cause of this non-converging was investigated. Some fit versions resulted in unrealistic values of Seiliger parameters.

In Chapter 4, the trend of the Seiliger parameters as a function of the engine operating conditions (e.g. the power output, engine speed) for the full operating range of the engine was investigated for all Seiliger fit versions that converged to a solution. Also the error in the equivalence criteria that were not used was presented for the full range of operating conditions in order to decide on the most preferable fit version to use as a basis for modelling and characterizing the combustion.

5.2 Conclusions

The conclusions from Chapter 2 are:

- (1) The 'Heat of combustion' is temperature dependent in this thesis and results in a slightly higher heat of combustion than the constant value at reference temperature (e.g. the often used $4.27 \cdot 10^7 \text{ J/kg}$).
- (2) The 'Energy of fuel' as defined in this thesis, causes an 'Effective heat of combustion' which is lower than the nominal value at reference temperature, since fuel in a diesel engine enters at a low energy (as a liquid and at a relatively low temperature) and the additional heat to evaporate and heat up the fuel is taken from the heat released by the fuel.
- (3) The Woschni model is used to evaluate the heat loss to the walls, which affects the gross heat release considerably. Therefore, the constants in Woschni's model could be selected to fit the total gross heat release when this is known from a fuel flow measurement..
- (4) The TDC (Top Dead Centre) shift has effect on the shape of the heat release. A theoretical exercise proved that the effect is not as large as expected and that it is impossible to get the heat release at zero before SOC (Start of Combustion) by a proper choice of TDC shift only. Therefore a constant value for the shift of 0.7 degree is used in this thesis.
- (5) The method of smoothing the combustion reaction coordinate as obtained from the raw in-cylinder pressure signals and then simulating the cylinder temperature and pressure potentially gives a better signal quality than mathematically (up-front) smoothed signals.

The conclusions from Chapter 3 are:

- (1) In the basic Seiliger process the polytropic exponents during compression and expansion have an effect only on work and heat loss. The polytropic efficiency is used to verify whether the polytropic exponent indicates the net heat correctly as a negative heat flow (heat loss).
- (2) If very late combustion is present, the polytropic exponent during expansion can be used to describe an extra combustion phase in the advanced Seiliger process.

The polytropic efficiency is used to verify whether the polytropic exponent indicates the net heat correctly as a positive heat flow (heat input).

- (3) It is possible to fit heat and work (and thus efficiency) together with maximum pressure and temperature of a Seiliger process to a measured engine cycle, but it is apparently difficult to fit the temperature at the moment of opening the exhaust valve (EO) right.
- (4) When the temperature at Exhaust Open (EO) is selected as equivalence criterion, the process of fitting a Seiliger cycle to a measured engine cycle does not always converge owing to the fact that actually no solution exists. Therefore temperature at EO should be abandoned and preference should be given to the peak temperature as an equivalence criterion.
- (5) The fit process requires the net apparent heat release and thus can be obtained without the uncertainties of the heat loss model. Characterizing the combustion in terms of Seiliger parameters however is a characterization of combustion and heat loss. The mean value first principle model that uses the Seiliger parameters must also include a heat loss model.

The conclusions from Chapter 4, for a classic injection system as tested in this research, are:

- (1) The Seiliger parameter a and b , whatever the Seiliger fit version, behave in a clear and unambiguous way.
- (2) Seiliger parameter c seems to behave erratic and dependent on the Seiliger fit version, but it need not to be modelled in a basic Seiliger cycle with three combustion stages.
- (3) In the basic Seiliger cycle at part load the parameter a first increases and then decreases. Seiliger parameter b is the first to become unity (and its value must be frozen), then parameter a goes to unity.
- (4) In the advanced Seiliger cycle the polytropic exponent during expansion (n_{exp}) can help to better describe *very* late combustion: parameter b still goes to unity, but less quickly.
- (5) The qualitative description given in (3) and (4), together with graphs of the parameters versus load and speed, or even better of the associated heat fractions, can serve as an objective characterization of the net heat release of the cylinder

process.

- (6) When comparing the results of all the Seiliger fit versions, two versions are preferred:
- a) If the engine combustion is assumed to have three combustion stages, the results from the basic Seiliger cycle with fit parameters a , b , c and n_{exp} and equivalence criteria maximum pressure (p_{max}), net heat input (Q_{in}), indicated work (W_i) and maximum temperature (T_{max}) (version **V4-4**) can be used.
 - b) If very late combustion is present then the results from an advanced Seiliger cycle with the same fit parameters a , b , c and n_{exp} and the same equivalence criteria p_{max} , Q_{in} , W_i and T_{max} (version **V4-6**) should be used.

5.3 Recommendations

The recommendations for further work following the research presented in this thesis are:

- (1) The temperature and air fraction dependent gas properties such as specific heat, enthalpy, entropy etc. are calculated in the 'Properties library', which was presented in Chapter 2. However a weak point of the present property library is that it cannot handle humid air. How to implement this effectively should be researched.
- (2) The Woschni model is used to evaluate the heat loss to the walls. There are uncertainties in the determination of the constants in the formula. Especially the overall multiplying parameter C_l , (refer equation [2.9]) should be reconsidered. C_l is used to correct the final value of the normalized reaction co-ordinate to arrive at unity in three typical operating points in Chapter 2 and Chapter 3. This is not applied in all measurements in Chapter 4 because it is not needed for the process analysis. Further investigation of the variations in C_l as a function of load and speed is necessary to model the heat loss more accurately.
- (3) The uncertain factors in the new smoothing method (presented in section 2.4), such as the selection of starting points and the type of iteration to use, make that the user needs to have experience in numerical analysis and have knowledge of diesel engine combustion in order to get good results. The traditional, purely mathematical, method is simpler and apparently can achieve the same goals to some extent. These two methods should be compared in detail to gain knowledge on their applicability and boundary conditions.
- (4) The in-cylinder process simulation model in this thesis is based on a single zone cylinder process model, assuming a direct relation between injection, evaporation, mixing and combustion. If differences between injection rate, evaporation rate and combustion rate are to be included in the model it must be extended to a 'few-zone model', i.e. next to the gas zone also a droplet zone, and perhaps a combustion zone, should be defined. In this way a more detailed description of the in-cylinder process can be made.
- (5) In the basic Seiliger process model, stage 1-2 and 5-6 include the heat loss

process during compression and expansion, which are modelled with polytropic exponents, and the other three stages are for net heat input. In the advanced Seiliger process, only stage 1-2 indicates heat loss (again modelled with a polytropic exponent) and the other four stages result in a net heat input. In the DE B4 simulation model heat loss during 2-3, 3-4 and 4-5 is modelled using the Woschni heat loss model, albeit only at maximum cylinder temperature (point 4). Heat loss during combustion, and preferably also during compression and expansion in the basic and advanced Seiliger process should be based on the Woschni model, but then applied in the finite stations of the Seiliger cycle. In a continuous cylinder process simulation, the Woschni heat loss model is based on crank angle and can easily be evaluated continuously. In the Seiliger process there are seven finite stations for which the pressures and temperatures are only known after calculation of the heat losses, introducing an essential algebraic loop. How to introduce a Woschni (-like) heat loss model rigorously in a finite stage in-cylinder process model deserves further attention.

- (6) In this research, the Seiliger parameters as function of work and engine speed were investigated. However, when modelling Seiliger parameters in the DE B4 model, other relations between Seiliger parameters and engine operating conditions could be used. For example the air excess ratio, which indicates the relative air supply to the engine, could be used as an input. In general, the non-dimensional Seiliger parameters should preferably be expressed in non-dimensional operating parameters.
- (7) The analysing approach in this thesis is proposed to be used in the modern engines with such as high pressure injection equipment, later injection timing and common rail. The comparison of Seiliger parameters behaving in the classic and modern engine could give more information on characterising the combustion.
- (8) The research in this thesis can be used to characterize combustion in general and as such could be applied to condition monitoring of diesel engines.
- (9) Similar analysis based on the experimental data could be used to investigate the Vibe combustion model parameters as function of engine load and speed. Although this has been done before (a.o. [Watson, 1980]), it is perhaps time do it again on modern engines using the improved heat release analysis developed in this thesis.

Appendix

Appendix I. Single-zone combustion model¹

In the control volume, the in-cylinder *gas* is considered to be single-zone. The *fuel droplets* are a zone within the control volume but their dwelling time is assumed to be zero (i.e. the injection rate and the evaporating rate are the same). Also the dwelling time of the *fuel gas* after evaporating is assumed to be zero (evaporating rate and combustion rate are the same).

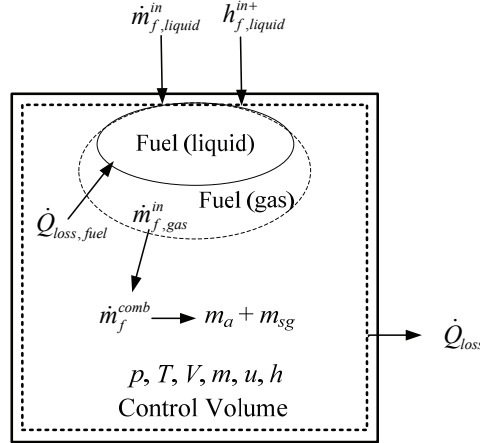


Figure I.1 Scheme of the control volume

The energy and mass balance for an open control volume in general is:

$$d(m \cdot u) = h^{in+} \cdot dm^{in} - h^{out+} \cdot dm^{out} + \delta Q - \delta W \quad [I.1]$$

$$dm = dm^{in} - dm^{out} \quad [I.2]$$

The + in the upper index of (total) enthalpy indicates that the kinetic term may be included. Divide equation [I.1] and [I.2] by time difference 'dt' and introduce mass-, heat- and workflow:

$$\frac{d(m \cdot u)}{dt} = h^{in+} \cdot \dot{m}^{in} - h^{out+} \cdot \dot{m}^{out} + \dot{Q} - \dot{W} \quad [I.3]$$

$$\frac{dm}{dt} = \dot{m}^{in} - \dot{m}^{out} \quad [I.4]$$

¹ Part of the text of in this appendix is reprinted with permission from ©Copyright Royal Netherland Naval College, 2009 [Stapersma, 2009c].

Now applied to the system in Figure I.1, there is no mass flow out of the control volume:

$$\dot{m}^{out} = 0 \quad [I.5]$$

The inflow only consists of liquid fuel:

$$\dot{m}^{in} = \dot{m}_{f,liquid}^{in} \quad [I.6]$$

with its (total) enthalpy:

$$h^{in+} = h_{f,liquid}^{in+} \quad [I.7]$$

Equation [I.3] and [I.4] become:

$$\frac{d(m \cdot u)}{dt} = h_{f,liquid}^{in+} \cdot \dot{m}_{f,liquid}^{in} + \dot{Q} - \dot{W} \quad [I.8]$$

$$\frac{dm}{dt} = \dot{m}_{f,liquid}^{in} \quad [I.9]$$

In the gas phase of the control volume, it is assumed that fuel vapor enters the system from the liquid phase. The result is that fuel vapor (f) and air (a) are present in the control volume. They combine by a chemical reaction (combustion) producing stoichiometric gas (sg). The total mass at any moment is:

$$m = m_f + m_a + m_{sg} \quad [I.10]$$

Also the internal energy within the control volume is the sum of these constituents and the ‘first law of thermodynamic’ for this system becomes:

$$\frac{d(m_f \cdot u_f + m_a \cdot u_a + m_{sg} \cdot u_{sg})}{dt} = h_{f,liquid}^{in+} \cdot \dot{m}_{f,liquid}^{in} + \dot{Q} - \dot{W} \quad [I.11]$$

Now proceed by differentiating the left hand side:

$$m_f \cdot \frac{du_f}{dt} + m_a \cdot \frac{du_a}{dt} + m_{sg} \cdot \frac{du_{sg}}{dt} = h_{f,liquid}^{in+} \cdot \dot{m}_{f,liquid}^{in} - u_f \cdot \frac{dm_f}{dt} - u_a \cdot \frac{dm_a}{dt} - u_{sg} \cdot \frac{dm_{sg}}{dt} + \dot{Q} - \dot{W} \quad [I.12]$$

If the dwelling time of the fuel vapour is assumed zero:

$$m_f = 0 \quad [I.13]$$

Assuming that air and stoichiometric gas behave as ideal gases:

$$du_a = c_{v,a}^{\text{ideal}} \cdot dT \quad [I.14]$$

$$du_{sg} = c_{v,sg}^{\text{ideal}} \cdot dT \quad [I.15]$$

The total change of the specific internal energy for the mixture as occurring in the first law is:

$$m_a \cdot \frac{du_a}{dt} + m_{sg} \cdot \frac{du_{sg}}{dt} = (m_a \cdot c_{v,a} + m_{sg} \cdot c_{v,sg}) \cdot \frac{dT}{dt} = m \cdot c_v \cdot \frac{dT}{dt} \quad [I.16]$$

Then the energy balance:

$$m \cdot c_v \cdot \frac{dT}{dt} = h_{f,liquid}^{in+} \cdot \dot{m}_{f,liquid}^{in} - u_f \cdot \frac{dm_f}{dt} - u_a \cdot \frac{dm_a}{dt} - u_{sg} \cdot \frac{dm_{sg}}{dt} + \dot{Q} - \dot{W} \quad [I.17]$$

Each mass balance of substance has a term that represents the amount that is disappearing or appearing as a result of the combustion taking place in the cylinder (= control volume). This term is super-indexed 'comb'. The mass balances of substance then are:

$$\frac{dm_f}{dt} = \dot{m}_{f,gas}^{in} - \dot{m}_f^{comb} \quad \text{for fuel vapor} \quad [I.18]$$

$$\frac{dm_a}{dt} = -\dot{m}_a^{comb} \quad \text{for air} \quad [I.19]$$

$$\frac{dm_{sg}}{dt} = \dot{m}_{sg}^{comb} \quad \text{for stoichiometric gas} \quad [I.20]$$

The mass balance for the combustion reaction process (*reaction balance*) is:

$$\dot{m}_f^{comb} + \dot{m}_a^{comb} = \dot{m}_{sg}^{comb} \quad [I.21]$$

The ratio of the air (required for the combustion) to the amount of fuel is – by definition – the stoichiometric ratio:

$$\dot{m}_a^{comb} = \sigma \cdot \dot{m}_f^{comb} \quad [I.22]$$

Then, using the mass balance of the reaction, the amount of stoichiometric gas is:

$$\dot{m}_{sg}^{comb} = (1 + \sigma) \cdot \dot{m}_f^{comb} \quad [I.23]$$

Define the reaction rate (on kg basis) as the fuel combustion (or fuel burn) rate:

$$\xi = \dot{m}_f^{comb} \quad [I.24]$$

Substitute the reaction equations into the mass balances of air and stoichiometric gas in equation [I.18] – [I.20]:

$$\frac{dm_f}{dt} = \dot{m}_{f,gas}^{in} - \xi \quad \text{for fuel vapor} \quad [I.25]$$

$$\frac{dm_a}{dt} = -\sigma \cdot \xi \quad \text{for air} \quad [I.26]$$

$$\frac{dm_{sg}}{dt} = (1 + \sigma) \cdot \xi \quad \text{for stoichiometric gas} \quad [I.27]$$

Substitute the mass balances of substance, equation [I.25] – [I.27] into the energy balance [I.17]:

$$m \cdot c_v \cdot \frac{dT}{dt} = h_{f,liquid}^{in+} \cdot \dot{m}_{f,liquid}^{in} - u_f \cdot (\dot{m}_{f,gas}^{in} - \xi) + u_a \cdot \sigma \cdot \xi - u_{sg} \cdot (1 + \sigma) \cdot \xi + \dot{Q} - \dot{W} \quad [I.28]$$

Since the dwelling time within the droplet zone is assumed zero, the mass flow of the liquid fuel into the cylinder will be equal to the mass flow of fuel evaporating as gas from the fuel droplets:

$$\dot{m}_{f,liquid}^{in} = \dot{m}_{f,gas}^{in} = \dot{m}_f^{in} \quad [I.29]$$

After sorting terms ultimately the energy balance becomes

$$m \cdot c_v \cdot \frac{dT}{dt} = \dot{m}_f^{in} \cdot (h_{f,liquid}^{in+} \cdot -u_f) + \xi \cdot [(u_f + \sigma \cdot u_a - (1 + \sigma) \cdot u_{sg})] + \dot{Q} - \dot{W} \quad [I.30]$$

If the kinetic energy caused by the fuel injection pressure is not neglected in the energy balance:

$$h_{f,liquid}^{in+} = h_{f,liquid}^{in} + \frac{v^2}{2} \quad [I.31]$$

The kinetic energy can be estimated if it is assumed that it is fully converted to a

permanent pressure drop across the injector:

$$p_{inj} = p + \frac{\rho_{f,liquid} \cdot v^2}{2} \quad [I.32]$$

Now the ‘combustion heat flow’ (\dot{Q}_{comb}) is introduced:

$$\dot{Q}_{comb} = \xi \cdot \left[(u_f + \sigma \cdot u_a - (1 + \sigma) \cdot u_{sg}) \right] \quad [I.33]$$

Also the ‘energy flow of fuel’ (\dot{E}_f) is defined as the (negative) effect of energy transport of liquid fuel into the cylinder when compared with the ultimate energy within the volume:

$$\dot{E}_f = \dot{m}_{f,in} \cdot (h_{f,liquid}^{in+} - u_f) \quad [I.34]$$

One can view this energy flow also as the heat flowing from the gas phase to the (liquid) fuel and required to heat up and evaporate the fuel before combustion ($\dot{Q}_{loss,fuel}$ in Figure I.1).

Assume the indicated work is reversible and the heat loss to the wall gives rise to a negative term in the equation [I.30], then it becomes:

$$m \cdot c_v \cdot \frac{dT}{dt} = \dot{Q}_{comb} - \dot{Q}_{loss} - p \cdot \frac{dV}{dt} + \dot{E}_f \quad [I.35]$$

Eventually:

$$\frac{dT}{dt} = \frac{\dot{Q}_{comb} - \dot{Q}_{loss} - p \cdot \frac{dV}{dt} + \dot{E}_f}{m \cdot c_v} \quad [I.36]$$

Appendix II. Properties library

The in-cylinder gas consists of air and stoichiometric gas. In these two constituents, the air is the a mixture of Nitrogen (N₂), Oxygen (O₂), Argon (Ar) and Carbondioxide (CO₂); the stoichiometric gas is the mixture of of Nitrogen (N₂), Argon (Ar), Carbondioxide (CO₂), Sulphuroxide (SO₂) and Water (H₂O). For each species in air and stoichiometric gas, they are considered to be ideal but non-perfect gases and then the mixture behaves as ideal but non-perfect as well. Therefore the specific heat, enthalpy, and internal energy of air and stoichiometric gas are functions of only temperature and the mixture fractions. The latter is well defined for air and for stoichiometric gas it can be calculated based on fuel composition and a fuel reaction mass balance. Ultimately the properties of the in-cylinder gas are functions of only temperature and air fraction in the cylinder.

A power series of the (normalized) temperature (equation [II.1]) is used to fit these property data for all the species in both air and stoichiometric gas and then the properties of air and stoichiometric gas can be known on the basis of ideal mixture. Finally the composition x is used to calculate the in-cylinder gas property data.

$$c_p = a_1 + a_2 \cdot \theta + a_3 \cdot \theta^2 \dots a_k \cdot \theta^{k-1} \dots a_m \cdot \theta^{m-1}$$

$$= \sum_{k=1}^m a_k \cdot \theta^{k-1} \quad \text{[II.1]}$$

With $\theta = \frac{T - T_{shift}}{T_{norm}}$

T_{shift} – the Kelvin temperature is shifted to a non-zero point, usually $T_{shift} = 0$ K.

T_{norm} – normalized temperature, usually $T_{norm} = 1000$ K.

It is mentioned that T_{shift} is usually higher such as 273 K, 800 K or even 1000 K. In this case 0 K was chosen in order later to integrate for entropy.

There are several reasons for using a power series to obtain the specific heat at constant pressure. Firstly, given the power series of the specific heat at constant pressure, it is easy to integrate them resulting in the enthalpy difference relative to a certain reference according to equation [II.2]. In addition, the number of terms of the

power series can be selected according to the required accuracy. In this case generally 6 terms are used to cover a range between 200 – 2500 K with reasonable accuracy (Table II.1) and based on data from [Zeise, 1954] valid for this range.

$$dh = c_p \cdot dT \quad [\text{II.2}]$$

$$du = c_v \cdot dT \quad [\text{II.3}]$$

$$ds = c_p \cdot \frac{dT}{T} - R \frac{dp}{p} \quad [\text{II.4}]$$

First of all, the properties of each species in air, stoichiometric gas and fuel are calculated:

$$c_{v,j} = c_{p,j} - R_j = \sum_{k=1}^m a_{k,j} \cdot \theta^{k-1} - R_j \quad [\text{II.5}]$$

$$\Delta h_j = h_j - h_j^{ref} = \sum_{k=1}^m \frac{a_{k,j}}{k} \cdot T_{norm} \cdot \theta^k - \sum_{k=1}^m \frac{a_{k,j}}{k} \cdot T_{norm} \cdot \theta_{ref}^k \quad [\text{II.6}]$$

$$u_j = \Delta u_j + u_j^{ref} = h_j - R_j \cdot T \quad [\text{II.7}]$$

$$\begin{aligned} \Delta s_j &= s_j - s_j^{ref} + R_j \cdot \ln \left(\frac{p_j}{p_{ref}} \right) \\ &= \left(a_{1,j} \cdot \ln \left(\frac{\theta}{\theta_{ref}} \right) - \sum_{k=2}^m \frac{a_{k,j}}{k-1} \cdot \theta_{ref}^{k-1} + \sum_{k=2}^m \frac{a_{k,j}}{k-1} \cdot \theta^{k-1} \right) \end{aligned} \quad [\text{II.8}]$$

With $T_{ref} = 25 \text{ }^\circ\text{C}$.

$$p_{ref} = 0.1 \text{ Mpa.}$$

h_{ref} and s_{ref} are the specific enthalpy and entropy at reference condition (T_{ref} and p_{ref}) and their values for different species are given in Table II.2.

Then the properties of air (in fact dry air) can be calculated summing the properties of each species weighted by the mass fractions of the species (equation [II.9] – [II.11]). The expressions for the stoichiometric gas are the same as for air, the index ‘sg’ (stoichiometric gas) taking the place of index ‘da’ (dry air) in equation [II.9] – [II.12].

$$c_{v,da} = c_{p,da} - R_{da} = \sum_j x_j^{da} \cdot c_{p,j} - \sum_j x_j^{da} \cdot R_j \quad [\text{II.9}]$$

$$h_{da} = \sum_j x_j^{da} \cdot h_j \quad [\text{II.10}]$$

$$u_{da} = \sum_j x_j^{da} \cdot u_j \quad [\text{II.11}]$$

The calculation of the entropy of a mixture of air is more complicated than for the other properties above since it is, even for ideal gas, not only a function of temperature and mass fraction but also of pressure

$$s_{da} = \sum_j x_j^{da} \cdot \left(\Delta s_j + s_j^{ref} - R_j \cdot \ln \left(\frac{p_{da}}{p_{ref}} \right) - R_j \cdot \sum_j y_j^{da} \cdot \ln \left(y_j^{da} \right) \right) \quad [\text{II.12}]$$

In the dry air, j are the components: N₂, O₂, Ar and CO₂; in the stoichiometric gas, j are the components: N₂, Ar, CO₂, H₂O and SO₂.

Finally, together with the air mass fraction calculated in equation [2.5], the in-cylinder gas properties are calculated:

$$c_v = x \cdot c_{v,air} + (1-x) \cdot c_{v,sg} \quad [\text{II.13}]$$

$$h = x \cdot h_{air} + (1-x) \cdot h_{sg} \quad [\text{II.14}]$$

$$u = x \cdot u_{air} + (1-x) \cdot u_{sg} \quad [\text{II.15}]$$

$$s = x \cdot \left(\Delta s_{da} + s_{da}^{ref} - R_{da} \cdot \ln \left(\frac{p}{p_{ref}} \right) \right) + (1-x) \cdot \left(\Delta s_{sg} + s_{sg}^{ref} - R_{sg} \cdot \ln \left(\frac{p}{p_{ref}} \right) \right) - R_g \cdot \sum_j y_j^g \cdot \ln \left(y_j^g \right) \quad [\text{II.16}]$$

With:

$$R_g = (1-x) \cdot R_{sg} + x \cdot R_{da} \quad [\text{II.17}]$$

$$y_j^g = x_j^g \cdot \frac{M_g}{M_j} \quad [\text{II.18}]$$

$$x_j^g = (1-x) \cdot x_j^{sg} + x \cdot x_j^{da} \quad [\text{II.19}]$$

$$\frac{1}{M_g} = \frac{1-x}{M_g} + \frac{x}{M_g} \quad [\text{II.20}]$$

y – the mole fraction [--]

p – in-cylinder pressure [pa]

The calculation of the properties of liquid fuel is somewhat different from the gaseous fuel. The enthalpy of the liquid fuel is based on the definition:

$$h_{f,liquid} = u_{f,liquid} + \frac{p}{\rho_{f,liquid}} \quad [\text{II.21}]$$

The first item in the right hand side is calculated based on:

$$du = c_v \cdot dT \quad \text{ref [II.3]}$$

Then the internal energy of liquid fuel is:

$$u_{f,liquid} = u_f^{ref} + c_{v,f,liquid} \cdot (T - T_{ref}) \quad [\text{II.22}]$$

The diesel fuel is assumed to consist of an alkane ($C_{13}H_{28}$) and a benzene ($C_{13}H_{10}$), the idea being that the chosen species are typical for all alkanes and aromatics and that the specific heat of alkanes and aromatics differ both at reference temperature and in their temperature dependence. The fraction of $C_{13}H_{28}$ and $C_{13}H_{10}$ is calculated from the carbon percentage of the fuel, which is known when the fuel type is determined. The $c_{v,f,liquid}$ can be then be calculated with the data in Table II.1, which for the moment is not temperature dependent. The reference value u_f^{ref} equals h_f^{ref}

minus the volume work (p_{ref} / ρ_f^{ref}) at the same reference temperature. The

reference enthalpy h_f^{ref} of the fuel was used to match the effective heat of combustion to a real measured value or a value determined according to [BSI, 1982], as explained in Chapter 2 of this thesis. The evaporation heat of the two typical fuel constituents at reference condition can be estimated based on [Borman, 1998] (See Table II.3).

The density of liquid fuel can be taken according to [Stapersma, 2011c]

$$\rho_{f,liquid} = \rho_f^{15} - 0.68 \cdot (\theta - 15) \quad [\text{II.23}]$$

With ρ_f^{15} is the fuel liquid density at 15 °C.

Table II.1 The coefficients for the polynomial to calculate c_p [Stapersma, 2009f], [Yaws, 1986], [Borman, 1998]

	a_1	a_2	a_3	a_4	a_5	a_6	range (K)
N ₂	3.5463	0.5773	1.8224	1.1149	0.2731	0.0239	200-2500
O ₂	3.0845	1.8622	-1.0049	0.2817	-0.0320	0.0007	200-2500
Ar	2.500	0.000	0.000	0.000	0.000	0.000	200-2500
CO ₂	2.5468	8.0614	-5.9398	2.2908	-0.4380	0.0327	200-2500
H ₂ O	3.9800	-0.4380	2.5797	-1.4469	0.3244	-0.0264	200-2500
SO ₂	2.7915	8.9226	-8.4591	4.1789	-1.0431	0.1038	200-2500
C ₁₃ H ₁₀ (g)*	-74.758	1018.70	-717.21	221.40	-20.28	0.000	200-1500
C ₁₃ H ₂₈ (g)*	110.40	533.21	739.84	1021.20	324.23	0.000	150-1500
C ₁₃ H ₁₀ (l)&	2210	0	0	0	0	0	0
C ₁₃ H ₂₈ (l)&	1700	0	0	0	0	0	0

* (g) means fuel in gas phase

& (l) means fuel in liquid phase and this coefficient is used to calculate $c_{v,f,liquid}$

Table II.2 The reference values of enthalpy and entropy at $p = 0.1$ MPa, $T = 25^\circ\text{C}$ [Baehr, 2006]

	h_{ref} (kJ/mol)	s_{ref} (J/mol/K)
N ₂	0	191.609
O ₂	0	205.152
Ar	0	154.846
CO ₂	-393.51	213.785
H ₂ O	-241.83	188.835
SO ₂	-296.8	248.22

Table II.3 Evaporation heat of fuel composition at $p = 0.1$ MPa, $T = 25^\circ\text{C}$.

	h_{evap}^{ref} (kJ/kg)
C ₁₃ H ₁₀	339
C ₁₃ H ₂₈	246

Appendix III. Curve Fitting Techniques Using Least Square Theory

The strategy of least square regression is to minimize the sum of squares of the residual S_r resulting in a unique curve for 'best' fit [Chapra, 2006].

$$S_r = \sum_{i=1}^n e_i^2 = \sum_{i=1}^n (y_{i,measured} - y_{i,fitting})^2 \quad [III.1]$$

Since equation [2.24] is nonlinear in the coefficients, the nonlinear least square method should be used. The relation between the fit equation f (where a_m are the parameters in the equation) and measured data (x_i and y_i) can be expressed generally as:

$$y_i = f(x_i; a_0, a_1, \dots, a_m) + e_i \quad [III.2]$$

The nonlinear equation f can be expanded in a Taylor series at the initial value of the parameters and curtailed after the first derivative. A two parameters case is taken as an example:

$$f(x_i)_{j+1} = f(x_i)_j + \frac{\partial f(x_i)_j}{\partial a_0} \Delta a_0 + \frac{\partial f(x_i)_j}{\partial a_1} \Delta a_1 \quad [III.3]$$

Where: j – the initial guess;

$j+1$ – the prediction;

$$\Delta a_0 = a_{0,j+1} - a_{0,j};$$

$$\Delta a_1 = a_{1,j+1} - a_{1,j}$$

Up to now, equation [III.3] has been linearized with respect to the parameters a_0 and a_1 . Equation [III.3] can be substituted in to equation:

$$y_i - f(x_i)_j = \frac{\partial f(x_i)_j}{\partial a_0} \Delta a_0 + \frac{\partial f(x_i)_j}{\partial a_1} \Delta a_1 + e_i \quad [III.4]$$

A matrix form of equation [III.4] can be obtained:

$$\{D\} = [Z_j] \{\Delta A\} + \{E\} \quad [III.5]$$

$[Z_j]$ is the matrix of partial derivatives of the function evaluated at the initial guess j , n is the number of measured data point.

$$[Z_j] = \begin{bmatrix} \partial f_1 / \partial a_0 & \partial f_1 / \partial a_1 \\ \partial f_2 / \partial a_0 & \partial f_2 / \partial a_1 \\ \vdots & \vdots \\ \partial f_n / \partial a_0 & \partial f_n / \partial a_1 \end{bmatrix} \quad \text{[III.6]}$$

The vector $[D]$ contains the differences between the measurements and the function values,

$$\{D\} = \begin{bmatrix} y_1 - f(x_1) \\ y_2 - f(x_2) \\ \vdots \\ y_n - f(x_n) \end{bmatrix} \quad \text{[III.7]}$$

The vector $[A]$ contains the change of the parameter values,

$$\{\Delta A\} = \begin{bmatrix} \Delta a_0 \\ \Delta a_1 \\ \vdots \\ \Delta a_n \end{bmatrix} \quad \text{[III.8]}$$

Then the linear least square theory can be applied in equation [III.5] to get the normal formula:

$$[[Z_j]^T [Z_j]] \{\Delta A\} = \{[Z_j]^T \{D\}\} \quad \text{[III.9]}$$

Thus, the approach consists of solving equation [III.9] for $\{\Delta A\}$, which can be employed to compute improved values for the parameters, as in

$$a_{0,j+1} = a_{0,j} + \Delta a_0 \quad \text{and} \quad a_{1,j+1} = a_{1,j} + \Delta a_1 \quad \text{[III.10]}$$

This procedure is repeated until the solution converges — that is, until

$$|\mathcal{E}_a|_k = \left| \frac{a_{k,j+1} - a_{k,j}}{a_{k,j+1}} \right| \quad \text{[III.11]}$$

falls below an acceptable stopping criterion.

Appendix IV. Fitting residual analysis

Assume that in the fit process, y is the measured data, \hat{y} is the corresponding fit value and \bar{y} is the mean value of the measured data. The residual r is defined:

$$r = y_i - \hat{y}_i \quad [\text{IV.1}]$$

There are several goodness-of-fit statistics for the fit model, with which the goodness of the fit result can easily be evaluated [MATLAB, 2008].

- **Sum of square due to error (SSE)**

$$SSE = \sum_{i=1}^n (y_i - \hat{y}_i)^2 \quad [\text{IV.2}]$$

If SSE is closer to 0, the fit results in a smaller random error and will give a more accurate prediction.

- **R-square**

R-square is defined as the ratio of squares of regression (SSR) and the total sum of squares (SST). In fact it is the square of the correlation between the fit values and the predicted fit value, in which the mean value of the measured data is used as the benchmark.

$$R\text{-square} = \frac{SSR}{SST} \quad [\text{IV.3}]$$

With
$$SSR = \sum_{i=1}^n (\hat{y}_i - \bar{y})^2 \quad \text{and} \quad SST = \sum_{i=1}^n (y_i - \bar{y})^2 \quad [\text{IV.4}]$$

According to equation [IV.2] and [IV.4], the R-square can be expressed as:

$$R\text{-square} = \frac{SSR}{SST} = \frac{SST - SSE}{SST} = 1 - \frac{SSE}{SST} \quad [\text{IV.5}]$$

R-square can have a value between 0 and 1, where a value closer to 1 means that a large proportion of variance is accounted for in the fitting model. For example, an

R-square value 0.8234 means that the fit explains 82.34% of the total variation in the data around the average.

When increasing the number of fitted coefficient (fit parameters b_k and m_k), the *R-square* becomes larger although the fit may not improve in a practical sense. In order to describe the fit properly, the adjusted *R-square* is introduced considering the residual degree of freedom (*DFE*). The residual degree of freedom u is defined as the number of the measured data n minus the fitted parameters number k :

$$u = n - k \quad [IV.6]$$

And adjusted *R-square* is:

$$\text{Adjusted } R\text{-square} = 1 - \frac{SSE(n-1)}{SST(u)} \quad [IV.7]$$

Appendix V. Polytropic Process¹

V.1 Introduction

The polytropic process is a process for which the heat exchange is reversible and can take the general form:

$$\delta Q^{\text{rev}} = T \cdot dS = c \cdot m \cdot dT \quad [\text{V.1}]$$

where the specific heat c is anything between the specific heat at constant pressure and the one at constant volume. Remember that the internal energy for an ideal gas is:

$$dU = c_v^{\text{ideal}} \cdot m \cdot dT \quad [\text{V.2}]$$

Then substitute the last two equations into Gibbs equation:

$$dU = T \cdot dS - p \cdot dV \Rightarrow c_v \cdot m \cdot dT = c \cdot m \cdot dT - p \cdot dV \quad [\text{V.3}]$$

Rearranging yields:

$$(c - c_v) \cdot m \cdot dT = p \cdot dV \quad [\text{V.4}]$$

Assume ideal gas:

$$p \cdot V = m \cdot R \cdot T \quad [\text{V.5}]$$

$$c_p - c_v^{\text{ideal}} = R \quad [\text{V.6}]$$

Then in equation [V.3] replace m and p with the gas law by T and V :

$$\frac{c - c_v}{c_p - c_v} \cdot \frac{dT}{T} = \frac{dV}{V} \quad [\text{V.7}]$$

With the ideal gas law for constant mass in logarithmic form:

¹ Part of the text of in this appendix is reprinted with permission from ©Copyright Royal Netherland Naval College, 2002 [Stapersma, 2007].

$$\frac{dp}{p} + \frac{dV}{V} \stackrel{\text{ideal}}{=} \frac{dT}{T} \quad [\text{V.8}]$$

The temperature can be eliminated:

$$\frac{c - c_v}{c_p - c_v} \cdot \left(\frac{dp}{p} + \frac{dV}{V} \right) = \frac{dV}{V} \Rightarrow \frac{dp}{p} + \frac{c - c_p}{c - c_v} \cdot \frac{dV}{V} = 0 \quad [\text{V.9}]$$

Now introduce the polytropic exponent n :

$$n = \frac{c - c_p}{c - c_v} \quad [\text{V.10}]$$

and its relation to the general specific heat c and the isentropic index κ :

$$n = \frac{\frac{c}{c_v} - \gamma}{\frac{c}{c_v} - 1} \Rightarrow \frac{c}{c_v} = \frac{n - \gamma}{n - 1} \quad [\text{V.11}]$$

then:

$$\frac{dp}{p} + n \cdot \frac{dV}{V} = 0 \Rightarrow p \cdot V^n = \text{constant} \quad [\text{V.12}]$$

This way of introducing the polytropic process is that right at the beginning *reversible* heat exchange is assumed as the only cause for entropy change, which is the right assumption for compression and expansion in diesel engines. In [Stodola, 1922] and [Baehr, 1989] a more general basis, applicable to both *reversible* and *irreversible* processes is introduced. The following derivation for a closed volume process is taken from [Stapersma, 2007],

V.2 Polytropic efficiency and exponent for closed systems

The ‘polytropic efficiency’ for a closed system is defined by the ratio between the reversible work and change in internal energy of a small step change within the process:

$$\eta_{pol}^u \stackrel{\text{def}}{=} \frac{-p \cdot dV}{du} \quad [\text{V.13}]$$

With Gibbs and the second law the polytropic efficiency for the closed system can be written as:

$$\eta_{pol}^u = \frac{-p \cdot dV}{-p \cdot dV + T \cdot ds} = \frac{-p \cdot dV}{-p \cdot dV + \delta q + T \cdot \delta s_{irr}} \quad [V.14]$$

It can be seen very precisely that both *reversible heat input* (or loss) and/or *irreversible entropy production* will result in a polytropic efficiency different from unity since both cause a change of the entropy. The state of change – in terms changes of temperature, pressure and specific volume – is completely determined by the polytropic efficiency. This will be investigated in the following.

For ideal gas:

$$du^{ideal} = c_v \cdot dT \quad [V.15]$$

$$p = \frac{R \cdot T}{v} \Rightarrow p \cdot dv^{ideal} = R \cdot T \cdot \frac{dv}{v} \quad [V.16]$$

The polytropic efficiency becomes:

$$\eta_{pol}^u \overset{ideal}{=} - \frac{R \cdot \frac{dv}{v}}{c_v \cdot \frac{dT}{T}} \quad [V.17]$$

Therefore equation [V.17] can be written as differential equations for the change of temperature as function of the change of specific volume:

$$\frac{dT}{T} \overset{ideal}{=} - \frac{1}{\eta_{pol}^u} \frac{R}{c_v} \cdot \frac{dv}{v} \quad [V.18]$$

Then the relation between polytropic efficiency and polytropic exponents will be presented. For ideal gas:

$$\frac{R}{c_v} \overset{ideal}{=} \frac{c_p - c_v}{c_v} = \gamma - 1 \quad \text{with} \quad \gamma = \frac{c_p}{c_v} \quad [V.19]$$

Define in the same way:

$$\frac{1}{\eta_{pol}^u} \cdot \frac{R}{c_v} \stackrel{\text{ideal}}{=} n - 1 \quad [\text{V.20}]$$

where n again is the polytropic exponent. Rearrange equation [V.20], the relating between polytropic efficiency and polytropic exponent is:

$$\eta_{pol}^u \stackrel{\text{ideal}}{=} \frac{\gamma - 1}{n - 1} \quad [\text{V.21}]$$

or reversed:

$$n \stackrel{\text{ideal}}{=} 1 + (\gamma - 1) \cdot \frac{1}{\eta_{pol}^u} \quad [\text{V.22}]$$

Note that the definition of polytropic efficiency in an expansion process will be reversed, so the polytropic efficiency according to [V.21] must be reversed for expansion, i.e.:

$$\eta_{pol,comp}^u \stackrel{\text{ideal}}{=} \frac{\gamma - 1}{n_{comp} - 1} \quad [\text{V.23}]$$

$$\eta_{pol,exp}^u \stackrel{\text{ideal}}{=} \frac{n_{exp} - 1}{\gamma - 1} \quad [\text{V.24}]$$

Next the derivation of the inclination of a polytropic line in the T - S diagram (dT/ds) is presented.

The entropy equation of state as following from the Gibbs equation is:

$$ds \stackrel{\text{ideal}}{=} c_v \cdot \frac{dT}{T} + R \cdot \frac{dv}{v} \quad [\text{V.25}]$$

Rearrange equation [V.17]:

$$\frac{dv}{v} \stackrel{\text{ideal}}{=} -c_v \cdot \frac{dT}{R \cdot T} \cdot \eta_{pol}^u \quad [\text{V.26}]$$

Substitute equation in entropy state equation [V.25]:

$$ds \stackrel{\text{ideal}}{=} c_v \cdot \frac{dT}{T} - c_v \cdot \frac{dT}{T} \cdot \eta_{pol}^u \quad [\text{V.27}]$$

Sort the equation:

$$\frac{dT^{ideal}}{ds} = \frac{1}{c_v \cdot (1 - \eta_{pol}^u)} \cdot T \quad [V.28]$$

Note that the definition of polytropic efficiency in an expansion process will be reversed, so the inclination according to [V.28] must be reversed for expansion, i.e.:

$$\frac{dT^{ideal}}{ds} = \frac{T}{c_v \cdot (1 - \eta_{pol,comp}^u)} \quad [V.29]$$

$$\frac{dT^{ideal}}{ds} = \frac{T}{c_v \cdot \left(1 - \frac{1}{\eta_{pol,exp}^u}\right)} \quad [V.30]$$

According to equation [V.28] and [V.30], it can be concluded that when the polytropic factor η is assumed to be constant, the curves of polytropic compression and expansion in T - s diagram are *not* straight lines but change with temperature, in fact with the ratio of temperature and specific heat..

Substitute equation [V.23] and [V.24] in [V.28] and [V.30] respectively, and then the inclination in T - s diagram can be expressed in the polytropic exponent, and is the same for compression and expansion:

$$\frac{dT^{ideal}}{ds} = \frac{n-1}{n-\gamma} \cdot \frac{T}{c_v} \quad [V.31]$$

Note that the factor appearing here is the inverse of the ratio c/c_v in equation [V.11]. With equation [V.31] the tendency of the curves for stage 1-2 (polytropic compression) and 5-6 (polytropic expansion) in the Seiliger process when plotted in T - s diagram can be explained (refer to Figure 3.7, Figure 3.9(d), etc.).

Appendix VI. Investigation of diverging in Newton-Raphson numerical method

In the Seiliger fit versions, there are three fit versions, *V4-1*, *V4-5* and *V5-2*, diverging when using Newton-Raphson iteration method to find solutions of the system of equations in the SIMULINK environment. In order to investigate whether there are either no solutions of the equations or the Newton-Raphson method does not find the solution, the algebraic equations for the equivalence criteria are taken from the simulation model and after some simplification will be directly applied to get some information of the roots of the equations.

Firstly, the Seiliger fit version *V4-3*, which is converging when using the Newton-Raphson method, is investigated to verify the solutions of the equations as found. Then the diverging version *V4-5* will be investigated.

VI.1 Seiliger fit version *V4-3* (converging)

In *V4-3*, the equivalence criteria are p_{max} , q_{in} , w_i and T_{EO} and the Seiliger parameters are a , b , c and n_{exp} . The gas properties will now assumed to be constant in the equations for the equivalence criteria, although they are dependent on the temperature and air fraction in the simulation model. However the purpose of this investigation is not to get the precise solutions but to see whether there are solutions. The constants listed in Table VI.1 are the fit results of *V4-3* in the SIMULINK environment. The nominal point (100% speed, 100% power) is used in the following investigation.

Table VI.1 The constant used in the equivalence criteria equations

parameter	value	unit
p_l	$2.1446 \cdot 10^5$	Pa
r_c	13.11	[-]
n_{comp}	1.36	[-]
$c_{v,23}$	867.79	J/kg/K
T_l	348.65	K
$c_{p,34}$	1221.20	J/kg/K
R_{34}	286.92	J/kg/K
R_{45}	286.78	J/kg/K

parameter	value	unit
$q_{in, measured}$	$1.1199 \cdot 10^6$	J/kg
p_{max}	$9.319 \cdot 10^6$	Pa
w_{12}	$-4.240 \cdot 10^5$	J/kg
w_{56}	$3.041 \cdot 10^5$	J/kg
r_{26}	0.0923	[-]
$w_{i, measured}$	$5.211 \cdot 10^5$	J/kg
$T_{EO, measured}$	1119.60	K

1) Peak pressure p_{max} :

The equivalence criterion of p_{max} based on the Seiliger definition is:

$$p_{max} = p_1 \cdot r_c^{n_{comp}} \cdot a \quad [VI.1]$$

Substitute the parameters which are constant as listed in Table VI.1 and fit the maximum pressure to the smoothed measurement:

$$a = \frac{p_{max}}{p_1 \cdot r_c^{n_{comp}}} = \frac{93.139}{2.144 \cdot 13.11^{1.36}} = 1.3129 \quad [VI.2]$$

2) Net heat input q_{in} :

The equivalence criterion for q_{in} based on the *basic* Seiliger process definition is:

$$\begin{aligned} q_{in} &= q_{23} + q_{34} + q_{45} \\ &= c_{v,23} \cdot T_1 \cdot r_c^{n_{comp}-1} \cdot (a-1) + c_{v,34} \cdot T_1 \cdot \gamma \cdot r_c^{n_{comp}-1} \cdot a \cdot (b-1) \\ &\quad + c_{v,45} \cdot T_1 \cdot (\gamma-1) \cdot r_c^{n_{comp}-1} \cdot a \cdot b \cdot \ln c \\ &= c_{v,23} \cdot T_1 \cdot r_c^{n_{comp}-1} \cdot (a-1) + c_{p,34} \cdot T_1 \cdot r_c^{n_{comp}-1} \cdot a \cdot (b-1) \\ &\quad + R_{45} \cdot T_1 \cdot r_c^{n_{comp}-1} \cdot a \cdot b \cdot \ln c \end{aligned} \quad [VI.3]$$

Substitute the parameters which are constant as listed in Table VI.1 and fit the heat input to the smoothed measurement:

$$2.3906 + 14.116 \cdot (b-1) + 3.3149 \cdot b \cdot \ln(c) = 11.199 \quad [VI.4]$$

Thus:

$$\boxed{14.116 \cdot b + 3.3149 \cdot b \cdot \ln(c) - 22.9244 = 0} \quad [VI.5]$$

3) Indicated work w_i :

The equivalence criterion for w_{in} based on the Seiliger process definition is:

$$\begin{aligned}
 w_i &= w_{12} + w_{34} + w_{45} + w_{56} \\
 &= -c_{v,12} \cdot T_1 \cdot \frac{\gamma - 1}{n_{comp} - 1} \left(1 - r_c^{n_{comp} - 1}\right) + c_{v,34} \cdot T_1 \cdot (\gamma - 1) \cdot r_c^{n_{comp} - 1} \cdot a \cdot (b - 1) \\
 &\quad + c_{v,45} \cdot T_1 \cdot (\gamma - 1) \cdot r_c^{n_{comp} - 1} \cdot a \cdot b \cdot \ln c \\
 &\quad + c_{v,56} \cdot T_1 \cdot \frac{\gamma - 1}{n_{exp} - 1} \cdot r_c^{n_{comp} - 1} \cdot a \cdot b \cdot \left(1 - b^{n_{exp} - 1} \cdot c^{n_{exp} - 1} \cdot r_{26}^{n_{exp} - 1}\right) \\
 &= w_{12} + R_{34} \cdot T_1 \cdot r_c^{n_{comp} - 1} \cdot a \cdot (b - 1) + R_{45} \cdot T_1 \cdot r_c^{n_{comp} - 1} \cdot a \cdot b \cdot \ln c \\
 &\quad + \frac{R_{56}}{n_{exp} - 1} \cdot T_1 \cdot r_c^{n_{comp} - 1} \cdot a \cdot b \cdot \left(1 - b^{n_{exp} - 1} \cdot c^{n_{exp} - 1} \cdot r_{26}^{n_{exp} - 1}\right)
 \end{aligned} \tag{VI.6}$$

Substitute the parameters which are constant as listed in Table VI.1 and fit the indicated work to the smoothed measurement:

$$\begin{aligned}
 &-4.2398 + 3.3166 \cdot (b - 1) + 3.3149 \cdot b \cdot \ln(c) \\
 &\quad + \frac{3.3123}{n_{exp} - 1} \cdot b \cdot \left(1 - (0.0923 \cdot b \cdot c)^{n_{exp} - 1}\right) = 5.211
 \end{aligned} \tag{VI.7}$$

Thus:

$$\boxed{
 \begin{aligned}
 &3.3166 \cdot b + 3.3149 \cdot b \cdot \ln(c) \\
 &\quad + \frac{3.3123}{n_{exp} - 1} \cdot b \cdot \left(1 - (0.0923 \cdot b \cdot c)^{n_{exp} - 1}\right) - 12.7669 = 0
 \end{aligned}
 } \tag{VI.8}$$

4) Temperature at opening of exhaust valve T_{EO} :

The equivalence criterion for T_{EO} based on the Seiliger process definition is:

$$\begin{aligned}
 T_{EO} &= \frac{T_5}{r_e^{n_{exp} - 1}} \\
 &= T_1 \cdot r_c^{n_{comp} - 1} \cdot a \cdot b \cdot \left(\frac{V_6}{b \cdot c \cdot V_2}\right)^{1 - n_{exp}} \\
 &= T_1 \cdot r_c^{n_{comp} - 1} \cdot a \cdot b \cdot \left(b \cdot c \cdot \frac{V_2}{r_6}\right)^{n_{exp} - 1} \\
 &= T_1 \cdot r_c^{n_{comp} - 1} \cdot a \cdot b^{n_{exp}} \cdot c^{n_{exp} - 1} \cdot r_{26}^{n_{exp} - 1}
 \end{aligned} \tag{VI.9}$$

Substitute the parameters which are constant as listed in Table VI.1 and fit the temperature at Exhaust Opening to the smoothed measurement:

$$1155.9 \cdot b^{n_{exp}} \cdot (0.0923 \cdot c)^{n_{exp}-1} - 1119.6 = 0 \quad [VI.10]$$

Thus:

$$b^{n_{exp}} \cdot (0.0923 \cdot c)^{n_{exp}-1} - 0.9686 = 0 \quad [VI.11]$$

From equation [VI.5] parameter c can be made explicit:

$$\ln(c) = \frac{22.9244 - 14.116 \cdot b}{3.3149 \cdot b} \quad [VI.12]$$

Therefore:

$$c = e^{\frac{22.9244 - 14.116 \cdot b}{3.3149 \cdot b}} \quad [VI.13]$$

Eliminate variable c in equation [VI.8] and [VI.11] using equation [VI.13]:

$$3.3166 \cdot b + (22.9244 - 14.116 \cdot b) + \frac{3.3123 \cdot b}{n_{exp} - 1} \cdot \left(1 - \left(0.0923 \cdot b \cdot \left(e^{\frac{22.9244 - 14.116 \cdot b}{3.3149 \cdot b}} \right) \right)^{n_{exp}-1} \right) - 12.7669 = 0 \quad [VI.14]$$

$$b^{n_{exp}} \cdot \left(0.0923 \cdot e^{\frac{22.9244 - 14.116 \cdot b}{3.3149 \cdot b}} \right)^{n_{exp}-1} - 0.9686 = 0 \quad [VI.15]$$

Then the ‘ezplot’ command in MATLAB is used to plot the equation [VI.14] and [VI.15]. The result is shown in Figure VI.1, from which it is obvious that there is an intersection point in the *realistic range* of the two parameters. In this point $b = 1.602$, $n_{exp} = 1.285$, $c = 1.1619$ while the fit results with Newton-Raphson method gives $b = 1.247$, $n_{exp} = 1.283$, $c = 3.766$ (refer Table 3.30). The result could be accepted since the difference is mainly caused by the gas properties constant setting instead of variables when using Newton-Raphson in simulation model. It can be concluded that using a graphical solution for the algebraic equations of the equivalence criteria is a reliable way to verify whether there are roots of the equations or not.

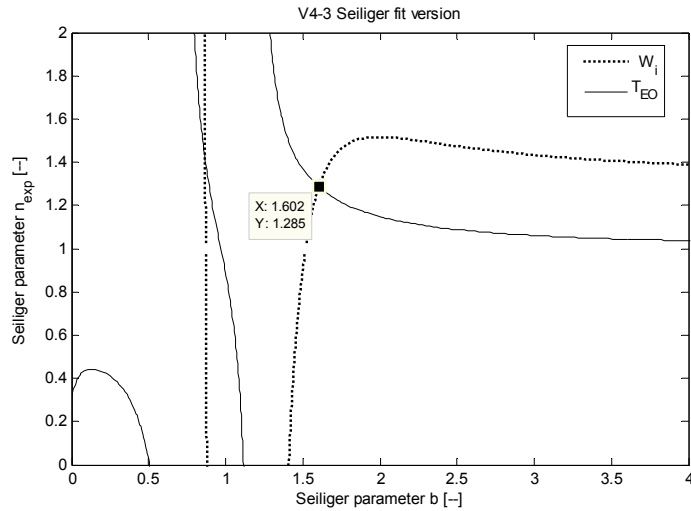


Figure VI.1 Equivalence criteria equations of V4-3

VI.2 Seiliger fit version V4-5 (diverging)

In V4-5, the equivalence criteria are p_{max} , q_{in} , w_i and T_{EO} and the Seiliger parameters are a , b , c and n_{exp} . Since this version is diverging when using the Newton-Raphson method, the constants listed in Table VI.2 are from fitting results of V4-6 in the SIMULINK environment, for which the solution of V4-5 must be close by (if it exists).

Table VI.2 The constant used in the equivalence criteria equations

parameter	value	unit
p_1	$2.1446 \cdot 10^5$	Pa
r_c	13.11	[-]
n_{comp}	1.36	[-]
$c_{v,23}$	867.79	J/kg/K
T_1	348.65	K
$c_{p,34}$	1232.72	J/kg/K
R_{34}	286.92	J/kg/K
R_{45}	286.73	J/kg/K
$q_{in, measured}$	$1.1199 \cdot 10^6$	J/kg
p_{max}	$9.319 \cdot 10^6$	Pa

parameter	value	unit
w_{12}	$-4.240 \cdot 10^5$	J/kg
r_{26}	0.0923	[-]
$w_{i, \text{measured}}$	$5.211 \cdot 10^5$	J/kg
$T_{EO, \text{measured}}$	1119.60	K
$c_{v,56}$	963.84	J/kg/K
γ_{56}	1.2974	[-]

1) Peak pressure p_{max} :

The equivalence criterion of p_{max} based on Seiliger definition is:

$$p_{max} = p_1 \cdot r_c^{n_{comp}} \cdot a \quad \text{Ref [VI.1]}$$

Substitute the parameters which are constant listing in Table VI.2 and fit to the smoothed measurement:

$$a = \frac{p_{max}}{p_1 \cdot r_c^{n_{comp}}} = \frac{93.139}{2.144 \cdot 13.11^{1.36}} = 1.3129 \quad \text{Ref [VI.2]}$$

2) Net heat input q_{in} :

The equivalence criterion for q_{in} based on the *advanced* Seiliger process definition is:

$$\begin{aligned} q_{in} &= q_{23} + q_{34} + q_{45} + q_{56} \\ &= c_{v,23} \cdot T_1 \cdot r_c^{n_{comp}-1} \cdot (a-1) + c_{v,34} \cdot T_1 \cdot \gamma \cdot r_c^{n_{comp}-1} \cdot a \cdot (b-1) \\ &\quad + c_{v,45} \cdot T_1 \cdot (\gamma-1) \cdot r_c^{n_{comp}-1} \cdot a \cdot b \cdot \ln c \\ &\quad + c_{v,56} \cdot T_1 \cdot \left(1 - \frac{\gamma-1}{n_{exp}-1}\right) \cdot r_c^{n_{comp}-1} \cdot a \cdot b \cdot \left(1 - b^{n_{exp}-1} \cdot c^{n_{exp}-1} \cdot r_{26}^{n_{exp}-1}\right) \quad \text{[VI.16]} \\ &= c_{v,23} \cdot T_1 \cdot r_c^{n_{comp}-1} \cdot (a-1) + c_{p,34} \cdot T_1 \cdot r_c^{n_{comp}-1} \cdot a \cdot (b-1) \\ &\quad + R_{45} \cdot T_1 \cdot r_c^{n_{comp}-1} \cdot a \cdot b \cdot \ln c \\ &\quad + c_{v,56} \cdot T_1 \cdot \left(1 - \frac{\gamma-1}{n_{exp}-1}\right) \cdot r_c^{n_{comp}-1} \cdot a \cdot b \cdot \left(1 - b^{n_{exp}-1} \cdot c^{n_{exp}-1} \cdot r_{26}^{n_{exp}-1}\right) \end{aligned}$$

Substitute the parameters which are constant as listed in Table VI.2 and fit the heat input to the smoothed measurement:

$$\begin{aligned}
 & 2.3906 + 14.249 \cdot (b-1) + 3.3143 \cdot b \cdot \ln(c) \\
 & - 11.41 \cdot \left(\frac{n_{exp} - 1.2974}{n_{exp} - 1} \right) \cdot b \cdot \left(1 - (0.0923 \cdot b \cdot c)^{n_{exp}-1} \right) = 11.199 \quad [VI.17]
 \end{aligned}$$

Thus:

$$\boxed{
 \begin{aligned}
 & 14.249 \cdot b + 3.3143 \cdot b \cdot \ln(c) \\
 & - 11.41 \cdot \left(\frac{n_{exp} - 1.2974}{n_{exp} - 1} \right) \cdot b \cdot \left(1 - (0.0923 \cdot b \cdot c)^{n_{exp}-1} \right) - 23.0574 = 0
 \end{aligned}
 } \quad [VI.18]$$

3) Indicated work w_i :

The equivalence criterion for w_{in} based on the Seiliger process definition is:

$$\begin{aligned}
 w_i &= w_{12} + w_{34} + w_{45} + w_{56} \\
 &= -c_{v,12} \cdot T_1 \cdot \frac{\gamma-1}{n_{comp}-1} \left(1 - r_c^{n_{comp}-1} \right) + c_{v,34} \cdot T_1 \cdot (\gamma-1) \cdot r_c^{n_{comp}-1} \cdot a \cdot (b-1) \\
 &\quad + c_{v,45} \cdot T_1 \cdot (\gamma-1) \cdot r_c^{n_{comp}-1} \cdot a \cdot b \cdot \ln c \\
 &\quad + c_{v,56} \cdot T_1 \cdot \frac{\gamma-1}{n_{exp}-1} \cdot r_c^{n_{comp}-1} \cdot a \cdot b \cdot \left(1 - b^{n_{exp}-1} \cdot c^{n_{exp}-1} \cdot r_{26}^{n_{exp}-1} \right) \quad \text{Ref [VI.6]} \\
 &= w_{12} + R_{34} \cdot T_1 \cdot r_c^{n_{comp}-1} \cdot a \cdot (b-1) \\
 &\quad + R_{45} \cdot T_1 \cdot r_c^{n_{comp}-1} \cdot a \cdot b \cdot \ln c \\
 &\quad + \frac{R_{56}}{n_{exp}-1} \cdot T_1 \cdot r_c^{n_{comp}-1} \cdot a \cdot b \cdot \left(1 - b^{n_{exp}-1} \cdot c^{n_{exp}-1} \cdot r_{26}^{n_{exp}-1} \right)
 \end{aligned}$$

Substitute the parameters which are constant as listed in Table VI.2 and fit the indicated work to the smoothed measurement:

$$\begin{aligned}
 & -4.2398 + 3.3166 \cdot (b-1) + 3.3143 \cdot b \cdot \ln(c) \\
 & + \frac{3.3138}{n_{exp}-1} \cdot b \cdot \left(1 - (0.0923 \cdot b \cdot c)^{n_{exp}-1} \right) = 5.211 \quad [VI.19]
 \end{aligned}$$

Finally:

$$\boxed{
 \begin{aligned}
 & 3.3166 \cdot b + 3.3143 \cdot b \cdot \ln(c) \\
 & + \frac{3.3138 \cdot b}{n_{exp}-1} \cdot \left(1 - (0.0923 \cdot b \cdot c)^{n_{exp}-1} \right) - 12.7669 = 0
 \end{aligned}
 } \quad [VI.20]$$

4) Temperature at opening of exhaust valve T_{EO} :

The equivalence criterion for T_{EO} based on the Seiliger process definition is:

$$\begin{aligned}
 T_{EO} &= \frac{T_5}{r_e^{n_{exp}-1}} \\
 &= T_1 \cdot r_c^{n_{comp}-1} \cdot a \cdot b \cdot \left(\frac{V_6}{b \cdot c \cdot V_2} \right)^{1-n_{exp}} \\
 &= T_1 \cdot r_c^{n_{comp}-1} \cdot a \cdot b \cdot \left(b \cdot c \cdot \frac{V_2}{r_6} \right)^{n_{exp}-1} \\
 &= T_1 \cdot r_c^{n_{comp}-1} \cdot a \cdot b^{n_{exp}} \cdot c^{n_{exp}-1} \cdot r_{26}^{n_{exp}-1}
 \end{aligned}
 \tag{VI.9}$$

Substitute the parameters which are constant as listed in Table VI.2 and fit the temperature at Exhaust Opening to the smoothed measurement:

$$1155.9 \cdot b^{n_{exp}} \cdot (0.0923 \cdot c)^{n_{exp}-1} - 1119.6 = 0 \tag{VI.21}$$

Finally

$$b^{n_{exp}} \cdot (0.0923 \cdot c)^{n_{exp}-1} - 0.9686 = 0 \tag{VI.22}$$

From equation [VI.21], the variable b can be expressed in c and n_{exp} :

$$b = \left(\frac{0.9686}{(0.0923 \cdot c)^{n_{exp}-1}} \right)^{\frac{1}{n_{exp}}} \tag{VI.23}$$

Eliminate variable b in equation [VI.18] and [VI.20] using equation [VI.23]:

$$\begin{aligned}
 &14.249 \cdot \left(\frac{0.9686}{(0.0923 \cdot c)^{n_{exp}-1}} \right)^{\frac{1}{n_{exp}}} + 3.3143 \cdot \left(\frac{0.9686}{(0.0923 \cdot c)^{n_{exp}-1}} \right)^{\frac{1}{n_{exp}}} \cdot \ln(c) \\
 &- 11.41 \cdot \left(\frac{n_{exp} - 1.2974}{n_{exp} - 1} \right) \cdot \left(\frac{0.9686}{(0.0923 \cdot c)^{n_{exp}-1}} \right)^{\frac{1}{n_{exp}}} \cdot (1 - (0.0923 \cdot b \cdot c)^{n_{exp}-1}) \\
 &- 23.0574 = 0
 \end{aligned}
 \tag{VI.24}$$

$$\begin{aligned}
 & 3.3166 \cdot \left(\frac{0.9686}{(0.0923 \cdot c)^{n_{exp}-1}} \right)^{\frac{1}{n_{exp}}} + 3.3143 \cdot \left(\frac{0.9686}{(0.0923 \cdot c)^{n_{exp}-1}} \right)^{\frac{1}{n_{exp}}} \cdot \ln(c) \\
 & + \frac{3.3138}{n_{exp} - 1} \cdot \left(\frac{0.9686}{(0.0923 \cdot c)^{n_{exp}-1}} \right)^{\frac{1}{n_{exp}}} \cdot \left(1 - \left(0.0923 \cdot \left(\frac{0.9686}{(0.0923 \cdot c)^{n_{exp}-1}} \right)^{\frac{1}{n_{exp}}} \cdot c \right)^{n_{exp}-1} \right) \\
 & - 12.7669 = 0
 \end{aligned}$$

[VI.25]

The ‘ezplot’ command in MATLAB is again used to plot the equation [VI.24] and [VI.25]. The result is shown in Figure VI.2, from which it is obvious that **no** intersection point exists in the *realistic range* of the two parameters. Therefore it can be concluded that the system of equations for the Seiliger fit version **V4-5** has *no roots*. On the other hand, the solid and dash lines between $c = 1 - 4$ are pretty close, which means that if a relative wide range for the error of the equivalence criteria is acceptable, there could be "solutions" for the equations. (e.g. the error of T_{EO} in fitting results of **V4-6** is 1.30%; if this is acceptable, the fit result of **V4-6** can be considered to be a solution of **V4-5**, refer to Table 3.30).

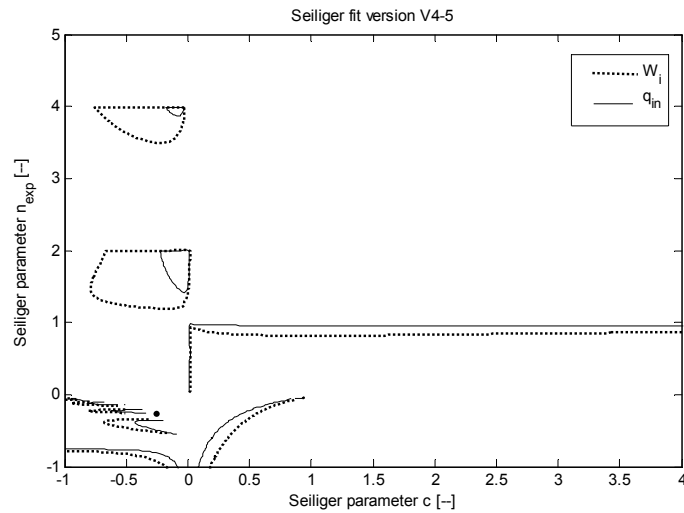


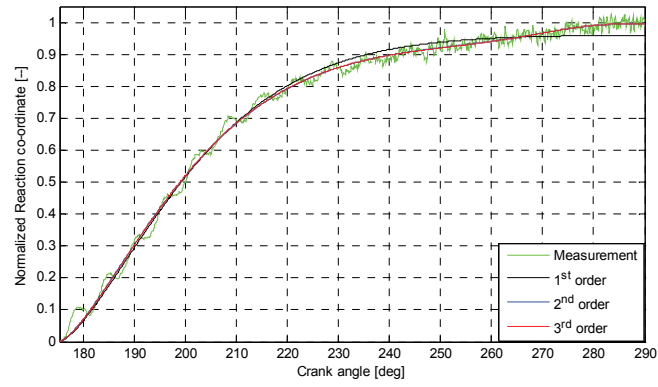
Figure VI.2 Equivalence criteria equations of **V4-5**

Appendix VII. Smoothed heat release measurement of the other three cylinders and cylinder 1 with original hole position

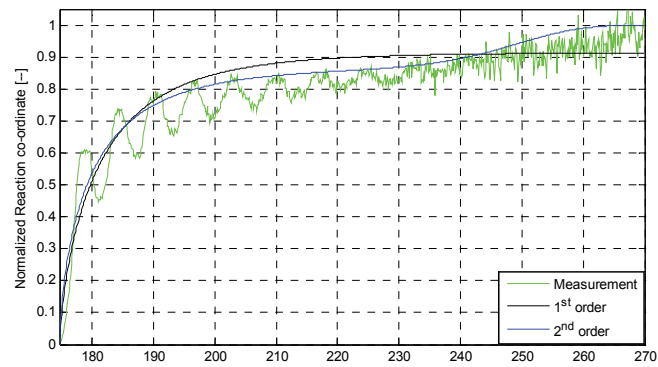
VII.1 Cylinder 2

Table VII.1 Vibe parameters for fit functions (cylinder 2)

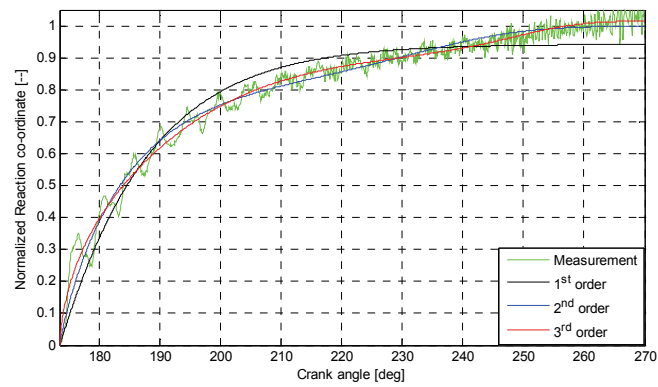
Operating point	Vibe Function	1		2		3	
		b_1	m_1	b_2	m_2	b_3	m_3
(A)	First order	0.962	0.414				
	Second order	0.943	0.054	0.386	10.8		
	Third order	0.989	0.409	0.057	10.78	-0.049	1.034
(B)	First order	0.914	-0.240				
	Second order	0.853	-0.312	0.137	5.264		
(C)	First order	0.943	0.024				
	Second order	0.848	-0.099	0.153	3.618		
	Third order	0.526	-0.310	0.101	7.595	0.390	0.458



(a) Operating point (A)



(b) Operating point (B)



(c) Operating point (c)

Figure VII.1 Fitting the reaction coordinate with multiple Vibe function (cylinder 2)

Appendix VII. Smoothed heat release measurement of the other three cylinders and cylinder 1 with original hole position

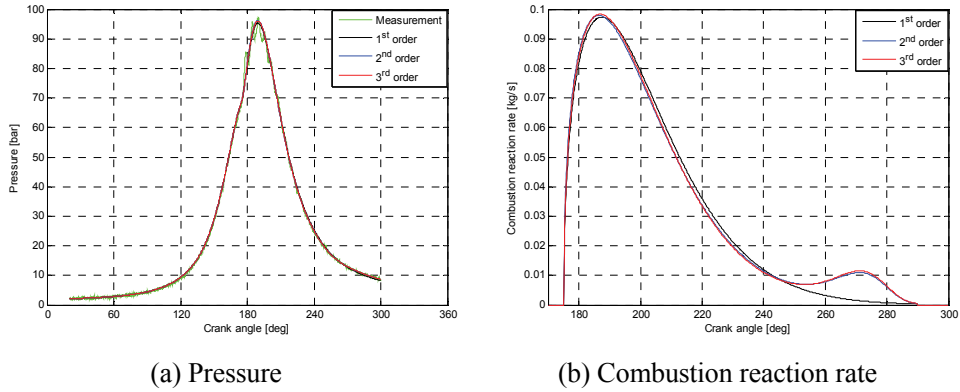


Figure VII.2 Smoothed pressure and combustion reaction rate (point (A), cylinder 2)

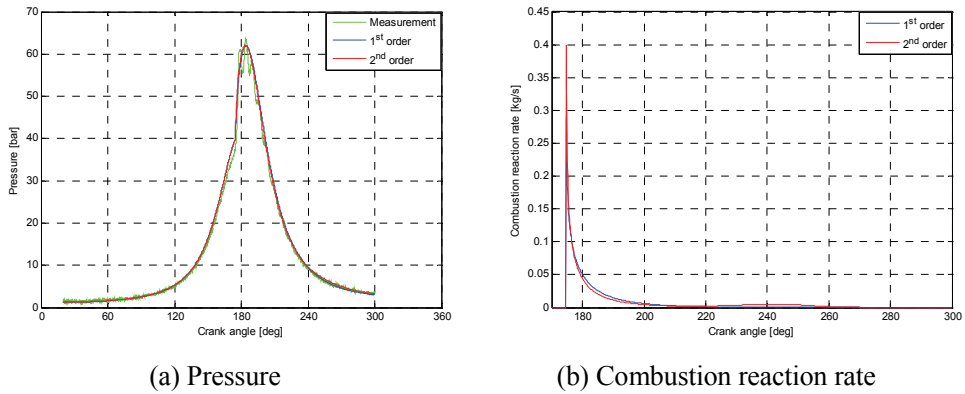


Figure VII.3 Smoothed pressure and combustion reaction rate (point (B), cylinder 2)

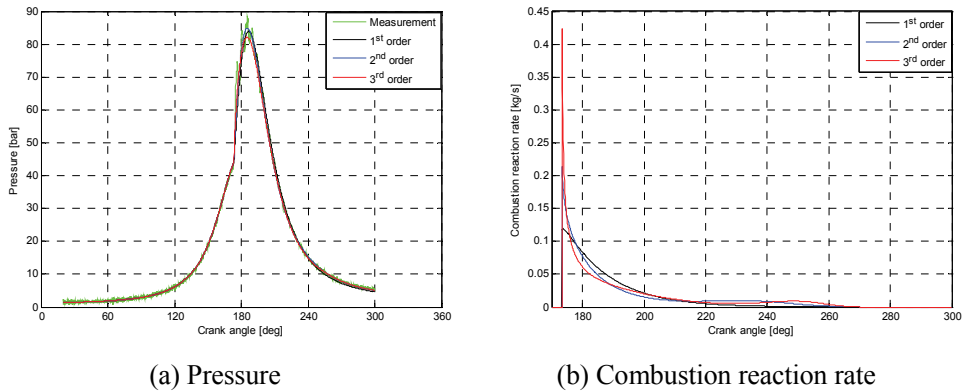
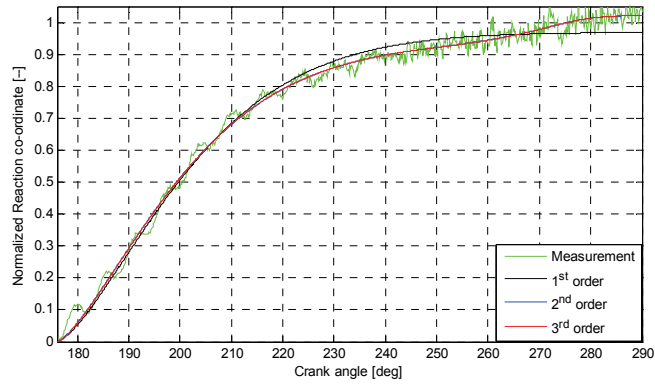


Figure VII.4 Smoothed pressure and combustion reaction rate (point (C), cylinder 2)

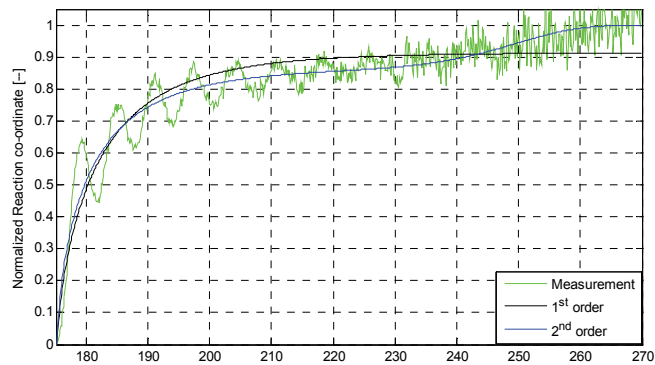
VII.2 Cylinder 3

Table VII.2 Vibe parameters for fit functions (cylinder 3)

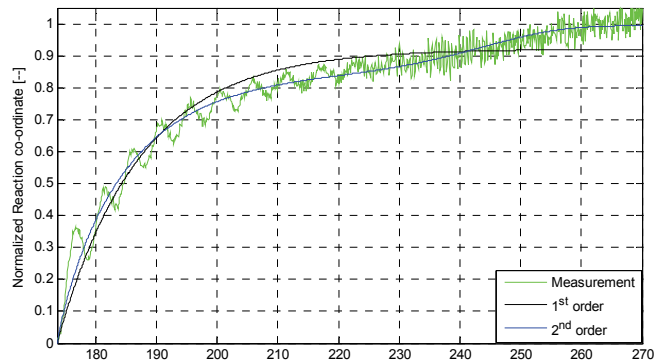
Operating point	Vibe Function	1		2		3	
		b_1	m_1	b_2	m_2	b_3	m_3
(A)	First order	0.941	0.405				
	Second order	0.917	0.370	0.072	11.72		
	Third order	0.959	0.401	0.079	10.08	-0.051	1.539
(B)	First order	0.922	-0.258				
	Second order	0.874	-0.315	0.136	7.348		
(C)	First order	0.921	-0.013				
	Second order	0.855	-0.101	0.140	5.806		



(a) Operating point (A)

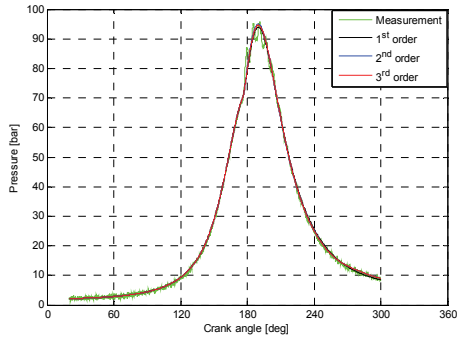


(b) Operating point (B)

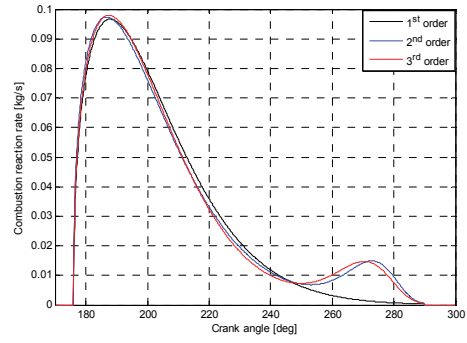


(c) Operating point (c)

Figure VII.5 Fitting the reaction coordinate with multiple Vibe function (cylinder 3)

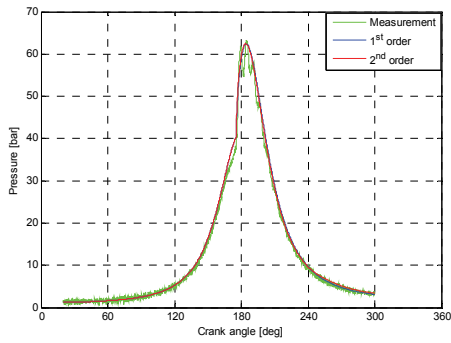


(a) Pressure

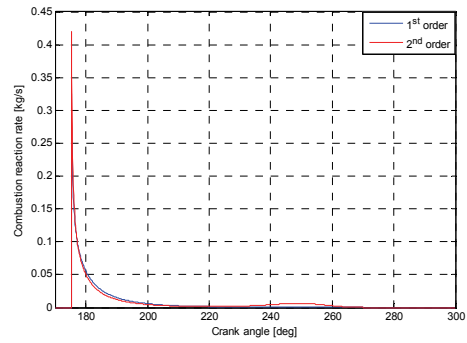


(b) Combustion reaction rate

Figure VII.6 Smoothed pressure and combustion reaction rate (point (A), cylinder 3)

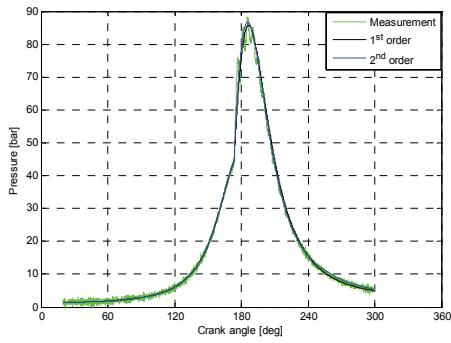


(a) Pressure

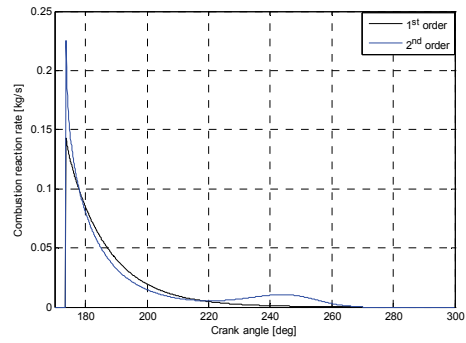


(b) Combustion reaction rate

Figure VII.7 Smoothed pressure and combustion reaction rate (point (B), cylinder 3)



(a) Pressure



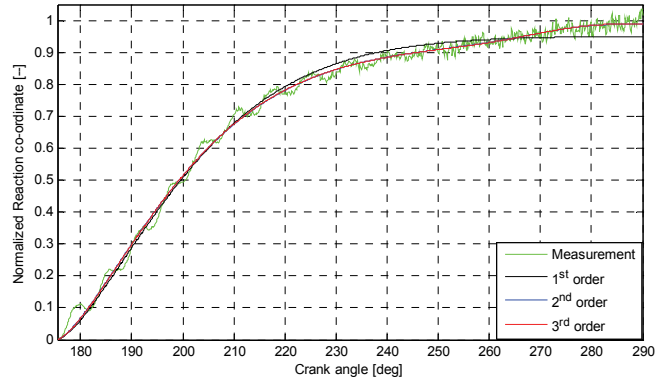
(b) Combustion reaction rate

Figure VII.8 Smoothed pressure and combustion reaction rate (point (C), cylinder 3)

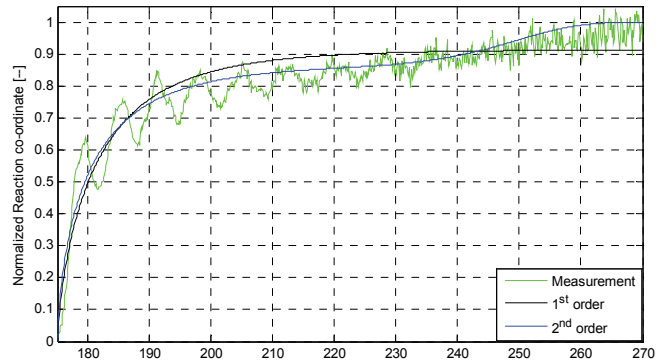
VII.3 Cylinder 4

Table VII.3 Vibe parameters for fit functions (cylinder 4)

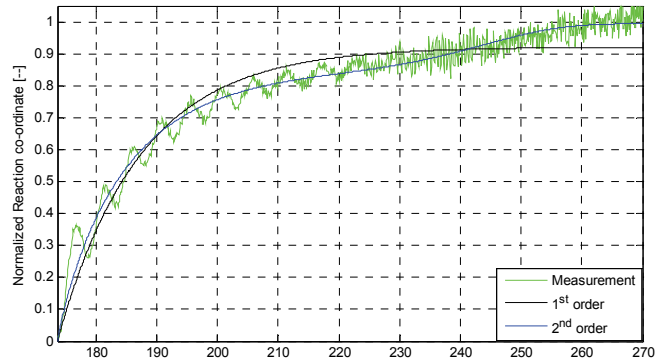
Operating point	Vibe Function	1		2		3	
		b_1	m_1	b_2	m_2	b_3	m_3
(A)	First order	0.953	0.415				
	Second order	0.929	0.381	0.061	9.842		
	Third order	0.971	0.403	0.064	9.831	-0.044	1.035
(B)	First order	0.893	-0.274				
	Second order	0.843	-0.332	0.117	5.482		
(C)	First order	0.917	-0.006				
	Second order	0.833	-0.115	0.139	3.761		



(a) Operating point (A)



(b) Operating point (B)



(c) Operating point (c)

Figure VII.9 Fitting the reaction coordinate with multiple Vibe function (cylinder 4)

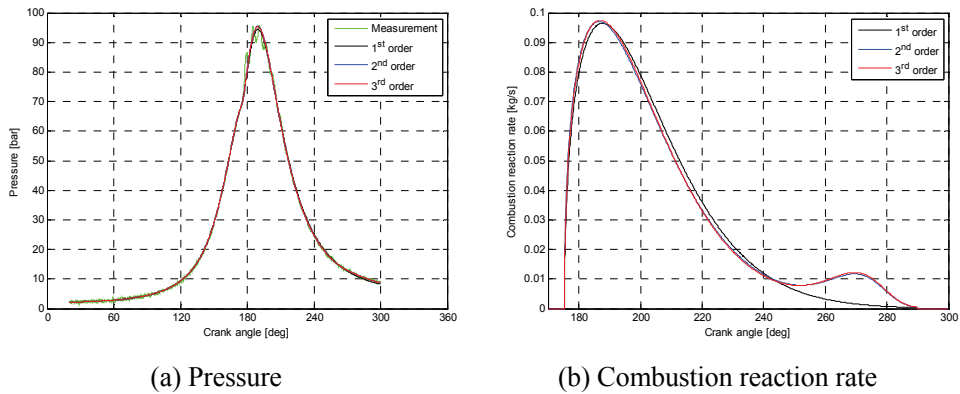


Figure VII.10 Smoothed pressure and combustion reaction rate (point (A), cylinder 4)

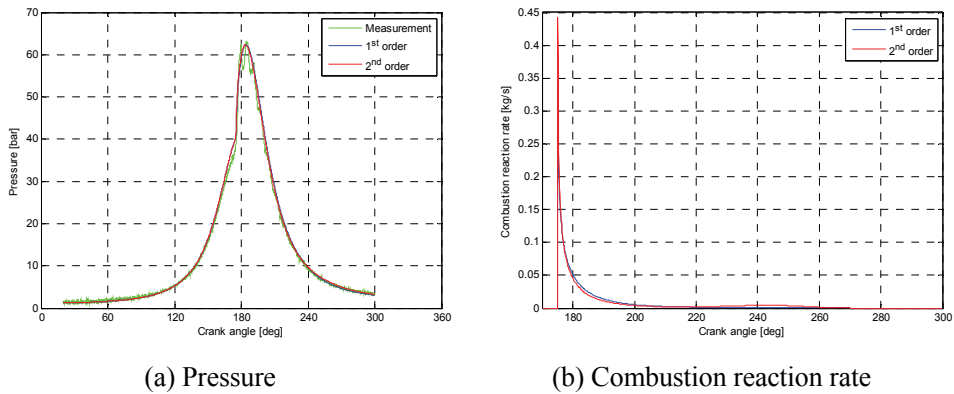


Figure VII.11 Smoothed pressure and combustion reaction rate (point (B), cylinder 4)

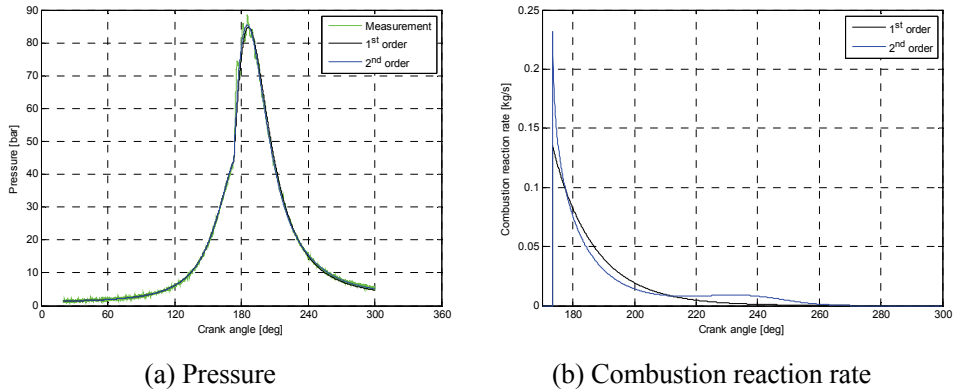
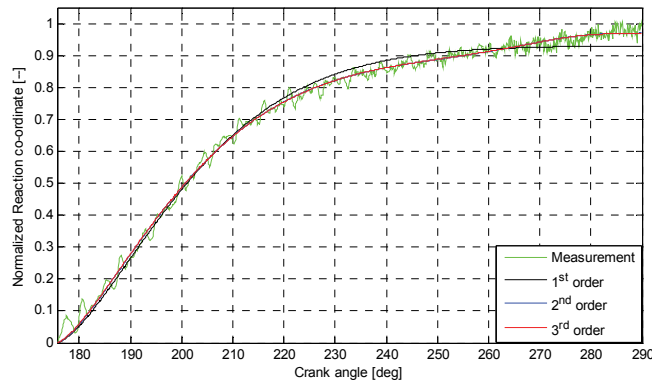


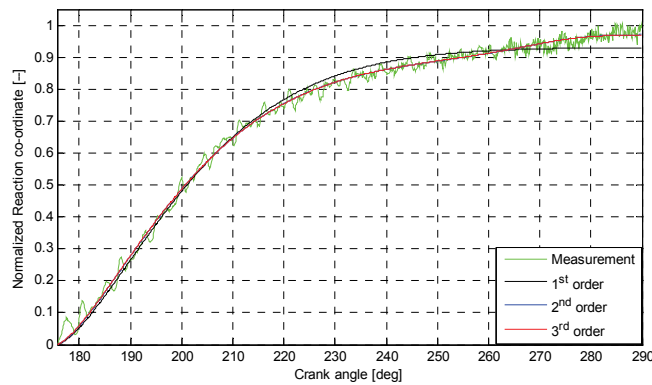
Figure VII.12 Smoothed pressure and combustion reaction rate (point (C), cylinder 4)

VII.4 The measurement of different measured holes

The original hole was located at the low side of the cylinder head which was only possible on cylinder 1. In order to carry out measurements on cylinder 2, 3 and 4, the measuring hole on all cylinders was moved to the top of the cylinder head, resulting in a longer channel. For cylinder 1 pressure measurements using the original hole were carried out in order to judge the differences. Two operating points are analysed: operating point I is 1000 rev/min, 100% power; operating point II is 800 rev/min, 61% power.



(a) Operating point (I)



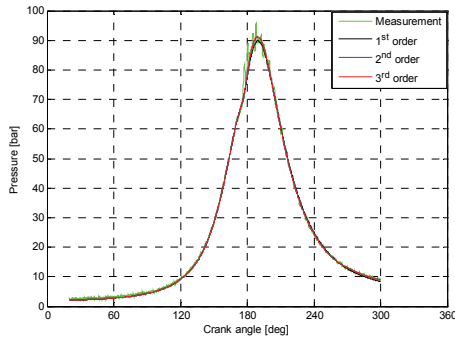
(b) Operating point (II)

Figure VII.13 Fitting the reaction coordinate with multiple Vibe function (cylinder 1, original hole)

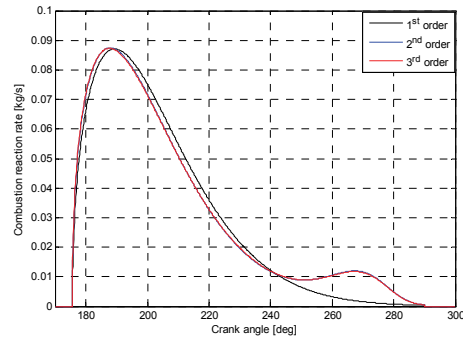
Appendix VII. Smoothed heat release measurement of the other three cylinders and cylinder 1 with original hole position

Table VII.4 Vibe parameters for fit functions (cylinder 1, original hole)

Operating point	Vibe Function	1		2		3	
		b_1	m_1	b_2	m_2	b_3	m_3
(I)	First order	0.931	0.457				
	Second order	0.902	0.413	0.070	8.855		
	Third order	0.861	0.396	0.068	8.842	0.042	0.807
(II)	First order	0.898	0.038				
	Second order	0.823	-0.062	0.123	3.874		
	Third order	0.211	-0.490	0.096	5.783	0.646	0.139

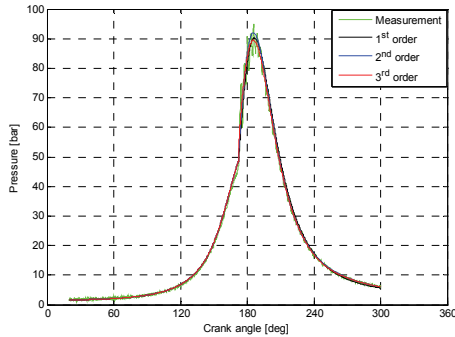


(a) Pressure

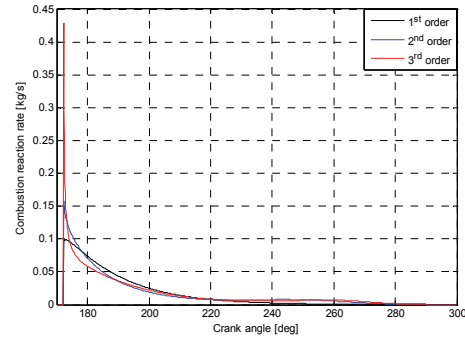


(b) Combustion reaction rate

Figure VII.14 Smoothed pressure and combustion reaction rate (point (I), cylinder 1, original hole)



(a) Pressure



(b) Combustion reaction rate

Figure VII.15 Smoothed pressure and combustion reaction rate (point (II), cylinder 1, original hole)

Appendix VIII. Description of the measurement system (based on manufacturer's data)

VIII.1 Pressure sensor

The pressure sensor used in the measurement system is a KISTLER 7061B, which is a water-cooled precision pressure sensor especially suited for duty in internal combustion engines for high-precision thermodynamic measurement. The technical data of this sensor is shown in Table VIII.1.

Table VIII.1 KISTLER 7061B pressure sensor technical data

Parameters	Unit	Value
Range	bar	0 – 250
Calibrated partial ranges	bar	0 – 50 0 – 5
Overload	bar	300
Sensitivity	pC/bar	≈ -80
Natural frequency	kHz	≈ 45
Linearity all ranges (cooling)	%FSO	≤ ±0.5
Acceleration sensitivity (axial) with cooling	bar/g	<0.01
Operating temperature range Without cooling	°C	-50 – 350
Sensitivity shift cooled 50 ± 35 °C	%	≤ +2
non-cooled 200 ± 150 °C	%	≤ ±0.5
Load-change drift (Drop of zero line after cutting the ignition)	bar/s	≤ ±0.5

Parameters	Unit	Value
Thermo shock at 1500min ⁻¹ , 9bar IMEP		
Δp	bar	< ± 0.1
ΔIMEP	%	< ± 0.5
Δp_{max}	%	< ± 0.5
Insulation torque at 20 °C	TΩ	
Tightening torque	Nm	25
Cooling water pressure	bar	≤ 6
Capacitance (incl. cable)	pF	11 (117)
weight	g	27
Plug, ceramic insulator	Type	10 – 32 UNF

The temperature conditioning unit (KISTLER Type 2621E) has a pressure control system for the cooling circuit, an electronic flow monitoring system and a standardized monitoring/alarm signaling system, and can be operated from a variety of wall power. Features of the unit are:

- For up to 10 sensors
- Cooling circuit with pressure regulation
- Electronic flow monitoring system
- Standardized monitoring/alarm signalling system

Water-cooled cylinder pressure sensors are used for precision measurements where minimum long term drift is required and when a suitable mounting space is available in the engine. Cooling adapters are mainly used for cooling piezoresistive absolute pressure sensors in intake and exhaust manifolds. The temperature conditioning unit should be mounted on the engine test bench and the distributor as close as possible to the engine.

VIII.2 Charge Amplifier

The mains-operated, microprocessor controlled single-channel charge amplifier Type 5011B converts the electrical charge produced by piezoelectric sensors into a proportional voltage signal.

- Large measuring range
- Wide frequency range
- Automatic zero correction
- Adjustable low-pass filter and time constant
- Various options and versions provide optimum adaptation to the measuring problem
- Conforming to CE

This amplifier serves mainly to measure mechanical quantities, e.g. pressure, force or acceleration. The instrument dimensions are DIN standardized and it can be supplied in a desktop or rack mount case.

The principle measurement without calculation:

- Set sensor sensitivity
- Select display scale
- Sensor sensitivity and scale are displayed
- Set the signal output of the data acquisition unit (recorder, oscilloscope...), for example to 1 V/unit (1 V/cm)
- The display appears directly in mechanical units according to the display scale selected

Table VIII.2 KISTLER 5011B charge amplifier technical data

<i>Basic unit</i>		
Parameters	Unit	Value
Measuring range for 10 V FS	pC	±10 – ±999 000
Sensor sensitivity [T]. (M.U. = Mechanical units)	pC/M.U	±10 – ±9 990
Scale [S]	M.U./V	0.001 –9,990,000
Output voltage	V	±10
Output current (short-circuit protected)	mA	±5

Appendix VIII. Description of the measurement system based on manufacturer's data

Parameters	Unit	Value
Output impedance	Ω	10
Frequency range (-3dB, Filter 'OFF')	kHz	$\approx 0 - 200$
Low-pass filter upper cutoff frequency -3dB Butterworth, 2 pin 8 stages (1, 3, 10 ...)	kHz (%)	0.01 - 30 (± 10)
Time constant [TC] (high pass filter)		
Long	s	>1 000 - 100 000
Medium ($T = R_g \cdot C_g$)	s	1 - 10 000
Short ($T = R_g \cdot C_g$) 0,01 ... 100	s	0.01 - 100
Error		
< ± 100 pC FS (max./typ.)	%	< ± 3 / < ± 2
$\geq \pm 100$ pC FS (max./typ.)	%	< ± 1 / < ± 0.5
Linearity	% FS	< ± 0.05
Noise	mV_{rms}	< 0.5 (< 1.5)
9.99 pC/V (1 pC/V)	mV_{pp}	< 4 (< 8)
Loss due to cable capacitance	pC_{rms}/pF	< $2 \cdot 10^{-5}$
Drift at 25 °C	pC/s	< ± 0.07

General Data

Parameters	Unit	Value
Operating temperature range	$^{\circ}C$	0 - 50
Connections		
Measuring input/signal output	--	BNC negative
Remote control	--	Connector 6 pin
(Operate, Overload, ...)	--	DIN 45322
Power plug	--	IEC 320 C 14
Conformity to EC Directive		
Safety		EN 61010-1
EMC Interference Emission		EN 50081-1/EN 50081-2
EMC Interference Immunity		EN 50082-1/EN 50082-2
Power, switchable	VAC (%)	230/115 (-22/+15)
(Protection class I)	Hz (VA)	48 - 62 (20)
Voltage between protection and measuring ground	V_{rms}	< 50

Parameters	Unit	Value
Dimensions		
with desktop case Type 5747A1	mm	94*141*195
for rack mounting	mm	71.12*128.7*169
Front panel according to	HE (mm)	3 (128.7)
DIN 41494 (Part 5)	TE (mm)	14 (71.12)
Weight (incl. IEEE-488 or RS-232C)	kg	≈ 2

VIII.3 Precision balance talent TE6101

The fuel flow is determined by measuring the time required for a certain amount of fuel to be consumed. The amount of fuel was such that the time was something like 60 – 150 seconds. The time was measured by a chronometer and the amount of fuel was weighed by a precision balance.

The Precision balance is from ‘Sartorius mechatronics’. The standard features are:

- High-grade stainless steel weighing pan
- Large, high-contrast LCD
- High level of operating convenience, thanks to keys with positive click action and 2 tare keys
- Built-in application programs: counting, weighing in %, net-total formulation; averaging; toggling between 2 units
- Battery- operable (eight 1.5-V Mignon AA batteries) or runs on line current (AC adapter included as part of the equipment supplied)
- Bidirectional RS-232C data interface port
- ISO/GLP-compliant logging capability for calibration, adjustment and weighing data in conjunction with the optional YDP03-0CE data printer
- Four digital filter levels for adaptation of the balance to the conditions at the place of use
- Mechanical protection of the weighing system against side impact and overloading
- Rugged construction; compact size; reliable weighing technology

Table VIII.3 SARTORIUS Precision balance Talent TE6101

Readability	0.1 g
Weighing capacity	6,100 g
Response time (avg.)	2 s
Housing (W*D*H)	200*270*70 mm
Reproducibility	$\leq \pm 0.1$ g
Linearity	$\leq \pm 0.2$ g
<hr/>	
Key accessories	Order no.
Data printer with date, time and statistics functions	YDP03-0CE
Data transfer software SartoConnect with RS-232C standard cable (1.5 m);	YSC01L
Test and calibration weight: 5,000 g, accuracy class F2	YCW6548-00
External rechargeable battery pack	YRB08Z
Carrying case	YDB01TE
Dust cover	6960TE03

VIII.4 Measured parameters in the test bed

Table VIII.4 Measured parameters in the test bed

	Parameter	Unit
1	Atmosphere Pressure	mbar
2	Fuel Leakage	--
3	Fuel Control Rod	--
4	Fuel Vessel	--
5	CO Emission	--
6	CO2 Emission	--
7	Cylinder Cool Water Pressure	bar
8	CxHy Emission	--
9	Pressure after Turbine in Exhaust Pipe Point 1	bar

	Parameter	Unit
10	Sea Water Pressure	bar
11	Fuel Pressure before Engine	bar
12	Central Cool Water Pressure	bar
13	Cylinder 1 Pressure	bar
14	Cylinder 2 Pressure	bar
15	Cylinder 3 Pressure	bar
16	Cylinder 4 Pressure	bar
17	Inlet Receiver Pressure	bar
18	Nozzle Pressure	bar
19	Water Brake Pressure	bar
20	Pressure before Turbine in Exhaust Pipe Above	bar
21	Pressure before Turbine in Exhaust Pipe Beneath	bar
22	Total Efficiency	%
23	Fuel Flow	kg/s
24	Central Cool Water Flow for both Cylinder Water Cooler and Lubricating Oil	kg/s
25	Central Cool Water Flow for Inter Cooler	kg/s
26	Cylinder Cool Water Flow	kg/s
27	Lubricating Oil Flow	kg/s
28	Average Toque	N·m
29	Average Temperature for Exhaust	N·m
30	Load	--
31	High Level of Fuel Weighter	--
32	High level of Leakage Tank	--
33	Kisler Cooler	--
34	Toque	N·m

Appendix VIII. Description of the measurement system based on manufacturer's data

	Parameter	Unit
35	Torque Set Point	--
36	Fuel Leakage	--
37	Air consumption	kg/s
38	NOx Emission	--
39	DO Tank Level	--
40	HFO Tank Level	--
41	O2 Emission	--
42	Governor	--
43	Relative Humidity	%
44	SFC	
45	Lubricating Oil Pressure	bar
46	Fly Wheel Signal	--
47	Inlet Air Temperature	°C
48	Temperature after Turbine in Exhaust Pipe	°C
49	Fuel Temperature Before Engine	°C
50	Central Cool Water Temperature after Cylinder Water Cooler	°C
51	Central Cool Water Temperature after Inter Cooler	°C
52	Central Cool Water Temperature after Lubricating Oil Cooler	°C
53	Central Cool Water Temperature Before Cylinder Cool Water Cooler	°C
54	Central Cool Water Temperature before Inter Cooler	°C
55	Central Cool Water Temperature before Lubricating Oil Cooler	°C
56	Cylinder Cool Water Temperature after Cooler	°C
57	Cylinder Cool Water Temperature after Engine	°C

	Parameter	Unit
58	Cylinder Cool Water Temperature before Cooler	°C
59	Cylinder Cool Water Temperature before Engine	°C
60	Inlet Receiver Temperature	°C
61	Air Temperature After Compressor	°C
62	Temperature after Turbine	°C
63	Sea Water Temperature to Bolnes	°C
64	Sea Water Temperature to MAN	°C
65	Lubricating Oil Temperature after Cooler	°C
66	Lubricating Oil Temperature after Engine	°C
67	Lubricating Oil Temperature before Cooler	°C
68	Lubricating Oil Temperature before Engine	°C
69	Exhaust Temperature for Cylinder 1	°C
70	Exhaust Temperature for Cylinder 2	°C
71	Exhaust Temperature for Cylinder 3	°C
72	Exhaust Temperature for Cylinder 4	°C
73	Temperature before Turbine in Exhaust Pipe Above	°C
74	Temperature before Turbine in Exhaust Pipe Beneath	°C
75	Time	s
76	Fuel Weighter Time	s
77	Turbocharger Speed	*1000 rpm
78	Engine Speed	rpm
79	Heat Input from Fuel	J
80	Power	kW
81	Water Brake Control	%

Nomenclature

Nomenclature

Abbreviation

TU Delft	Delft University of Technology
NLDA	Netherlands Defence Academy
MVFP	Mean Value First Principle
DE	Diesel Engine
CFD	Computational Fluid Dynamics
CRR	Combustion Reaction Rate
IC	Inlet valve Closed
EO	Exhaust valve Open
SOI	start of injection
SOC	start of combustion
EOC	end of combustion
TDC	Top Dead Centre
BDC	Bottom Dead Centre
RCO	Reaction coordinate
CRR	Combustion Reaction Rate
NAHRR	Net Apparent Heat Release Rate
GAHRR	Gross Apparent Heat Release Rate
EO	exhaust open condition

Symbol

A	area	m^2
A_b	bore	m^2
D_b	bore	m^2
E_f	energy of flow	J
\dot{E}_f	energy of fuel flow	W

Nomenclature

H	enthalpy	J
\dot{H}	enthalpy flow	J/s
L_s	stroke	m
P_i	indicated power	W
Q_{comb}	combustion heat	J
\dot{Q}_{comb}	combustion heat flow	W
\dot{Q}_{loss}	heat loss flow	W
Q_f	heat from fuel	J
Q_i	heat input	J
Q_{in}	net heat input in Seiliger process	J
S	entropy	J
T	temperature	K
U	internal energy	J
\dot{U}	internal energy flow	J/s
V	volume	m ³
V_s	stroke volume	m ³
X	normalized reaction rate	[--]
Z	normalized rate of combustion	[--]
a	Vibe parameter linked to combustion efficiency	[--]
a	Seiliger parameter	[--]
b	Seiliger parameter	[--]
b_k	Weight factors in multiple Vibe function (k=1,2,3,...)	[--]
c	Seiliger parameter	[--]
c_m	mean piston speed	m/s
c_p	specific heat at constant pressure	J/kg/K
c_v	specific heat at constant volume	J/kg/K
e_f	specific energy of flow	J/kg
h	specific enthalpy	J/kg
k	Reaction speed constant	[--]
m	mass	kg

m_k	Form factors in multiple Vibe function ($k=1,2,3,\dots$)	[--]
\dot{m}	mass flow	kg/s
n_{comp}	compression exponent	[--]
n_{exp}	expansion exponent	[--]
n_{eng}	engine speed	rev/s
m_{fr}	fuel consumption ratio	[--]
p	pressure	Pa
r_c	effective compression volume ratio	[--]
r_e	effective expansion volume ratio	[--]
t	time	s
t_{comb}	duration of combustion	s
u	specific internal energy	J/kg
u_{comb}	heat of combustion	J
x	air mass fraction	[--]
α	crank angle	[degree]
α_{g-w}	heat loss to the walls coefficient	W/m ² /K
η_{comb}	Combustion efficiency	[--]
η_{comp}	compression factor	[--]
η_{exp}	expansion factor	[--]
η_e	effective efficiency	[--]
η_{hl}	heat loss efficiency	[--]
η_i	indicated efficiency	[--]
η_m	mechanical efficiency	[--]
η_{td}	thermodynamic efficiency	[--]
ε	geometric compression ratio	[--]
ξ	fuel burn rate (or combustion reaction rate)	kg/s
λ	air excess ratio	[--]
λ_{CR}	radius to length ratio	[--]
μ	multiplication factor	[--]
σ	air/fuel ratio	[--]
ρ	density	kg/m ³
τ	Normalized time t/t_{comb}	[--]

Subscript

0	no fuel injected condition
1	trapped condition
f	fuel
inj	injection
max	maximum
ref	reference
sg	stoichiometric gas

Superscript

in	into the system
out	out of the system
comb	combustion
ref	reference

Reference

Reference

- [Arregle, 2003] J. Arregle, J. J. Lopez, J. M. Garcia and C. Fenollosa.
Development of a zero-dimensional diesel combustion
model. Part 1 & Part 2.
Applied Thermal Engineering, 23 (11), 1301-1331, 2003.
- [Baan, 1998] P. Baan.
Doorontwikkeling Modulair Simulatiemodel van een
dieselmotor (Further development of a Modular
Simulation model of a Diesel Engine) (in Dutch).
Report OvS 98/25, Delft University of Technology;
Internal report, 1998.
- [Baehr, 2006] H.D. Baehr.
Thermodynamik, Springer Verlag, Berlin, Heidelberg,
New York, 7. auflage, 1989.
ISBN 3-540-50773-6.
- [Baehr, 2006] H. D. Baehr and S. Kabelka
Thermodynamik (in German).
Springer, Germany, 2006.
- [Borman, 1998] G.L Borman, K.W. Ragland.
Combustion Engineering
McGraw-Hill, 1998
ISBN 0-07-006567-5
- [Benkenida, 2004] A. Benkenida and C. Angelberger.
Toward a three-dimensional CFD model for HCCI
combustion in diesel engines.
Combustion Science and Technology, 176 (5), 667- 683,
2004.

- [Betz, 1986] Alois Betz and Gerhard Woschni.
Energy conversion rate and rate of heat release of turbocharged diesel engines under transient conditions (in German).
MTZ, 1986, 47(7/8), 263–267, 1986.
- [Boëtius,1998] D. Boëtius, P. Baan.
Modulair simulatiemodel van een dieselmotor, Versie 1.0 (Modular simulation model of a diesel engine, Version 1.0) (in Dutch).
Report OvS 98/09, Delft University of Technology, Internal report, 1998
- [Boëtius, 1999] D. Boëtius.
Modelleren van een langzaamlopende dieselmotor (Modelling of a Slow Speed Diesel Engine) (in Dutch).
Report OvS 90/05, Delft University of Technology; Internal report, 1999.
- [Boot, 1991] Ph. Boot, J. Klein Woud and B.J. ter. Riet
A Mathematical Model of a Turbocharged 4 stroke diesel engine, suitable for simulation of the dynamic behaviour of complete drive systems.
Fourth International Marine Systems Design Conference. Kobe, Japan, 1991.
- [Brown, 1996] Benjamin Robert Brown.
Combustion data acquisition and analysis.
Master thesis, Loughborough University, UK, 1996.
- [BSI, 1982] BS MA 100 – 82.
British Standards Institution Specification for Petroleum Fuels for Marine Oil Engines and Boilers.
BSI, 1982

- [Chapra, 2006] S. C. Chapra and R. P. Canale.
Numerical methods for engineering, 5th edition.
McGraw-Hill, USA, 2006.
- [Chen, 1965] S.K. Chen and P. Flynn.
Development of a compression ignition research engine.
SAE Paper no. 650733, 1965.
- [de Vos, 2008] P. de Vos.
Dynamic modelling of a diesel-fuelled PEMFC system
for electric power generation.
Master Thesis, Delft University of Technology, The
Netherlands, 2008.
- [Dijkstra, 2003a] C. Dijkstra.
Modelling the gas exchange process in a low speed
two-stroke diesel engine.
Master thesis, Delft University of Technology, The
Netherlands, 2003.
- [Dijkstra, 2003b] C. Dijkstra.
Mean value diesel engine model for simulating the
off-design performance of 2- and 4-stroke diesel engines.
Master thesis, Delft University of Technology, The
Netherlands, 2003.
- [Ding, 2009] Y. Ding, D. Stapersma and H. T. Grimmelius.
Cylinder process simulation with heat release analysis in
diesel engine.
In Proceedings of the APPEEC2009, Wuhan, China, 2009.
- [Ding, 2010] Y. Ding, D. Stapersma, H. Knoll and H. T. Grimmelius.
Characterising heat release in a diesel engine: A
comparison between Seiliger process and Vibe model.
In Proceedings of the 28th CIMAC World Congress,
Bergen, Norway, 2011.

- [Ding, 2011b] Y. Ding, D. Stapersma and H. T. Grimmelius.
Simulation techniques for heat release calculation of diesel engines.
In Proceedings of the APPEEC2011, Wuhan, China, 2011.
- [Ding, 2011a] Y. Ding, D. Stapersma, H. Knoll and H. T. Grimmelius.
A new method to smooth the in-cylinder pressure signal for combustion analysis in diesel engines.
Proc. IMechE Part A: Journal of Power and Energy, 225 (3), 309 – 318, DOI: 10.1177/2041296710394298.
- [Grimmelius,1999a] H.T. Grimmelius, D. Boëtius, P. Baan.
The influence of sequential turbocharging control on propulsion behavior.
12th Ship Control Systems Symposium, Proceedings Volume II, The Hague, The Netherlands, 1999
- [Grimmelius, 1999b] H.T. Grimmelius, D. Boëtius and H.N. van den Oever.
The application of mean value first principle modelling in engine room simulators.
4th International Conference on Engine Room Simulators (ICERS4); San Francisco, 1999.
- [Grimmelius, 2000a] H.T. Grimmelius, D. Boëtius.
Advanced applications of simulation models in Marine Engineering.
INEC 2000, Conference Proceedings Part I, pp. 173 – 181, Hamburg, 2000.
- [Grimmelius , 2000b] H.T. Grimmelius, D. Stapersma.
Control optimisation and load prediction for marine diesel engines using a mean value simulation model.
ENSUS 2000 Conference Proceedings, pp. 212 - 229, Newcastle, 2000.

- [Grimmelius, 2007] H.T. Grimmelius, E. Mesbahi, P.J.M. Schulten, D. Stapersma.
The use of Diesel engine simulation models in ship propulsion plant design and operation.
In Proceedings of the 25th CIMAC Conference, Vienna, 2007.
- [He, 1988] Xueliang He and Xiaoping Xu.
The determination and comparison of start and end of combustion of diesel engines (in Chinese).
Introducing Journal of China Ordnance, issue 2, 1988.
- [He, 1990] X. L. He and S. S. Li.
Combustion in the internal combustion engine (in Chinese), pp.97.
China Machine Press, China, 1990.
- [Heywood, 1988] John B. Heywood.
Internal combustion engine fundamentals. pp491-566.
McGraw-Hill, USA, 1988.
- [Hiroyasu, 1983] Hiroyuki HIROYASU, Toshikazu KADOTA and Masataka ARAI
Development and Use of a Spray Combustion Modeling to Predict Diesel Engine Efficiency and Pollutant Emission (Part 1 –Part 3)
Bulletin of JSME 26 (214), 569-591, 1983.
- [Hua, 1984] J. Hua and Z. Wang.
Calculation and application of combustion heat release rate in high speed diesel engine (in Chinese).
Trans. CSICE, issue 2, 103–123, 1984.
- [Klein woud, 2002] J. Klein Woud and D. Stapersma.
Design of propulsion and electric power generation system.
IMarEST, London, UK, 2002.

- [Knobbe, 2001] E. M. Knobbe and D. Stapersma.
Some new ideas for performing heat release analysis.
In Proceedings of the 23rd CIMAC World Congress,
Hamburg, Germany, 2001.
- [Kom, 2004a] M. Kom.
Vergelijking van het Seiliger model met het dubbel Vibe
model.
Report DMS 04/09, Delft University of Technology;
Internal report, 2004.
- [Kom, 2004b] M. Kom.
Nieuwe fit voor de Seiliger parameters.
Report DMS 04/08, Delft University of Technology;
Internal report, 2004.
- [Kraaij, 2002] G.J. Kraaij.
DESIRE; Technical specification for full size system.
Energieonderzoek Centrum Nederland, Petten, The
Netherlands, 2002.
- [Lapuerta, 2000] M. Lapuerta, O. Armas and V. Bermúdez.
Sensitivity of diesel engine thermodynamic cycle
calculation to measurement errors and estimated
parameters. *Applied Thermal Engineering*, 20(9), 843–
861, 2000.
- [MATLAB, 2008] MATLAB.
Curve fitting Toolbox™ Users guide, pp. 2–10, pp. 2–16,
pp. 4–4, pp. 4–9.
MathWorks Inc, USA, 2008.
- [Merker, 2006] G. P. Merker, C. Schwarz, G. Stiesch and F. Otto.
Simulating combustion
Springer, Germany, 2006.

- [Millington, 1968] B. W. Millington and E. R. Hartles.
Frictional Losses in Diesel Engines.
SAE Paper no.680590, 1968.
- [Moran, 2003] M. J. Moran and H. N. Shapiro.
Fundamental of engineering thermodynamics.
Wiley Higher Education, 6th edition, USA, 2007.
- [Rietz, 1995] R. D. Reitz and C. J. Rutland.
Development and testing of diesel engine CFD models.
Progress in Energy and Combustion Science, 21(2), 173
- 196, 1995.
- [Sahin, 2008] Zehra Sahin and Orhan Durguna.
Multi-zone combustion modeling for the prediction of
diesel engine cycles and engine performance parameters.
Applied Thermal Engineering, 28 (17-18), 2245 – 2256,
2008.
- [Seiliger, 1922] M. Seiliger.
Graphische thermodynamik und berechnen der
verbrennungs – maschinen und turbinen (in German).
Julius Springer, Berlin, Germany, 1922.
- [Schulten, 1998] P.J.M. Schulten.
Quasi stationair model voor het cilinderproces van een
diesel motor (Quasi-stationary model for the cylinder
proces of a Diesel Engine) (in Dutch).
Report OvS 98/06, Delft University of Technology,
Internal report, 1998.
- [Schulten, 2003] P. J. M. Schulten and D. Stapersma.
Mean value modelling of the gas exchange of a 4-stroke
diesel engine for use in powertrain applications.
SAE paper no. 2003-01-0219, 2003.

- [Schulten, 2005] P. J. M. Schulten.
The interaction between diesel engines, ship and propeller during a maneuvering.
PhD thesis, TU Delft, The Netherlands, 2005.
- [Stapersma, 1997] D. Stapersma.
A general model for off-design performance of a single stage turbomachine.
Report nr: KIM-PFS-97-111, issue A.
Royal Netherlands Naval College, The Netherlands, 1997.
- [Stapersma, 2001] D. Stapersma and H. T. Grimmelius.
Concept exploration applied to diesel engines.
In Proceedings of the 23rd CIMAC World Congress, Hamburg, Germany, 2001.
- [Stapersma, 2002a] D. Stapersma
Diesel engines, Volume 1: Performance analysis, 2nd print.
Royal Netherlands Naval College, The Netherlands, 2002.
- [Stapersma, 2002b] D. Stapersma
Diesel engines, Volume 2: Turbocharging, 2nd print.
Royal Netherlands Naval College, The Netherlands, 2002.
- [Stapersma, 2007] D. Stapersma
Diesel engines, Volume 5: thermodynamic principles (I),
Royal Netherlands Naval College, The Netherlands, 2007.
- [Stapersma, 2009c] D. Stapersma
Diesel engines, Volume 3: Combustion, 5th print,
636-660.
Royal Netherlands Naval College, The Netherlands, 2009.

- [Stapersma, 2009d] D. Stapersma
Diesel engines, Volume 4: Emissions and heat transfer,
5th print, 822-831.
Royal Netherlands Naval College, The Netherlands, 2009.
- [Stapersma, 2009f] D. Stapersma
Diesel engines, Volume 6: thermodynamic principles (II),
4th print, 163-195.
Royal Netherlands Naval College, The Netherlands, 2008.
- [Stapersma, 2010a] D. Stapersma
Diesel engines, Volume 1: Performance analysis, 8th print,
29-36.
Royal Netherlands Naval College, The Netherlands, 2009.
- [Stiesch, 2003] G. Stiesch.
Modeling engine spray and combustion processes.
Springer, Germany, 2003.
- [Stodola, 1922] A. Stodola
Dampf- und Gasturbinen
5. Aufl, Berlin, Springer 1922.
Reprint: Düsseldorf, VDI Verlag 1986.
- [Struckmeier, 2010] Daniel Struckmeier, Daisuke Tsuru, Hiroshi Tajima.
New application and modeling of low ignitability fuel for
marine engines.
In Proceedings of the 28th CIMAC World Congress,
Bergen, Norway, 2011.
- [Tauzia, 2006] Xavier Tauzia, Alain Maiboom, Pascal Chesse, Nicolas
Thouvenel.
A new phenomenological heat release model for
thermodynamical simulation of modern turbocharged
heavy duty diesel engines.
Applied Thermal Engineering, 26 (16), 1851–1857,
2006.

- [Van Oosten, 2004] B.T.W. Van Oosten.
Dynamic modeling of a fuel cell with reformer.
Graduation report, Delft University of Technology, The Netherlands, 2004.
- [Vibe, 1970] I. Vibe.
Brennverlauf und Kreisprozeß von
Verbrennungsmotoren (in German).
VEB Verlag Technik, Berlin, Germany, 1970
- [Watson, 1980] N. Watson and A.D. Pilley.
A combustion correlation for diesel engine simulation.
SAE paper no. 800029, 1980.
- [Woschni, 1967] G. Woschni.
A universally applicable equation for the instantaneous
heat transfer coefficient in the internal combustion engine.
SAE paper no. 670931, 1967.
- [Yaws, 1986] Carl L. Yaws.
Handbook of thermodynamic diagrams, Volume 3.
Gulf Publication Company, Houston, Texas, USA, 1986.
- [Zeise, 1954] H. Zeise.
Thermodynamische Tafels Band III/I.
Hüzel Verlag, Leipzig 1954.
- [Zhan, 2004] Y. Zhan, B. Wan, X. Wang and Y Hu.
A simulation model for the main engine of the modern
container ship.
Proceedings of the Third International Conference on
machine learning and cybernetics, Shanghai, China,
2004.
- [Zinner, 1980] K. Zinner.
Aufladung von Verbrennungsmotoren (in German).
Springer, Germany, 1980.

Summary

Summary

Characterising combustion of diesel engines is not only necessary when researching the instantaneous combustion phenomena but also when investigating the change of the combustion process under variable engine operating conditions. An effective way to achieve this goal is to parameterize the combustion process using a finite combustion stage cylinder process model and then the parameters can be modeled to give a global description of diesel engine combustion.

The main objective of this thesis is getting information how to calculate (simulate) the parameters defining the finite stage cylinder process model using both theoretical and experimental methods. The latter is essential but also complicated.

Heat release analysis is an important tool in the research of the combustion process in diesel engines. An 'in-cylinder process model' is described firstly which is the basis of the 'heat release calculation' model. Moreover it can be used independently to simulate the in-cylinder process to investigate the main features of the cylinder process of the engine. Then the reversed and anti-causal 'heat release calculation model' is presented together with the results for three engine operating points. Then a new smoothing method based on multiple Vibe functions is presented in order to acquire a smoother and more reliable pressure signal.

In order to fit the measured engine cycle to the Seiliger process and to calculate the parameters which define the finite stage cylinder process model, the theory of a basic and advanced Seiliger process is presented. Then a systematic investigation of the Seiliger parameters and the effects on in-cylinder process is carried out. The more important investigation is how to fit the measured engine cycle to the Seiliger process. Several combinations of equivalence criteria are used to make this transformation and set up the applicable systems of equations for the Seiliger parameters. A Newton-Raphson iteration method then is applied to find the solutions of these systems of equations.

Three representative operating points (nominal point, nominal speed and 25% power, low speed and 50% power) are applied in the fitting of the real engine cycle with a Seiliger process firstly. The differences of the Seiliger parameters coming out of

several fit procedures for the three operating points were compared and their global behaviour as function of power and speed could be seen. Finally the behaviour of the Seiliger parameters over the full operational range of the MAN 4L20/27 diesel engine is shown based on one extensive series of measurements. Also the error in the equivalence criteria that were not used was presented for the full range of operating conditions in order to decide on the most preferable fit version to use as a basis for modelling and characterizing the combustion.

The analysing approach in this thesis has been verified on an ancient engine, i.e. MAN 4L20/27. However it can be used for characterising combustion in modern engines with late injection timing, high pressure injection equipment, and even common rail since the simulation models and Seiliger model are based on basic principles of physics.

Samenvatting

Het karakteriseren van de verbranding in dieselmotoren is niet alleen noodzakelijk voor het onderzoek van het verloop van de verbranding op enig moment, maar ook bij het onderzoek naar de verandering van het verbrandingsproces in de motor bij andere bedrijfsomstandigheden dan nominaal. Een effectieve manier om dit doel te bereiken is om het verbrandingsproces te parametriseren met behulp van een model van het cilinder proces met eindige verbrandingsfasen waarna de parameters kunnen worden gemodelleerd om te komen tot een globale beschrijving van het verbrandingsproces in de dieselmotor.

De belangrijkste doelstelling van dit proefschrift is om informatie te verkrijgen hoe de parameters, die het cilinder process model met een eindig aantal verbrandingsfasen definiëren, berekend (en dus gesimuleerd) kunnen worden, gebruikmakend van zowel theoretische als experimentele methoden. Die laatste zijn essentieel, maar ook lastig.

De analyse van de warmte vrijgave is een belangrijk hulpmiddel in het onderzoek van het verbrandingsproces in dieselmotoren. In het proefschrift wordt eerst een 'gesloten cilinder proces model' beschreven dat de basis is van het model van de "warmte vrijgave berekening". Tevens kan dit model onafhankelijk worden gebruikt om het gesloten cilinder proces te simuleren en de belangrijkste kenmerken van het cilinder proces van de motor te onderzoeken. Vervolgens is het omgekeerde (in feite anti-causale) 'warmte vrijgave rekenmodel' gepresenteerd samen met de resultaten voor drie motorbedrijfspunten. Ten slotte is een nieuwe smoothing methode op basis van meerdere Vibe functies ontwikkeld met als doel tot een gelijkmatiger en meer betrouwbaar druksignaal te komen.

Om de gemeten motorcyclus af te beelden op het Seiliger proces en om de parameters, die dat cilinder proces-model met een eindig aantal verbrandingsfasen definiëren, te berekenen, is een theorie voor een basaal en een geavanceerd Seiliger proces ontwikkeld. Vervolgens is een systematisch onderzoek van de Seiliger parameters en de effecten op het in-cilinder proces uitgevoerd. Het belangrijkste onderzoek is hoe de gemeten motorcyclus moet worden afgebeeld op het Seiliger proces. Meerdere combinaties van equivalentie criteria worden gebruikt om deze transformatie uit te

voeren en de van toepassing zijnde systemen van vergelijkingen voor de Seiliger parameters op te stellen. Een Newton-Raphson iteratie methode wordt dan toegepast om de oplossingen van deze stelsels van vergelijkingen te vinden.

Drie representatieve bedrijfspunten (een nominaal punt, een punt bij nominaal toerental en 25% vermogen, een punt bij lage toerental en 50% vermogen) worden gebruikt om de echte motorcyclus tot een Seiliger proces te transformeren. De verschillen van de Seiliger parameters voor verschillende combinaties van equivalentie criteria zijn voor de drie werkpunten met elkaar vergeleken en hun globale gedrag als functie van de belasting en toerental kan worden bestudeerd. Uiteindelijk is het gedrag van de Seiliger parameters over het volledige werkgebied van de MAN 4L20/27 dieselmotor onderzocht op basis van een uitgebreide reeks metingen. Ook de fout in de equivalentie criteria die niet werden gebruikt, werd voor alle operationele omstandigheden gepresenteerd om te kiezen wat de meest te prefereren fit-versie is als basis voor het modelleren en karakteriseren van de verbranding.

De analyse methode, ontwikkeld in dit proefschrift, is geverifieerd op een gedateerde motor, d.w.z. een MAN 4L20/27. Niettemin kan de methode worden gebruikt voor het karakteriseren van de verbranding in moderne motoren met een later inspuitmoment, hoge druk injectie-apparatuur, en zelfs common rail, omdat de simulatie modellen en het Seiliger model zijn gebaseerd op de basisprincipes van de fysica.

摘 要

柴油机燃烧的特征化分析不仅研究柴油机瞬时燃烧现象,而且研究燃烧过程随工况变化而变化的情况。达到这个目标行之有效的的方法是,应用有限燃烧阶段的缸内过程模型参数化燃烧过程,从而应用参数的全局模型表述柴油机的燃烧过程。

本论文的主要目标是如何应用理论和试验的方法计算(仿真)缸内有限燃烧阶段模型中的参数,试验方法是重要的同时也是复杂的。

柴油机燃烧放热率的分析是研究燃烧过程的一个比较重要工具。本论文首先描述了“放热率计算模型”的基础,即“缸内过程模型”。“缸内过程模型”可以独立应用于模拟柴油机缸内过程,进而研究柴油机缸内过程的主要特征。接着本论文陈述了其反因果的逆模型“放热率计算模型”,同时计算并得到了三个运行工况点的结果。然后,论文阐述了基于多 Vibe 方程的平滑方法,从而得到更平滑且可靠性高的压力曲线。

为了应用 Seiliger 过程拟合实际测量的柴油机工作循环,从而计算出定义有限阶段的缸内过程的参数,本文阐述了基本 Seiliger 过程和高级 Seiliger 过程的基本理论。接着本文系统化研究了 Seiliger 参数以及这些参数对柴油机缸内过程的影响。论文较重要的部分是如何应用 Seiliger 模型拟合实际测量的柴油机的工作循环。几种等价标准的组合用于转化和建立方程组来求解 Seiliger 参数。同时应用 Newton-Raphson 迭代法来求解方程组。

本文首先应用了具有代表性的三个运行工况点(标准工况,额定转速和 25%功率,低转速和 50%功率)进行柴油机实际测量的工作过程与 Seiliger 过程的拟合。对比了不同的拟合方程得出的相应的 Seiliger 参数,并得到了这些参数随功率和转速变化的全局特性。最后,本论文依据一个系列的测量,列出了 Seiliger 参数随 MAN 4L20/27 柴油机整个运行范围的特性。同时分析了未使用的等价标准在相应方程组中的误差,进而决定了较好的拟合组合用于建模和特征化柴油机燃烧的基础。

本论文应用了一台比较古老的柴油机,即 MAN20/27,验证了本文所用到的分析方法。然而,由于本文所用到的仿真模型和 Seiliger 模型都是基于基本物理理论的模型。所以这种方法还可以应用于特征化分析现代柴油机,比如说,应用延迟喷油正时,高压喷油装置,共轨燃油系统等先进技术的柴油机。

Acknowledgement

The engine measurements used in this thesis were prepared and carried out at the ‘Medemblik’ laboratory of the Netherlands Defence Academy (NLDA) in Den Helder from May 2009 to January 2010. During the nine months of my stay in Den Helder I got a lot of help from the staff in the laboratory, Chris Dijkstra, Arek Wojtalik, Marco Gademan, etc. Without their help and technical support, it would have been impossible for me to finish the measurements.

I must thank in particular Henk Knoll at NLDA. During the measurements, he gave me a lot of directions how to carry out experimental work and learnt me the ins and outs of the test facilities. When afterwards processing the measurements with the simulation tools, we had plenty of discussions how to make the simulations more accurate and efficient. In particular regarding programming issues, I learnt a lot from him. In the end he also participated in reviewing the thesis.

I am grateful to the corporation of China Scholarship Council (CSC) and TU Delft who financed my living and studying in the Netherlands. I should also thank Harbin Engineering University (HEU) to allow me to come to TU Delft in order to pursue my doctor’s degree.

Finally but more importantly, I would like to thank my supervisors professor Douwe Stapersma and Dr Hugo Grimmelius. During these four years, they gave me a lot of encouragement and support. Thanks to their rigorousness, tolerance and patience, I succeeded in finishing my PhD project in the end.

Curriculum Vitae

Ding Yu (in Chinese order) was born on 25th of January, 1980 in Qiqihar, China. In 1999, he went to Harbin Engineering University (HEU) in Harbin for his bachelor study and in 2003 he received a bachelor degree in ‘Thermal and Power Engineering’, after which he became an employee in HEU and continued his study for a master degree on the subject called ‘The performance analysis of diesel engine crankshaft and the research into a calculation method of crankshaft fatigue strength’. In 2006, he obtained a master degree in ‘Marine Engineering’ at HEU. In 2007, he got a scholarship from China Scholarship Council (CSC) and went to Delft University of Technology to start his PhD project.